Titre: Title:	Extrusion Catalytic Depolymerization of PMMA
Auteur: Author:	Yanfa Zhuang
Date:	2025
Type:	Mémoire ou thèse / Dissertation or Thesis
Référence: Citation:	Zhuang, Y. (2025). Extrusion Catalytic Depolymerization of PMMA [Thèse de doctorat, Polytechnique Montréal]. PolyPublie. https://publications.polymtl.ca/65859/

POLYTECHNIQUE MONTRÉAL
affiliée à l'Université de Montréal

Extrusion catalytic depolymerization of PMMA

YANFA ZHUANG
Département de génie chimique

Thèse présentée en vue de l'obtention du diplôme de *Philosophiæ Doctor*
Génie chimique

Mars 2025

POLYTECHNIQUE MONTRÉAL
affiliée à l'Université de Montréal

Cette thèse intitulée :

Extrusion catalytic depolymerization of PMMA

présentée par **Yanfa ZHUANG**
en vue de l'obtention du diplôme de *Philosophiæ Doctor*
a été dûment acceptée par le jury d'examen constitué de :

Charles DUBOIS, président
Gregory PATIENCE, membre et directeur de recherche
Abdellah AJJI, membre et codirecteur de recherche
Jean-Marie RAQUEZ, membre
Milan MARIC, membre externe

DEDICATION

Dedicated to
My deceased mother
My beloved family
Thank you for your love and support

ACKNOWLEDGEMENTS

Pursuing a Ph.D. has been one of the most significant decisions of my life. Over six years of doctoral study, I encountered numerous challenges, hardships, dedication, and sacrifices, but it also completely transformed my understanding and equipped me with many new skills. Throughout my Ph.D., there were many moments when I considered giving up, especially during the COVID-19 pandemic, which profoundly disrupted my initial enthusiasm for academic research. However, with the unwavering support of my supervisors, family, and friends, I persevered and completed my doctoral project.

Among all those who supported me, I am most grateful to my doctoral supervisor, Prof. Gregory S. Patience. His unwavering support was instrumental in my ability to complete this project. He consistently provided the guidance and assistance I needed, especially during the most critical times. Beyond the doctoral project, he taught me valuable workplace habits and social skills that are difficult to learn in school but will benefit me throughout my life. Without his support, my doctoral project would not have been possible. I extend my highest respect and gratitude to Prof. Gregory S. Patience.

I am also profoundly thankful to my co-supervisor, Prof. Abdellah Ajji, for his strong support. I appreciate the experimental and testing platform for polymer research he provided and his assistance with the extrusion experiments. When I started this Ph.D. project, I had minimal knowledge of polymers. Thanks to Prof. Abdellah Ajji, I gained a deeper understanding of polymers.

I extend my gratitude to Prof. Daria C. Boffito for her support and the laboratory platform she provided. I also thank Dr. Jean-Luc Dubois for his guidance and help in the project's progress.

I am very fortunate to have had many wonderful colleagues, and I am deeply grateful for their help and support during my Ph.D. In particular, I must thank Dr. Nooshin Saadatkhah for her assistance with my project and personal growth. From her, I learned the character and qualities that an excellent person should possess. I also thank my colleague Tien-Dat Nguyen for his significant help with my experiments.

I am grateful to my former and current colleagues Dr. He Li, Dr. Zhenni Ma, Dr. Gianluca Pauletto, Prof. Federico Galli, Nooshin Moradi, Dr. Zahra Khani, Dr. Mahdi Sharifian, Jacopo De Tommaso, Dalma Schieppati, Paula-andrea Rivera-Quintero, Fellipy Rocha, Yuxiang Song, Maoline Houndedoke, Dr. Tugce N. Eran, Mario Ferreiro González, and Adrien D'Oliveira for their support of my project. I also thank my interns, Mack Grigg and Tianhua Xu from UBC, and Clive Yi Jie Ng from Nanyang Polytechnic in Singapore, for their help with my doctoral experiments. I am also grateful to Matthieu Gauthier and Claire Cerclé from CREPEC for their experimental support and professional instrument training. Special thanks go to Technician Jean Ghantous for his great help with my doctoral project, and to the other technical staff, Rafael Rios, Alejandro Velez Garcia, and Alexis Thivierge.

I would like to express my special thanks to my Chinese friends, Dr. Chunyu Wang, Dr. Zhaohui Chen, Dr. Chi Zhang, Jingsi Jiang, Shihao Pei, Peiyu Wang, Dr. Xin Zhou, and Xinxin Pi, for their help with my doctoral work and life in Montreal. Thanks to all my friends who have supported me over the past six years in Montreal.

Finally, I want to thank my mother, who passed away last year. She was the only person in the world who supported me unconditionally. For all my major life choices, including selecting a major, studying abroad, pursuing a Ph.D., career choices, and starting a business, she was my greatest supporter. Perhaps the person who most wanted to see me graduate with my Ph.D. was my mother. It is a pity she cannot witness this moment with her own eyes. I am also very grateful to my other family members for their selfless and strong support. My family has been my biggest motivation to complete this doctoral degree. Thank you to my family for their support and companionship.

I am still myself, but no longer the naive and young person I once was. The Ph.D. journey has ended, but the vast world ahead is still waiting for me.

RÉSUMÉ

L'industrie génère chaque année 400 millions de tonnes de déchets plastiques, mais seulement 9 % sont recyclés. Plus de 80 % sont mis en décharge, incinérés ou rejetés dans l'environnement. Un type de plastique largement non recyclé est le polyméthacrylate de méthyle (PMMA). Également connu sous les noms de verre acrylique, Plexiglas, Perspex, Altuglas et Lucite, le PMMA est un thermoplastique optiquement transparent, réputé pour sa bonne résistance à la traction et à la flexion, ainsi que pour son excellente résistance aux UV et aux rayures. Chaque année, 4 millions de tonnes de PMMA sont produites pour diverses applications industrielles, notamment dans les domaines de l'optique, de l'électronique, de la signalisation, de la construction, des pièces automobiles et des revêtements. Au Canada, moins de 10 % des déchets de PMMA sont recyclés, tandis qu'en Europe, environ 30 000 tonnes de PMMA ont été recyclées en 2019, ce qui représente environ 10 % de la production totale de déchets de PMMA. À l'échelle mondiale, l'industrie génère chaque année entre 800 000 et 1 000 000 tonnes de déchets de PMMA qui ne sont pas valorisés. Le recyclage du PMMA peut être réalisé par des méthodes mécaniques ou chimiques. Le recyclage mécanique entraîne souvent une détérioration des propriétés du matériau après plusieurs cycles. En revanche, le recyclage chimique offre une solution plus efficace, en particulier pour les déchets de PMMA en fin de vie, en les convertissant en produits chimiques à valeur ajoutée avant qu'ils ne soient mis en décharge ou incinérés.

La dépolymérisation thermique du PMMA à des températures supérieures à 350 °C dans une atmosphère inerte permet d'obtenir une pureté du monomère de méthacrylate de méthyle (MMA) supérieure à 90 %, avec un rendement en monomère compris entre 70 % et 90 %. L'objectif principal du recyclage chimique industriel des déchets de PMMA est de produire du monomère de MMA, qui doit ensuite être purifié pour permettre une éventuelle repolymérisation.

Les charges et additifs présents dans les déchets de PMMA en fin de vie peuvent nuire à la pureté et au rendement du monomère de MMA produit lors de la thermolyse, en introduisant des impuretés qui compliquent les processus de purification en aval et augmentent les coûts. Le MMA régénéré brut (r-MMA) contient souvent des oligomères et des impuretés ayant des points d'ébullition ou des structures moléculaires similaires à ceux du MMA, tels que l'acrylate de méthyle, l'acrylate d'éthyle, le propionate de méthyle ou d'éthyle, et

l'isobutyrate de méthyle. Par exemple, l'acrylate d'éthyle a un point d'ébullition d'environ 100 °C, très proche de celui du MMA (101 °C). Ces impuretés nécessitent des processus de purification plus étendus et coûteux, dont certains sont difficiles à éliminer complètement. Par conséquent, la présence de ces impuretés limite l'utilisation du r-MMA dans les marchés strictement réglementés où un PMMA de haute qualité est requis.

Ce projet vise à produire du MMA et/ou de l'acide méthacrylique (MAA) en utilisant une méthode d'extrusion réactive (REX). Le MAA, en plus du MMA, est un monomère fonctionnel précieux et polyvalent, largement utilisé dans des applications telles que les peintures, les agents de traitement pour le cuir et les textiles, les adhésifs et les résines échangeuses d'ions. Il est également employé dans la synthèse de copolymères avec d'autres monomères, ses esters (par exemple, le MMA), et les sels de MAA. Le recyclage du PMMA en MAA par hydrolyse permet d'atténuer les difficultés associées à l'élimination des impuretés dans la voie de recyclage conventionnelle du PMMA en MMA. Contrairement à la thermolyse, qui génère divers sous-produits volatils, l'hydrolyse permet non seulement d'obtenir directement du MAA, mais aussi de convertir les composés dérivés de la thermolyse en composants acides plus facilement séparables du produit final. Par exemple, la thermolyse du PMMA produit de l'isobutyrate de méthyle (point d'ébullition : 90 °C) et de l'acrylate d'éthyle (point d'ébullition : 100 °C), qui peuvent ensuite être hydrolysés en acide isobutyrique (point d'ébullition : 155 °C, point de fusion : −47 °C) et en acide acrylique (point d'ébullition : 141 °C), respectivement. Le MAA a un point d'ébullition de 162 °C et un point de fusion de 15 °C, ce qui facilite sa séparation des sous-produits issus du recyclage du PMMA. Étant donné la co-existence du MMA et du MAA lors du recyclage chimique du PMMA et leur forte valeur industrielle, ce projet se concentre sur l'obtention d'un flux de MMA et/ou de MAA de haute pureté en une seule étape de traitement.

La première étape de ce projet a consisté à examiner le procédé REX, notamment ses principes de fonctionnement, ses composants, ses applications, ses réactions, sa modélisation, ses considérations d'échelle et ses limitations. Parmi les trois types d'extrudeuses réactives — monovis, bivis à contre-rotation et bivis à co-rotation —, nous avons déterminé que l'extrudeuse bivis à co-rotation est la plus efficace pour les milieux visqueux en raison de ses performances supérieures en matière de mélange, de contrôle de la température et du temps de séjour, ainsi que de son mécanisme autonettoyant. Le REX montre un potentiel pour le recyclage dégradatif des polymères.

Dans la deuxième étape, nous avons développé un réacteur à lit fixe à l'échelle du laboratoire pour évaluer des catalyseurs commerciaux à base de zéolithes, y compris la zéolithe Y, la zéolithe β, la mordenite et la ZSM-5, pour la valorisation du PMMA en MAA. L'hydrolyse directe du PMMA sur la zéolithe Y de type H (rapport $SiO_2/Al_2O_3 = 80$) a permis d'obtenir un rendement en MAA de 56 % et une sélectivité de 58 % à 350 °C. Nous avons élucidé le mécanisme de réaction de l'hydrolyse du PMMA en analysant les produits gazeux et liquides ainsi que les résidus solides réagis. Le dépôt de coke dans les structures des zéolithes à larges pores a provoqué une désactivation réversible des sites acides de Brønsted et de force moyenne. Bien que la décarboxylation catalytique du MMA génère de l'acétone et du CO, la décarboxylation du MAA produit principalement de l'acétone et du CO. Par ailleurs, l'hydrolyse directe des chaînes de PMMA a formé du méthanol et des copolymères Poly(MMA-co-MAA), qui se déshydratent davantage en anhydride glutarique à six chaînons.

Un réacteur à lit fixe à l'échelle du laboratoire a permis une exploration approfondie du mécanisme d'hydrolyse directe du PMMA et a identifié la zéolithe Y comme le catalyseur optimal pour l'hydrolyse en REX. L'hydrolyse du PMMA se déroule par des réactions en tandem : dépolymérisation radicalaire en MMA, suivie de l'hydrolyse catalytique du MMA en MAA. Les deux composés, MMA et MAA, sont cogénérés lors de l'hydrolyse du PMMA.

Dans la phase finale de ce projet, nous avons démontré un système d'extrusion réactive en deux étapes à l'échelle du laboratoire pour le recyclage continu des déchets de PMMA de qualité injection ou extrusion en MMA et/ou MAA à des températures comprises entre 330 °C et 370 °C. Ce système utilise une extrudeuse monovis comme dispositif d'alimentation pour injecter le PMMA fondu dans une extrudeuse bivis à co-rotation servant de réacteur d'hydrolyse, où la dépolymérisation du PMMA et l'hydrolyse du MMA se produisent. Les tests de distribution des temps de séjour ont caractérisé l'hydrodynamique de la configuration des vis, montrant que des vitesses de vis et des taux d'alimentation plus faibles prolongeaient les temps de réaction moyens. Un plan Plackett–Burman a identifié la température et le type de catalyseur comme des facteurs significatifs influençant l'hydrolyse du MMA. Nous avons comparé les catalyseurs solides (zéolithe Y, γ-Al_2O_3), les catalyseurs acides liquides (acide phosphotungstique hydraté et H_2SO_4) et un catalyseur liquide caustique (KOH) pour l'hydrolyse en REX du PMMA. Dans des conditions optimales, l'extrusion d'hydrolyse sans catalyseur a atteint le rendement en MMA le plus élevé (89 %) et une conversion du PMMA de 96 %. L'extrusion d'hydrolyse des déchets de PMMA de qualité injection avec 10 % de zéolithe Y de type H (rapport $SiO_2/Al_2O_3 = 80$) a donné 5.3 % de MAA, 67 % de MMA et une conversion quasi complète du PMMA à 370 °C. Les catalyseurs acides liquides ont hydrolysé

directement le PMMA en copolymères Poly(MMA-co-MAA) et/ou Poly(acide méthacrylique) (PMAA), suivis d'une déshydratation pour former de l'anhydride glutarique à six chaînons. De manière similaire, KOH a hydrolysé le PMMA en Poly(MMA-co-MAA) et/ou en sel de potassium du PMMA.

ABSTRACT

The industry generates 400 million tonnes of plastic waste each year, but only 9 % is recycled. Over 80 % is either landfilled, incinerated, or released into the environment. One type of plastic that remains largely unrecycled is Polymethyl methacrylate (PMMA). Also known as acrylic glass, Plexiglas, Perspex, Altuglas, and Lucite, PMMA is an optically transparent thermoplastic renowned for its good tensile and flexural strength, as well as its excellent UV and scratch resistance. Annually, 4 million metric tonnes of PMMA are produced for various industrial applications, including optics, electronics, signage, construction, automotive parts, and coatings. In Canada, less than 10 % of PMMA waste is recycled, while Europe recycled approximately 30,000 tonnes of PMMA in 2019, which represents around 10 % of total PMMA waste production. Globally, the industry generates between 800 000 to 1 000 000 tonnes of PMMA waste each year that remains unaddressed. Recycling PMMA can be approached through mechanical or chemical methods. Mechanical recycling often results in deteriorated material properties after several cycles. In contrast, chemical recycling offers a more effective solution, particularly for end-of-life PMMA scraps, by converting them into value-added chemicals before they are sent to landfills or incinerated. Thermal depolymerization of PMMA at temperatures above 350 °C in an inert atmosphere yields over 90 % methyl methacrylate (MMA) monomer purity with a monomer yield ranging from 70 % to 90 %. The focus of industrial chemical recycling of waste PMMA is on generating MMA monomer, which then requires purification for potential re-polymerization.

Fillers and additives present in end-of-life PMMA can negatively impact the purity and yield of MMA monomer during thermolysis, introducing impurities that complicate downstream purification processes and increase costs. The crude regenerated MMA (r-MMA) often contains oligomers and impurities with similar boiling points or molecular structures to MMA, such as methyl acrylate, ethyl acrylate, methyl or ethyl propionate, and methyl isobutyrate. For instance, ethyl acrylate has a boiling point of approximately 100 °C, which is very close to the boiling point of MMA (101 °C). These impurities necessitate more extensive and costly purification processes, some of which are challenging to eliminate entirely. Consequently, the presence of these impurities restricts the use of r-MMA in strictly regulated markets where high-quality PMMA is required.

This project aims to produce MMA and/or methacrylic acid (MAA) using a reactive ex-

trusion (REX) method. MAA, in addition to MMA, is a valuable and versatile functional monomer widely used in applications such as paints, leather and textile treatment agents, adhesives, and ion-exchange resins. It is also employed in the synthesis of copolymers with other monomers, its esters (e.g., MMA), and MAA salts. Recycling PMMA into MAA via hydrolysis mitigates the challenges associated with impurity removal in the conventional PMMA-to-MMA recycling pathway. Unlike thermolysis, which generates various volatile by-products, hydrolysis not only yields MAA directly but also converts thermolysis-derived compounds into acid-phase components that are more readily separable from the MAA product. For instance, PMMA thermolysis produces methyl isobutyrate (boiling point: 90 °C) and ethyl acrylate (boiling point: 100 °C), which can be subsequently hydrolyzed into isobutyric acid (boiling point: 155 °C, melting point: −47 °C) and acrylic acid (boiling point: 141 °C), respectively. MAA has a boiling point of 162 °C and a melting point of 15 °C, which facilitates its separation from PMMA recycling by-products. Given the co-existence of MMA and MAA during the chemical recycling of PMMA and their high industrial value, this project focuses on achieving a high-purity stream of MMA and/or MAA in a single processing step.

The first step of this project involved reviewing REX, including its working principles, apparatus components, applications, reactions, modeling, scale-up considerations, and limitations. Among the three types of reactive extruders—single-screw, counter-rotating twin-screw, and co-rotating twin-screw—we determined that the co-rotating twin-screw extruder is the most effective for viscous media due to its superior mixing, temperature and residence time control, and self-wiping performance. REX demonstrates potential for polymer degradative recycling.

In the second step of this project, we developed a lab-scale fixed-bed reactor to evaluate commercial zeolite catalysts, including zeolite Y, zeolite β, Mordenite, and ZSM-5, for the upcycling of PMMA to MAA. Direct hydrolysis of PMMA over H-type zeolite Y (SiO_2/Al_2O_3 ratio = 80) achieved an MAA yield of 56 % and selectivity of 58 % at 350 °C. We elucidated the PMMA hydrolysis reaction mechanism through analysis of gaseous and liquid products, as well as reacted solid residues. Coke deposition within the frameworks of large-pore zeolites caused reversible deactivation of Brønsted and medium-strength acid sites. While MMA catalytic decarboxylation generates acetone and CO, the decarboxylation of MAA predominantly produces acetone and CO. Additionally, direct hydrolysis of PMMA chains formed methanol and Poly(MMA-co-MAA) copolymers, which further dehydrated to six-member glutaric anhydride.

A lab-scale fixed-bed reactor enabled in-depth exploration of the direct hydrolysis mechanism of PMMA and identified zeolite Y as the optimal catalyst for REX hydrolysis. PMMA hydrolysis proceeds through tandem reactions: radical depolymerization to MMA, followed by MMA catalytic hydrolysis to MAA. Both MMA and MAA are co-generated during PMMA hydrolysis.

In the final phase of this project, we demonstrated a lab-scale two-stage reactive hydrolysis extrusion system for continuous recycling of injection- and extrusion-grade PMMA scraps into MMA and/or MAA at 330 °C to 370 °C. The system utilized a single screw extruder as a feeder to inject molten PMMA into a co-rotating twin-screw extruder serving as the hydrolysis reactor, where PMMA depolymerization and MMA hydrolysis occur. Residence time distribution tests characterized the screw configuration's hydrodynamics, showing that lower screw speeds and feeding rates extended average reaction times. A Plackett–Burman design identified temperature and catalyst type as significant factors affecting MMA hydrolysis. We compared solid catalysts (zeolite Y, γ-Al_2O_3), liquid acid catalysts (phosphotungstic acid hydrate and H_2SO_4), and a caustic liquid catalyst (KOH) for the REX hydrolysis of PMMA. Under optimized conditions, catalyst-free hydrolysis extrusion achieved the highest MMA yield (89 %) and PMMA conversion (96 %). Hydrolysis extrusion of injection-grade PMMA scrap with 10 % H-type zeolite Y (SiO_2/Al_2O_3 ratio = 80) yielded 5.3 % MAA, 67 % MMA, and near-complete PMMA conversion at 370 °C. Liquid acid catalysts directly hydrolyzed PMMA to Poly(MMA-co-MAA) copolymers and/or Poly(methacrylic acid) (PMAA), with subsequent dehydration forming six-membered glutaric anhydride. Similarly, KOH hydrolyzed PMMA into Poly(MMA-co-MAA) and/or PMMA potassium salt.

TABLE OF CONTENTS

LIST OF TABLES

LIST OF FIGURES

LIST OF SYMBOLS AND ACRONYMS

PMMA	Polymethyl methacrylate
PMAA	Poly(methacrylic acid)
MMA	Methyl methacrylate
r-MMA	Regenerated methyl methacrylate
MAA	Methacrylic acid
REX	Reactive extrusion
BP	Boiling point
MP	Melting point
ACN	Acetone-cyanohydrin
DOE	Design of Experiments
PTA	Phosphotungstic acid
RTD	Residence time distribution
SDF	Strain distribution function
LCA	Life cycle assessment
MA	Methyl acrylate
EA	Ethyl acrylate
CSBR	Conical spouted bed reactor
TSE	Twin-screw extruder
LSLF	Low-speed late fusion
HSEI	High-speed energy input
SF	Single flight
SME	Screw mixing element
ZME	Zester mixing element
PLLA	Polylactic acid
CNT	Carbon nanotube
ABS	Acrylonitrile butadiene styrene
GMA	Glycidyl methacrylate
NP	Nanoparticle
LDPE	Low density polyethylene
PA6	Polyamide 6
PBT	Polybutylene terephthalate
PBAT	Polybutylene adipate terephthalate
PET	Polyethylene terephthalate

PP	Polypropylene
PLLA	Poly(l-lactide)
MA	Maleic anhydride
TC	Thermocouples
IR	Infrared
UV	Ultra-violet
NIR	Near-infrared
MIR	Mid-infrared
ATR-IR	Attenuatedtotal-reflection infrared
CFD	Computational fluid dynamics
PFRs	Plug-flow reactors
CSTRs	Continuous stirred-tank reactors
FVM	Finite volume method
FEM	Finite element method
PE	Polyethylene
PS	Polystyrene
PVC	Polyvinyl chloride
TPU	Thermoplastic urethane
PPE	Personal protective equipment
SOS	Safe operating space
XRD	X-ray powder diffraction
BET	Brunauer-Emmett-Teller
BJH	Barrett-Joyner-Halenda
PSD	Particle size distribution
SEM	Scanning electron microscopy
EDS	Energy dispersive spectroscopy
TEM	Transmission electron microscopy
SAED	Selected area electron diffraction
XPS	X-ray photoelectron spectroscopy
NH_3-TPD	Ammonia temperature-programmed desorption
FTIR	Fourier-transform infrared spectroscopy
GPC	Gel permeation chromatography
RI	Refractive index
THF	Tetrahydrofuran
TGA	Thermogravimetric analysis
DSC	Differential scanning calorimetry

TCD	Thermal conductivity detector
MSD	Mass selective detector
UI	Ultra inert
SIM	Selected ion monitoring
DME	Dimethyl ether
Py-IR	Pyridine-adsorbed FT-IR
LAS	Lewis acid sites
BAS	Brønsted acid sites
RFI	Relative fluorescence intensity
T	Temperature
T_{g}	Glass transition temperature
X_{PMMA}	PMMA conversion, %
S_{i}	Selectivity of product component i, %
Y_{i}	Yield of product component i, %
m/z	Mass-to-charge ratio
N_{Pe}	Peclet number
N_{TSE}	Screw speed of twin-screw extruder, rpm
Q_{PMMA}	PMMA feeding rate, $\mathrm{g\,h^{-1}}$ or $\mathrm{kg\,h^{-1}}$
Q_{H2O}	Liquid H_2O injection rate, $\mathrm{mL\,min^{-1}}$
$Q_{\mathrm{cat.}}$	Feeding rate of catalyst, $\mathrm{g\,h^{-1}}$
S_{BET}	Surface area measured by Brunauer-Emmett-Teller method, $\mathrm{m^2\,g^{-1}}$
V_{tot}	Total pore volume, $\mathrm{cm^3\,g^{-1}}$
V_{micro}	Volume of micropores, $\mathrm{cm^3\,g^{-1}}$
S_{micro}	Specific surface area of micropores, $\mathrm{m^2\,g^{-1}}$
S_{meso}	Specific surface area of mesopores, $\mathrm{m^2\,g^{-1}}$
D_{v}	Pore size measured by Barrett-Joyner-Halenda model, Å
d_{p}	Particle size, µm
F	Degree of fill
L/D	Length to diameter ratio
M_{w}	Molecular weight, $\mathrm{g\,mol^{-1}}$
C	Normalized relative fluorescence intensity
θ	Non-dimensional time
ξ	Non-dimensional length
u	Melt velocity
$\bar{t}$	Mean residence time
σ	Shear stress

η	Melt viscosity
E_{a}	Activation energy

CHAPTER 1 INTRODUCTION

1.1 Background and problem identification

Polymethyl methacrylate (PMMA), also known as Plexiglas, acrylic glass, Perspex, Altuglas, and Lucite, is an optically transparent thermoplastic renowned for its excellent tensile and flexural strength, UV resistance, and scratch resistance [1, 2]. The industry produces 4 million tonnes of PMMA annually, serving applications in automotive, construction, electronics, signage, and coatings. Despite its widespread use, PMMA recycling rates remain critically low. In the European Union, only 10 % of PMMA waste is collected and recycled each year. In Canada, less than 10 % of waste PMMA is recycled. Globally, the industry generates 800,000 to 1,000,000 tonnes of waste PMMA annually, much of which is landfilled, incinerated, or improperly disposed of, often polluting natural environments, including oceans. Recycled PMMA primarily originates from post-industrial sources, such as cast sheets, extrusion sheets, and injection-molded parts. This waste is typically processed through mechanical recycling to produce new PMMA products or composites, or through thermolysis to generate regenerated MMA (r-MMA) for repolymerization.

Mechanical recycling is often limited to processing post-industrial PMMA waste due to its lower levels of fillers and impurities. However, the material properties of mechanically recycled PMMA deteriorate after several cycles, reducing its long-term utility [3]. In contrast, chemical recycling offers a more promising solution for recycling end-of-life PMMA, which constitutes the majority of global PMMA waste.

Thermal depolymerization of PMMA at temperatures above 350 °C in an inert atmosphere yields 70 % to 90 % monomer yield, with r-MMA purity exceeding 90 % [4]. However, fillers and additives in end-of-life PMMA, such as metals, glass fibers, granite, and colorants, reduce r-MMA yield and introduce impurities, increasing the costs of downstream purification [5].

Crude r-MMA often contains oligomers and impurities, including methyl acrylate, ethyl acrylate, methyl pyruvate, methyl or ethyl propionate, methyl isobutyrate, and methyl 2-methylbutyrate [6–8]. Many of these impurities share similar physicochemical properties with MMA, such as close boiling points and molecular structures, complicating downstream separation and purification processes. For instance, ethyl acrylate (BP = 100 °C) has a boil-

ing point nearly identical to that of MMA (BP = 101 °C) and an odor threshold over 20 times lower than MMA, making its complete removal particularly challenging [9, 10]. Currently, some impurities in crude r-MMA are difficult to eliminate entirely during purification. These limitations hinder the use of r-MMA for producing high-quality PMMA, especially for applications in strictly regulated markets.

To reduce the downstream purification costs of crude r-MMA and enhance the value of PMMA thermolysis, we propose upcycling PMMA to produce methacrylic acid (MAA) instead of MMA. MAA, as a functional monomer and specialty chemical, is widely used in the synthesis of copolymers, esters, and salts. The market is showing increasing interest in the supply of MAA due to its versatile applications in paints, adhesives, leather and textile treatments, fiber processing, and ion-exchange resins [11, 12]. The demand for MAA is expected to grow further as new MMA production facilities utilizing ethylene as a feedstock are set to come online in the coming years. Unlike traditional MMA plants, these facilities do not coproduce MAA, creating additional market opportunities for MAA.

Hydrolyzing PMMA not only converts r-MMA to MAA but also breaks down ester impurities, such as ethyl acrylate, into acid components. This process simplifies the separation of MAA from the hydrolysis products, making it a more efficient pathway for high-purity MAA production. Based on differences in boiling points, distillation can be employed to separate the hydrolysis products. Similarly, low-temperature crystallization can be utilized to separate components with distinct melting points. Since MAA (BP = 162 °C, MP = 15 °C) exhibits different volatility and melting characteristics compared to other hydrolysis-derived acids such as isobutyric acid (BP = 155 °C, MP = −47 °C) and acrylic acid (BP = 141 °C) [13], a combination of distillation and low-temperature crystallization holds promise for producing high-purity MAA.

Industry primarily produces MAA through the acetone-cyanohydrin (ACN) process and the oxidation of isobutylene or ethylene-derived methacrolein [14,15]. The ACN process requires hazardous feedstocks such as hydrogen cyanide and cyanide intermediates, while the oxidation pathway depends on fossil fuel-derived raw materials. In contrast, the hydrolysis of post-industrial and end-of-life PMMA offers a sustainable alternative for MAA production. This approach not only addresses the challenge of solid PMMA waste management but also provides significant technical, economic, and market advantages. MAA has a distinct and valuable market of its own. However, given the co-existence of both MAA and MMA in the

hydrolysis products, there is also the option to reproduce PMMA by converting MAA into MMA, followed by a repolymerization step. This closed-loop pathway offers a potential route for PMMA reproduction.

Reported reactors for PMMA hydrolysis to MAA are currently limited to lab-scale fluidized or fixed-bed reactors [5, 16] and stirred tank reactors [17], all of which operate in batch or semi-batch modes. Developing a continuous process is essential to enable the industrial-scale application of PMMA hydrolysis for MAA production. However, reactor design for continuous PMMA recycling remains unexplored. Additionally, the reaction mechanisms of direct PMMA hydrolysis, including often-overlooked side reactions, require further investigation.

Reactive extrusion (REX) is a continuous process used for polymer modification, synthesis, or degradation through the use of extruders. Reviewing the applications of REX in polymer functionalization, polymerization, and depolymerization provides critical insights for designing a REX system tailored for PMMA extrusion hydrolysis. A co-rotating twin-screw extruder equipped with distinct functional zones (PMMA feeding, liquid injection, reaction, degassing, and compression) demonstrates potential for continuous PMMA hydrolysis recycling. However, technical validation and detailed investigations remain lacking. Key operational parameters, including temperature, feeding rate, and screw rotation speed, critically influence PMMA depolymerization and hydrolysis processes. Both MMA and MAA are valuable products of PMMA extrusion hydrolysis and are pivotal in chemical recycling. Nevertheless, the co-generation ratio of MMA to MAA during REX remains unclear and requires further study.

The production of MAA relies on the use of hydrolysis catalysts, with zeolites emerging as promising candidates for PMMA/MMA hydrolysis. Screening zeolites for direct PMMA hydrolysis using small sample loading provides valuable insights into the reaction mechanism and helps identify the most effective zeolite for PMMA upcycling to MAA in a twin-screw extruder.

1.2 Objectives

The main objective of this project is to develop a continuous reactive hydrolysis extrusion process for recycling waste PMMA into MAA and/or MMA. Both MAA and MMA are highly

desirable and valuable products. To achieve this main objective, the project is structured around four specific objectives:

1. Identify applications of REX in polymer processing, including polymer functionalization, polymerization, and depolymerization.
    - Review the principles, equipment, characteristics, applications, design considerations, and simulation aspects of the REX process.
    - Identify the functions of different zones within a reactive extruder, including feeding, melting, mixing, and degassing.
    - Determine the most suitable extruder type for degradative extrusion processes.
    - Summarize the limitations, technical challenges, and future perspectives of REX.
2. Identify the most effective zeolite catalysts for PMMA upcycling to MAA using a lab-scale fixed-bed reactor.
    - Screen zeolite catalysts, including zeolite Y, zeolite β, ZSM-5, and Mordenite, for PMMA upcycling to MAA.
    - Elucidate the detailed reaction mechanism of PMMA direct hydrolysis over zeolite catalysts.
    - Investigate the effect of the SiO_2/Al_2O_3 molar ratio of the zeolites on the hydrolysis upcycling of PMMA.
    - Investigate the formation mechanism of coke deposition.
    - Examine the impact of acidity and micropore shape-selectivity of zeolites on the hydrolysis upcycling of PMMA.
    - Determine the optimal reaction temperature.
    - Evaluate the activity of desilicated and regenerated zeolite Y.
3. Develop a lab-scale, two-stage reactive hydrolysis extrusion system for the continuous conversion of PMMA into MMA and/or MAA.
    - Analyze the hydrodynamics of the twin-screw configuration using an axial dispersion model.
    - Optimize the extrusion conditions, including temperature, screw rotation speed, and feeding rate, for the first-stage single screw extruder and the second-stage twin-screw extruder.

- Investigate the impact of degassing methods (vacuum degassing versus atmospheric degassing) on product recovery.
- Determine the mean residence time of PMMA melt in the reaction, degassing, and compression zones of the twin-screw extruder.

4. Study the activity of hydrolysis catalysts in PMMA reactive hydrolysis extrusion.

   - Determine the optimal reaction conditions for PMMA catalytic hydrolysis extrusion using Design of Experiments (DOE).
   - Investigate the catalytic activity of solid catalysts (zeolite Y and Al_2O_3) and liquid catalysts (phosphotungstic acid (PTA), H_2SO_4, and KOH).
   - Examine the effect of catalyst feeding percentage and liquid injection rate on MAA yield.
   - Characterize the solid extrusion residues.
   - Investigate the different reaction mechanisms catalyzed by liquid and solid catalysts.
   - Characterize the PMMA scraps used in reactive hydrolysis extrusion tests.

CHAPTER 2 COHERENCE OF THE CHAPTERS

A brief description of the chapters and their interconnections is provided below.

2.1 Chapter 1

The first chapter highlights the current state of PMMA production and recycling, emphasizing the urgent need for more effective and valuable methods to manage and recycle post-industrial and end-of-life PMMA. It briefly discusses the challenges associated with PMMA pyrolysis, the most widely used chemical recycling method for producing MMA monomer. To address these challenges, an alternative approach is proposed to upcycle PMMA into MAA instead of MMA, aiming to reduce the potential purification costs and complexities of crude r-MMA. The primary objective focuses on developing a continuous PMMA reactive hydrolysis extrusion process for the production of MAA and/or MMA.

2.2 Chapter 2

Provide a concise overview of all chapters and their interconnections.

2.3 Chapter 3

In this chapter, we review and compare various PMMA recycling methods and examine the mechanisms of PMMA depolymerization. The chapter provides an overview of PMMA extrusion depolymerization techniques used in industrial applications and laboratory studies, highlighting the principles of extrusion degassing and factors that improve devolatilization. Additionally, we explore current industrial synthesis routes for MAA and evaluate potential hydrolysis catalysts for converting MMA to MAA.

2.4 Chapter 4

In this chapter, we review the working principles, apparatuses, applications, reaction types, simulation and modelling approaches, scale-up considerations, limitations, technical challenges, and future perspectives of REX. Our analysis concludes that REX is an ideal process for polymer functionalization, polymerization, and depolymerization. This literature study provides the theoretical foundation and key considerations for designing a degradative REX

system. The findings of this research have been published in **The Canadian Journal of Chemical Engineering**.

2.5 Chapter 5

This chapter presents a sustainable recycling method for directly hydrolyzing PMMA into MAA using a fixed-bed reactor. The study evaluates the hydrolysis activity of various commercial zeolite catalysts, including zeolite Y, zeolite β, ZSM-5, and Mordenite, as well as regenerated and desilicated zeolite Y. We examine the effects of the SiO_2/Al_2O_3 molar ratio, hydrolysis temperature, zeolite pore size, and acidity on PMMA hydrolysis activity. Additionally, we elucidate the comprehensive reaction mechanism by investigating the primary MAA production pathway and side reactions that reduce MAA yield. The study identifies H-type zeolite Y with an SiO_2/Al_2O_3 molar ratio of 80 as the most effective catalyst for PMMA hydrolysis. The findings from this work have been published in **Reaction Chemistry & Engineering**.

2.6 Chapter 6

This chapter presents a lab-scale, two-stage reactive hydrolysis extrusion system for the continuous recycling of injection- and extrusion-grade PMMA scraps into MMA and/or MAA at temperatures ranging from 330 °C to 370 °C. The study characterizes the hydrodynamics of the designed screw configuration through residence time distribution (RTD) tests and analysis, and determines the optimized extrusion conditions using DOE. The research validates the hydrolysis activity of commercial H-type zeolite Y with an SiO_2/Al_2O_3 molar ratio of 80 within the developed reactive hydrolysis extrusion system. It further evaluates and compares the hydrolysis activity of liquid catalysts (PTA, H_2SO_4, and KOH) with solid catalysts (zeolite Y and Al_2O_3) under optimized extrusion conditions. The results of this work have been published in **Chemical Engineering Journal**.

2.7 Chapter 7

This section summarizes the results obtained and provides a general discussion of the results.

2.8 Chapter 8

This section summarizes the project, discusses the limitations of PMMA reactive hydrolysis extrusion, and offers recommendations for future research.

CHAPTER 3 LITERATURE REVIEW

3.1 Recycling methods of waste PMMA

Plastic products have become an essential part of our daily lives due to their exceptional durability, ease of processing, lightweight nature, low production costs, and strong resistance to chemical corrosion. However, their widespread consumption has created significant environmental challenges. Recycling plastic waste not only reduces the environmental burden by minimizing waste in nature and conserving the natural resources used in plastic production but also provides economic advantages by enabling the recovery of energy and the reproduction of value-added materials, such as monomers.

Recycling waste from polymer materials can be categorized into four main methods (Fig. 3.1) [18]: reuse (i.e., primary recycling), mechanical recycling (i.e., secondary recycling), chemical recycling (i.e., tertiary recycling), and energy recovery (i.e., quaternary recycling). Mechanical recycling transforms polymeric waste into reusable polymer without breaking the polymer chains, while chemical recycling involves breaking down polymer chains into feedstock for producing monomers, fuels, or chemicals. Reuse preserves the original properties of the polymer to the greatest extent. In contrast, energy recovery breaks down polymer chains through combustion to release the energy stored in the material [19].

Some vinyl-based polymers, such as PMMA and PS, undergo free-radical depolymerization mechanisms that enable efficient recovery of their monomers (with yields exceeding 70 %) at elevated temperatures [3, 21, 22]. In contrast, other vinyl-based polymers—such as PVC, PE, and PP—tend to degrade into complex mixtures of smaller molecules rather than regenerating the original monomer. PMMA is an ideal recyclable polymer due to its unique ability to be depolymerized back into its original monomer. The purified monomer can then be re-polymerized into new PMMA resins. Theoretically, this cycle represents a sustainable process, as it ensures the properties of the newly produced materials remain uncompromised.

3.1.1 Reuse

PMMA reuse involves repurposing PMMA items for the same or different functions without changing their chemical structure or processing them through mechanical means, such

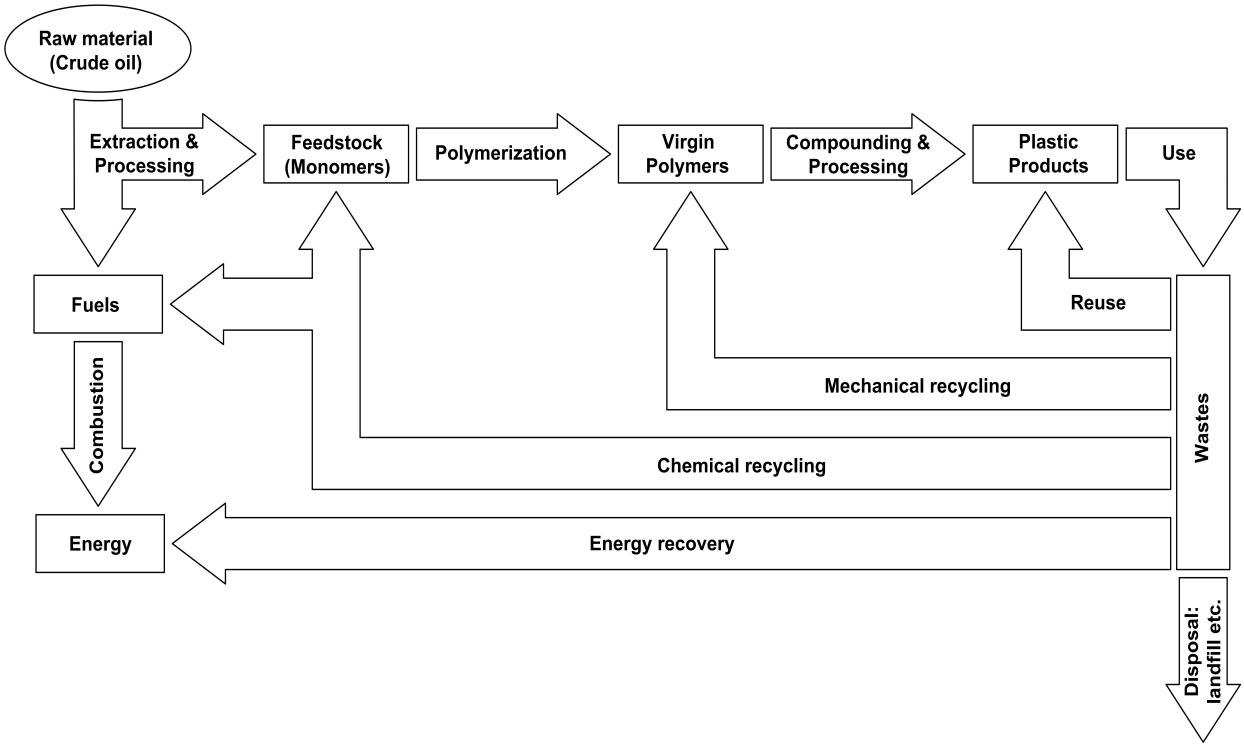

Figure (3.1) Industrial ecology for plastics [18, 20]

as shredding, melting, and reprocessing. This method extends the life of PMMA products, reducing the need for new materials. Reuse results in lower environmental impacts because it avoids the energy and resources required for manufacturing new products. Within the framework of Life Cycle Assessment (LCA), reuse is typically prioritized over recycling due to its lower environmental impacts [23]. PMMA reuse typically involves cleaning used PMMA products without obvious degradation of properties. However, the significantly larger volume of end-of-life PMMA, which often contains additives, fillers, and compounding polymers, reduces the possibility of reuse and necessitates the development of alternative and more feasible recycling methods.

3.1.2 Mechanical recycling

This process converts waste polymers, separable from their associated contaminants, into granules or products using conventional extrusion techniques. The primary drawback of mechanical recycling is the inevitable degradation of material properties after each cycle, caused by the reduction in molecular weight during extrusion [3]. Prado et al. [24] demonstrated the production of optical fibers for sensor systems by thermally extruding cleaned PMMA

scraps originally used in LCD monitors. The fibers produced using a mini extruder showed minimal degradation of PMMA at 220 °C to 230 °C. Additionally, waste PMMA serves as valuable filler material in composite production. For instance, Kočevar and Kržan [25] successfully removed most glass fibers from composite waste consisting of glass fiber-reinforced polyester bound to a layer of cross-linked PMMA. The processed material was extruded with fresh PMMA, PP and ABS, yielding composites that successfully passed industrial tests for bathtub production.

Efficient separation of target polymers from impurities is crucial for recycling plastic composites before extrusion. Unlike other mechanical recovery methods, such as manual sorting and flotation, PMMA recycling via solvent extraction—using techniques like dissolution/reprecipitation and supercritical fluid extraction—achieves more effective purification of recovered PMMA [26]. However, the higher operational costs associated with these methods limit their industrial-scale application. Gouli et al. [27] successfully recovered virgin PMMA in granular form from decorative sheets using a dissolution/reprecipitation process at temperatures of 40 °C to 50 °C. The selected solvent/nonsolvent system (toluene/n-hexane) efficiently removed additives from the PMMA sheets while preserving the critical properties of the recovered material. Nevertheless, the recycled granules required an extended drying time of 2 h at 70 °C in the toluene/n-hexane system [28].

3.1.3 Energy recovery

This process reduces the volume of waste PMMA and recovers the energy stored in PMMA through incineration [29]. Due to the limited availability of efficient recycling technologies, incineration and landfill remain the primary methods for disposing of end-of-life PMMA. However, incinerating high-energy PMMA represents a significant loss of resources, given the non-renewable nature of fossil fuel-derived plastics. Moreover, it is an ecologically unsustainable practice, as it poses health risks from the release of toxic combustion byproducts, such as dioxins (particularly in chlorine-containing polymers) [29].

3.1.4 Chemical recycling

Although mechanical recycling requires less energy, the degradation of recycled plastics' properties is inevitable after several processing cycles. An alternative to efficiently recycling waste plastics is chemical recycling, which converts polymers into various products, including

monomers, oligomers, fuels, and mixtures of hydrocarbon compounds, through the application of heat and/or chemical agents [3, 30].

Chemical recycling is a promising solution for disposing of end-of-life PMMA, particularly due to its potential for high-yield recovery of MMA monomer. PMMA undergoes thermal depolymerization to produce MMA monomer with a purity exceeding 90 % at >350 °C. The primary chemical recycling processes for waste PMMA include pyrolysis and catalytic cracking.

Pyrolysis

Pyrolysis is a thermal treatment process that decomposes materials at elevated temperatures in the absence of oxygen. Thermal depolymerization, a specific form of pyrolysis, breaks down plastics and other polymers into monomers and oligomers. Smolders and Baeyens [31] reported that PMMA thermal pyrolysis results in nearly 97 % recovery of MMA monomer at temperatures between 400 °C to 500 °C. PMMA undergoes nearly complete decomposition into monomer at temperatures exceeding 400°C [32, 33]. Thermal depolymerization is most efficient at relatively mild pyrolysis temperatures (230 °C to 600 °C) [3], while higher temperatures may reduce monomer yield and lead to the cracking of monomers or heavier hydrocarbons into lighter molecules such as CO_2, CO, and light hydrocarbons [31, 34].

Main products of pyrolysis PMMA pyrolysis contributes to a very high monomer recovery rate (90 % to 98 %) through the depolymerization steps. The yield of MMA is primarily influenced by the residence time of the monomer gas in the reactor and, to a lesser extent, by the reaction temperature [31]. The temperature for low-temperature pyrolysis typically is at 350 °C to 600 °C, while the type of reactor is critical for determining product selectivity at higher temperatures (i.e., >600 °C) [3]. Low-temperature pyrolysis results in a large fraction of liquid products (99 %), with a small percentage of gaseous by-products and residues (Table 3.1). The liquid fraction predominantly consists of MMA monomer, with a small percentage of esters and other organic compounds. At elevated temperatures, MMA yield decreases due to the increased production of undesired gaseous by-products and reduced selectivity to MMA in the liquid fraction [35, 36]. Purification of the obtained monomer is crucial, as the presence of impurities in the pyrolysis oil fraction can lead to a lower polymerization rate and inferior polymer properties [29].

Table (3.1) Composition (%) of the pyrolysis products of the pure PMMA (M_w = 350000) and the commercial PERSPEX (PMMA purity > 99 %) at 450 °C [29]

Composition in fraction (wt.%)	**Pure PMMA**	**PERSPEX**
Gaseous fraction (wt% in total)	**0.6**	**0.8**
CO_2	52.4	50.2
CO	25.8	29.5
CH_4	17.0	10.0
C_2H_4	0.8	1.2
C_3H_6	1.7	3.7
C_4	1.2	4.4
iC_5	1.1	1.0
Liuqid fraction (wt% in total)	**99.3**	**98.7**
Methyl methacrylate	99.0	96.7
Methyl Propanoic acid, methyl ester	0.1	0.5
Methyl Propanoic acid, 2-methyl-, methyl ester	0.1	0.7
Propanoic acid, 2,2- dimethyl-, methyl ester	0.2	0.4
Cyclohexanecarboxylic acid, ethenyl ester	0.1	0.2
Cyclohexane, 1-methyl-2- pentyl	0.1	0.2
1,3-Pentadiene, 2,4- dimethyl	0.0	0.3
Butanedioic acid, methylenedimethyl ester	0.2	0.3
1,4-Cyclohexanedicarboxylic acid, dimethyl ester	0.1	0.4
Cyclohexanone, 2,5- dimethyl-2-(1-methyl)	0.0	0.2
Other compounds	0.1	0.1
Residue (wt% in total)	**0.1**	**0.5**
Total monomer recovery	**98.3**	**95.4**

Mechanism of PMMA depolymerization The PMMA depolymerization proceeds via a radical degradation mechanism, in which generated free radicals decompose the polymer backbone into monomers or gaseous fragments [31]. The thermal stability of PMMA varies depending on its end groups, which are determined by the polymerization process. PMMA with saturated end groups (PMMA–H) exhibits higher thermal stability, with a decomposition temperature at 300 °C to 400 °C, compared to vinyl-terminated PMMA (PMMA–CH=CH_2), which depolymerizes at a lower temperature at 230 °C to 300 °C [37]. The degradation process of PMMA is a radical chain reaction comprising three irreversible steps: initiation, depropagation (the reverse of polymerization), and termination [38].

Initiation: The degradation initiation of vinyl-terminated and saturated PMMA occurs at

different temperatures. For vinyl-terminated PMMA, radical formation begins through an end-chain scission mechanism at temperatures above 230 °C (Fig.3.2a). At higher temperatures (>300 °C), a combination of end-chain and random chain scission mechanisms becomes predominant. In contrast, the initiation of PMMA with saturated end groups exclusively involves random chain scission, occurring only at temperatures above 300 °C. This process generates tertiary and primary alkyl radicals through random cleavage of the polymer chain (Fig.3.2b). The specific initiation temperature for random chain scission varies within 300 °C to 400 °C, depending on the properties of the degraded PMMA material.

Depropagation: Depropagation is the reverse of the propagation step in the MMA polymerization process. During this stage, the tertiary alkyl radicals generated in the initiation step undergo further degradation. This involves cleavage of the C–C bond at the β position of the tertiary alkyl site, producing a new tertiary alkyl radical and an MMA molecule as the primary product (Fig. 3.2). This unzipping mechanism predominantly releases MMA. Additionally, primary alkyl radicals can form methallyl-terminated species, which subsequently generate new tertiary alkyl radicals [39]. Depropagation is the dominant process in PMMA degradation, and its rate follows first-order kinetics in weight loss [38].

Termination: Termination occurs through the interaction of radical pairs, leading to the reformation of a polymer chain [38]. However, at higher degradation temperatures (>360 °C), the depropagation process progresses to the end of the PMMA chain, significantly reducing the occurrence of termination [40].

The scission of head-to-head linkages is the least thermally stable degradation pathway for PMMA produced via free radical polymerization [41]. This process occurs at relatively low temperatures, below 200 °C. However, its overall contribution to PMMA's thermal depolymerization is minimal because polymerization dominates at such low temperatures.

To enhance the thermal stability of PMMA, mercaptans are commonly added during production to saturate thermally unstable double bonds. Additionally, copolymerization of MMA with comonomers such as methyl acrylate (MA) or ethyl acrylate (EA) improves thermal stability by reducing the unzipping degradation reaction, which subsequently lowers MMA yield [36, 42].

The key factors influencing PMMA thermal depolymerization include the polymer's molecu-

lar weight, the type and proportion of comonomers, and the presence of mercaptans. Minor factors, such as cross-linking, pigments, and dyes in the polymer matrix, also affect the depolymerization behavior [42]. Variations in the molecular weight and grade of PMMA can lead to different depolymerization results [3].

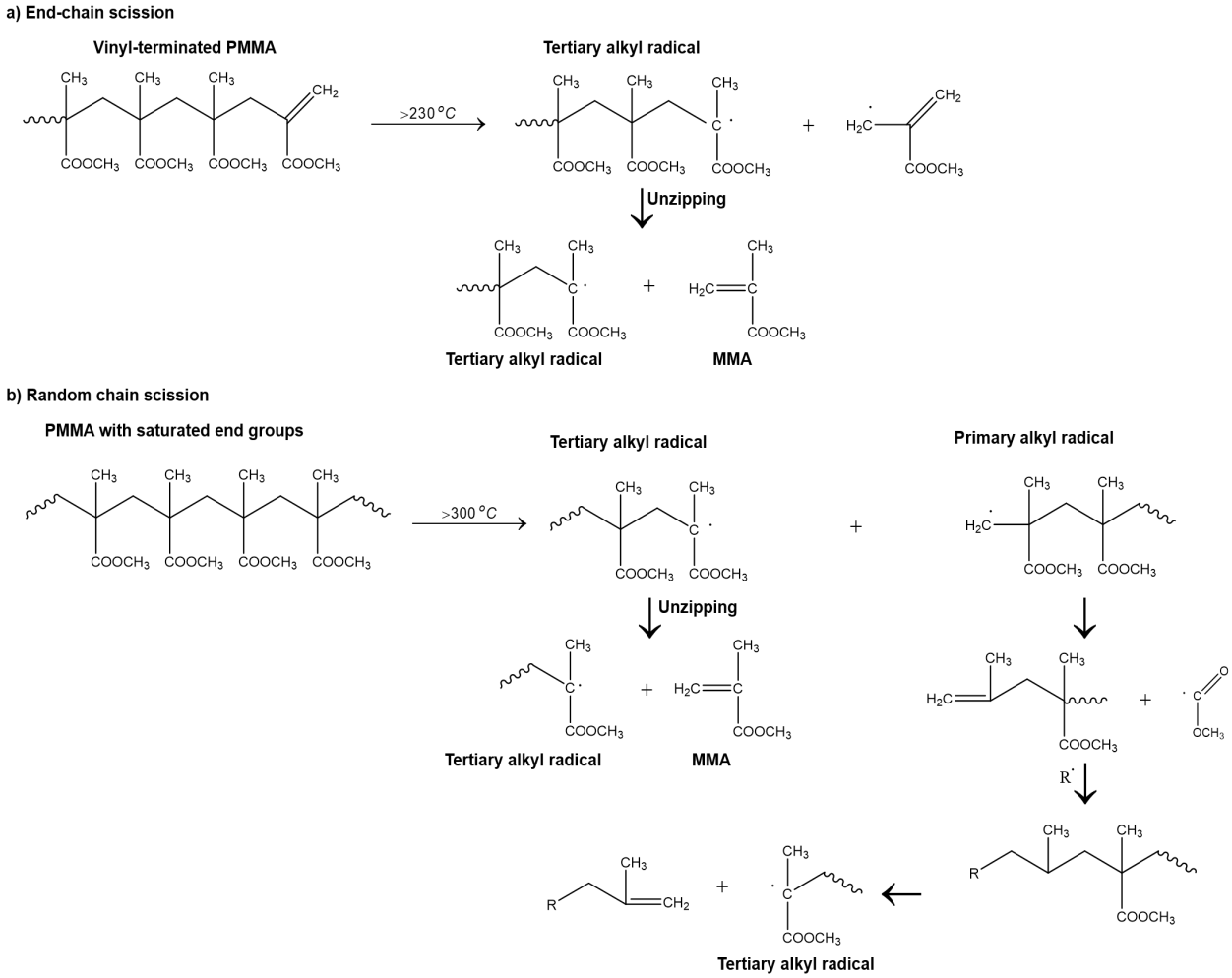

Figure (3.2) Mechanism of PMMA thermal depolymerization [3, 37, 39, 43]

Kinetics of PMMA thermal depolymerization reaction Thermal depolymerization of PMMA begins at temperatures above 220 °C to 230 °C, while polymerization dominates at lower temperatures. The process is a heterogeneous reaction in which solid or molten PMMA thermally degrades into gaseous products, primarily at elevated temperatures. According to Barlow et al. [44], PMMA depolymerization proceeds through three distinct reaction mechanisms, depending on the initial molecular weight and reaction temperature (Table 3.2). At

low to moderate temperatures, the intrinsic reaction rate is relatively unaffected by the chain length of the PMMA.

Measuring the intrinsic reaction rate necessitates eliminating mass and heat transfer limitations, making it inherently more challenging than determining the apparent reaction rate. As described by the Arrhenius equation, the intrinsic reaction rate constant, k_{m}, is solely a function of temperature and is expressed as:

$$dx/dt = Aexp(-\frac{E_{\mathrm{a}}}{RT})f(x) \tag{3.1}$$

The theoretical activation energy of the overall depolymerization reaction is available according to the activation of the elementary reaction steps (Table 3.3).

Thermal depolymerization of PMMA in solution is an ideal approach for determining the intrinsic kinetic parameters, as heat and mass transfer are sufficiently high under specific conditions in a solution system [38]. However, in practical industrial applications, mass and heat transfer limitations significantly restrict the rate of PMMA depolymerization. During the pyrolysis of PMMA, heat is transferred to the polymer via forced convection in the surrounding medium. As a result, the overall depolymerization process of PMMA is governed by a combination of intrinsic chemical kinetics and the accompanying physical transfer processes [31].

The apparent reaction rate constant, k', is a product of the intrinsic reaction rate constant, k, and the transfer coefficient, k_{c}. This combination arises from a two-step process, where heat transfer occurs initially, followed by the depolymerization reaction. The global apparent reaction rate constant is therefore given by:

$$\frac{1}{k'} = \frac{1}{k_{\mathrm{c}}} + \frac{1}{k} \tag{3.2}$$

Applying equation (6.1) to (6.2), the temperature dependence of the apparent reaction rate constant is:

$$k' = \frac{Ak_{\mathrm{c}}exp(-E_{\mathrm{a}}/RT)}{k_{\mathrm{c}} + Aexp(-E_{\mathrm{a}}/RT)} \tag{3.3}$$

where the transfer coefficient, k_{c}, exhibits a slight dependence on temperature. Two scenarios

Table (3.2) Mechanisms and Intrinsic reaction rate equations for PMMA depolymerization steps [31, 44]

Elementary reaction steps	**Intrinsic reaction rate equations**	**Conditions**
Mechanism 1		
Random initiation, followed by complete depropagation	$R_{\mathrm{P}} = -2k_{\mathrm{ir}}x_0C_{\mathrm{p}}$ $R_{\mathrm{M}} = 2k_{\mathrm{ir}}{x_0}^2C_{\mathrm{p}} = k_{\mathrm{m}}{x_0}^2C_{\mathrm{p}}$	High temperature (430 °C to 460 °C) & small chain length (D_{p}: 105-570)
Mechanism 2		
Random initiation, depropagation and termination by disproportionation	$R_{\mathrm{P}} = 2k_{\mathrm{ir}}xC_{\mathrm{p}}$ $R_{\mathrm{M}} = 2k_{\mathrm{d}}\sqrt{\frac{k_{\mathrm{ir}}x}{k_{\mathrm{td}}}}{C_{\mathrm{p}}}^{\frac{1}{2}} = k_{\mathrm{m}}{C_{\mathrm{p}}}^{\frac{1}{2}}$	• High temperature (430 °C to 460 °C) & small chain length D_{p}: 570-2970 • Moderate temperature (400 °C to 430 °C)
Mechanism 3		
End initiation, depropagation and termination by disproportionation	$R_{\mathrm{P}} = 0$ $R_{\mathrm{M}} = k_{\mathrm{d}}\sqrt{\frac{2k_{\mathrm{ie}}}{k_{\mathrm{td}}}}{C_{\mathrm{p0}}}^{\frac{1}{2}} = k_{\mathrm{m}}{C_{\mathrm{p0}}}^{\frac{1}{2}}$	Low temperature (330 °C to 400 °C)

Table (3.3) Theoretical activation energy of PMMA depolymerization steps [31]

Mechanism	$k_{\mathbf{m}} \propto$	$E_{\mathbf{a}} =$
Mechanism 1	k_{ir}	$E_{\mathrm{ir}} = 287\,\mathrm{kJ\,mol^{-1}}$
Mechanism 2	$k_{\mathrm{d}}\sqrt{k_{\mathrm{ir}}/k_{\mathrm{td}}}$	$E_{\mathrm{d}} + 0.5(E_{\mathrm{ir}} - E_{\mathrm{td}}) = 190\,\mathrm{kJ\,mol^{-1}}$
Mechanism 3	$k_{\mathrm{d}}\sqrt{k_{\mathrm{ie}}/k_{\mathrm{td}}}$	$E_{\mathrm{d}} + 0.5(E_{\mathrm{ie}} - E_{\mathrm{td}}) = 75\,\mathrm{kJ\,mol^{-1}}$

With $E_{\mathrm{td}} = 12\,\mathrm{kJ\,mol^{-1}}$, $D_{\mathrm{R}} = 275\,\mathrm{kJ\,mol^{-1}}$, $E_{\mathrm{d}} = E_{\mathrm{ie}} = 54\,\mathrm{kJ\,mol^{-1}}$

can simplify equation (6.3) [31]:

$*$ **Low temperature**: $k_{\mathrm{c}} \gg Aexp(-E_{\mathrm{a}}/RT)$ or $k_{\mathrm{c}} = Aexp(-E_{\mathrm{a}}/RT)$. In this chemical-controlled regime, external heat transfer occurs much faster than the chemical reaction. The apparent activation energy is then determined by the slope of the plot of $ln(k_0)$ versus $1/T$.

$*$ **High temperature**: $k_{\mathrm{c}} \ll Aexp(-E_{\mathrm{a}}/RT)$ or $k' = k_{\mathrm{c}}$. In this heat-diffusion-controlled regime, the chemical reaction occurs faster than heat transfer. Under these conditions, the apparent reaction rate constant is equal to the transient convective heat transfer coefficient.

At low temperatures, the depolymerization is governed by kinetic control, while at high temperatures, the reaction shifts to being heat-transfer controlled [31].

Pyrolysis equipment for PMMA The development of pyrolysis apparatuses should consider both technological feasibility and economic viability. PMMA pyrolysis is an energy-intensive process, and achieving high monomer recovery purity is crucial for its economic viability, potentially leading to significant economic benefits. Currently, the most commonly used pyrolysis systems for PMMA include fluidized bed reactors, molten media bath reactors, and conical spouted bed reactors (CSBRs).

Fluidized bed reactor: The fluidized bed reactor is well-suited for pyrolysis due to its ability to provide high heat and mass transfer rates, along with maintaining constant temperatures. PMMA pyrolysis in a fluidized bed reactor achieves the highest yield of MMA monomer [3]. Sasse and Emig [42] demonstrated a laboratory-scale fluidized bed setup that included a fluidized reactor, screw feeder, fluidizing gas, product processing, and product analysis components. Quartz sand with varying grain sizes was selected as the fluidization medium, providing a surface for the reaction. Similarly, Kaminsky and Eger [34] developed a

mini pilot plant for the pyrolysis of filled PMMA, with throughputs of $1\,\mathrm{kg\,h^{-1}}$ and $30\,\mathrm{kg\,h^{-1}}$ (Fig. 3.3), achieving a 98 wt.% MMA yield at 450 °C.

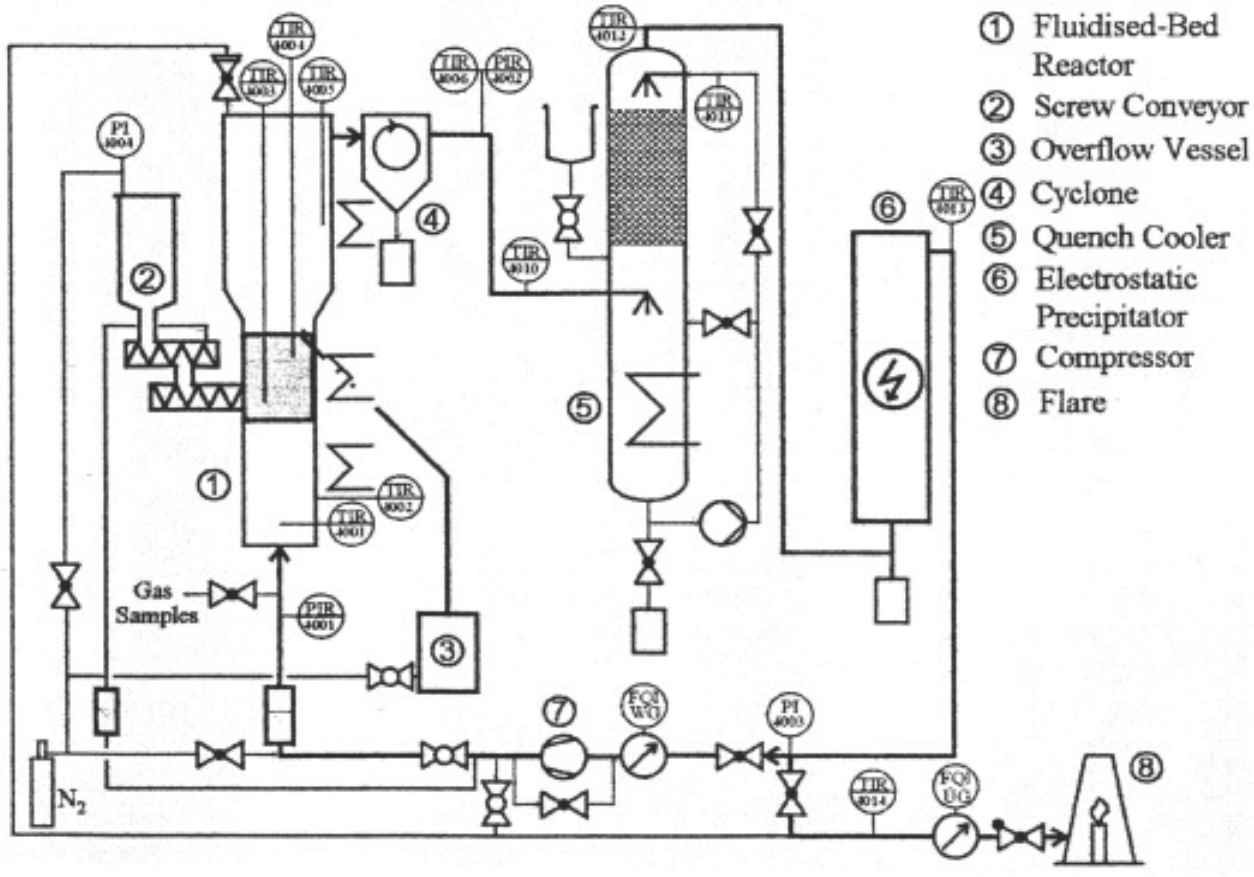

Figure (3.3) Scheme of PMMA pyrolysis plant [34]

The particle bed is fluidized using either an inert purge gas or a reactive precursor to maintain the reaction zone. Inadequate purging velocity can lead to particle elutriation into the filters, while splashing of the reactive precursor into the splash zone may cause soft agglomeration [3, 45].

However, a significant drawback of PMMA pyrolysis using a fluidized bed reactor is its high energy consumption. The thermal depolymerization temperature typically exceeds 450 °C [8], requiring substantial heat input. In addition to the high energy demands, the fluidized bed is sensitive to the presence of fillers in the polymer, such as metals, fibers, and other additives, which can affect the process [46].

Molten media bath reactor: The molten media bath process offers a promising alternative for PMMA depolymerization due to its high heat capacity and thermal inertia [47]. The molten media options include materials such as iron, slag, tin, lead, and salts (e.g., KCl and $MgCl_2$). In the UK, the depolymerization industry recovers MMA monomer by floating PMMA scrap on the surface of a molten lead bath (Fig. 3.4) [48]. The MMA yield in the molten media bath process is generally lower than that achieved in a fluidized bed reactor. Kaminsky et al. [49] achieved an 80 % MMA yield at 500 °C using a molten salt bath of KCl and $MgCl_2$, but the yield dropped to 30 % at 700 °C. Smolders and Baeyens [31] reported an 87 % MMA yield in a lab-scale molten lead bath reactor.

Although this process offers high heat transfer capacity, it has several significant drawbacks. The metal media used (typically lead) and other by-products often contaminate the recovered MMA [42]. Additionally, lead-contaminated waste formed during depolymerization in the molten lead bath impedes heat transfer, which negatively affects the efficiency of PMMA thermal depolymerization [50]. Furthermore, additional product purification steps, such as distillation, increase energy consumption [50].

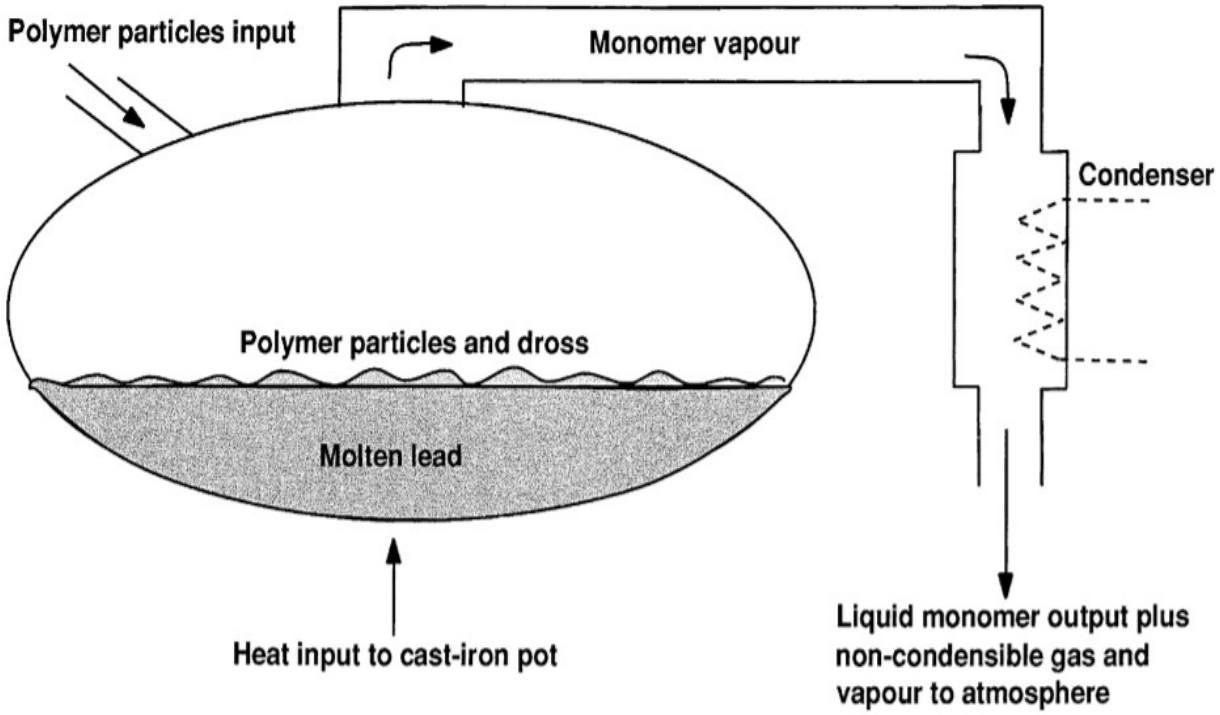

Figure (3.4) Scheme of molten lead bath reactor for PMMA depolymerization [50]

Conical spouted bed reactor: The conical spouted bed reactor is a promising candidate for PMMA pyrolysis due to its excellent hydrodynamic behavior, high heat transfer efficiency, and versatility. It presents an alternative to the fluidized bed reactor for PMMA pyrolysis, offering several advantages [35]. Compared to a fluidized bed, the conical spouted bed has a lower pressure drop (nearly half) and can accommodate particles with a wide range of sizes and densities without segregation. The gas residence time in the reactor ranges from 1 s to 20 ms, which helps minimize secondary reactions within the reactor.

The conical spouted bed is characterized by a single central inlet orifice that introduces fluid gas and particles into the spouted bed (Fig. 3.5) [3]. It consists of three typical zones: (a) the spout zone, which is the central core of the reactor where the air flows; (b) the annular zone, the surrounding area outside the central inlet orifice; and (c) the fountain zone, where particles continue to move upward due to inertia.

The conical spouted bed is essentially an enhanced version of the fluidized bed, designed to avoid the defluidization issues that can occur in fluidized beds [35]. Lopez et al. [35] conducted PMMA depolymerization at 400 °C to 550 °C using a conical spouted bed reactor, achieving a maximum monomer yield of 86.5 % at 400 °C. The pyrolysis process also produced a significant amount of ethyl acrylate (EA) at the same temperature. However, the maximum MMA yield in the conical spouted bed was lower than that achieved in the fluidized bed.

Catalytic cracking

Unlike thermal cracking or pyrolysis, catalytic cracking involves the use of catalysts in the pyrolysis reactor to lower the required cracking temperature while simultaneously adjusting the product distribution. The catalytic cracking process generates ionic species on the catalyst surface, leading to the formation of shorter and more branched-chain products during pyrolysis [3].

Khangkham [51] screened several zeolite catalysts—ZSM-5, zeolite β, HUSY, and dealuminated USY—through batch experiments to identify the most suitable catalyst for PMMA cracking. ZSM-5 was selected for further use in a continuous catalytic degradation unit (Fig. 3.6). The study found that the acid properties of the zeolite, including both the quantity and strength of acid sites, played a crucial role in determining the product distribution during batch experiments. Additionally, the shape selectivity of micropores influenced the

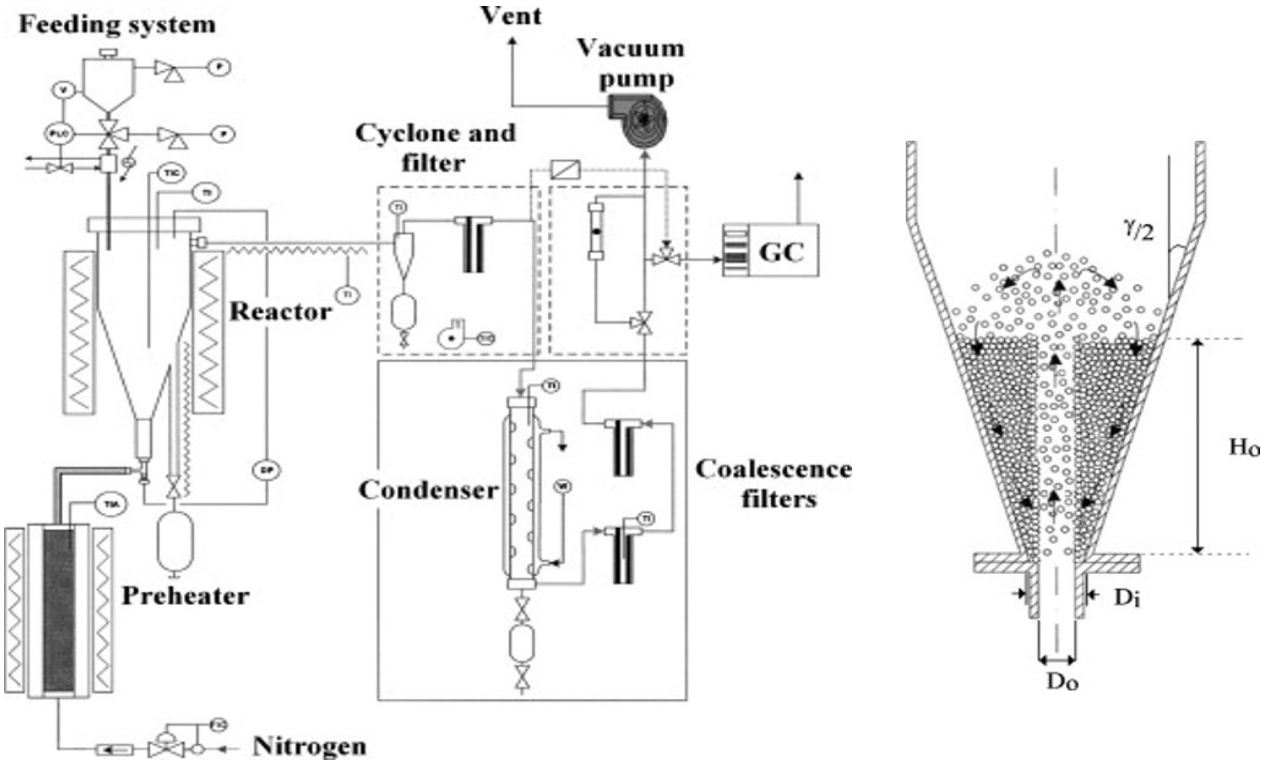

Figure (3.5) Scheme of PMMA pyrolysis bench scale plant (left) and dimensions of a conical spouted bed reactor (right) [35]

composition of the liquid fraction. In a continuous fixed-bed reactor, the yield of liquid products increased as the reaction temperature was raised from 200 °C to 270 °C. However, temperatures exceeding 270 °C led to further cracking of light products into gaseous compounds over the catalysts' active sites. The precise MMA yield was difficult to determine due to the limited performance of the condenser during the experiment [51].

3.2 Extrusion depolymerization of PMMA

Extruder-based plastic recycling technology has been gaining increasing attention in recent years. An extruder, which consists of one or more rotating screws within a barrel, is a simple yet effective machine used for various extrusion processes. It is widely employed in industries such as food, rubber, ceramics, and plastic processing. Extruder-based reactors, also referred to as screw reactors, screw tubular reactors [42], or auger reactors [52], are emerging as promising technologies for plastic recycling.

Screw extruders can operate both in continuous and batch modes [42]. These reactors consist

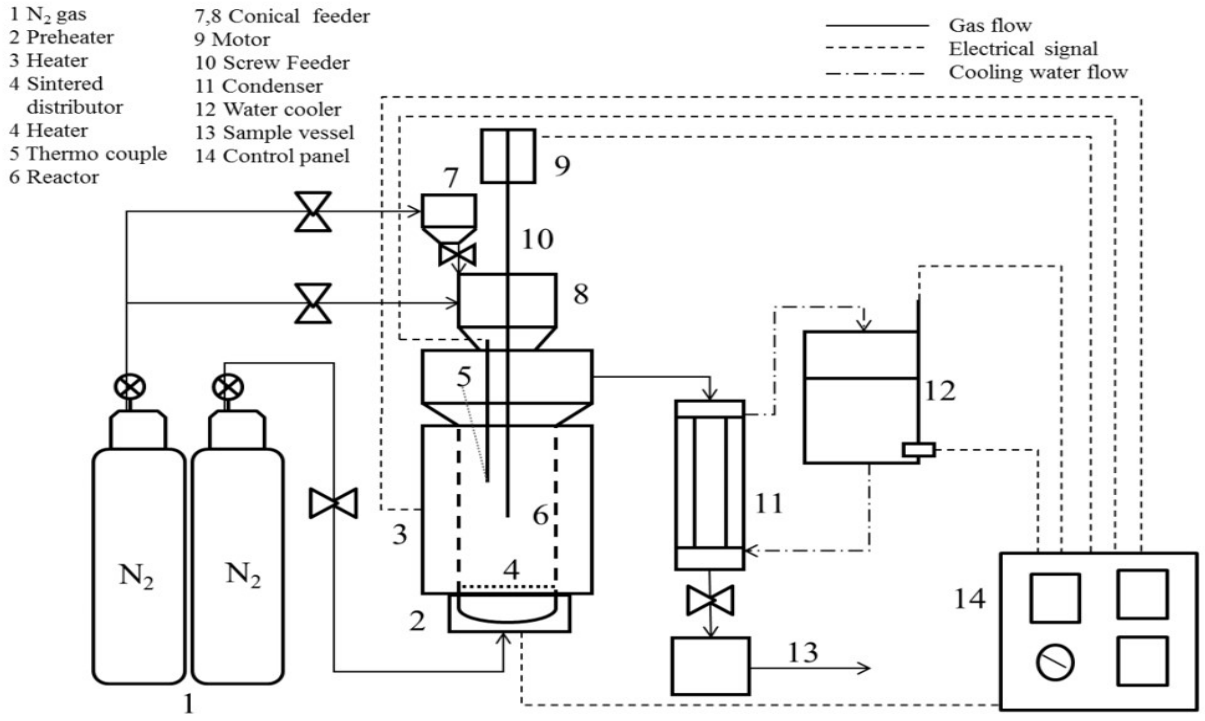

Figure (3.6) Scheme of PMMA continuous catalytic degradation unit [51]

of several distinct zones: the feeding zone, melting zone, reaction zone, venting zone, and pumping zone. The specific configuration of these zones depends on the type of screw reactor (single screw, twin-screw, or multi-screw) and the process requirements. Among these, the most commonly used screw reactors are single screw and twin-screw reactors. The key advantages of screw reactors include [42, 52]:

* Ease of vapor product extraction through the venting zone.
* Configurable and controllable temperature and pressure profiles.
* Adjustable mixing performance via screw design and configuration.
* High heat transfer capacity.
* Variable residence times along the horizontal reactor.

3.2.1 Degradative extrusion recycling process

Screw reactors are widely used, particularly in biomass pyrolysis. Xtrudx Technologies, Inc. [53] patented a continuous supercritical fluid depolymerization technology for polymer waste. The process involves three distinct zones: (1) the extruder-based conveying zone, where biomass or waste plastics are melted and conveyed into (2) the supercritical fluid

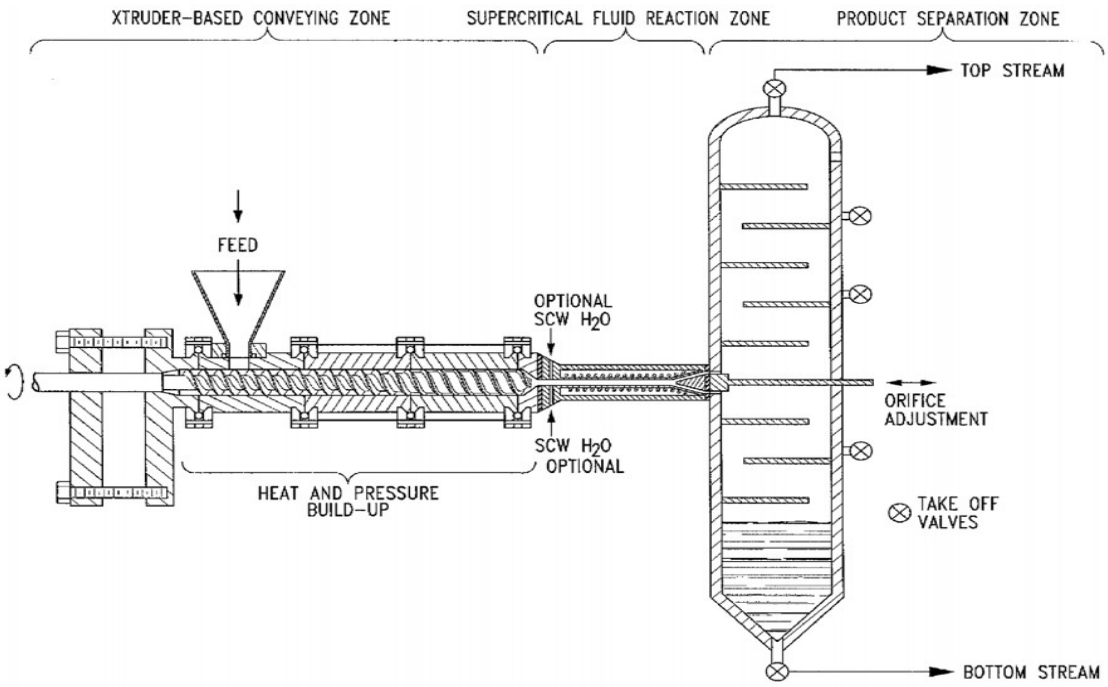

Figure (3.7) Scheme of continuous supercritical fluid depolymerization of polymer waste [53]

reaction zone, where hot compressed water reacts with the melt, producing gaseous and liquid products, which then enter (3) the product separation zone (i.e., separation chamber) (Fig.3.7). Furthermore, the Faculty of Bioscience Engineering at Ghent University developed a continuous biomass pyrolysis apparatus using two tandem screw extruders (Fig.3.8). This apparatus is capable of simultaneously recycling both liquid and solid products.

In 1974, Japan Steel Works, Ltd. developed a continuous thermal degradation system using a single screw extruder as the reactor to recycle synthetic macromolecular materials (Fig.3.9). Similarly, Michaeli and Breyer [55] described a degradative extrusion process using a co-rotating, closely intermeshing twin-screw extruder to depolymerize PMMA (Fig.3.10), based on an unpublished report. The co-rotating twin-screw extruder effectively inputs thermal and mechanical energy through barrel heating and the use of kneading blocks and left-hand thread elements. A gravimetric metering station feeds PMMA scraps into the twin-screw extruder, where the machine heats the PMMA to the depolymerization temperature, followed by the depolymerization reaction. Nitrogen gas strips monomer gases from the extruder's venting zone and channels them into a condensation unit. Non-depolymerized PMMA residues and contaminants are extruded through the die. The self-cleaning feature of the intermeshing twin screws ensures continuous operation. In this process, the MMA content in the condensate ranged from 89 % to 97 % at 380 °C to 400 °C.

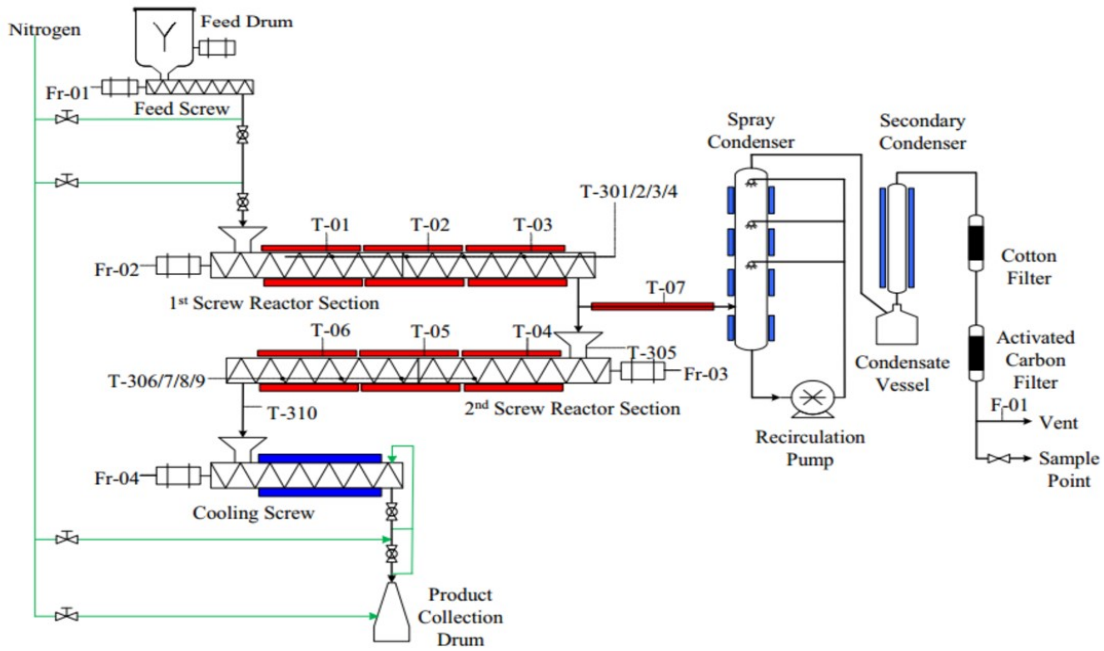

Figure (3.8) Process flow diagram of continuous pyrolysis of biomass using screw reactor [52]

More recently, the European MMAtwo project [56] successfully demonstrated a pilot-scale pyrolysis extrusion process for depolymerizing extrusion, injection, and cast-grade PMMA scraps and cuttings into MAA monomers. This process achieves a plastic-to-monomer yield of 80 % to 90 %, with an MMA purity of 99.8 % following downstream purification.

The MMAtwo process relies on thermolysis to produce MMA without the use of catalysts or steam, with PMMA undergoing thermal depolymerization as the main reaction. In contrast, the PMMA recycling process proposed in this thesis employs a catalytic hydrolysis extrusion method. By introducing catalysts and steam, this approach enables the co-generation of both MMA and MAA. Unlike the MMAtwo process, this thesis targets MAA as a key product. The overall reaction involves a tandem process within a single extruder: PMMA is first thermally depolymerized into MMA, which is subsequently hydrolyzed into MAA.

3.2.2 Devolatilization

Devolatilization involves removing volatile components from the melt through the extruder's venting zone. Tadmor and Gogos [57] proposed that a foaming-boiling process, in which

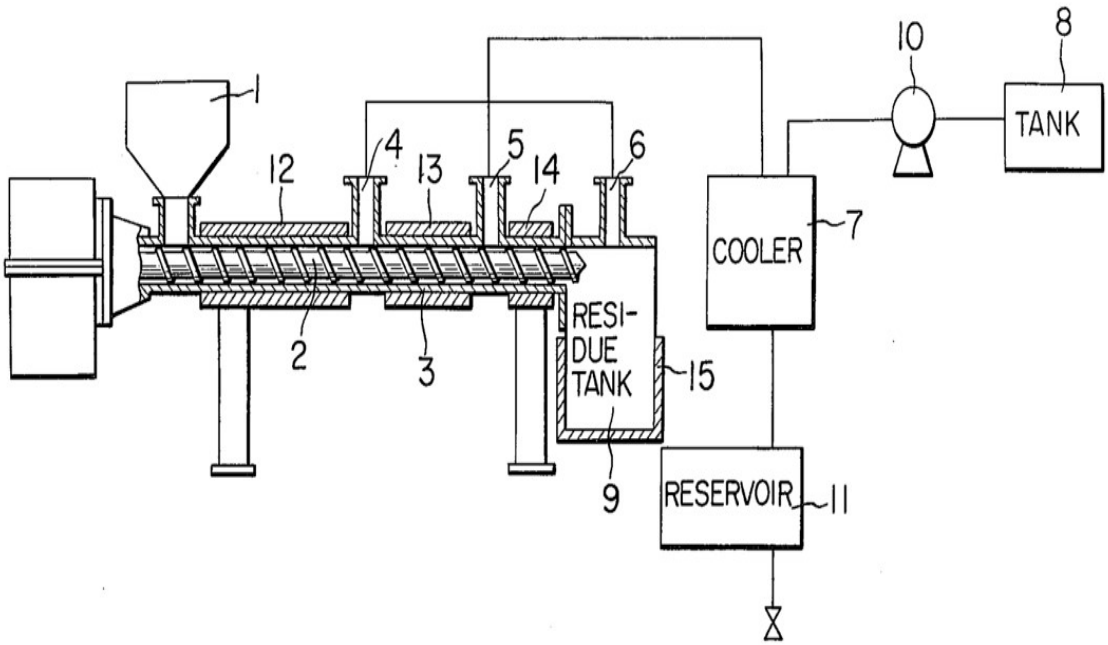

Figure (3.9) Continuous thermal degradation system for synthetic macro-molecule materials [54]

bubbles play a key role in the transport of volatiles, drives devolatilization. In a twin-screw extruder, devolatilization is a mass-transfer process that depends on shear forces [58]. Martin and Haight [58] identified five key factors influencing devolatilization efficiency: (1) residence time under the vents (longer times are preferred), (2) the melt surface area (larger surface areas are preferred), (3) the surface renewal rate of the melt pool (higher rates are preferred), (4) the presence of bubbles, and (5) the strength of the vacuum applied to the vents.

Highly viscous melts that hinder bubble movement require longer residence times for effective devolatilization. Twin-screw extruders generally exhibit higher devolatilization efficiency compared to single screw extruders [59]. The use of a vacuum or stripping agents significantly enhances the removal of volatiles from the melt. Lowering the vapor pressure of the volatiles also facilitates their extraction [59]. Additionally, reducing the melt pressure promotes more efficient devolatilization.

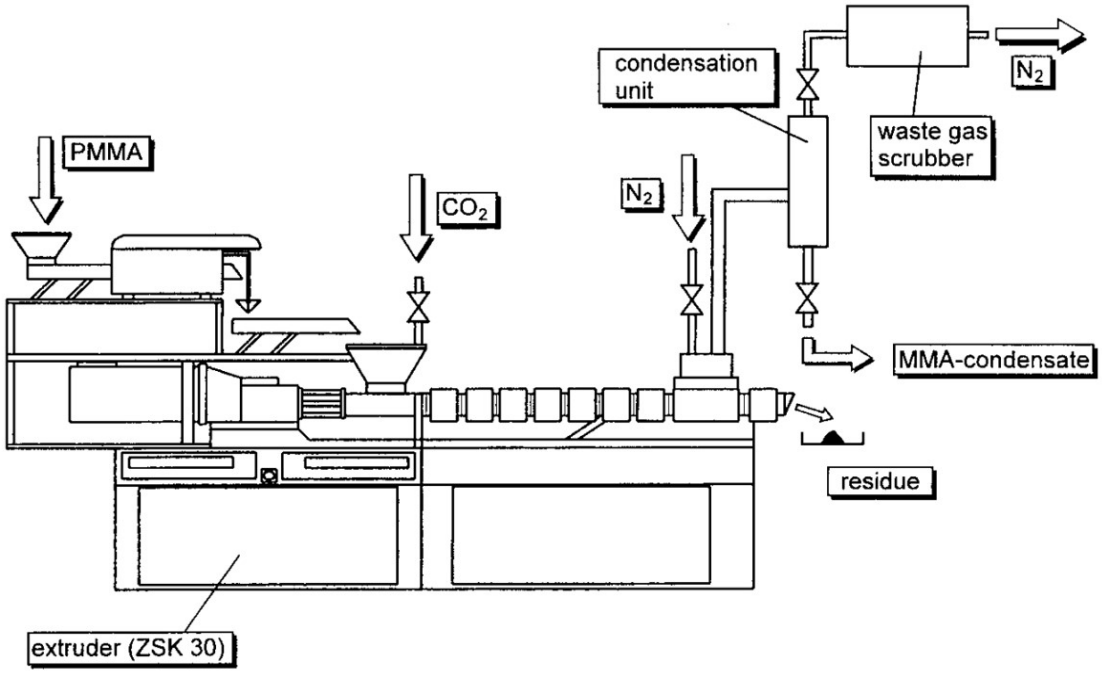

Figure (3.10) Scheme of extrusion depolymerization process of PMMA developed by Aachen University [55]

3.3 MAA preparation

MAA is a colorless carboxylic acid with a strong, unpleasant odor. It is produced on a large scale in industry as a precursor to its esters, particularly MMA, which is a crucial monomer for PMMA production [60]. The esterification of MAA to MMA offers an effective process for producing high-purity MMA and serves as an environmentally friendly alternative to the traditional acetone-cyanohydrin (ACH) route. The ACH process, which involves the reaction of acetone and hydrogen cyanide to form MMA, is widely used in the commercial production of MMA but is less environmentally sustainable due to the involvement of toxic intermediates such as hydrogen cyanide and acetone cyanohydrin [14].

3.3.1 MAA synthesis route

MAA is a key precursor to MMA in industrial applications. The production of MAA typically coincides with MMA manufacturing. There are three main production routes in the industry, each tailored to specific hydrocarbon raw materials: the C3 route, the C4 route, and the C2 route [60].

The commercial viability of the MAA/MMA production route is influenced by factors such as raw material costs, production efficiency, operating costs, waste disposal costs, plant capital investment, and environmental impact. Until 1982, the ACH process (C3 route) dominated MMA/MAA production (Fig. 3.11). However, the ACH process leads to high waste handling costs, as each ton of MMA produced generates 1.5 tons of ammonium bisulfate due to the use of corrosive sulfuric acid [60]. In 2014, Evonik Röhm GmbH developed and patented a more sustainable technology for converting methacrylic esters to MAA [61]. This innovative process involves four key steps: (a) the preparation of acetone cyanohydrin using acetone and hydrocyanic acid as reactants; (b) the conversion of acetone cyanohydrin to methacrylamide through reaction with concentrated sulfuric acid; (c) esterification of methacrylamide to methacrylic esters in the presence of alcohols; and (d) the hydrolysis of methacrylic esters to MAA using heterogeneous catalysts.

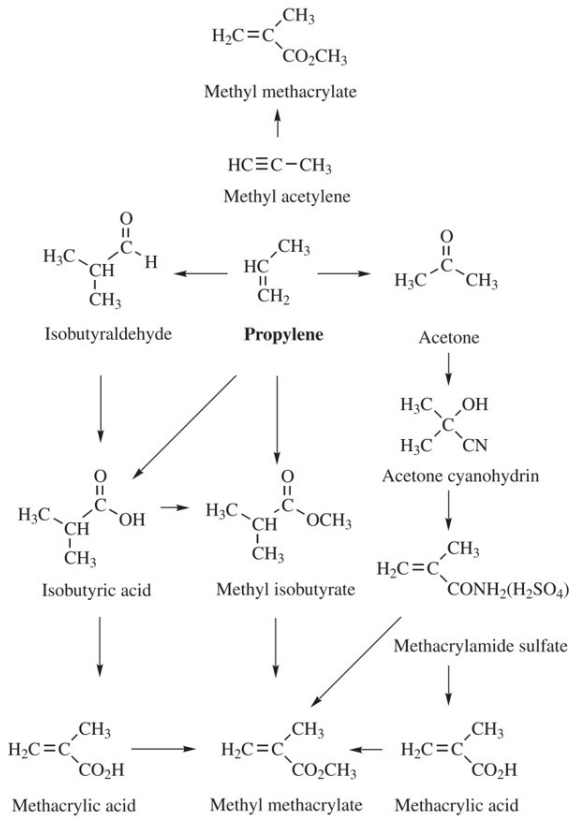

Figure (3.11) C3 route for MAA/MMA production [60]

In 1982, Nippon Shokubai Kagaku Kogyo Co. introduced an alternative to the ACH process, utilizing isobutylene (C4 route) (Fig.3.12). In this process, isobutylene undergoes a two-stage, gas-phase oxidation to form MAA, with methacrolein serving as an intermediate [60]. In 1990,

BASF launched an ethylene-based production plant (C2 route) in Germany (Fig.3.13). The C2 route produces MMA/MAA through intermediates such as propionic acid, propanal, or methyl propionate [60].

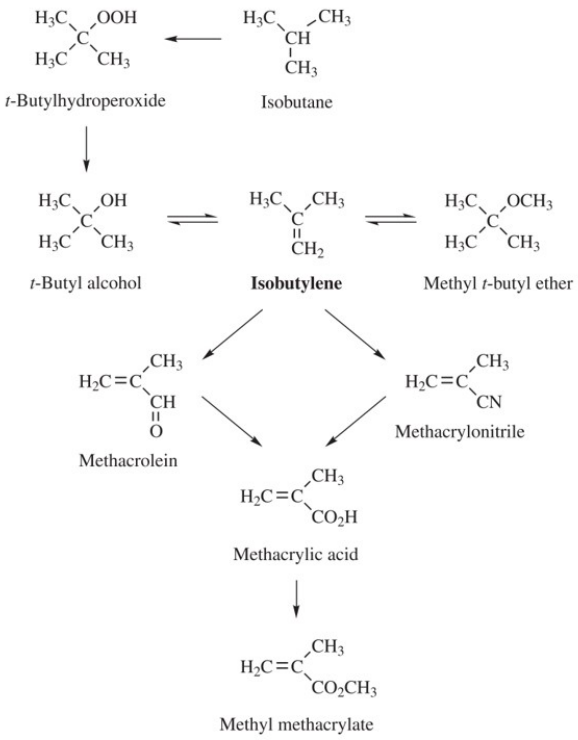

Figure (3.12) C4 route for MAA/MMA production [60]

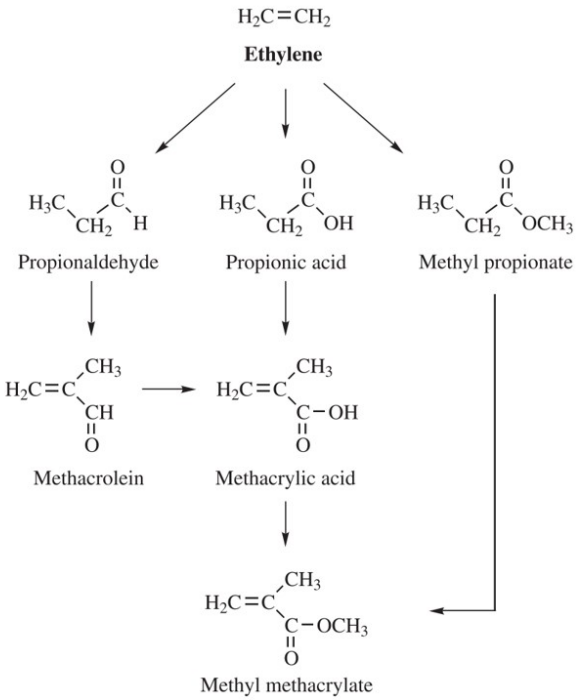

Figure (3.13) C2 route for MAA/MMA production [60]

The final step in MMA synthesis primarily involves the esterification of MAA. As such, the production of high-purity MAA is crucial, given its significant demand in MMA manufacturing.

In contrast, Arkema France [62] patented an innovative process for producing MAA monomer directly from PMMA. This process involves two key steps: the depolymerization of PMMA into MMA, followed by the hydrolysis of the resulting MMA to MAA.

3.3.2 Hydrolysis of PMMA to MAA

Hydrolysis catalysts

The most straightforward and direct method for synthesizing MAA is through the hydrolysis of MMA. This reaction occurs in the presence of either acidic or alkaline catalysts. Hydrolysis catalysts are typically classified into two categories: homogeneous catalysts and heterogeneous catalysts.

Common homogeneous catalysts for ester hydrolysis include:

∗ Strong acid catalysts: e.g., sulfuric acid.
∗ Basic catalysts: e.g., sodium hydroxide or potassium hydroxide.

Acidic hydrolysis of an ester produces a carboxylic acid and an alcohol, while basic hydrolysis yields a carboxylate salt and an alcohol. In the case of basic hydrolysis, the basic catalyst also participates as a reactant in the reaction.

Heterogeneous catalysts offer several advantages over homogeneous catalysts for MMA hydrolysis [60]. On one hand, they are easier to separate from the reaction products. On the other hand, their use reduces the reliance on corrosive sulfuric acid, thereby minimizing the environmental impact of waste acid. Suitable heterogeneous catalysts for hydrolysis include [61–63]:

∗ Zeolites: higher SiO_2/Al_2O_3, higher the stability of the zeolite under hydrothermal conditions.
∗ Ion exchange resins: acidic polymeric resins, such as Amberlyst 15, Amberlyst 36, Lewatit K1221, and Lewatit K2431, are effective catalysts
∗ Metal oxides or hydroxides: MgO, CaO, $Ca(OH)_2$, $Al(OH)_3$, $Mg(OH)_2$ etc.;
∗ Amorphous acid catalysts: include silica, alumina, silica-alumina, silica-zirconia, silica-titania, and aluminum phosphate gels.

PMMA hydrolysis to MAA

In a recent study, Chub et al. [16] reported a tandem reaction process for converting virgin PMMA to MAA using a lab-scale fluidized bed reactor. They evaluated the activity of various solid catalysts and mediums, including Al_2O_3, FCC, Cs – HPA, zeolite Y, $ZrO_2MoO_{3/}SiO_2$, and sand, for the direct hydrolysis of PMMA in a fluidized bed. Among these, zeolite Y demonstrated the highest MAA yield of 33 %. The MAA production process involved a tandem reaction mechanism where PMMA first underwent thermal depolymerization to MMA, followed by the catalytic hydrolysis of MMA to MAA. While the study proposed a simplified mechanism for MAA production from PMMA, it did not explore in detail the effects of zeolite properties, such as acidity and micropore shape-selectivity, and detailed side reactions, on MAA yield and product distribution.

In a follow-up study, Chub et al. [64] introduced a tandem reactor system combining a fluidized sand bed with a fixed bed to convert virgin PMMA to MAA. In this setup, PMMA was first depolymerized in a fluidized sand bed to generate MMA, which was subsequently hydrolyzed to MAA over zeolite Y in a fixed bed reactor. The system achieved a maximum PMMA conversion of 53 % and an MAA yield of up to 48 %. However, the tandem reactor faced operational challenges, including unstable flow and significant pressure drops between the two reactors, leading to rapid deactivation. All experiments were conducted in batch mode using virgin PMMA as the feedstock.

De Tommaso et al. [17] developed a stirred tank reactor system for converting waste artificial marble into MMA and MAA under hydrothermal conditions. Waste artificial marble, a type of end-of-life PMMA, is characterized by its low PMMA content and high Al-containing filler content.

3.4 Summary and perspectives

Clean and post-industrial PMMA waste represent the primary feedstocks for reuse and recycling efforts. These materials can be reprocessed via mechanical methods to produce new products with a reduced carbon footprint. However, the majority of PMMA waste comes from end-of-life products, which lack efficient management and utilization. A significant portion is landfilled, incinerated, or improperly discarded into the environment [65, 66].

Compared to energy recovery or untreated disposal, chemical recycling offers a more sustainable pathway by converting PMMA into monomers or other valuable chemicals. Current technologies—such as fluidized bed reactors, molten metal beds, extruders, and conical spouted beds—are mainly focused on recycling post-industrial waste PMMA [3, 67, 68]. Vinyl-based plastics like PMMA and PS can undergo free radical thermal depolymerization to yield their monomers. This non-catalytic pyrolysis route simplifies monomer recovery.

To date, commercial PMMA chemical recycling technologies have largely aimed at producing MMA monomer. However, they remain insufficient for handling the large volumes of end-of-life PMMA waste.

In contrast to the MMA-focused pathway, MAA-oriented recycling presents an alternative

route for managing and utilizing waste PMMA. MAA is produced industrially as a precursor for ester synthesis, particularly MMA [14]. Although MAA's market is about 10 % the size of MMA's, its independent demand is growing.Traditionally, MAA is cogenerated during MMA production. However, new MMA plants that use ethylene as a feedstock will not produce MAA as a by-product, which is expected to boost market demand for MAA. Utilizing waste PMMA to produce MAA thus creates a dual benefit: addressing plastic waste while supplying a high-demand chemical.

PMMA hydrolysis proceeds via two tandem reactions: thermal depolymerization to MMA, followed by catalytic hydrolysis of MMA to MAA [5, 69]. Although fluidized bed [5] and stirred-tank reactors [17] have shown potential in this conversion, their batch or semi-batch operation complicates cleaning and limits scalability. Therefore, continuous operation is preferred. A novel continuous reactor design is needed to efficiently convert PMMA into MAA, and reactive extrusion offers significant promise for this purpose.

Effective hydrolysis requires suitable catalysts. Identifying catalysts that improve MAA yield while reducing energy and steam consumption will enhance the technical and economic viability of the PMMA-to-MAA route. A detailed mechanistic study is also critical to guide reactor and process design, and to identify the formation pathways of key by-products that affect product purity.

CHAPTER 4 ARTICLE 1 – EXPERIMENTAL METHODS IN CHEMICAL ENGINEERING: REACTIVE EXTRUSION

Yanfa Zhuang, Nooshin Saadatkhah, Mahdi Salehi Morgani, Tianhuai Xu, Charlie Martin, Gregory S. Patience, and Abdellah Ajji

Published in The Canadian Journal of Chemical Engineering on July 10, 2022

4.1 Abstract

Reactive extrusion (REX) is a manufacturing technique that combines traditional melt extrusion with chemical reactions, including polymerization, polymer functionalization, and depolymerization (chemical recycling). Single screw, counter-rotating, and co-rotating twin-screw extruders (TSE) are possible configurations, but the TSE is most effective for viscous media with better mixing capability, temperature and residence time distribution control, and self-wiping (cleaning) performance. Compared to traditional polymer processing where monomers react in tanks, followed by compounding and pelletizing, REX can operate solvent-free in a single step. This simplifies the downstream separation and saves equipment and operational costs. However, the short residence times (on the order of seconds to minutes) of extruders limit their applications to fast reactions. For longer reactions, a sequential design and string extruders with batch reactor extend residence times. Furthermore, the surface-to-volume ratio decreases with increasing scale, which introduces design complexity to remove the heat of reaction. Here, we review REX working principles, apparatuses and their elements, applications and reactions, modelling and scale-up considerations, as well as limitations and recommendations. Web of Science indexed 579 articles that mention reactive extrusion between 2017 and 2021. A bibliometric analysis of these articles identified five research clusters: composite, nano-composite, and thermal properties; degradation, crosslinking, rheology, and acid; crystallization, polypropylene, maleic anhydride, and rheological properties; morphology, compatibilization, and copolymer; and oxidative stress and mechanisms.

4.2 Introduction

Reactive extrusion (REX) is a continuous manufacturing technology to process chemicals and polymers: conveying, reaction (synthesis), melting, mixing, devolatilization, pumping,

and sequential shaping. [70–74] An extruder typically has a single or twin-screw (Fig. 4.1), but multiple screws are also available. The screws of a twin-screw extruder (TSE) typically intermesh (intermeshing) and rotate in the same direction or in opposite directions.

A co-rotating TSE has higher capacity and better heat-management and cleaning capability compared to single screw and counter-rotating configurations. [75] Dow Chemical Company patented the first REX to polymerize styrene in 1950 [76] and 23 years later Meyuhas et al. [77] published the theoretical principles of REX.

Low-speed late fusion (LSLF) TSEs operate up to 50 rpm, and high-speed energy input (HSEI) TSEs run up to 1200 rpm and more. HSEI TSEs apply to compounding, reactive processing, and devolatilization.

LSLF counter-rotating TSEs mix materials at low shear and pump at a constant pressure. In the HSEI market, demand for co-rotating intermeshing TSEs with self-wiping flow capability exceeds that of the counter-rotating intermeshing and non-intermeshing TSEs (Fig. 4.2). High torque shaft geometries include splined, asymmetrical splined, hammered, key-way, and hexagonal.

Each section of a REX segmented barrel and screw design may operate at different temperature and pressure and comprises sections to feed liquids and solids, and zones for melting, mixing, reaction, degassing, pumping, and shaping. Side-feeding ports and devolatilization zones facilitate adding solvents and removing reaction products. [75] REX normally requires less solvent or even zero solvent compared to the traditional polymer synthesis processes. Strong shear stress from rotating screws in the first block melts solid polymer within seconds. In the latter zones, a die (and auxiliary equipment) shapes the melt into various forms, such as pellets, sheets, and films.

REX processes have several limitations and constraints: [78] because of the high cost per unit reaction volume, only high throughput is economically feasible. [75] Also, thermal runaway accelerates parasitic reactions that compromises product quality. Industry applies REX for polymerization (polyaddition, polycondensation, free radical copolymerization, ionic polymerization, and anionic copolymerization), grafting, and depolymerization. [79] A well-known industrial example of REX is the polymerization of thermoplastic polyurethane which has the capacity of producing 60 % of thermoplastic polyurethane global demand. [78] Current REX

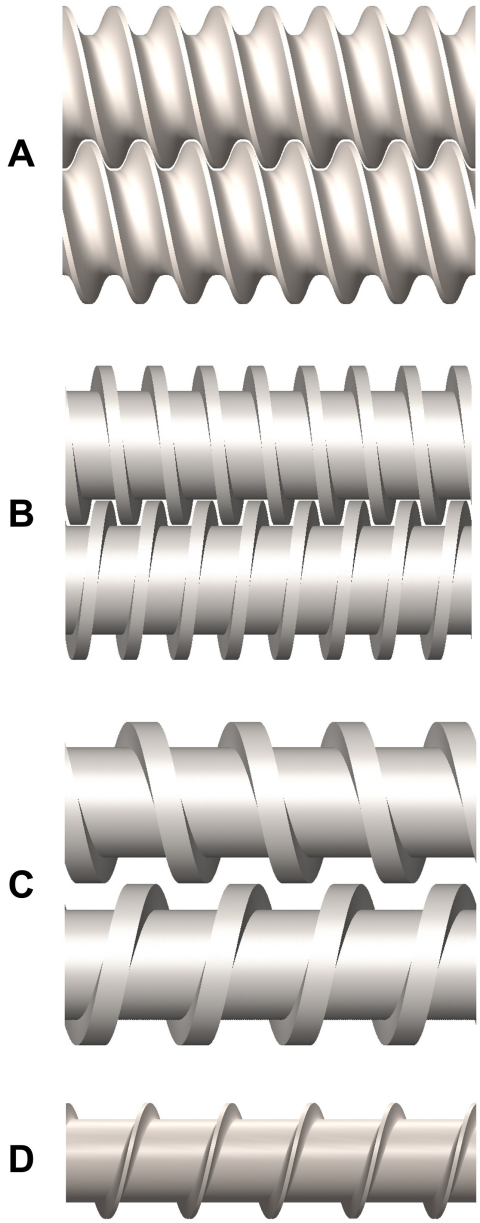

Figure (4.1) 90 % of commercially available screw configurations is (A) intermeshing co-rotating, and other configurations ((B) intermeshing counter-rotating, (C) non-intermeshing counter-rotating, and single screw (D)) apply in specialty products

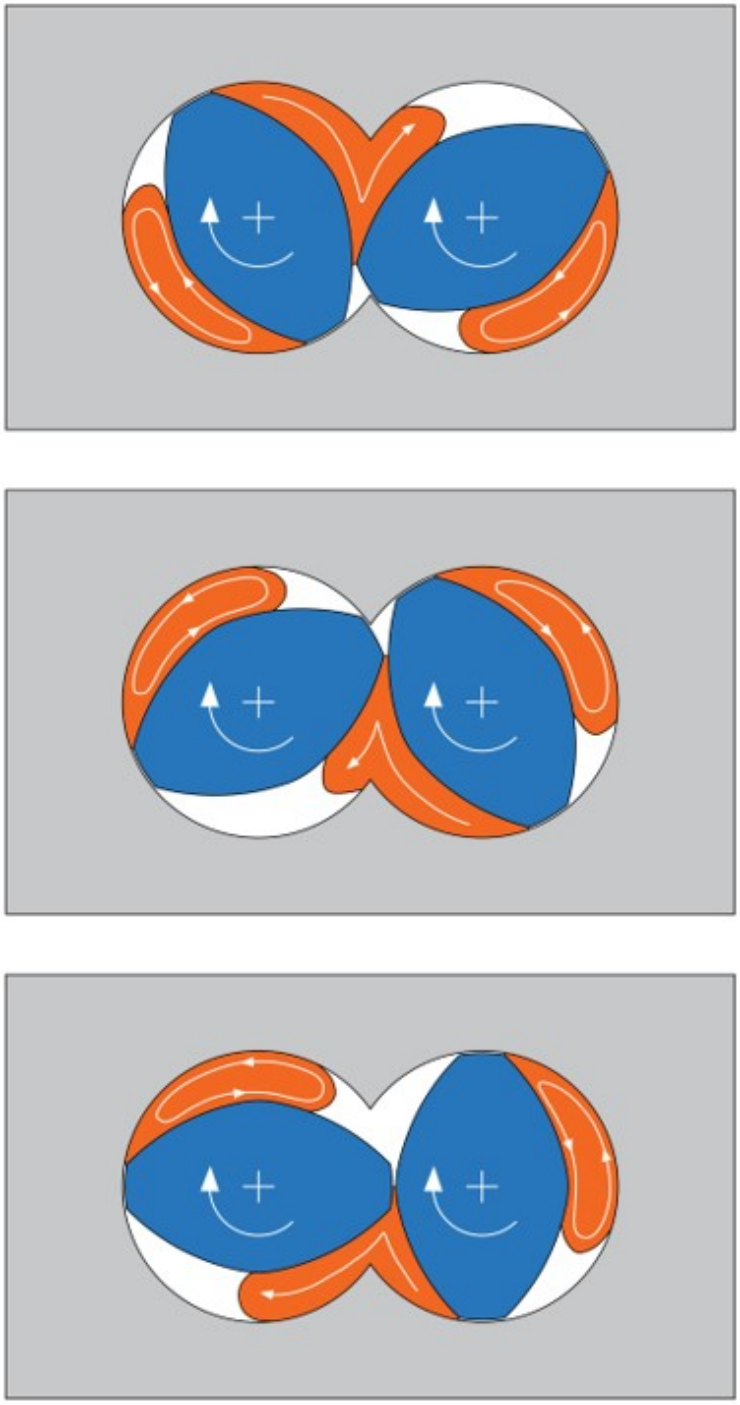

Figure (4.2) Self-wiping capability of co-rotating twin-screw extruders (TSEs)

research focuses on biomass value-added conversion, [80] thermoplastic devulcanization, [81] degradative extrusion, [82], bio-based or highly-valued polymer synthesis, [83–85], process scale-up, and to produce or recycle value-added products.

This article belongs to a special series dedicated to experimental methods in chemical engineering. [86] These articles highlight the salient features of the methods to help readers quickly grasp their applications, limitations, and uncertainties. Here, we review the REX process and describe its modelling and scale-up considerations for practical design and operation.

4.3 REACTIVE EXTRUSION

4.3.1 Working principles

Reactive extruders are continuous chemical reactors to treat and transform viscous materials and polymer melts. [87] During reactive extrusion, extruders serve a dual role by functioning as both reactors and mixers. Reactive extruders polymerize monomers, graft polymer chains,functionalize polymers, and treat end-of-life plastics. [88–90] Among polymers produced by REX, polyethylene terephthalate, polyurethane, polyamide, and polystyrene-maleic anhydride are the most prevalent. [78]

The three steps in the production of polymers consist of polymerization, compounding, and post-treatment processing. Stirred tank and tubular reactors are applied to polymerize monomers but they are inadequate for viscous liquids and require solvents (solution polymerization). [91] The solvents promote side reactions and add cost to distill/evaporate the solvent.

REX and subsequent compounding and processing in a single or twin-screw extruder is an economic alternative to solution polymerization. [78] High-temperature operation, dispersive and distributive mixing, controlled reaction time, and processing high viscosity melts are other advantages. [59] The main limitation is the extruder length and low surface-to-volume ratio. Polymer melts have low thermal conductivity [59] and this combined with the limited barrel wall surface area excludes highly exothermic or endothermic reactions like partial oxidations. [87] For example, compatibilization, a conventional REX process, has a very low reaction heat per volume. [87]

A co-rotating, intermeshing TSE is the most common type of extruder for REX and is suitable for melting, mixing, and pumping polymers through dies for pelletizing. TSE offers heating flexibility for chemical reactions because of its segmented heating and shear heating by tightly intermeshing screw elements. [78] TSE screw elements convey fluids (feeding and pumping), mix, and compartmentalize reactants in zones (Fig. 4.3).

Mixing elements have various geometries and distribute and disperse monomer, polymer, nanoparticles, and liquids. Zoning elements work as a restrictive barrier to limit mixing and movement from different areas, and also seal for the venting ports. Screw geometry parameters of conveying element include (Figure 4.4): pitch (the distance between two consecutive flights), channel depth (the distance from the screw roots to the inner barrel surface), channel width (the distance across the screw channel in a direction perpendicular to the flight), flight clearance (the distance between the screw flight and the inner barrel surface), flight width (the distance across one flight in a direction perpendicular to the flight), and flight angle (the angle between the flight and the direction perpendicular to the screw axis). Inner diameter (ID), outer diameter (OD), and centre diameter (C) between two shafts define TSE cross section.

Reactive extruders heat the reactants to initiate the reaction. The screw length, configuration, and rotation speed determine the residence time distribution and, coupled with the temperature profile, control the extent of reaction. Furthermore, feeding additives (liquid and solid) is possible at multiple positions in the extruder, which is an interesting feature for heat-sensitive compounds. Feeding inert gases reduces the oxygen concentration, which minimizes product degradation. [78, 92]

4.3.2 Equipment and its characteristics

The typical TSE length to diameter ratio (L/D) varies from 32:1 to 48:1, and up to 100:1. The barrel of a TSE consists of several sections (modular) with individually controlled heating and liquid cooling (Fig. 4.5).

Closed barrels are suitable for pumping, melting, and mixing, while open barrels are either for feeding or for devolatilization. The motor provides the shear energy to rotate the screws. Parameters like screw speed (rpm), feed rate, sectional temperature, and venting vacuum levels affect the whole process including melt pressure and temperature, and motor amper-

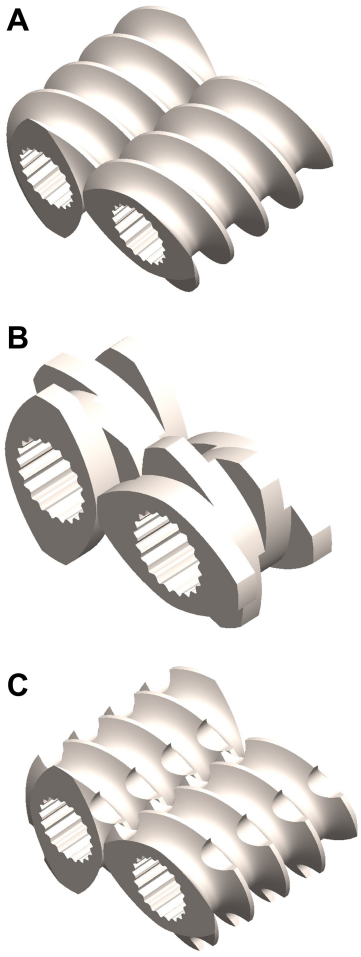

Figure (4.3) TSE screw elements: **A** conveying; **B** mixing; and, **C** mixing and zoning

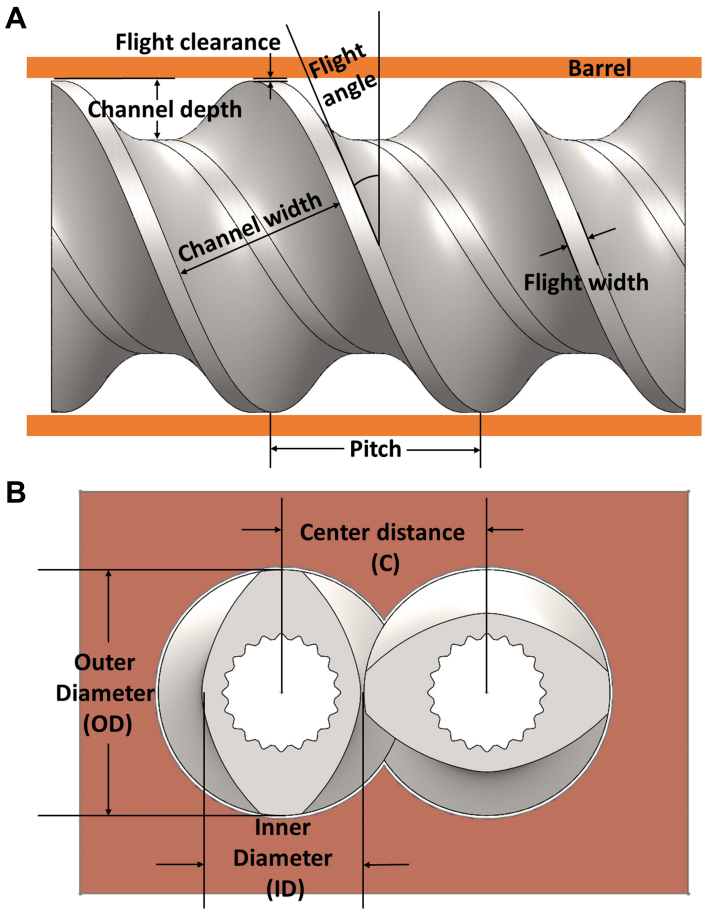

Figure (4.4) Screw geometry of: **A** conveying element; and, **B** twin-screw extruder (TSE) cross section view

age or torque. Screws are equipped with elements for three main tasks: conveying, melting, and mixing.

Conveying elements carry materials either forward (to pump materials to downstream locations and discharge) or reverse (to broaden the residence time distribution for reaction or to create a dynamic seal between zones). The kneading element, depending on its width, might melt materials and reduce their particle size (dispersion). Distributive mixing elements distribute particles in the matrix and homogenize morphology. [78] Pressure at the die is a function of the feeding rate and melting consistency.

Feeding

In a TSE, throughput is independent of screw rotational speed (rpm): The feed rate determines the output rate at steady state. The screw rotation speed controls degree of fill (F) in the barrel section and thereby affects its residence time distribution. [93]

$$F = \frac{0.2777 \times \mathrm{Q}}{\mathrm{SV} \times (\mathrm{rpm}/60) \times \mathrm{SG} \times \mathrm{Ef}} \tag{4.1}$$

where Q is flow rate in $\mathrm{kg\,h^{-1}}$, SV is the free volume of extruder in cc/diameter, rpm is the screw rotation speed, SG is the specific gravity of the material, and Ef is the average forwarding efficiency being processed.

We feed materials at different positions in the extruder based on the reaction and their physico-chemical properties (heat-sensitive materials, solid particles, or low viscosity liquids). [94] It is possible to feed materials downstream of the extruder but it requires reducing the pressure to the ambient pressure.

Polymers in the shape of pellets, powders, or flakes are better fed upstream in the first extruder sections for melting. In a commercial TSE or tangential single screw extruder, the first extruder section has a larger channel depth and handles larger particle sizes.

To feed large granules and flakes ($> 50\,\%$ of the channel depth) or fine powders ($< 100\,\mu\mathrm{m}$) requires special screw designs. In the devolatilization zone, extruders reduce pressure and extract vapours or volatiles with a vacuum pump. These two operations are necessary to

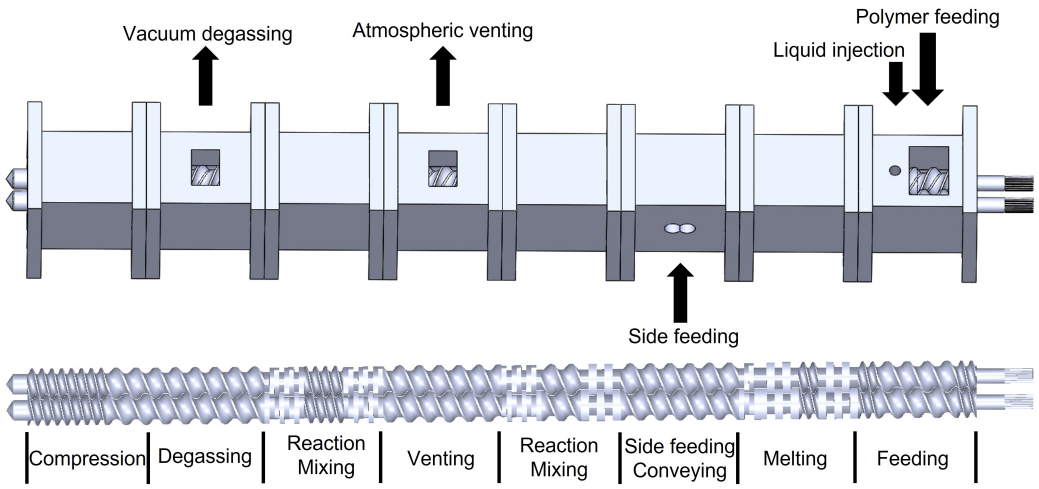

Figure (4.5) Typical twin-screw zones and barrels in a reactive extrusion (REX) system

introduce powder to the extruder, otherwise the vapours and volatiles will flow upwards through the vertical pipe of the powder feeder and compromise feed rate control. Some screw elements like increased volume (undercut) or single flight (SF) are specially designed to block gas in the primary melting zones of the extruder. [78]

Feeding location depends on the purposes of additives, for example, pigments must be added before the melting zone, and fibres after the melting zone. Vents on the feed opening allow gases to exhaust from the barrel. Liquids must be injected into the zero pressure zones and require fast mixing. Pressurized injection pumps inject non-viscous liquids into the fully filled distributive mixing section.

Liquid additives can lubricate unmelted pellets and agglomerates in the primary zone but can also cause agglomeration. [78] Restrictive elements increase the degree of fill in the extruders. The excessive number of restrictive elements increases the residence time, produces temperature buildup, and consequently degrades materials.

Melting

Electrical elements or furnaces heat the exterior wall of the barrel. Another source of energy is the friction between the screws and the materials in the barrel—mechanical energy. Kneading elements produce the highest mechanical energy including two-lobe or three-lobe eccentric kneading blocks, shoulder kneading blocks, and conveying kneading blocks. [95]

Screw configuration, screw rotational speed, and the volume determine the amount of mechanical energy generated. [78]

Mixing

Mixing is a critical factor in reactions and REX. Dispersive and distributive mixing are the two main mixing mechanisms (Fig. 4.6). Dispersive mixing disperses the particles and reduces their size, while distributive mixing homogenizes particles and inhibits agglomeration. Each extruder must be designed concerning the input feed and the desired products.

Narrow kneading blocks maximize the number of flow divisions and increase distributive mixing. Wide-disk kneading blocks increase dispersive mixing, maximize shear stresses on the material, and homogenize particles. Kneading blocks, special mixing bushings (such as toothed mixing units and blister rings), and screw elements (such as zester mixing element—ZME), screw mixing element (SME), Igel mixing element, SG segment screw, and ZB gear mixer) are the main mixing components in a co-rotating TSE. [78, 95, 96]

Dividing the mixing section into several zones minimizes thermal runaway versus a single zone, thereby reducing the degradation rate. Conveying sections between mixing sections lets polymer materials relax before entering the next mixing section.

Devolatilization

Devolatilization or degassing removes unwanted gas components from the molten polymer and prevents contamination during REX. Depending on the process and type of volatiles, single or multiple stage, linear or rotary stage vacuum setups or atmospheric vents remove excessive moisture, gas products, or trapped air from the materials during reactive extrusion.

Devolatilization systems function better on the high residence time locations and where the channel degree of fill is low. A low degree of fill gives time, surface, surface renewal, and space to remove volatiles from molten polymer.

Typically, screw bushings with a long pitch assist in the removal of volatiles. [78] The degree of fill or fill percent in a TSE is an approximation of the percentage of the available volume

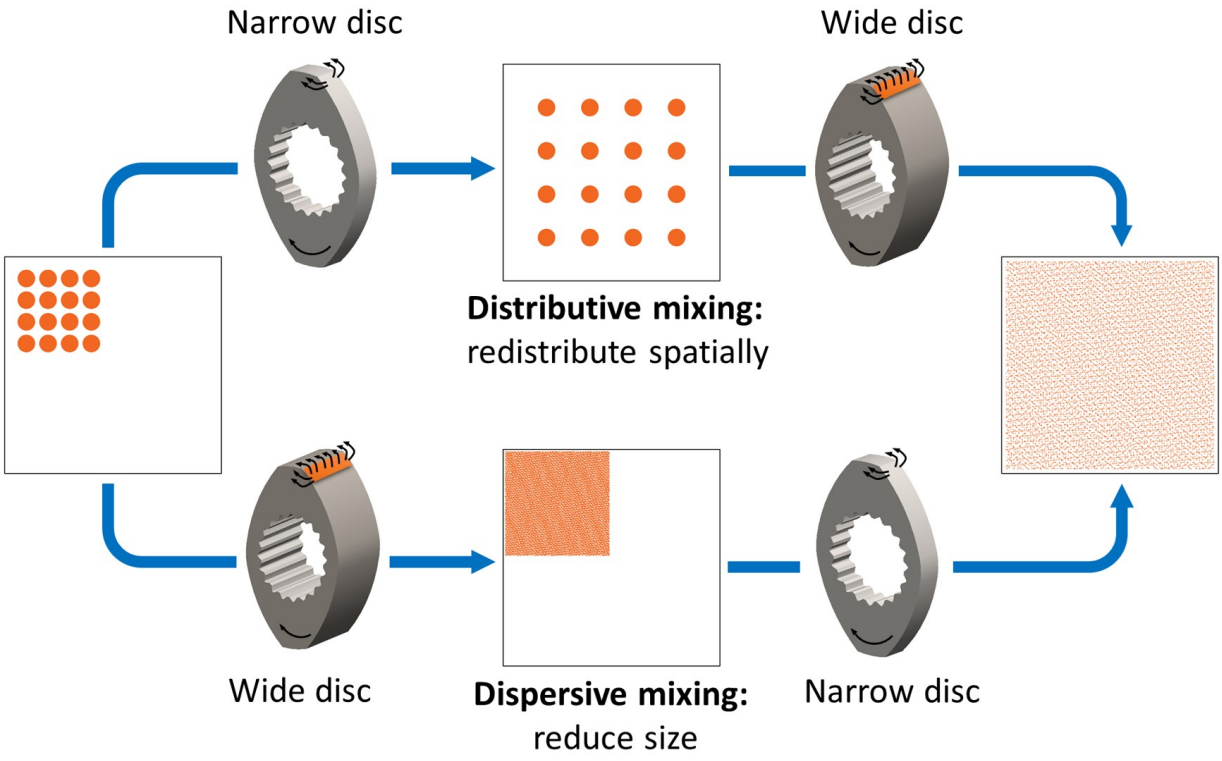

Figure (4.6) Distributive & dispersive mixing processes. The orange dots represent particles of different sizes. Distributive mixing (top path) spatially homogenizes particles and dispersive mixing (bottom path) disperses the particles and reduces their size

in the process section.

4.4 APPLICATIONS

4.4.1 Bibliometric map

Over 579 articles indexed by WOS (*Web of Science*) mentioned reactive extrusion in the last five years (2017–2021). [97] Most articles were in the category of mechanical properties (occurred in 214 articles), followed by polylactic acid (177), polymer blend (134), morphology (98), and crystallization (85). VOSViewer software grouped keywords into five clusters based on WOS bibliometric data (Fig. 4.7) The size of circles and texts are proportional to the number of occurrences in the keywords. Crystallization, rheology, maleic anhydride, polypropylene, and polyethylene are among the most frequently cited keywords in the red cluster with 25 of the top 99 keywords. The green cluster has the second-highest number of keywords (19) and includes crosslinking, degradation, functionalization, lignin, peroxide, and fiber.

Barrier properties, thermoplastics, bio-polymers, bio-degradation, cellulose, and surface modification are the keywords from the third-ranked cluster (blue) with 19 keywords. The fourth cluster (yellow) with 18 keywords includes mechanical properties, thermal degradation, bio-composites, nano-composites polylactic acid (PLLA), nucleation, immiscible blends, and carbon nanotubes (CNTs). The magenta cluster only has 13 keywords and includes blend, co-polymer, compatization, morphology, plasticization, hydrolysis, rubber, and pH.

4.4.2 Reaction types and mechanisms

Conventional reaction categories in which industry applies extruders include:

- **Controlled depolymerization/degradation** A free radical initiator breaks polymers into a controlled molecular weight distribution, recycles (or hydrolyses) polymers to their original monomers, or creates a higher concentration of reactive sites to graft. [59, 79] Recycling polybutylene succinate [99] and depolymerization of poly(ethylene terephthalate) are examples. [89, 100]
- **Polycondensation** Monomers or low molecular weight polymers chemically bond and produce longer chains with higher molecular weight, like polycondensation of

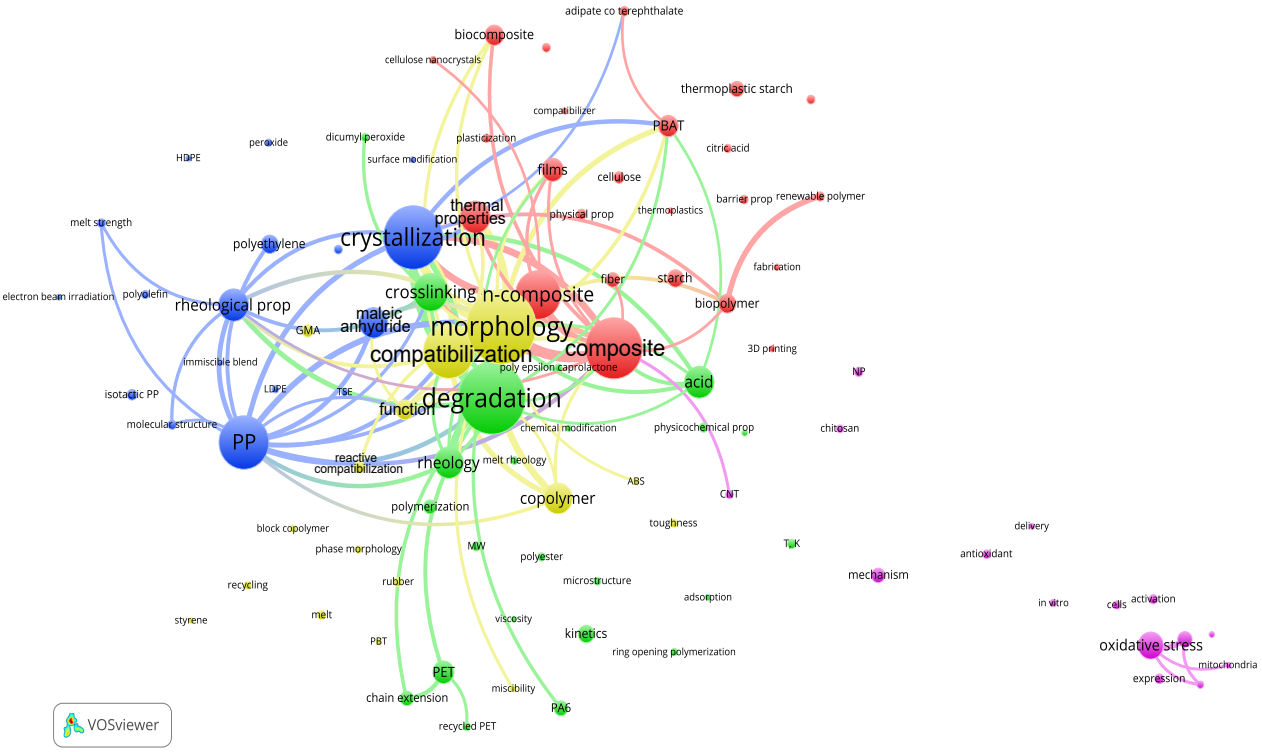

Figure (4.7) VOSViewer keyword bibliometric map based on keywords (reactive extrusion) derived from articles that WOS indexed from 2017 to June 2021. [97, 98] The text font size and diameter of the circles are proportional to the number of occurrences in the 579 articles indexed during this time. The map comprises the 99 most often mentioned keywords that the software groups together in clusters with the same colour: red-composite (25 keywords), green-degradation (23), blue-crystallization (18), yellow-mechanical properties (16), and magenta-oxidative stress (15) The map excludes the following keywords because the number of occurrences is so large, they dwarf the others and would have overlapped too many: green-reactive extrusion (345 occurrences), red-mechanical proper ties (295), red-polylactic acid (247), and red-blends (199). The smallest circles represent 13 articles. Lines represent citation links. Abbreviations: ABS-acrylonitrile butadiene styrene, CNT-carbon nanotube, GMA-glycidyl methacrylate, MW-molecular weight, n-composite-nanocomposite, NP-nanoparticle, LDPE-low density polyethylene, PA6-polyamide 6, PBT-polybutylene terephthalate, PBAT-polybutylene adipate terephthalate, PET-polyethylene terephthalate, PP-polypropylene, T-temperature, TSE-twin screw extruder.

ammonium polyphosphate [101] and synthesis of biobased poly(hexamethylene sebacate). [102]

- **Cross-linking** Polymer chains form covalent bonds or short strings of chemical bonds like cross-linking of polypropylene by peroxide and multifunctional monomers, [103] cross-Linking of poly(butylene terephthalate) by epoxy-vitrimer chemistry, [104] and cross-linking poly(l-lactide) (PLLA) with three peroxide groups. [105]

- **Grafting monomers or mixture of monomers** onto the existing polymers to modify polymers and improve properties as in the grafting of maleic anhydride (MA) onto polyolefins polypropylene (PP), [106, 107] copolymers of poly(L-lactide) and poly(ϵ-caprolactone) or poly(ethylene glycol). [108] Free radical initiators and ionizing radiation initiate the grafting reactions.

- **Functionalizing resin backbones** Fibre/fillers with highly reactive groups initiate the reaction for composites and alloys. Polymer functionalization and grafting are interconnected. In many grafting processes, the primary step involves producing a reactive or functionalized polymer substrate. [109] REX introduces functional groups like isocyanate, amine, anhydride, carboxylic acid, epoxide, and oxazoline to polymers or resins in a short residence time. [110] Examples are strengthening of poly (lactic acid) by epoxy- functionalized chains [111] and functionalization of polypropylene with maleic anhydride through the Alder-ene reaction. [112]

- **Copolyester exchange reactions** Copolyesters from during melting and mixing processes via alcoholysis, acidolysis, and ester-ester exchange: [113] alcoholysis of ethylene and vinyl acetate copolymers, transesterification of ethylene and alkyl acrylate, copolymers (EAA), and aminolysis of alkyl acrylate copolymers. [107]

- **Bulk (or mass) polymerization** An initiator launches the solventless polymerization of a monomer. The main problem in the process is the heat dissipation as in bulk polymerization of methyl methacrylate, [114] polyurethane synthesis, [115] and bulk polymerization of styrene. [116]

- **Compatibilizing** This operation increases polymer stability by adding a substance to an immiscible blend of polymers, like for immiscible mixtures of polypropylene/poly(butylene terephthalate) (PP/PBT) blends [117] and polyolefin and polystyrene via Friedel–Crafts alkylation. [118]

4.5 EXPERIMENTAL CONSIDERATION AND SCALE-UP

4.5.1 Parameters

Measurable or possible readouts in reactive processing are melt temperature, melt pressure, motor amperage (torque), viscosity, [119] residence time distribution (RTD), [120] and chemical conversion.

Temperature

In reactive processing, the temperature is a measurable and controllable parameter, even though temperature control is problematic because of the low heat conductivity of polymers, self-heating by viscous dissipation, or exothermic/endothermic reactions. [121] Viscous dissipation introduced by shear results in local overheating, which excites undesired side reactions, like thermal degradation: Kneading highly viscous materials creates heat due to shear.

Extrusion systems are instrumented with thermocouples (TC), resistance temperature detectors (RTD), and infrared (IR) detectors to monitor temperature. [122] RTDs have higher stability and accuracy compared to TC sensors, while TC sensors are cheaper and better for point measurements. [122, 123] IR probes allow non-contact surface and bulk temperature measurement by detecting the radiation emitted from the object.

TC sensors and RTDs are pressed into barrels to measure the temperature of the barrel wall. Barrel temperature is unequal with the real melt temperature due to heat transfer resistance.

However, immersion sensors tend to fail over time. TCs penetrate the melt and read the temperature at the point of the TC junction. [122] IR probes equipped with a sapphire window protrude into the melt and measure the radiation emitted from the polymer melt.

The measured temperature is the melt surface for opaque melt and bulk for transparent melt. [122] The TC and IR immersion depth and configuration affect the melt velocity profile in the channel. [121, 122] IR measurement has a shorter response time and wider monitor range compared to TC, although IR probes are more expensive.

Pressure

Melt pressure along a single-screw extruder rises gradually due to the flood feeding characteristic of the single-screw extruder. Unlike flood-fed single-screw extruders, pressure gradients vary along the barrel segments depending on the screw configuration (Fig. 4.8). [58] The venting and feeding zone operate at ambient pressure.

Fluctuations in die pressure indicates extrusion throughput variation, which may affect the dimensions of the extrudates (Fig. 4.9).

Excessive pressure may build up quickly in extruders, dissociate the die from the barrel, and even cause an explosion. [122] Peroxides as initiators increases the safety hazards caused by an over-pressure.

Monitoring pressure minimizes these risks. Instrumentation includes strain gauge transducers (including capillary and pushrod type), piezo-electric transducers, and pneumatic pressure transducers.

A strain gauge transducer contains two diaphragms in which only one contacts the polymer melt directly. [122] A pushrod connects the two diaphragms for pushrod strain gauges. and (mercury mostly) hydraulic in a capillary type strain gage. [122] Piezo-electric transducers and pneumatic type transducers are robust, but the former have a better dynamic response, lower error, and are less sensitive to temperature variations.

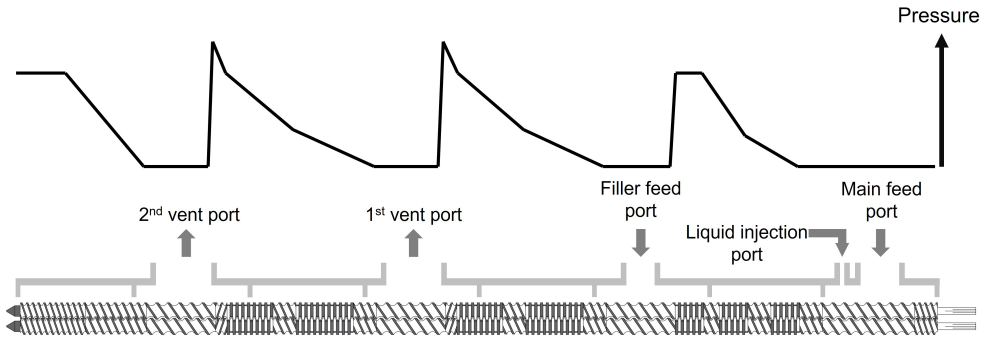

Figure (4.8) Pressure gradient along a starve-fed twin-screw extruder (TSE) [58]

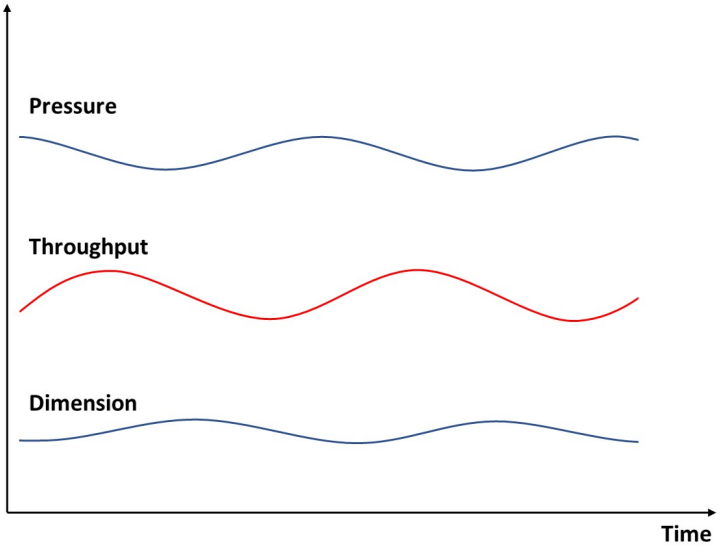

Figure (4.9) Change of die pressure, throughput, and dimension with time [122]

Residence time distribution (RTD)

The RTD characterized the probability distribution with respect to time that chemical species or particles remain in a vessel and is a diagnostic tool to identify flow anomalies. [120, 124] In reactive processing, RTD is a critical parameter to evaluate the mixing ability of an extruder [125] and compare the effect of changes of operating conditions and extruder design on screw reactor performance. [124] The RTD is determined by screw rotation speed, screw design, mass throughput, filling degree, material properties, and back pressure. [125] For co-rotating TSE, higher screw fill levels generate a narrower RTD and less shear, while lower fill levels cause broader RTD and more shear (Fig. 4.10).

In-line measurement with ultra-violet (UV) fluorescence tracers is the most common method. [121] Its advantages over other methods include [121, 126] that a UV fluorescence probe can generally be installed in ports for pressure sensors, a few milligrams of fluorescent tracer is sufficient, [127] and tracer grafted onto the polymer chain is a true measure of RTD. Radioactive tracers have similar capabilities as UV fluorescence but require more infrastructure (NaI scintillator detectors, for example).

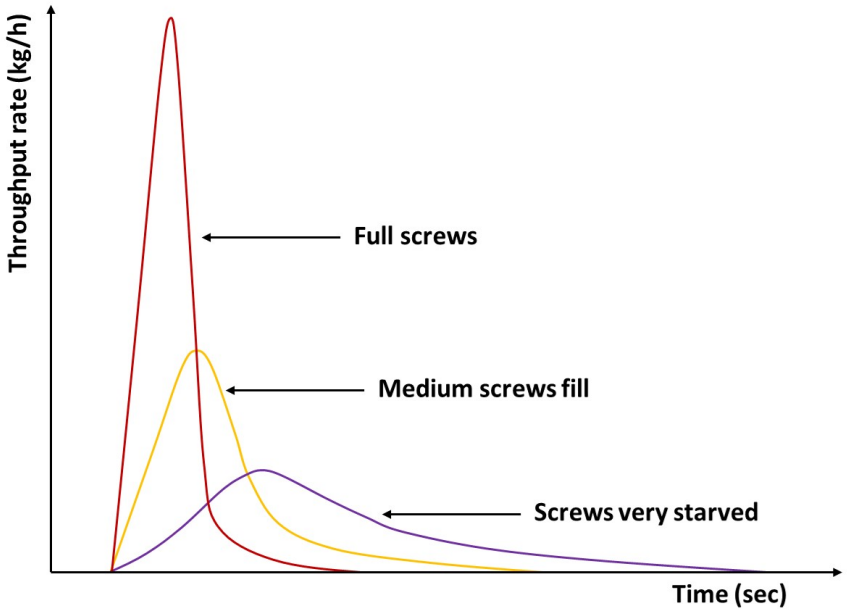

Figure (4.10) Residence time distribution of different levels of screw fill [93]

Rheology

Rheology (rheo-kinetics or rheo-chemistry), [78] the study of fluid flow and deformation under stress, is the most vital property in polymer melt processing. [119, 121] It depends on molecular weight, molecular weight distribution, macromolecular conformation, shear rate, temperature, and monomer content. [121, 128] We evaluate the degree of polymerization and blending quality based on viscosity. [121] However, for controlled degradation and bulk polymerization processes, the dramatic changes of the molecular weight and distribution introduce an extra level of complexity. Instruments include slit rheometers (in-line), capillary rheometers (on-line), and rotary rheometers (off-line), [119, 121] which adequately characterize thermally stable polymers. [78] The recorded torque of batch mixers, M, varies linearly with shear stress, σ, which is the product of shear rate and viscosity ($\dot{\gamma}\eta$):

$$\sigma = M \times K_{\sigma} \tag{4.2}$$

where K_{σ} is a stress constant that depends on geometry.

Recently, some commercial mixers or extruder systems coupled with torque rheometer (like the Haake PolyLab OS) are available to measure properties on-line.

Chemical conversion

Chemical conversion is a characteristic parameter in reactive processing to characterize reaction mechanisms. In-line reaction monitoring eliminates delay time versus off-line methods. [129] Reaction monitoring probes (near-infrared (NIR) spectroscopy, mid-infrared (MIR) spectroscopy, attenuated-total-reflection infrared (ATR-IR), and Raman spectroscopy), [78, 130, 131] are positioned on the extruder die exit.

Optical spectroscopy provides molecular information like composition and is sensitive to the morphological and structural features at numerous scales. [78, 121] Other monitoring techniques, such as ultrasonic attenuation, fluorescence spectroscopy, light scattering polarimetry, turbidity, and electric conductivity monitor reaction extent and quality. [78]

4.5.2 Rheo-kinetics

Rheo-kinetics combines rheology and kinetics to analyze changes in rheological properties during reactive processing and to reflect the underlying chemical transformations. [132] The reaction kinetics can even be derived during this process, as the viscosity varies with $\dot{\gamma}$, T, M_{w} (molecular weight), and α, the conversion extent: [133]

$$\eta = f(\dot{\gamma}, T, M_{\mathrm{w}}, \alpha) \tag{4.3}$$

Viscosity increases by 4 to 6 orders of magnitude for bulk polymerization that have dramatic increases in molecular weight and decrease for reactions like depolymerization.

Modelling the change of viscoelastic properties can predict the flow behaviour of reactive processes.

As the polymer chain length increases, viscosity increases mostly linearly for chain polymerzation (Fig. 4.11), while there is a long induction period for random polymerization. [133]

The Cross, power-law, Sisko, and Carreau models adequately characterize the shear-thinning viscosity of non-Newtonian fluids. [134] The Carreau–Yasuda model best describes the shear-thinning fluid behaviour of these fluids and provides an apparent viscosity, η_0 (viscosity at

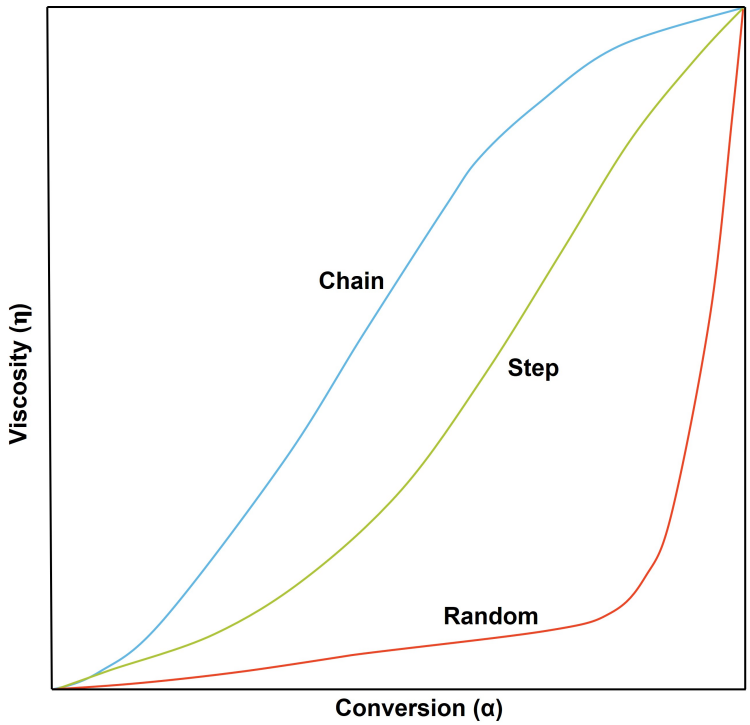

Figure (4.11) Viscosity (η) profiles as a function of reaction extent (α) for chain-propagation polymerization reactions [133]

zero shear rate):

$$\eta = \eta_0[1 + (\lambda\dot{\gamma})^a]^{\frac{n-1}{a}} \tag{4.4}$$

where λ is relaxation time, a is the Yasuda parameter that describes the transition region between the power-law and zero-shear-rate regions(2 in most cases), and n is power index.

Both η_0 and λ depend on temperature and M_w:

$$\eta_0 = A \exp\left[\frac{E_\mathrm{a}}{R}\left(\frac{1}{T} - \frac{1}{T_\mathrm{ref}}\right)\right] M_\mathrm{w}^{\mathrm{\l pha_v}} \tag{4.5}$$

$$\lambda = B \exp\left[\frac{E_\mathrm{a}}{R}\left(\frac{1}{T} - \frac{1}{T_\mathrm{ref}}\right)\right] M_\mathrm{w}^{\mathrm{\l pha_\tau}} \tag{4.6}$$

where E_a is the flow activation energy, T_ref is the reference temperature, and α_v and α_τ are power law exponents and are close to 3.4 for entangled polymers.

The Yasuda–Carreau model is reliable for simulation, but it poorly characterizes changes in viscoelastic properties with time.

Based on the dynamic molecular theory, Carrot et al. [135] proposed a model using a blending law of relaxation modulus $G(t)$:

$$G(t) = G^0 \int_{\ln Mc}^{\infty} \left[P(M)F^{0.5}(t, \lambda_M)\mathrm{d}(\ln M)\right]^2 \tag{4.7}$$

where $G(t)$ is named the plateau modulus and $F^{0.5}(t, \lambda_M)$ is the relaxation function:

$$F(t, \lambda_{\mathrm{Mw}}) = \exp\left(-\frac{t}{\lambda_{\mathrm{Mw}}}\right) \tag{4.8}$$

where λ_{Mw} is the relaxation time.

4.5.3 Diffusion

In degradative extrusion, small variations of molecular weight change polymer rheology dramatically. [121] The Deborah number, N_{De}, characterizes the diffusion character of polymer melts and is the ratio of the reptation time of the polymer chains λ_m to the characteristic time of the diffusion process θ_{d}: [121]

$$N_{De} = \frac{\lambda_m}{\theta_{\mathrm{d}}} \tag{4.9}$$

where θ_d is the ratio of the square of the thickness of the polymer layer, L, and the mutual diffusion coefficient, D_{12}

$$\theta_d = \frac{L^2}{D_{12}} \tag{4.10}$$

N_{De} compares the rate of conformational rearrangement against the rate of diffusion, which serves as an indicator to differentiate between various diffusion processes: when $N_{\mathrm{De}} > 1$ elastic diffusion predominates and when $N_{\mathrm{De}} < 1$ polymer behaves like a purely viscous fluid and Fick's second law of diffusion applies: [121]

$$\frac{\partial C}{\partial t} = D_{12} \cdot \Delta C \tag{4.11}$$

where C is the concentration of diffusing molecule and Δ is the Laplace operator, which denotes the second derivative.

Viscoelastic diffusion is another term to describe the diffusion behaviour when N_{De} approaches

1, which indicates that the molecular relaxation and mass transport occur in comparable time scales.

Due to the difficulty of directly measuring the diffusion coefficients in polymer melts at high temperatures, we estimate D_{12} considering diffusion theories. The free volume theory, a simplified expression of the self-diffusion coefficient D_1: [121]

$$D_1 = A \exp\left(-\frac{E_\mathrm{d}}{RT}\right) \exp\left(\alpha C\right) \tag{4.12}$$

where A and α are constants, E_d is the activation energy of the diffusion process, and C is the concentration of the diffusing molecule in the polymer.

The Flory–Huggins theory relates the mutual binary diffusion coefficient to the self-diffusion coefficient. Above the glass transition temperature T_g: [121]

$$D_{12} = D_1(1-f)^2(1-2\chi f) \tag{4.13}$$

where f is a ratio that compares the solvent volume to the polymer volume and χ is the Flory–Huggins interaction parameter.

These two expressions hold true when the assumption that self- diffusion only depends on the free volume (the free volume theory).

It is also assumes that solubility is independent of the M_w.

The limitation of theory-based models is that they are established from some arbitrary assumptions, which compromises accuracy.

4.5.4 Mixing

TSE mixing is categorized as distributive—the extent of homogeneity and dispersive (Fig. 4.6).

Distributive mixing is characterized by the homogeneity of distribution of single-phase elements in extruders, whereas dispersive mixing describes the process of disaggregation and

dispersion of solid particles, liquid droplets, or gas bubbles. [136]

We examine both radial and axial distributive mixing in extruders. The rotating screw elements induce flow leakage at the intermeshing zones and flight clearance (Fig. 4.3). The mixing action depends on the kinematic parameter of flow Λ, which is the product of the volumetric flow rate, Q, rotational speed, N, barrel diameter, D, and dimensionless volumetric flow rate term that depends on screw geometry: [136]

$$\Lambda = \frac{Q}{ND^3Q'} \tag{4.14}$$

Mixing quality is similar in screws for which the value of Λ is close. [136] Increasing the screw speed and reducing the material throughput improves distributive mixing (lower Λ). Negative Λ, in the case of reverse elements, has even better mixing: [136] a negative pressure gradient forms a fully filled region in the extruder, which gives it more time to mix.

In contrast to distributive mixing, which solely depends on flow kinetics, dispersive mixing varies with viscosity. For solid particles, a minimum shear stress is required to break up agglomerates. For liquid droplets and gas bubbles, a large shear stress must first overcome the surface tension before they are dispersed. The Weber number, the ratio of the product of γ, droplet diameter (d), and the viscosity of the continuous phase (η_c) to the surface tension (σ) characterizes this behaviour: [136]

$$N_{\mathrm{We}} = \frac{\gamma d \eta_c}{2\sigma} \tag{4.15}$$

The droplets deform and break up with increasing N_{We}. Other than shear forces, extensional forces also disperse liquid droplets. Extensional flows usually form when the flow path narrows (right before the fluid passes through the flight tips and the intermeshing zones). Extensional forces are more effective in deforming liquid droplets than pure shear stress and thus can be varied to enhance dispersion in TSEs. [136] The residence time distribution (RTD) depends on the screw rotation speed and the configuration of the screw elements. [137] Markers introduced in the feed track the change of concentration within the extruder.

The concentration profile of the markers at the exit represent the residence time density function and cumulative residence time function. [136] The width of the RTD curve correlates with how well the extruder disperses the tracer: a broad RTD curve gives better mixing quality (higher backmixing). The coefficient of variation, v, degree of segregation D_{s}, and

area stretch δ are other parameters to characterize mixing quality.

Considering n samples are collected with concentrations c_i, the coefficient v is: [136]

$$v = \frac{s}{\bar{c}} = \frac{\sqrt{\frac{1}{n-1}\sum_{i=1}^{n}\left(c_i - \bar{c}\right)^2}}{\bar{c}} \tag{4.16}$$

where s is the standard deviation and $\bar{c}$ is the mean value of concentration.

The degree of segregation is the product of v^2 and the ratio of the side-stream flow rate to the main-stream flow rate, φ: [136]

$$D_\mathrm{s} = \varphi v^2 \tag{4.17}$$

Mixing quality improves with lower values of v and D_s, which require a large sample size n to be statistically relevant.

The area stretch model, δ, focuses on the interfacial deformation caused by the stretching and reorientation of two fluids with similar properties. [138] Considering an infinitesimal area of $|\,\mathrm{d}A|$ with the normal direction $\overrightarrow{N}$ that transforms into an area of $|\,\mathrm{d}a|$ with the normal direction $\overrightarrow{n}$, the area stretch δ is: [138]

$$\delta = \frac{|\,\mathrm{d}a|}{|\,\mathrm{d}A|} \tag{4.18}$$

This parameter requires the definition of different tensors and normal directions, hence knowledge of the velocity field in extruders from simulation results. A high area stretch is better for distributive mixing. This model applies to laminar flow only and interfacial tension is negligible. [138]

4.5.5 Scale-up

Reactive extruders vary in diameter from 15 to 800 mm. The surface over volume ratio reduces proportionally when increasing the screw diameter, which reduces the heat transfer surface area, thereby modifying the radial temperature: higher temperature in the centre of the channel in the case of an exothermic reaction. [139] Heat transfer is the major limiting factor in scaling up. The larger the scale, the greater the temperature gradient between the centre of the channel and near the barrel walls.

Temperature gradients and polymer composition variations (due to reaction, for example) induce instabilities due to differences in viscosity that result in fluctuating throughput, and so lower conversion. A careful design of the experiments on a laboratory scale minimizes the risks of scaling up the process. [78, 79] Macro-balances quantify the contribution of thermal effects and determine the adiabatic temperature rise. The heat transfer coefficients of the barrel wall of the extruder (modelled as a scraped heat exchanger), vary between 400-600 $\mathrm{W\,m^{-2}\,K^{-1}}$. The heat transfer coefficient at the screw surfaces varies between 100–150 $\mathrm{W\,m^{-2}\,K^{-1}}$ (screw surface is not fully scraped). [140]

Scale-up depends on similarity in geometry, hydrodynamics, time, temperature, and chemical environment: [75] Geometric similarity occurs when the ratio between any two length parameters remains the same in the large- and the small-scale.

For a co-rotating TSE, the industrial-scale and laboratory-scale have the same type and the same L/D ratio. In counter-rotating TSEs, the complicated leakage gaps geometries require geometrical similarity between the small and commercial scales. In hydrodynamic scale-up, the dimensionless velocity profiles are held identical and both extruders have the same (dimensionless) filled length. Identical dimensionless flow profiles bring about identical shear rate profiles; the velocity gradients are similar, but not the absolute velocities (Fig. 4.12). For residence time scale-up, residence times are equal on both scales. In thermal scale-up, the absolute temperatures remain the same (based on overall energy balances), but not the temperature gradients (Fig. 4.13).

REX requires both chemical similarity and reaction progress similarity. However, chemical similarity depends on thermal similarity for the reaction rate, thermal similarity on hydrodynamics (viscosity), hydrodynamic similarity (velocity gradient), and geometric similarity. [75] So, scale-up depends on a series of equations relating geometrical and operating parameters to a power of the diameter ratio. These parameters include N (the rotation rate of the screws), P (the die pressure), μ (the viscosity), R (the fully filled length of the extruder), Q_b (the back flow), X (theoretical throughput), k (the reaction rate constant), r_V (the reaction rate), C (the concentration of the monomer), and τ (the residence time in the extruder) (Table 4.1). [75, 140]

The theoretical throughput or the maximum throughput, X, is the empty fraction in the

Table (4.1) Scale-up relations for geometric, hydrodynamic, residence time, thermal, and chemical similarities, $(\frac{Y}{Y_0}) = (\frac{D}{D_0})^y$ [75, 140]

Parameter (Y)	N	P	μ	R	Q	X	K	r_V	C	τ
Power (y)	n	p	ν	r	q	x	k	s	c	t
Geometric	Iso-viscous material with Newtonian behavior: $r = p - \nu - n - k$; For leakage flow: $q = n + x + 3$									
Hydro.	$x = 0$ so $q = n + 3$; $r = 0$ so $p = \nu + n$									
Residence t	Geometrical, hydrodynamic and iso-viscosities: r=n; n=0; p=ν; so q=3 Geometrical and hydrodynamic similarity: $r = n$; $p = 2n + \nu$; $q = n + 3$									
Thermal	Equal residence times, different filled lengths: $n = -2$; $r = -2$; and $p = \nu - 4$ so $q = 1$ For large Brinkmann: $q = \nu + 2n + 3$ With iso-viscous and hydrodynamic similarity: $n = 0$; $p = 0$, and $q = 3$									
Homo. Rx	$r = n$; $n = 0$; and $q = 3$; and $p = 0$									
Hetero. Rx	$r = p - \mu - n - k$; $r = 0$; $n = 0$; $q = 3$; $p = 0$ Large Damkohler IV: $q = 3 + s$; $s = 0$; $c = 0$; and $q = 3$ Small Damkohler IV: $2q = n + 4$; $n = 2$ but $n = 0$ for hydrodynamic So not possible to thermal scale-up									

feed zone:

$$X = 1 - F \tag{4.19}$$

In REX, scale-up requires hydrodynamic, thermal, and chemical similarity. To ensure equal residence time requires that the ratio of the the fully filled extruder length, R, to the product of the number of thread starts per screw, M, and rotation rate of the screws, N, is constant:

$$\frac{R}{MN} = \kappa \tag{4.20}$$

Since die pressure is proportional to viscosity and rotation speed ($P \propto \mu N$), to have equal viscosities, the die pressure needs to remain the same, while the back leakage increases with the screw diameter:

$$\frac{Q_{\mathrm{b}}}{Q_{\mathrm{b0}}} = \frac{D^3}{{D_0}^3} \tag{4.21}$$

The die pressure varies with the rotational speed of the screws:

$$\frac{P}{P_0} = \left(\frac{N}{N_0}\right)^2 \tag{4.22}$$

and the throughput changes according to:

$$\frac{Q}{Q_0} = \frac{ND^3}{N_0{D_0}^3} \tag{4.23}$$

Heat transfer in an extruder depends on conduction and convection and heat generation due to viscous dissipation and reaction.

The Brinkman number (heat generated by viscous dissipation over conduction) and the Péclet number (convective heat transfer over conductive heat transfer) characterize the relative significance of these mechanisms: [141]

$$N_{\mathrm{Br}} = \frac{\mu\nu^2}{\lambda\Delta T} \tag{4.24}$$

$$N_{\mathrm{Pe}} = \frac{\nu D}{\alpha} \tag{4.25}$$

where α is [142, 143]

$$\alpha = 2\sqrt{\frac{\lambda\rho C_P MN}{\pi}} \tag{4.26}$$

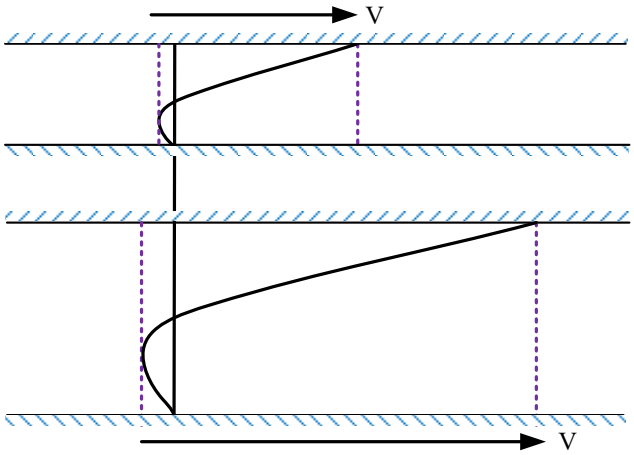

Figure (4.12) Hydrodynamic scale-up [75] where the velocity gradients are similar, but not the absolute velocities; dashed lines specify the smallest and the highest velocities

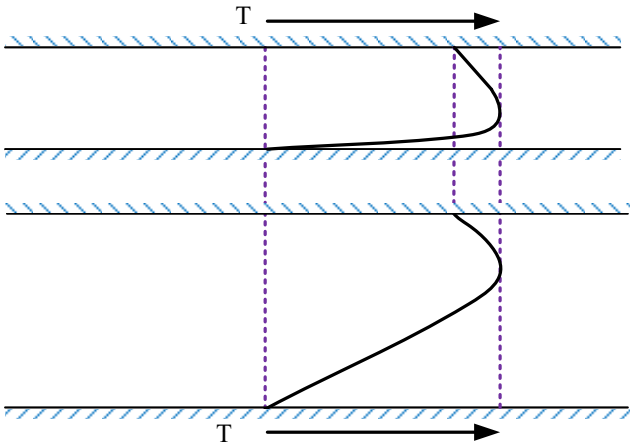

Figure (4.13) Thermal scale-up [75] where the absolute temperatures (and so the average) remains the same, but not the temperature gradients; dashed lines specify the highest temperature, as well as temperatures at the wall

For large $N_{\mathrm{Br}} > 2$, the extruder operates adiabatically.

The mass balance for a single component reaction is:

$$\frac{\partial C}{\partial t} = \nu \frac{\partial C}{\partial z} - r_{\mathrm{V}} \tag{4.27}$$

where r_{V} is the reaction rate and z is the axial co-ordinate.

For a first order reaction (and negligible change in volume), the Damköhler I number ($N_{\mathrm{Da,I}}$) is the ratio of reaction rate to convective mass transfer, which is a product of the rate constant, k and contact time, τ:

$$N_{\mathrm{Da,I}} = k\tau \tag{4.28}$$

and in terms of extruder geometry and for any reaction order it becomes

$$N_{\mathrm{Da,I}} = \frac{r_{\mathrm{V}} R}{C_0 N D} \tag{4.29}$$

where C_0 is the initial monomer concentration.

If the similarity in residence time is unachievable, $N_{Da,I}$ is constant only by changing the reaction constant through temperature. When the reaction heat is larger than the viscous dissipation (with many exothermic polymerization reactions), a balance on the conduction through the barrel wall, convective heat, and the heat of reaction make up the heat balance on the extruder: [75, 144]

$$Q\rho C_P \frac{\partial T}{\partial x} = \frac{\pi D H}{4} r_{\mathrm{V}} \Delta H_r + \pi D \alpha (T_w - T) \tag{4.30}$$

The dimensionless number to assess the relative heat generated by reaction to heat transfer by conduction, the Damköhler IV number ($N_{\mathrm{Da,IV}}$), is: [75, 144]

$$N_{Da,IV} = \frac{\Delta H_r r_{\mathrm{V}} R^2}{C_0 \lambda \Delta T} = \frac{\text{Heat of reaction}}{\text{Heat of conduction}} \tag{4.31}$$

For small $N_{Da,IV} (< 0.1)$, thermal and hydrodynamic similarity is impossible to achieve simultaneously in reactive extrusion.

For large $N_{Da,IV}$ (>10), the constraint for thermal similarity becomes:

$$\frac{\rho Q C_{\mathrm{P}} \partial T/\partial z}{\left(\frac{\pi}{4} DH\right) r_{\mathrm{V}} \Delta H_{\mathrm{r}}} = \kappa_2 \tag{4.32}$$

4.6 SIMULATION AND MODELLING

REX involves sophisticated process control, complex flow behaviour, temporal and spatial variation of rheology, and reaction kinetics. Experimental investigations are insufficient to characterize these processes, especially when applied for process optimization and scale-up. Model-driven simulation combined with experimental validation is recommended to adequately study REX phenomena and for commercial design. [145] De Smit et al. [145] reviewed REX modelling approaches from a multi-scale model point of view (i.e., the molecular scale considering elementary reactions, the changing viscosity at the micro-scale, mesoscale multiphase and morphological variation, and macro-scale equipment design and screw configurations) to guide polymer synthesis, modification, and recycling.

Modelling traditional extrusion process based on single and twin-screw configurations considers flow behavior and heat transfer phenomena. REX modelling must consider chemical phenomena, rheokinetics, and reaction heat (Fig. 4.14). Both chain growth reactions (e.g., polymerization, crosslinking, and grafting) and chain length decrease reactions (e.g., depolymerization, controlled degradation, and pyrolysis) may encounter average molecular weight variations and viscosity that change by orders of magnitude. Based on the three-dimensional (3D) computational fluid dynamics (CFD) simulation, Zhu et al. found viscous dissipation dominates in heat generation in a highly viscous system, while reaction heat becomes dominant in low-viscosity systems. [146] In chain length conservation reactions that are applied to either matrix compatibility improvement or functionalization, average molecular weight and viscosity keep a slight fluctuation with the increase of conversion.

REX simulation relies on the input of kinetic models developed by experimental data and transport models. Two common simulation strategies are adapted. [145] To simplify computation, an alternative strategy is to use tandem ideal plug-flow reactors (PFRs) and/or continuous stirred-tank reactors (CSTRs) as ideal models for extruders. The best approximation to the model (or combination) is evaluated based on residence time distribution measurements. [120] This reaction-driven approach provides detailed viscosity information but fewer details on flow parameters. Another simulation strategy is based on classical con-

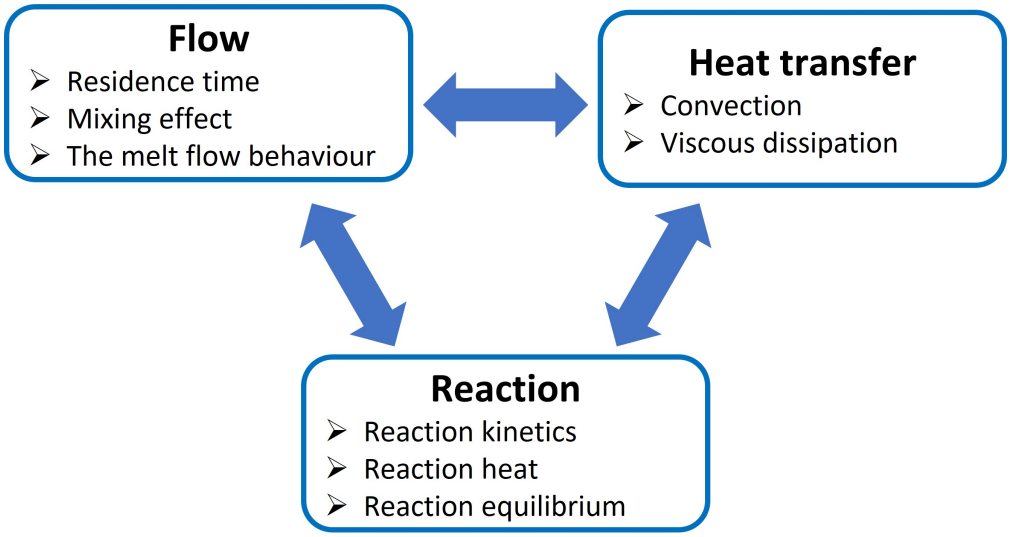

Figure (4.14) Coupling groups in reactive extrusion (REX) modelling [147]

tinuum mechanics, which is also known as the flow driven modelling approach. [145] Based on one-dimensional (1D), two-dimensional (2D), or 3D models, flow-driven modelling and simulation can demonstrate global or local fluid information along the length of single and twin-screw extruders. One popular commercial 1D/2D software designed for twin-screw extruder simulation is Ludovic that solves the Navier–Stokes equations for the extruder channel. [148] Berzin et al. [149] experimentally investigated the peroxide-induced degradation of polypropylene in a co-rotating TSE followed by a theoretical study based on Ludovic. The developed theoretical model can predict the primary process characteristics and describe the evolution of molecular weight and viscosity along the extruder.

More recently, Dubey et al. [150] applied upgraded Ludovic to simulate the ultrasound coupled REX of PLA and found further studies are required to fit the REX system with the coupling of alternative energy sources. 1D models have fewer assumptions and are computationally faster due to their simplified geometric features. Nevertheless, it is suitable for low screw rotation speed, low reaction heat, small screw diameter, and short fully-filled length. [151,152] 3D models simulate wider processing conditions and provide more abundant local information, even though they require more robust computational facilities and longer run times. Prominent software programs applied to 3D REX simulations include Fluent and Polyflow, which are based on CFD methods. Fluent uses the finite volume method (FVM), while Polyflow utilizes the finite element method (FEM).

Zhu et al. [146] studied the theoretical effects of screw rotating speed, screw element geometry, and initial conversion at the extruder inlet on polymerization of ϵ-caprolactone based on 3D fully-filled twin-screw conveying elements using Fluent. Zong et al. [153] experimentally researched the rheokinetics of Poly(p-phenylene terephthalamide) polycondensation and then theoretically compared flow pattern, temperature, and molecular weight distribution in the conveying screw, kneading element, and screw mixing element based on 3D geometric models on the Polyflow platform. More recently, Sun et al. [154] simulated reactive preparation of PP/TiO_2 nanocomposites in a TSE with two linked screws of conveying and mixing screw elements based on the Polyflow platform as well.

Reliable simulation results require experimental validation. Kinetic models based on experimental data are decisive in REX numerical simulation. Meshing is one crucial step in CFD simulation optimization and needs more consideration in simulation setup (Fig. 4.15).

Multiplex material models in complex processes as in the REX result in enormous numerical calculations and, as a result, low resolution. Machine learning techniques combined with physical models improve the accuracy of predictive models in REX systems. [155] Sparse regression (sPGD), Code2Vect (C2V), artificial neural networks (ANNs), support vector regression (SVR), and random forest regression (RF) are among the most commonly applied machine learning predictive models in chemistry and chemical engineering. [156,157] Application of artificial intelligence (AI) and machine learning techniques in REX, as other physical and chemical processes, is not limited to modelling the relationship between the input and output for quantitative prediction; it includes multidimensional data visualization, data classification, and creating dynamic data-driven systems. [155, 158]

In summary, the combination of experimental data and modelling is a powerful technique to describe the evolution of reaction, average molecular weight variation, viscosity change, and temperature profile along the extruder. Reliable REX simulation relies highly on kinetic models established by experimental data. A 1D/2D model is more favourable in global analysis despite the fact that they are limited under certain conditions. A 3D model is advantageous in local analysis and detailed investigation of flow and reaction on different types of screw elements.

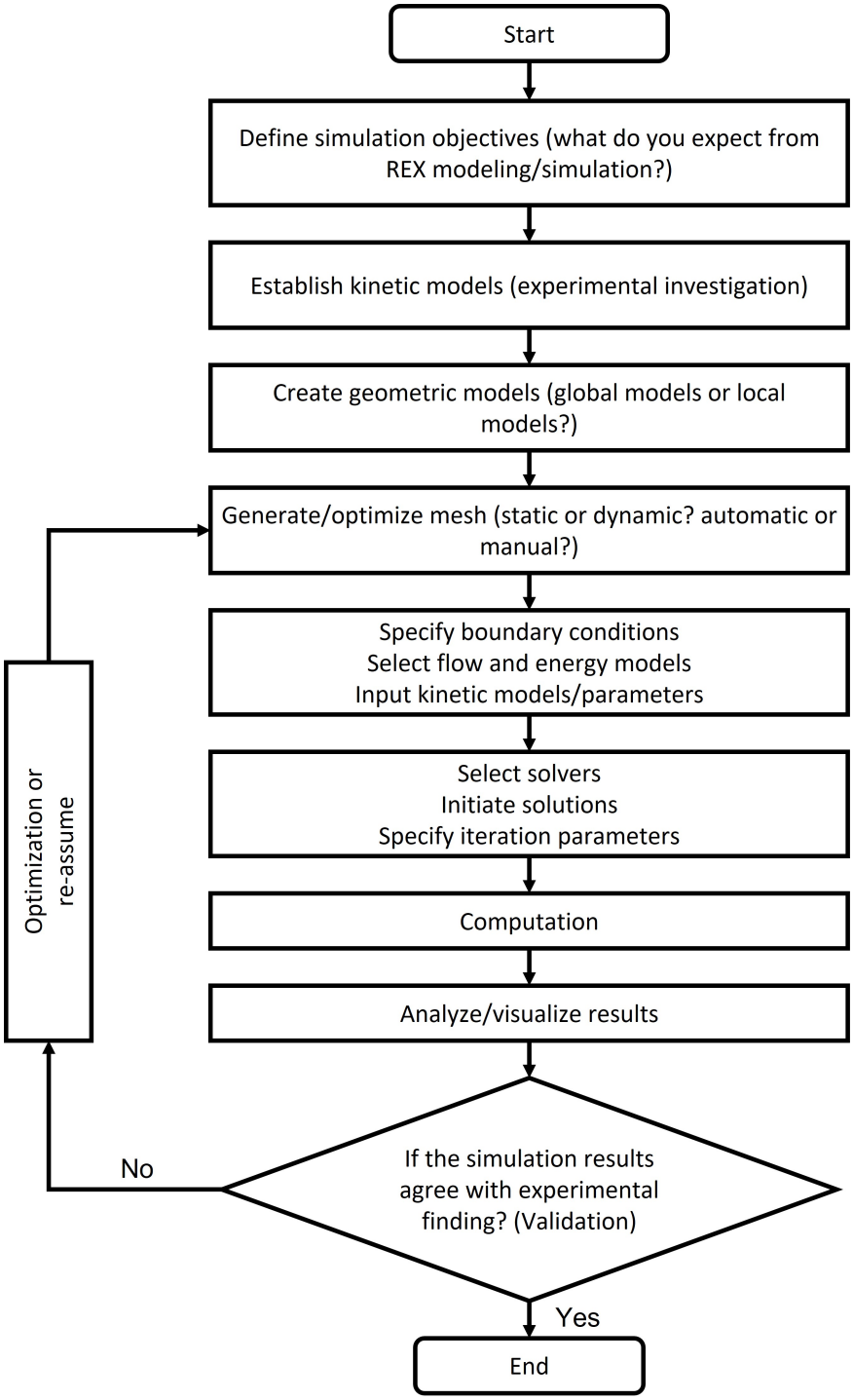

Figure (4.15) Flow chart of reactive extrusion (REX) computational fluid dynamics (CFD) simulation

4.7 UNCERTAINTIES

4.7.1 Limitations

Most polymerization reactions still rely on large stirred tank reactors, tubular reactors, fluidized bed reactors, or tower reactors. Highly exothermic reactions (chain-reaction polymerization, for example) generate too much heat for extruders to carry away. [75] Besides heat transfer surface, the limited residence times (a few seconds to a few minutes) limits applications with fast kinetics. [75] Because of the heat transfer limitations and short residence times, only a few polymerization reactions are carried out in reactive processing currently: polymethyl methacrylate (PMMA) bulk polymerization (and depolymerization), polyethylene (PE) controlled degradation, acrylic resin polymerization, nylon polycondensation, PC melt phase polycondensation, polyurethane polymerization, thermoplastic urethane (TPU) polymerization, and various grafting reactions (like maleic anhydride grafting). The main application of REX is to perform chain-modification reactions or improve the compatibility of two immiscible or partially miscible polymers.

4.7.2 Technical challenges

REX research involves multiple disciplines, i.e., chemical reaction engineering, rheology, polymer processing, and mechanics. Reactive processing creates value-added polymer products and chemicals via monomer-to-polymer, chain-modification, or polymer-to-monomer reactions. Many companies regard REX technology as an industrial secret. Technical challenges remain in developing a novel REX process or reforming an existing reactive extrusion production line.

Compared to a traditional compounding extrusion system, a REX system might require more upstream and downstream devices in addition to the extruders themselves. The upstream devices include liquid and powder feeding devices and polymer pre-treatment equipment. Pre-removal of impurities incorporated in polymer reactants is usually necessary for degradative extrusion recycling of polymer scraps since the closely intermeshing geometry of screws does not allow for the handling of large-sized infusible impurities. Serious screw seizing resulting from impurity blockage may result in screw torque, soar rise, and even screw fracture. Dosing a tiny stream of materials (like catalysts and compatibilizers) into an extruder is also a technical challenge, especially when the dosing rate is lower than 1 % on a lab-scale reactive extruder. Lab-scale REX equipment operates a throughput rate on the order of 5-40 $\mathrm{kg\,h^{-1}}$,

which is huge for a university environment as costs are enormous. Homogeneous and precise feeding of tiny streams demands costly equipment and is often technically unavailable.

The downstream devices contain cooling, sizing, and cutting equipment. Multiple atmospheric or vacuum vents are needed to trap and recover free reactants and undesirable by-products and volatiles. Filtration equipment is required to control contaminant content in products in some reactive processing cases, such as the production of silane-grafted cross-linkable PE where silane accumulation on screws and barrels can contaminate final products. [159] Furthermore, explosion-proof design and corrosion-resistant alloys are required if explosive and corrosive substances get involved in the production or are generated from reactions. In fact, REX often involves flammable monomers as reactants or products. All of these equipment considerations will inevitably increase the development difficulties and cost of lab-scale or industry-scale reactive extrusion systems.

The surface-to-volume ratio decreases as equipment is scaled up, which constrains heat transfer rates in a large-size reactive extruder. Severe thermal inhomogeneity may develop in production-size equipment but not at the lab-scale. [75] Large viscosity fluctuation exists in polymer-to-monomer and monomer-to-polymer reactive processing, which may bring about production instabilities (throughput fluctuation).

These instabilities are related to the scale of production equipment. [75] To achieve stable production, the whole reactive extrusion process also demands robust in-process monitor and control technology that needs further study.

4.7.3 Perspectives

REX processes mainly focus on standard polymer synthesis, such as TPU, modifying existing polymers, and upcycling. Future directions include flame-retardant polymers materials development, [160] green and solvent-free production of regular polymers (like LDPE and polyimides), [161, 162] REX intensified polymerization mechanisms, [163] proton exchange membranes for fuel cells, [164] compatibility blending of immiscible or partially miscible polymers, bio-based polymer production, [165] food packaging films processing, [166] polymer controlled degradation and depolymerization, and process intensification coupled REX. Alternative energy sources applied to REX include ultrasound, [150] microwave, and laser. Goto et al. [82] and Baek et al. [167] developed continuous supercritical decrosslinking extru-

sion to recycle crosslinked PE. Most recently, Arkema and JSW Europe successfully recycle MMA monomer from end-of-life PMMA using REX technology. [68] REX process control and monitoring is also an active area of research. In-line monitoring approaches (e.g., in-line Raman spectroscopy, [168] attenuated-total-reflectance ATR-FTIR, [169] and NIR spectroscopy [170]) are applied to explore reaction mechanisms in REX.

4.8 CONCLUSIONS

Reactive extruders handle highly viscous fluids. Their salient features include mixing capability, zoned temperature management, controlled residence time, segmented configuration of barrels and screw elements, and defined shear stress level. REX requires less or zero solvent and fewer processing units (pre- and post-treatments) and so can combine multiple chemical reactions in a single unit. However, they are best suited for fast and isothermic reactions. Design, safety considerations, scale-up, monitoring, and control of REXs are relatively more challenging than other processes. Due to relatively high equipment costs, reactive extrusion is best suited for high-value products or adding values to the existing polymers. Research in REX is directed toward polymer degradative recycling, polymerization of high-end monomers, polymer modification and functionalization, theory development, reaction mechanism investigation, and process simulation.

CHAPTER 5 ARTICLE 2 – UPCYCLING POLYMETHYL METHACRYLATE TO METHACRYLIC ACID

Yanfa Zhuang, Nooshin Saadatkhah, Tien-Dat Nguyen, Jacopo De Tommaso, Clive Yi Jie Ng, Chunyu Wang, Abdellah Ajji, Gregory S. Patience,

Published in Reaction Chemistry & Engineering on November 13, 2024

5.1 Abstract

Waste polymethyl methacrylate (PMMA) has become a more prominent contributor to global plastic waste in the aftermath of the COVID-19 pandemic. Recycling PMMA relies either on mechanical recycling or thermal depolymerization. Mechanical properties deteriorate after several mechanical recycling cycles. Depolymerization technologies operate in an inert atmosphere and requires costly monomer purifications d ownstream. Therefore, neither chemical nor mechanical recycling of PMMA is economically viable. Here, we demonstrate a sustainable recycling method through catalytic hydrolysis to upcycle PMMA while reaching higher product purity. PMMA reacts over zeolites and produce methacrylic acid instead of methyl methacrylate offering technical, economical, and market b enefits. Direct hydrolysis of PMMA over H-type zeolite with an SiO_2/Al_2O_3 ratio of 80 produced methacrylic acid with a yield of 56 % and selectivity of 58 %. Coke formed within the framework of large-pore zeolites, causing reversible deactivation of medium-strong acid sites and Brønsted acid sites. The catalytic decarboxylation of methacrylic acid primarily produces acetone and CO, and six-member glutaric anhydride forms in solid residues.

5.2 Introduction

Plastic waste is a continue challenge that spans generations. The Organization for Economic Cooperation and Development (OECD) reported that annual plastic production more than doubled 2000 to 2019, reaching 400 million tonne, [171] yet this number surged to 530 million tonne within just the first seven months of the COVID-19 pandemic [172]. The pandemic exacerbated the already existing plastic waste crisis [173].

The primary short-term impact of the pandemic was an unprecedented demand for personal protective equipment (PPE) in the healthcare and public sectors to combat the spread of

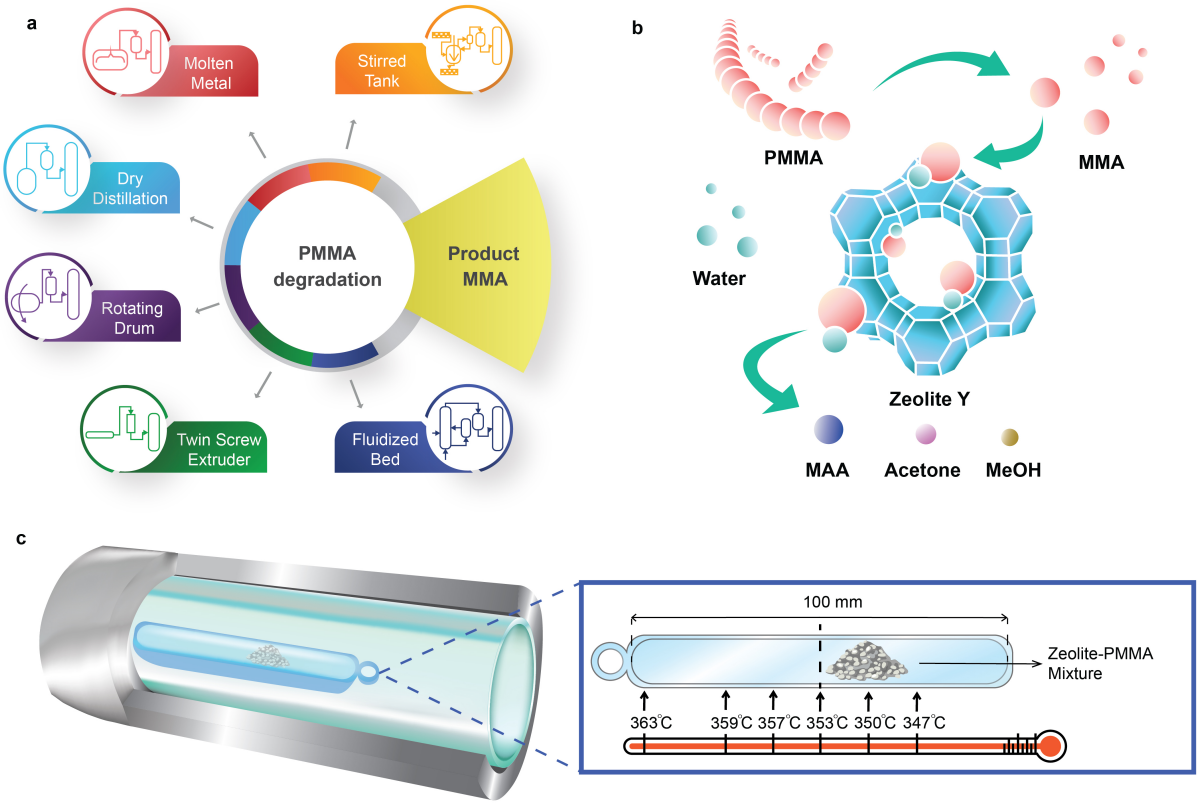

Figure (5.1) PMMA chemical recycling schemes. **a**, Conventional PMMA chemical recycling routes rely on PMMA thermal depolymerization to produce MMA monomer. **b**, In contrast to conventional PMMA chemical recycling, direct upcycling of PMMA to MAA monomer over zeolite catalysts yields a more versatile chemical block over MMA and so circumvents the issues related to MMA repolymerization. **c**, The double-layer 316L SS-quartz liner reaction tube and fused quartz boat with axial temperature difference for catalyst screening. Reaction temperature tolerance was ±3 °C.

the virus [174]. Simultaneously, single-use plastic ban legislation faced setbacks in many countries, including the USA, Canada, UK, France, India, and South Korea [175].

Fundamentally, the pandemic triggered a shift in behavior towards remote consumption modes, such as e-commerce and food delivery, which heavily rely on disposable plastics [172]. Consequently, the ongoing global economic slowdown, coupled with supply chain disruptions, has led to a reduction in post-industrial plastic waste and an increase in post-consumer waste, which is more challenging to collect and recycle. The disruption of recycling initiatives at both local and international levels has hindered the ability to manage this transition [171,176], particularly concerning single-use healthcare waste streams, where low manufacturing cost outweigh high collection and treatment expenses [177].

In the current scenario, to achieve absolute sustainability in human activities by 2030, defined as adhering to the Safe Operating Space (SOS) to prevent destabilizing the Earth's planetary system, hinges on a global mass-to-mass plastic recycling rate exceeding 71 % [178]. This target is unreachable, even with the current most advanced recycling technologies. By 2050, 94 % of plastic is projected to be recycled or incinerated, while 6 % is expected to be discarded [179]. In fact, even assuming the recycling of the maximum theoretically possible plastic amount (94 %), the material losses on the recycling chain impedes reaching complete sustainability. Achieving this target requires higher plastic-to-plastic yielding technologies (e.g. plastic to monomer or chemicals) [178].

Polymethyl methacrylate (PMMA), known as Plexiglas, Lucite, and Perspex, stands out as one of the prime candidates for achieving high yield plastic-to-plastic recycling [2]. PMMA attracted considerable attention during the pandemic, serving as protective barriers. This thermoplastic is distinguished by its tensile and flexural strength, UV resistance, and transparency, making it a versatile and multifunctional material. In 2021, the global PMMA market exceeded 4.5 billion USD, [2,180] and it is projected to reach an annual production of 3 million tonne by 2028, with its primary applications spanning the automotive, construction, electronics, signage, and coatings industries.

Europe, Asia Pacific, and America each account for roughly one-third of the global PMMA market, collectively representing 93 % of the market [181]. Despite Europe's above-average ranking in overall macro-regional plastic recycling [171], Europe recycled only 30 000 tonnes of PMMA in 2019, which is approximately 10 % of the total PMMA waste [182]. This results

in an annual volume of 800 000 t to 1 000 000 t of unaddressed waste PMMA worldwide [183].

PMMA has a ceiling temperature of 192 °C [184, 185] and pyrolyzes to MMA with a yield greater than 90 % between 350 °C and 450 °C [3, 67, 68] (Fig. 5.1a). The European MMAtwo project successfully demonstrated a pilot-scale, extrusion-based pyrolysis process to depolymerize selected cast, injection, and extrusion-grade scraps, achieving a plastic-to-monomer yield of 80 % to 90 % and a MMA purity of 99.8 % [56]. Pyrolysis of PMMA to MMA holds promise for maintaining carbon within the economy. However, it is not a universal solution for all types of PMMA-based waste.

Depending on the nature of the scraps or the depolymerization process, the resulting crude regenerated MMA (r-MMA) may contain impurities, such as methyl pyruvate, methyl or ethyl propionate, methyl isobutyrate, methyl acrylate, or ethyl acrylate, which have close boiling points and chemical structure with MMA [7, 8]. For example, ethyl acrylate shares the same boiling point as MMA (100 °C), and has an odour threshold 200 times higher [186], posing challenges for the pyrolysis process and the quality of the resulting product. PMMA polymerization follows a radical mechanism [67, 187], and acrylates generally create radicals more effectively than MMA in most situations, so even a small fraction triggers repolymerization at 25 °C to 180 °C [188–191], resulting in pipe blockages (Supplementary Fig. 5.8). Low quality scraps produce a lower quality r-MMA with more impurities [2, 182], which hinder its commercialization in strictly regulated markets, or those requiring high-quality monomer [192]. Similarly, some batch depolymerization technologies like dry distillation, or rotating drum maximize the contact between depolymerizing PMMA and the char formed from the reaction. This facilitates hydrogen transfer reactions of MMA, such as MMA to methyl isobutyrate, a volatile compound with the same boiling point as MMA [182].

PMMA upcycling to methacrylic acid (MAA) instead of MMA can enhance the polymer recycling capacity, and represents an alternative solution that offers significant technical, economic, and market benefits [16, 193]. MAA, as a functional monomer, is widely used in synthesis of copolymers with other monomers, its esters (e.g. MMA), and MAA salts. In addition, MAA serves as a valuable specialty chemical in applications such as paints, leather and textile treatment agents, adhesives, and ion-exchange resins [11,12]. In contrast to MMA, the market volumes of MAA (in terms of import and export) are approximately one-tenth the size, with roughly 150 000 t traded globally, compared to the 1 500 000 t of MMA [194] . Due to its smaller volumes and its niche applications, MAA has fewer suppliers, and there is

consumer interest in having new producers to enhance market elasticity and decouple MAA dynamics from those of MMA.

In a recent study, Chub et al. [16] synthesized MAA by integrating the depolymerization of virgin PMMA to MAA with its subsequent catalytic hydrolysis of MMA in a fluidized bed reactor. They evaluated the effect of various catalysts Al_2O_3, FCC, Cs−HPA, zeolite Y, $ZrO_2MoO_{3/}SiO_2$ and sand, and found that zeolite Y achieved the highest yield of MAA at 33 %. However, their study outlined a simplified mechanism for MAA production and did not fully explore side reactions that affect the overall yield. Additionally, it lacked detailed analysis of zeolite properties such as micropore shape-selectivity and the influence of the SiO_2/Al_2O_3 molar ratio. In follow-up research, the team developed a tandem reactor system, initially producing MMA in a fluidized sand bed, followed by MMA hydrolysis to MAA using zeolite Y in a fixed bed reactor [64]. Despite its innovative design, this system only achieved a maximum PMMA conversion of 53 % and an MAA yield of up to 48 %.

Here, we introduce a sustainable catalytic hydrolysis method to directly upcycle PMMA to MAA monomer over zeolite catalysts from 330 °C to 370 °C in a fixed bed reactor. Upcycling PMMA to MAA integrates PMMA thermal depolymerization and in-situ MMA hydrolysis (Fig. 5.1b). We investigated the activity of zeolite Y, ZSM-5, zeolite Beta, Mordenite (MOR) and desilicated zeolite Y in a double layer reaction tube (Fig. 5.1c). Direct hydrolysis of PMMA over zeolite Y-80 (SiO_2/Al_2O_3=80) exhibited the highest MAA yield (56 %) and MAA selectivity (58 %) at 350 °C. The MAA can be purified and converted to MMA for polymerization purposes, or sold as is.

5.3 Experimental

5.3.1 Materials

We purchased zeolites, including HY(80), HY(60), HY(30), Hβ(360), NH_4-MOR(20), NH_4-ZSM-5(200−400), and NH_4-ZSM-5(80), as well as virgin PMMA (Mw=550 000 g mol^{-1}) from Thermo Scientific Chemicals. All ammonium type zeolites were calcined at 550 °C for 2 hours (heating up by a 2 °C min^{-1} ramp) to form proton type HMOR (20), HZSM-5(200-400) and HZSM-5(80). Prior to each experiment, all samples were vacuum dried at 70 °C for 24 h. For all zeolites, the number in parenthesis indicates the SiO_2/Al_2O_3 mole ratio.

5.3.2 Preparation of desilicated Zeolite Y-80

Commercial HY(80) was desilicated in 0.05M, 0.1M, 0.2M and 0.3M NaOH solutions at 60 °C for 30 min, followed by filtration. The filtered samples were washed with deionized water until reaching neutral pH and dried overnight at 110 °C. The dried samples were further exchanged with 0.5M of NH_4NO_3 three times and then dried overnight at 110 °C. The NH_4^+ exchanged samples were finally calcined at 550 °C for 6 h in air. The desilicated HY(80) catalysts were labelled M0.5, M1, M2 and M3 corresponding to the NaOH solution concentration.

5.3.3 Regeneration of coked Zeolite Y-80

Reacted HY(80) at 350 °C for 35 min calcined at 550 °C for 6 h (2 °C min^{-1} ramp) to remove coke. R-HY(80) represents regenerated HY(80).

5.3.4 Characterization

X-ray powder diffraction (XRD)

The X-ray diffraction patterns of zeolites were measured by a Bruker D8 Advance Diffractometer with Cu Kα radiation in the 2θ angle range of 5° to 90° (scanning step=0.02°).

N_2 adsorption

Surface area and porosity were determined by N_2 adsorption at −196 °C on a Quantachrome Autosorb-1 analyzer. Prior to adsorption, samples were vacuum-degassed at 350 °C for 12 hours. The total specific surface area was estimated based on multi-point Brunauer-Emmett-Teller (BET) method in the $0.05 < P/P_0 < 0.30$. The total pore volume was determined according to the adsorbed N_2 volume at $P/P_0 = 0.99$. The volume of micropores and the specific surface area of mesopores were calculated by t-plot method in the t range of 3.5 Å to 5.0 Å. The Barrett-Joyner-Halenda (BJH) model was applied to determine the pore size distribution and the average pore size.

Particle size distribution (PSD)

The particle size distribution (PSD) was measured with a laser diffractometer (Horiba, LA950).

Scanning electron microscopy with energy dispersive X-ray spectroscopy (SEM/EDS)

A JEOL JSM-7600F Scanning Electron Microscopy (SEM, with a Schottky field emission gun) with an Oxford Instruments X-MaxN Energy Dispersive Spectroscopy (EDS) detector (with an active area of 80 mm^2 and a spectral resolution 123 eV) characterized the morphology and element mapping of zeolite and PMMA samples.

Transmission electron microscopy with energy dispersive X-ray spectroscopy (TEM/EDS)

A JEOL JEM-2100F Transmission Electron Microscope (TEM, operating with a high voltage 200 kV) with an Oxford TEM Xplore detector scanned C-HY(80) sample, and generated bright field images and EDS element maps based on selected area electron diffraction (SAED). C-HY(80) represented coked HY(80).

X-ray photoelectron spectroscopy (XPS)

The X-ray photoelectron spectroscopy (XPS) spectra was recorded using a VG Scientific Escalab 250Xi photoelectron spectrometer with a mono Al Kα radiation source. The pressure in the analysis chamber was 1.0×10^{-8} Torr. Spectra were recorded with a pass energy of 150 eV for the survey scans and 20 eV for the high resolution scans. The binding energies were corrected by the Si 2p core level (103.3 eV).

Ammonia temperature-programmed desorption (NH_3-TPD)

An AMI-300 Chemisorption Analyzer with a thermal conductivity detector measured ammonia temperature-programmed desorption (NH_3-TPD). Each sample dried under He at 350 °C for 5 h and adsorbed NH_3 at 50 °C for 1 h, followed by He flushing at 60 °C for 2 h. NH_3-TPD

curves were recorded by ramping the temperature from 60 °C to 550 °C at a rate of 2 °C min^{-1}.

Fourier-transform infrared spectroscopy (FTIR)

Functional groups of unreacted PMMA were investigated by a PerkinElmer Spectrum 65 FTIR spectrometer. Acetone dissolved unreacted PMMA in the solid residues and stood at room temperature for 12 h. The supernatant dropped on the surface of spectrometer's sample chamber and evaporated at room temperature for 10 min. The spectrometer scanned the PMMA film formed after acetone evaporation from 4000 to 600 cm^{-1}.

Pyridine-IR

The Fourier-transform infrared (FTIR) spectra of the pyridine adsorbed zeolites was recorded by a Bruker Tensor 27 FT-IR Spectrometer. Each sample was evacuated under vacuum (0.001 Pa) at 400 °C for 1 h. Pyridine vapor was introduced into the sample cells at room temperature and the adsorption was kept for 30 min. The desorption was performed under vacuum (0.001 Pa) at 150 °C and 350 °C, respectively, for 30 min. After cooling to room temperature, the desorbed samples were scanned from 1400 to 1700 cm^{-1}. The concentration of Lewis and Brønsted acid sites was determined by spectra bands at 1450 cm^{-1} and 1550 cm^{-1}.

Gel permeation chromatography (GPC)

A Thermo Scientific UltiMate 3000 HPLC system equipped with two tandem Shodex GPC KF-803L and KF-804L columns (target Mw range: 100–300,000 g mol^{-1}) measured the molecular weight (Mw) of unreacted PMMA. The GPC system, calibrated with the Shodex PMMA calibration kit STANDARD M-75 (Mw range: 2.79×10^3 to 1.01×10^6 g mol^{-1}, employed a Refractive Index (RI) detector and tetrahydrofuran (THF) as the eluent. The flow rate of THF eluent was 1 mm min^{-1}. The temperature of RI detector and column remained at 35 °C. THF dissolved unreacted PMMA in the solid residues and stood at room temperature for 12 h. The supernatant was injected into GPC system.

TGA under different atmospheres

A NETZSCH STA 449 F3 Jupiter Thermal Analyzer determined PMMA thermogravimetric degradation curve under steam and N_2 mixture atmosphere. The commercial PMMA powder equilibrated at 130 °C for 30 min followed by heating from 130 °C to 700 °C with a ramp of 5 °C min^{-1} under the mixture atmosphere of 70 mL min^{-1} of steam and 30 mL min^{-1} of N_2. A TA Instruments Q500 Thermogravimetric Analyzer determined PMMA thermogravimetric degradation curve under 60 mL min^{-1} of N_2. The same PMMA powder heated up from room temperature to 700 °C with a ramp of 5 °C min^{-1}.

Differential scanning calorimetry (DSC)

Differential scanning calorimetry (DSC) determined the glass transition temperature (T_g) of PMMA using DSC Q-2000 (TA Instruments). To eliminate the thermomechanical history, PMMA encapsulated in an aluminum pan thermally equilibrated at 135 °C for 10 min. After cooling to 40 °C, the sample heated up to 200 °C with a ramp of 10 °C min^{-1} with 50 mL min^{-1} of N_2 to protect all heating and cooling cycles.

5.3.5 Gas, liquid and solid products analysis

An Agilent 7890A GC system equipped with a Thermal Conductivity Detector (TCD) analyzed the gas effluent. The GC comprised a two-column system. An Agilent Hayesep Q 80/100 UltiMetal column (0.5 m×1/8"×2 mm) separated CH_4 and CO_2, while an Agilent J&W MolSieve 13X 80/100 UltiMetal column (1.5 m ×1/8"×2 mm) separated CO and H_2. An extra Agilent Hayesep Q 80/100 UltiMetal column (1 m×1/8"×2 mm) as a precolumn was used in a backflush to detector.
An Agilent 7890A GC system equipped with Agilent 7693 Autosampler and Agilent 5975C Mass Selective Detector (MSD) mass spectrometry qualitatively and quantitatively analyzed the liquid products. An Ultra Inert (UI) capillary column, Agilent J&W DB-Wax UI (polyethylene glycol stationary phases, length 30 m, inner diameter 0.25 mm, film thickness 0.25 µm), separated components. MSD scanned *m/z* (mass-to-charge ratio) from 29 to 500 in the qualitative analysis. Selected ion monitoring (SIM) mode was used to quantitatively analyze acetone (selected *m/z* 43 & 58) , methanol (selected *m/z* 31), MMA (selected *m/z* 41, 69 & 100) and MAA (selected *m/z* 41 & 86). The concentration of four components was determined by external calibration. External calibration standards were prepared by

mixing acetone (HPLC grade, $\geq$ 99.9 %, Sigma-Aldrich), methanol (HPLC grade, $\geq$ 99.9 %, Sigma-Aldrich), MMA ($\geq$ 99.6 %, stabilized with 6-tert-Butyl-2,4-xylenol, TCI America™) and MAA (99 %, containing 250 ppm MEHQ as inhibitor, Sigma-Aldrich) in the 4:1 (volume ratio) solvent mixture of ultrapure water (HPLC grade, Thermo Scientific™) and anhydrous ethanol (HPLC grade, Commercial Alcohols).

PMMA conversion (X_{PMMA}), product selectivity (S_{i}) and yield (Y_{i}) follow equations:

$$X_{\mathrm{PMMA}} = \frac{\text{corresponding MMA moles in degraded PMMA}}{\text{corresponding MMA moles in PMMA fed}} \times 100 \tag{5.1}$$

$$S_{\mathrm{i}} = \frac{\text{moles of comp. i produced} \times \text{No. of carbon in comp. i}}{\text{corresponding MMA moles in degraded PMMA} \times 5} \times 100 \tag{5.2}$$

$$Y_{\mathrm{i}} = \frac{\text{moles of comp. i produced} \times \text{No. of carbon in comp. i}}{\text{corresponding MMA moles in PMMA fed} \times 5} \times 100 \tag{5.3}$$

where i represents liquid product components (i.e. MMA, MAA, MeOH and acetone). The abbreviation comp. stands for component.

A TA Instruments Q500 Thermogravimetric Analyzer determined the mass of unreacted PMMA and the coke formed in the solid residues. The residue samples were heated from 25 °C to 700 °C with a ramp of 5 °C min^{-1} under 60 mL min^{-1} of air flow. A LECO CS744 analyzer equipped with an IR detector was applied to measure the mass fraction of total carbon remaining in the reacted solid residue by combusting samples at 1300 °C to 1400 °C with tungsten and iron accelerators.

5.3.6 Experimental set-up and procedure

PMMA was hydrolyzed in a 450 mm-long, ultra-high-polished 316L stainless steel (SS) tube (OD=25.4 mm, ID=22 mm; interior smoothness Ra=10), which was lined with a 450 mm-long quartz tube (OD=21.6 mm, ID=18 mm). A CARBOLITE GERO horizontal split tube furnace heated a 316L SS-quartz double-walled reaction tube. A mixture of 0.2 g PMMA and 0.2 g zeolite was placed in a fused quartz boat (100 mm × 15 mm × 7.5 mm) in the middle of the reaction tube. A thermocouple above the fused quartz boat recorded temperature in real time. A Swagelok 316L SS sample cylinder (150 mm) wrapped with a fibreglass heater

tape evaporated 2 mL min^{-1} of water and generated steam at 450 °C. Helium (170 mL min^{-1}) carried the steam into the reaction tube. To avoid interference with the H_2 peak during gas analysis, we opted for helium over nitrogen as the carrier gas. The gaseous products from the reaction tube condensed in a Synthware Graham condenser, followed by a Synthware liquid nitrogen cold trap. A Supel inert multi-layer foil gas bag collected all produced gases. Each reaction lasted for 35 min.

5.3.7 Kinetic diameter estimation

Kinetic diameter estimation referred to a universal electron density isosurface method proposed by Mehio et. al. [195] Gaussian 16W optimized and generated wavefunction of MMA and MAA molecules at PBE0/def2-TZVP level. Based on the wavefunction, Multiwfn program [196] quantitatively analyzed molecular surface using 0.0015 a.u. as an electron density isovalue, and yielded all surface vertices. VMD software visualized molecular surface vertices and measured the distance between two surface vertices reflecting kinetic diameter characteristic.

5.3.8 In-situ liquid and gas products analysis

A Synthware Graham condenser cooled down condensable gaseous products that were generated from 160 °C to 350 °C. Dozens of vials with 2 mm of ethanol collected liquid products from Graham condenser every minute. An Agilent 7890A-6975C GC-MSD analyzed each sample corresponding to a specific reaction temperature. A HIDEN HPR-20 QIC R&D quadrupole mass spectrometers online monitored gas composite after condensation.

5.4 Results and discussion

5.4.1 PMMA hydrolysis activities over zeolites

The temperature gradient along the axial direction of the fused quartz boat exceeded 16 °C (Fig. 5.1c). Consequently, we positioned the samples in a zone where the temperature ranged from 347 °C to 353 °C with a temperature setpoint at 350 °C. The evaporation of products during sample collection inevitably results in carbon loss (Fig. 5.2a & Supplementary Table 5.1). Also, a small fraction of liquid products evaporate and enter the gas bag, further

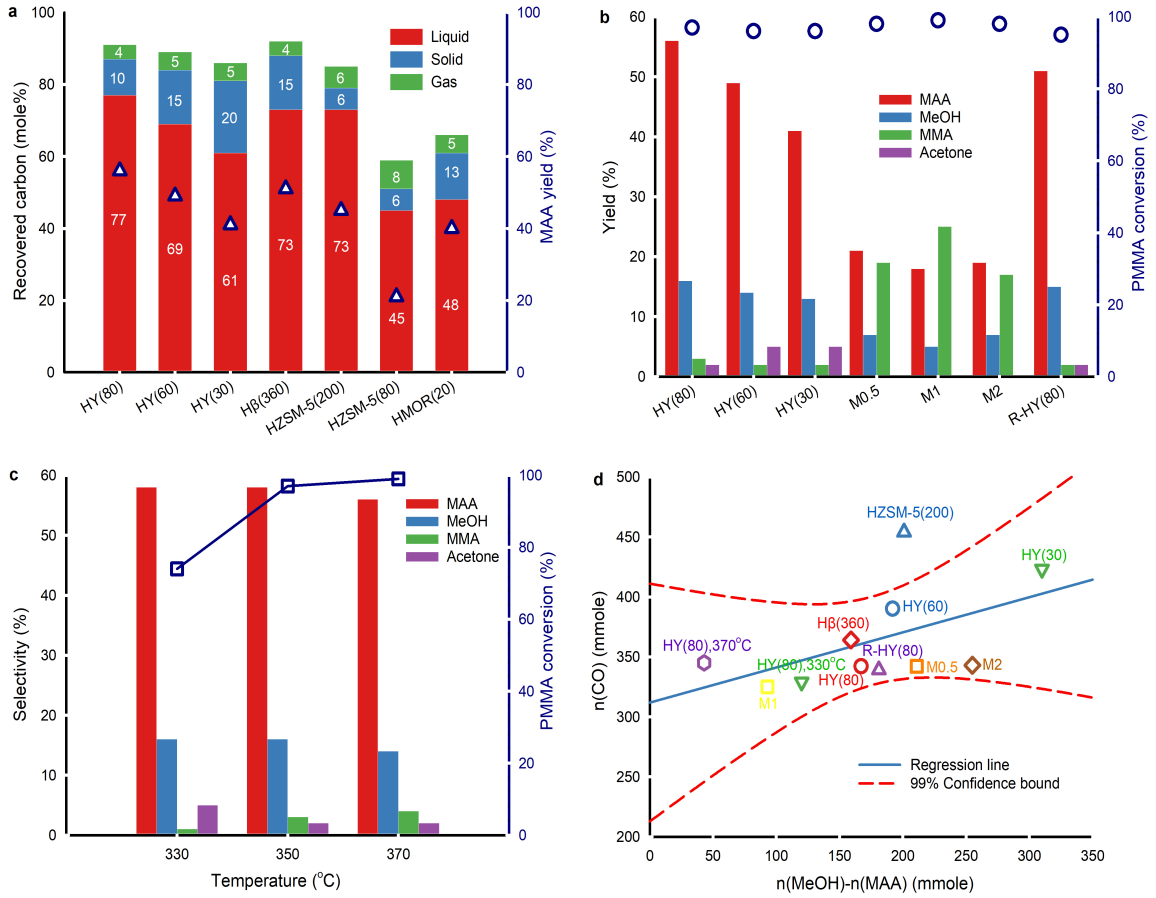

Figure (5.2) PMMA hydrolysis over fresh, activated, regenerated and desilicated zeolite catalysts. Each experiment contained 0.2 g virgin PMMA and 0.2 g zeolite. **a**, Recovered carbon, and MAA yield (right axis, hollow triangle) at 350 °C for 35 min with 2 mL min^{-1} liquid water injection. **b**, MAA, MeOH, MMA and acetone yield, and PMMA conversion (right axis, hollow circle) over fresh, desilicated and regenerated zeolite Y at 350 °C for 35 min with 2 mL min^{-1} liquid water injection. **c**, The effect of reaction temperature on the selectivity of MAA, MeOH, MMA and acetone, and PMMA conversion (right axis, hollow square) over fresh HY(80) with 35 min of reaction time and 2 mL min^{-1} liquid water injection. **d**, The correlation between the mole of CO and the difference of the mole of MeOH and MAA over various catalysts at 350 °C for 35 min with 2 mL min^{-1} of water injection. HMOR(20) and HZSM-5(80) excluded due to a huge deviation between n(CO) and n(MeOH)-n(MAA). All fresh, regenerated and desilicated zeolite Y, and Hβ(360) lied within 99% confidence interval.

restricting quantitative detection of liquid products. The carbon recovery over fresh zeolite Y with a SiO_2/Al_2O_3 ratio at 80, 60 and 30, and Hβ(360) was >85 % at 350 °C. The best carbon balance was 95 % over fresh HY(80) at 330 °C due to higher unreacted PMMA residues. Carbon content in solid residues is easier to quantify than liquid and gaseous products. In reactions over ZSM-5, MOR, and HY(80), carbon recovery falls below 85 %. The decrease in SiO_2/Al_2O_3 ratio on zeolite Y, from 80 to 30, and ZSM-5, from 200 to 80, led to a lower MAA yield, which corresponded to lower carbon recovery. The highest MAA yield was over HY(80) followed by Hβ(360). HZSM-5(80) and desilicated zeolite Y (M0.5, M1 and M2) had the lowest carbon balance ($\leq$ 60 %) and MAA yield ($\leq$ 24 %).

Based on the catalyst screening, Y type zeolite produced MAA with the highest yield. Consequently, we focused on Y type zeolite in this work. All fresh, desilicated and regenerated zeolite Y converted $\geq$ 95 % of PMMA at 350 °C (Fig. 5.2b). The acidity of zeolite Y influences the yields of MAA and methanol. A lower SiO_2/Al_2O_3 ratio, which corresponds to higher acidity (Supplementary Table 5.3), led to a decreased yield of MAA and methanol but an increased yield of acetone. From HY(80) to HY(30) (SiO_2/Al_2O_3=80 to SiO_2/Al_2O_3=30), the MAA yield decreased by 37 % (from 56 % to 41 %), and the methanol yield decreased by 23 % (from 16 % to 13 %), while the acetone yield increased 2.5-fold (from 2 % to 5 %). Specifically, the acetone yield was 4.8 % over HY(60) and 5.1 % over HY(30) based on the original experimental results. Due to rounding, both were represented as 5 % in the Fig. 5.2b. The more pronounced reduction in MAA yield compared to methanol, coupled with the rise in acetone production, suggests potential over-cracking of MAA and/or MMA into acetone. Desilicated zeolite Y, treated with varying concentrations of NaOH, produced more MMA but less MAA and methanol compared to fresh zeolite Y. Among the desilicated samples, M1 showed the highest yield of MMA but the lowest yields of MAA and methanol. Interestingly, none of the desilicated zeolites generated acetone. This suggests that specific active sites within the zeolitic framework are responsible for acetone formation. The desilication treatment may have compromised the zeolitic framework, leading to the loss of some active sites. R-HY(80) displayed equivalent MMA yield to fresh HY(80) but slightly lower yield of MAA, methanol and acetone.

The PMMA conversion increased by 31 % from 330 °C to 350 °C and slightly rose from 350 °C to 370 °C over fresh HY(80) (Fig. 5.2c). The selectivity to MAA and methanol remained constant at 330 °C and 350 °C, but decreased at 370 °C. At 330 °C, there was lower selectivity to MMA but higher selectivity to acetone compared to 350 °C and 370 °C. Higher temperature favoured faster PMMA depolymerization. Nevertheless, excessive temperature resulted in

lower selectivity to MAA and methanol due to further undesired reactions of both MMA and MAA. The optimal PMMA hydrolysis performance was on HY(80) at 350 °C.

PMMA depolymerizes to $CH_3O(CO)\cdot$ free radical fragment, converting to either methanol and CO or CO_2 and CH_4 via combining with one H· proton abstracted from other H-containing components [67]. Among all the catalysts, only HY(80) at 370 °C and HMOR(20) at 350 °C formed CH_4 ($\leq$ 0.1 mol %) (Supplementary Table 5.1). This confirmed that the $CH_3O(CO)\cdot$ fragment primarily formed CO and methanol.

PMMA hydrolysis without any catalyst at 350 °C with 2 mL min^{-1} of H_2O injection resulted in approximately the same CO_2 yield as PMMA hydrolysis over zeolites except M2 and unblended HY(80) on PMMA (Supplementary Table 5.1). We attributed the primary detected CO_2 to external sources, i.e. CO_2 entering during H_2O injection and gas collection. Small amounts of CO_2 might result from thermal degradation of MMA/MAA. If PMMA depolymerizes to MMA and partially to $CH_3O(CO)\cdot$ fragment, followed by MMA hydrolysis to MAA and methanol along with $CH_3O(CO)\cdot$ cracking to CO and methanol, the CO amount would theoretically equal to the mole difference between the collected methanol and MAA. The CO yield, however, did not correlate to the difference between methanol and MAA by 1:1 linear relationship over all zeolites (Fig. 5.2d). This discrepancy was attributed to the dehydration of methanol to dimethyl ether (DME) [16]. The formation of acetone is likely to also affect this relation. Fresh, regenerated and desilicated zeolite Y and Hβ(360) followed a linear distribution and fell within 99 % confidence intervals, indicating a similar reaction mechanism to generate CO and methanol among zeolites. HZSM-5(200), HZSM-5(80) and HMOR(20) significantly deviated from the linear regression confidence intervals. More aggressive cracking reactions occurred on ZSM-5 and MOR, resulting in more CO (Supplementary Table 5.3). As proton-type ZSM-5 is a common solid acid catalysts for methanol dehydration to DME [197], we attributed part of this deviation to more aggressive methanol dehydration.

As the acidity of fresh zeolite Y increased from HY(80) to HY(30), the CO yield gradually rose (Fig. 2d). At 350°C, PMMA hydrolysis produced 3.4 mol % CO over HY(80), 3.9 mol % CO over HY(60), and 3.9 mol % CO over HY(30) (Supplementary Table 5.1). Along with this increase in acidity, the acetone yield also increased, while the yield of MAA decreased. The similar upward trends of CO and acetone, as acidity increased, suggest that MAA cracking may co-generate both CO and acetone.

5.4.2 Effect of zeolite structure and acidity on PMMA hydrolysis

Commercial H-type zeolite Y and β, activated ZSM-5, and activated MOR displayed typical diffraction peaks compared with simulated XRD patterns for zeolites collected in ref. [198] (Fig. 5.3a and Supplementary Fig. 5.9). R-HY(80) retained the same crystallographic structure as fresh zeolite Y, indicating no framework destruction after regeneration at 550 °C. However, diffraction peaks nearly disappeared in M0.5, M1 and M2, suggesting a damaged crystal structure post-desilication. Only two small and broad crystal faces of (220) and (531) were detected. Broad peaks reveals smaller or zero crystallites on desilicated samples [199]. Even though desilication created meso-pores on HY(80), NaOH treatment corrupted the crystal structure.

Desilicated zeolite Y (M0.5, M1 and M2) exhibited low specific area from $43\,m^2\,g^{-1}$ to $128\,m^2\,g^{-1}$ and insignificant micropore volume, but higher average pore diameter (39 Å to 87 Å) compared to fresh HY(80) (Supplementary Table 5.2). In sample M3, the Si/Al ratio indicated that too concentrated NaOH solution caused excessive desilication. Even though desilication generated more mesoporous channels which facilitates molecular diffusion, the framework collapse weakened the microporous networks's shape-selectivity [200] and caused amorphous aluminosilicate with substantial mesoporosity [201].

NH_3-TPD identified and quantified weak acid sites at 100 °C to 250 °C and medium strong acid sites at 250 °C to 550 °C on fresh, regenerated, desilicated and coked zeolite Y (Fig. 5.3b and Supplementary Table 5.3) [202]. With the increase in SiO_2/Al_2O_3 ratio, fresh H-type zeolite Y displayed lower acidity on weak and medium strong acid sites simultaneously. The amount of weak acid sites and medium strong acid sites on R-HY(80) increased by 55 % and rose fourfold, respectively, compared with fresh HY(80). The Si/Al ratio of R-HY(80) was slightly higher than that of fresh HY(80) (Supplementary Table 5.2). A slight dealumination happened during catalyst regeneration at 550 °C. Weak acid mainly derives from NH_3 desorption from Si – OH groups and the extra-framework Al species, while medium strong acid principally comes from NH_3 desorption from bridging Si – OH – Al acidic hydroxyls in framework [203]. We attributed the increase of weak acid strength on R-HY(80) to the extra-framework Al species resulting from framework Al extraction. Meanwhile, partial extra-framework Al interacted with Si – OH – Al, which enhances medium strong acidity [204]. Surprisingly, medium strong acid sites on M0.5 and C-HY(80) disappeared entirely. NaOH

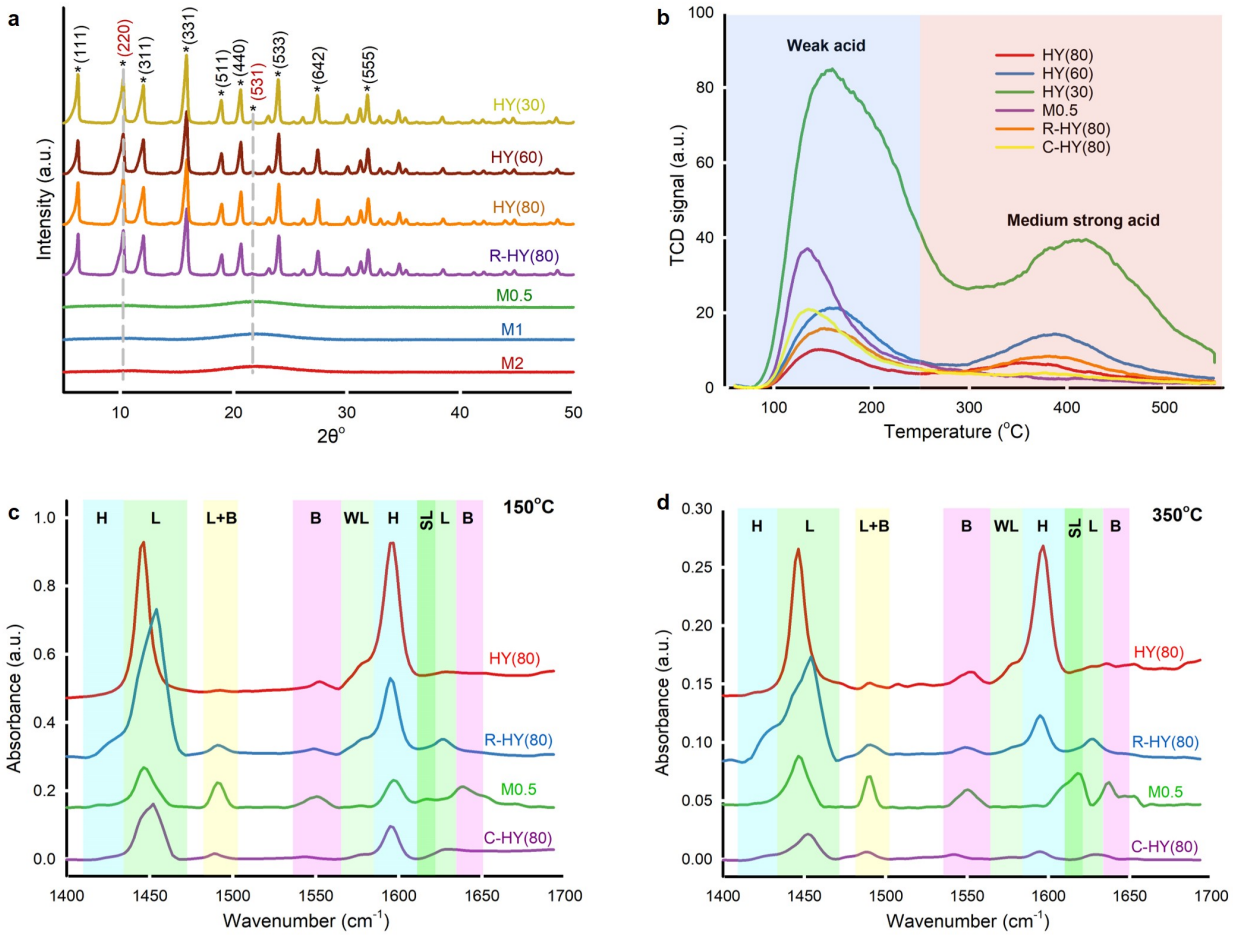

Figure (5.3) Characterization of fresh, activated, regenerated, desilicated and coked zeolite catalysts. **a**, X-ray powder diffraction over fresh, regenerated and desilicated zeolite Y. **b**, NH_3-TPD curves over fresh, desilicated, regenerated and coked zeolite Y starting from 50 °C to 550 °C. **c**, **d**, FTIR spectra of adsorbed pyridine on fresh, regenerated, desilicated and coked HY(80) with pyridine desorption temperature of 150 °C (**c**) and 350 °C (**d**). Characteristic bands identified hydrogen-bonded pyridine (H), Lewis acid site (L), Brønsted acid site (B), weak Lewis acid site (WL), strong Lewis acid site (SL) and the combination of Lewis and Brønsted acid site (L+B).

treatment at 60 °C destroyed the Si – O – Al bridge-linking framework of zeolite Y, and produced amorphous aluminosilicate that only exhibited weak acid sites. Zero medium strong acid sites on C-HY(80) confirmed coke mainly formed on the surface of Si – OH – Al groups in the zeolite framework and wholly deactivated these active sites and blocked zeolitic channels. A higher amount of weak acid strength on C-HY(80), compared to fresh HY(80), implied carbon-based solid residues may contain acid components interacting with the NH_3 probe molecule.

Pyridine-adsorbed FT-IR (Py-IR) analysis further distinguished Lewis and Brønsted acid sites on fresh, regenerated, desilicated and coked HY(80) at a pyridine desorption temperature of 150 °C and 350 °C (Fig. 5.3c & d and Supplementary Table 5.3). We attributed spectra bands at 1450, 1577, 1615 and 1628 cm^{-1} to C – C bond stretching vibrations of pyridine adsorbed on Lewis acid sites (LAS) [205, 206], and spectra bands at 1425 and 1596 cm^{-1} to hydrogen-bonded pyridine combined with zeolite surface's silanol groups [207, 208]. Pyridine ions protonated by Brønsted acid sites (BAS) generated two spectra bands at 1550 and 1640 cm^{-1} [205]. The spectra band at 1490 cm^{-1} corresponded to pyridine adsorbed on both of Lewis and Brønsted acid sites [209]. We further clarified weak LAS at 1577 cm^{-1} and strong LAS at 1615 cm^{-1} [206, 210]. The four-coordinate framework Al in zeolite Y contributes to BAS, yet extra-framework Al species generated by dealumination induced LAS [211, 212].

Compared with fresh HY(80), R-HY(80) had more LAS centered at 1450 cm^{-1} but less SiOH groups located at 1596 cm^{-1} and less BAS at 1550 cm^{-1}. Meanwhile, a new spectra band at 1425 cm^{-1} related to SiOH groups appeared on R-HY(80). Steam treatment reversibly transforms strong LAS into BAS, whereas thermal treatment causes an irreversible conversion of some BAS into LAS [213]. We attributed the reduction of BAS and the increase of LAS on R-HY(80) to zeolite dealumination during calcination at 550 °C. Desilication enhanced BAS located at 1550 cm^{-1} and acid sites corresponding to the combination of LAS and BAS at 1490 cm^{-1} band, but reduced both of LAS centered at 1450 cm^{-1} and SiOH groups stood at 1596 cm^{-1}. Presumably desilication caused some extra-framework Al species due to framework collapse and these Al species interacted with Si – OH – Al groups to strengthen peak at 1490 cm^{-1}. C-HY(80) showed only one predominant peak at 1450 cm^{-1} corresponding to LAS at a pyridine desorption temperature of 350 °C. The marked decline of BAS on C-HY(80) indicated coke primarily formed on the surface of BAS generated by Si – OH – Al in the zeolitic framework, which is consistent with the disappearance of medium strong acid sites on C-HY(80) measured by NH_3-TPD. Both of HY(80) and R-HY(80) presented weak LAS centered at 1577 cm^{-1} and lacked strong LAS located at 1615 cm^{-1}. Nevertheless, M0.5

displayed the exact opposite result. PMMA blended well with zeolite Y catalysts produced acetone during hydrolysis, but desilicated zeolites (M0.5, M1 and M1) entirely eliminated the production of acetone. This LAS type's transformation was likely to be responsible for the production of acetone.

5.4.3 Solid residue analysis

PMMA powder (Mw=550 000 g mol^{-1}) used in this work has a midpoint glass transition temperature T_g at 123 °C (Supplementary Fig. 5.13), which indicates an atactic tacticity [215]. Thermal depolymerization of this virgin PMMA powder underwent three weight loss stages (Fig. 5.4a) under either N_2 or steam. Steam caused less weight loss compared with inert atmosphere at stage I because steam thermogravimetric test kept sample at 130 °C for 30 min prior to temperature rise. We inferred that PMMA degradation had started since 130 °C during steam equilibrium, whereas PMMA weight loss began at 140 °C in N_2. Weight loss at stage II and III kept consistent under both of steam and inert gas atmospheres. PMMA non-catalytic depolymerization under inert gas and steam follows almost identical degradation behaviour. The thermogravimetric degradation of PMMA, synthesized via free radical polymerization, follows three distinct weight loss stages [67]. Stage I involved depolymerization initiated by the least stable head-to-head (H-H) linkages [41]. In Stage II, the weight loss was attributed to depolymerization initiated at the unsaturated vinyl ends, while Stage III was characterized by random scission within the polymer chains.

FTIR identified the functional groups of unreacted PMMA remaining in HY(80) (Fig. 5.4b). Spectra at 1728 cm^{-1} corresponded to carbonyl group C=O on PMMA chain. Solid residues obtained at 330 °C and 350 °C left unreacted PMMA, while band at 1728 cm^{-1} completely disappeared over residues obtained at 370 °C. Carbon balance showed 99 % of PMMA conversion over fresh HY(80) at reaction temperature of 370 °C (Fig. 5.2c & Supplementary Table 5.1). Notwithstanding analytic and statistic uncertainties, the data suggests PMMA completely degraded at 370 °C. PMMA residues reacting over HY(60) reached weight averaged molecular weight (Mw) at 18 000 g mol^{-1} measured by GPC (Supplementary Fig. 6.5). However, FTIR detected two small peaks at 1811 and 1762 cm^{-1} on HY(80) solid residues reacted at 350 °C. We attributed these two peaks to anhydride carbonyl twin peaks. Double peaks at 1811 and 1762 cm^{-1} were more likely to be intramolecular six-member glutaric anhydride formed between adjacent carboxyl groups [216, 217]. Polymethacrylic acid (PMAA)-PMMA copolymers were formed by direct hydrolysis of partial carbomethoxy groups on PMMA chain

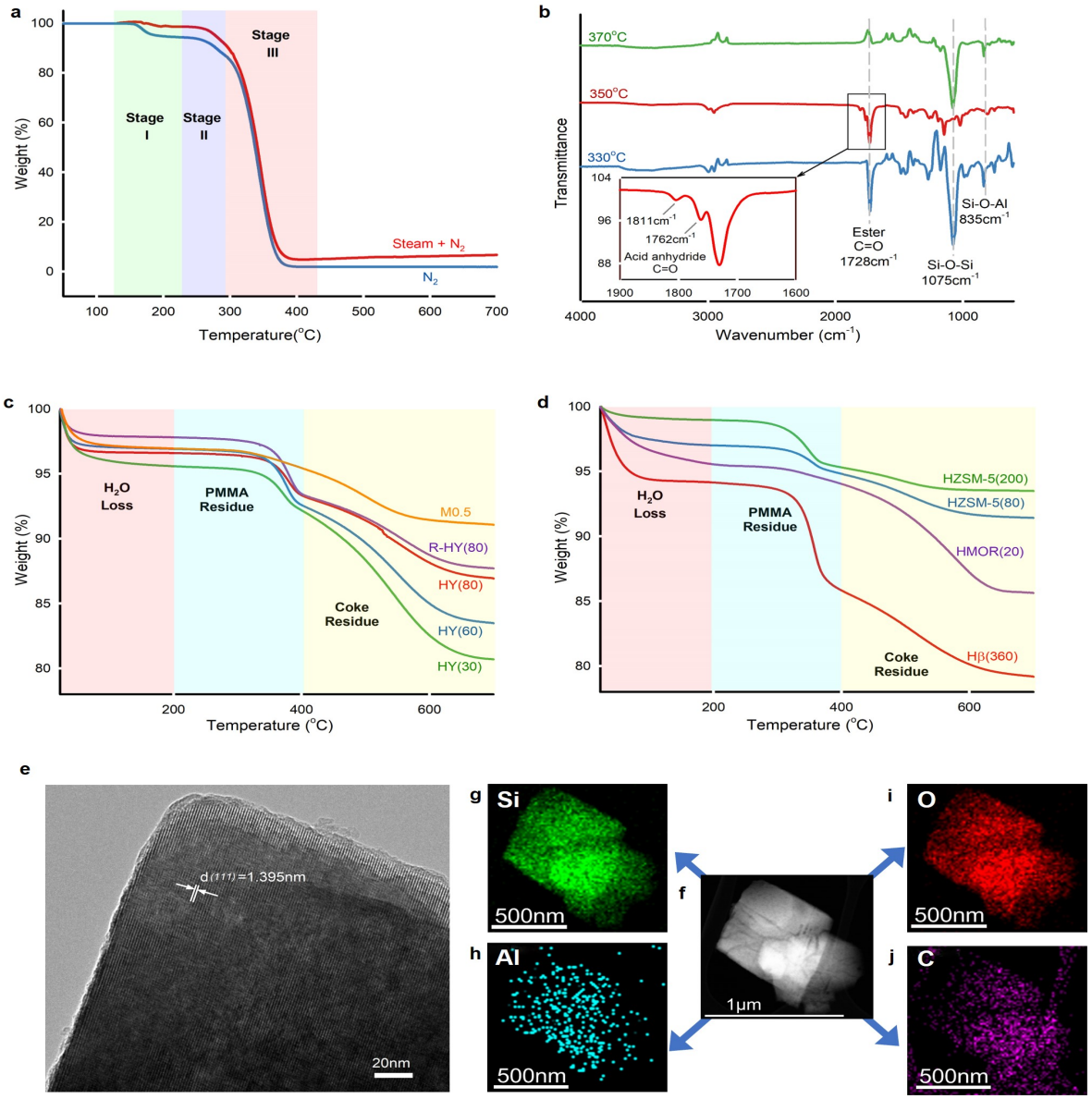

Figure (5.4) Solid residue analysis. **a**, Thermal gravimetric analysis of pure PMMA under N_2 atmosphere (60 mL min^{-1}, blue curve) and steam (mixture atmosphere of 70 mL min^{-1} of steam and 30 mL min^{-1} of N_2, red curve) with a heating ramp of 5 °C min^{-1}. **b**, FTIR spectra of acetone-dissolved residues on coked HY(80) reacted at 330 °C, 350 °C and 370 °C. Groups Si – O – Al and Si – O – Si were from HY(80) particle residues in acetone. **c**, **d**, Thermal gravimetric analysis of solid residues for fresh, regenerated and desilicated zeolite Y reacted at 350 °C (**c**), and activated HZSM-5(200), HZSM-5(80), HMOR(20) and fresh Hβ(360) reacted at 350 °C (**d**) under air atmosphere (60 mL min^{-1}) with a heating ramp of 5 °C min^{-1}. **e-j**, TEM images of coked HY(80) reacted at 350 °C. The interplanar spacing of 1.395 nm corresponded to the (111) plane in zeolite Y crystal (**e**). Dark-field TEM of C-HY(80) (**f**) element mapping images of Si (**g**), Al (**h**), O (**i**) and C (**j**) using an X-ray energy dispersive spectrometer (EDS).

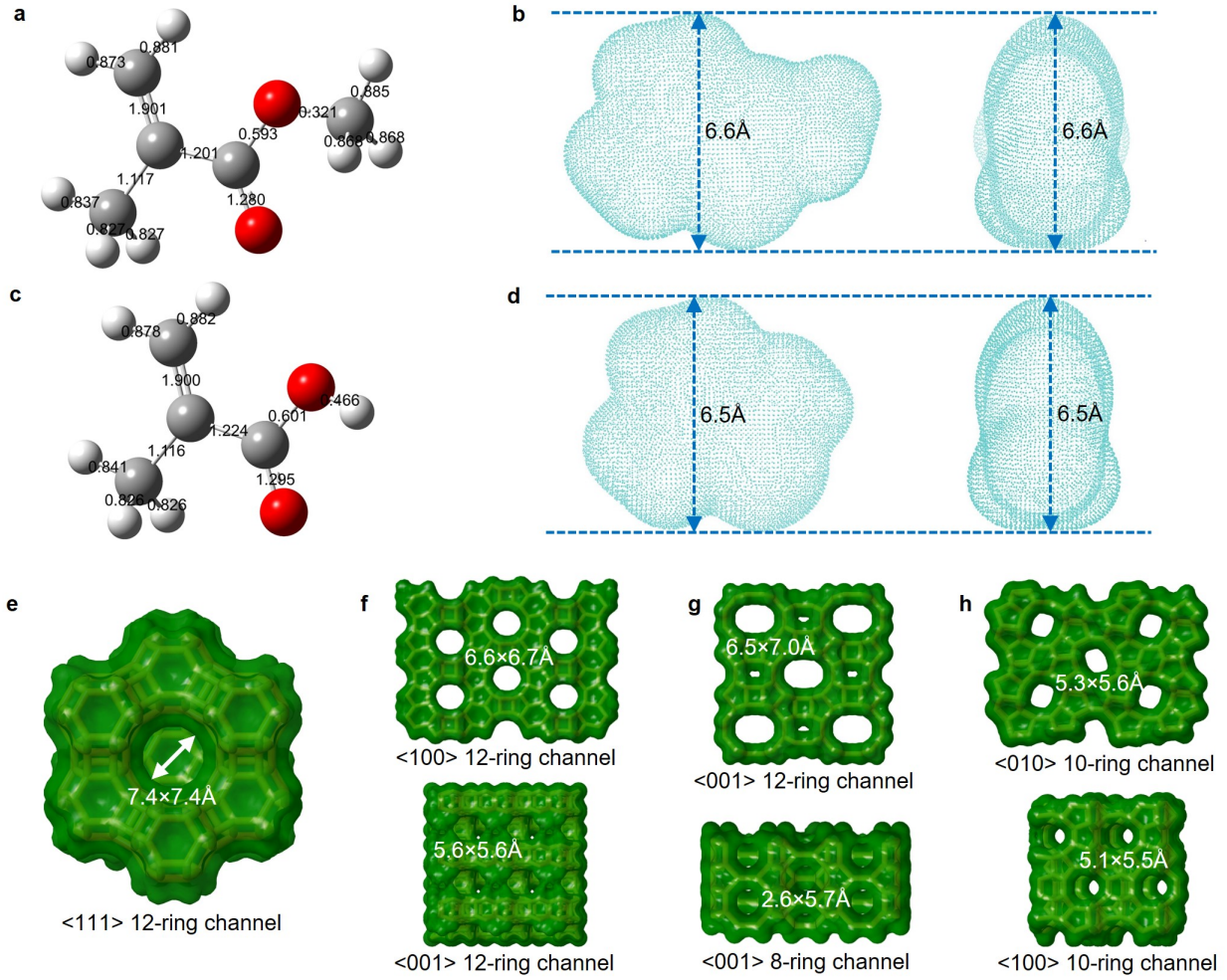

Figure (5.5) Relation between molecular kinetic diameter and zeolite structure size. **a-d**, 3D molecular ball-stick structure labelled with bond order of MMA (**a**) and MAA (**c**) via Gaussview 6, and electron density isosurface of MMA (**b**) and MAA (**d**) visualized by VMD. The estimated kinetic diameter is 6.6 Å for MMA (**b**) and 6.5 Å for MAA (**d**) based on electron density isovalue 0.0015 a.u. **e-h**, Channel diameter, ring size and crystal plane of zeolite Y (**e**), zeolite β (**f**), Mordenite (**g**) and ZSM-5 (**h**). All structure information referred to *Database of Zeolite Structures*. [214]

to carboxyl groups during PMMA depolymerization, followed by dehydration of two adjacent carboxyl groups to form six-member glutaric anhydride.

Thermogravimetric analysis (TGA) of solid residues under air recognized three weight loss stages (Fig. 5.4c & d). Weight loss below 200 °C belonged to H_2O adsorbed on solid residues, while weight loss between 200 and 400 °C, and above 400 °C corresponded to unreacted PMMA and coke deposits, respectively (Supplementary Fig. 5.14). Solid residues remaining in the fresh and regenerated zeolite Y displayed two distinct weight loss stages corresponding to PMMA and coke residues. With the decrease of SiO_2/Al_2O_3 ratio from 80 to 30 (so stronger acidity and higher amount of Al species), reacted zeolite Y presented more coke deposits. The increased coke deposits on lower SiO_2/Al_2O_3 ratio of zeolite Y confirmed that coke formed on the surface of Al sites and blocked Al-containing LAS and BAS as well as zeolite pore channels. Desilicated zeolite Y, M0.5, demonstrated strong cracking ability, which almost completely degraded PMMA and yielded a low amount of coke. We attributed the low coke deposits on M0.5 to the increased zeolite pore size. Further TGA investigation on reacted HZSM-5, HMOR(20) and Hβ(360) found zeolite pore size plays a decisive role in coke formation (Fig. 5.4d). HZSM-5(80) and HZSM-5(200) exhibited ultra-low coke deposits, even though HZSM(80) had higher coke formation than HZSM(200) owing to the strengthened acidity. HMOR(20) almost completely degraded PMMA, like M0.5, whereas accumulated more coke species than M0.5. Hβ(360) exhibited not only high PMMA residues, but also high coke deposits.

We further calculated the kinetic diameter of MMA and MAA molecules based on an electron density isosurface method [195]. Shape selectivity effect of zeolite limits molecules with a kinetic diameter higher than pore channel size to enter size-defined pores and access internal acid sites of zeolitic framework [218]. The kinetic diameter of MMA, 6.6 Å, is marginally higher than MAA kinetic diameter 6.5 Å (Fig. 5.5b & d). The four types of zeolites have specific pore dimensions (Fig. 5.5e-h and Supplementary Table 5.4). Owing to large-pore channels (7.4×7.4 Å), zeolite Y allows MMA and MAA to readily access its pores (Fig. 5.5e). Zeolite β owns 6.6×6.7 Å and 5.6×5.6 Å interconnected channels, which restricts the diffusion and transfer of MMA and MAA in the pores (Fig. 5.5f). Mordenite has 12-ring 6.5×7.0 Å large-pore channels as well as an 8-ring 2.6×5.7 Å micro-pore channel, which allows MMA and MMA to enter the pores but also confines the diffusion and transfer of MMA and MAA in the pores (Fig. 5.5g). ZSM-5 possesses 5.3×5.6 Å and 5.1×5.5 Å channels that only allows MMA and MAA to access its external surface (Fig. 5.5h).

Microporous confinement effect directly influences coke formation. Due to entire channel constraint, the reacted ZSM-5 exhibited mild coke deposits on external surface (Fig. 5.4d). Primary coke deposits formed on the internal surface of the pores over zeolite Y, β and MOR. Transmission electron microscope (TEM) of the reacted HY(80) at 350 °C demonstrated a 1.395 nm of interplanar spacing, which corresponds to the zeolite Y (111) crystal plane (Fig. 5.4e). Furthermore, element mapping scan found carbon distribution maintains consistent with Al, which confirmed coke mainly deposits on the surface of Al-containing acid sites (Fig. 5.4f-j).

Through kinetic diameter calculations of MMA and MAA, we determined that their diffusion within the zeolitic framework is a key factor in the deactivation of the zeolites. Both MMA and MAA can diffuse into the large-pore channels of zeolite Y, zeolite β, and MOR, leading to coke formation within the zeolitic framework. In contrast, the microporous channels of ZSM-5 prevent MMA and MAA from entering its internal pores, thereby avoiding coke formation. These kinetic diameter calculations provided us with a quantitative understanding of the relationship between zeolite deactivation and the diffusion behaviour of MMA and MAA within the zeolitic framework.

5.4.4 PMMA hydrolysis mechanism over HY(80)

PMMA thermolysis follows a free radical depolymerization mechanism [3]. TGA of PMMA degradation under steam without any catalysts confirms that PMMA thermal depolymerization in steam also follows a free radical depolymerization mechanism (Fig. 5.4a). To gain further insights into PMMA hydrolysis and its by-product, we conducted in-situ liquid and gas analysis using GC-MS, detecting MAA, methanol, MMA and acetone every minute (Fig. 5.6a). Two peaks appeared in product analysis at time zero and 15 min, corresponded to weight loss stage I and stage II & III together (Fig. 5.4a). PMMA hydrolysis over solid acid catalysts began with PMMA thermolysis to MMA, followed by catalytic hydrolysis of MMA to MAA and methanol [16]. We observed PMMA depolymerizes and MMA hydrolyzes immediately at the beginning of reaction. In lower temperature range (175 °C to 250 °C), we detected an equivalent amount of MAA, methanol and MMA. MMA hydrolysis over HY(80) produces MAA and methanol.

We observed the evolution of PMMA powder during melting to prepare highest contact between PMMA and catalyst. When feeding the reactor by mechanically blended PMMA and

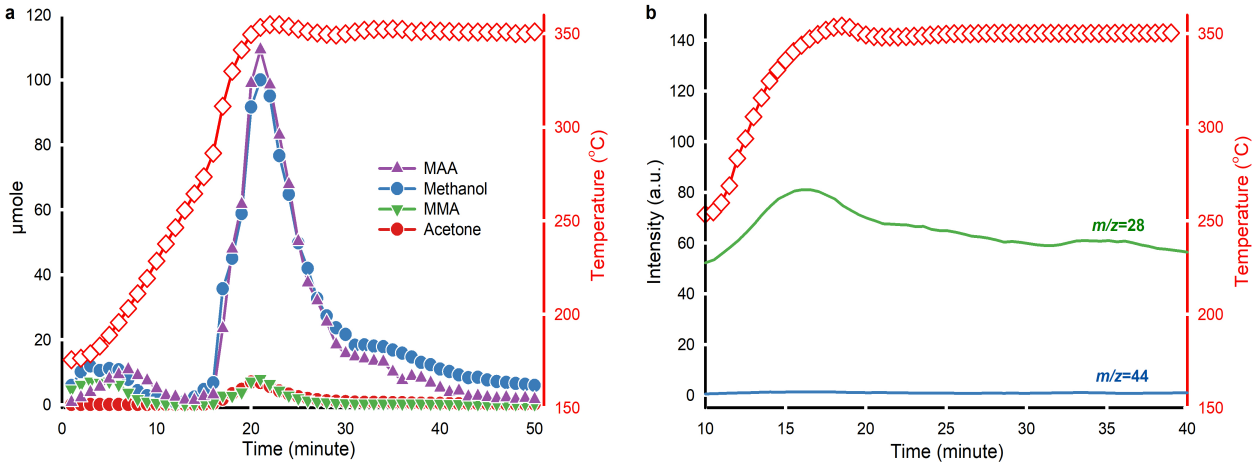

Figure (5.6) In-situ product monitoring. **a**, Mole of product measured every minute by GC-MS (left axis, solid symbols) to reaction temperature (right axis, red hollow squares). DME was excluded. **b**, Continuous mass-to-charge ratio (m/z) recorded by on-line mass spectrometer (left axis, green and blue curves) evolved with reaction temperature (right axis, red hollow squares) and reaction time. m/z=44 corresponds to CO_2, while m/z=28 represents CO.

HY(80), catalyst powder partially covered melted PMMA and so some of the produced MMA exit the reactor without passing through HY(80). In contrast, blanketing PMMA by HY(80) powder, kept PMMA covered even after melting (Supplementary Table 5.1). Slight melting of the PMMA spheres facilitated the adhesion of HY(80) particles onto their surfaces (Supplementary Fig. 5.10c & d).

PMMA underwent end-chain scission to produce MMA in the low-temperature zone (175 °C to 250 °C) [37], but did not form acetone. Above 250 °C, the yield of MAA and methanol increased because random chain scission started and accelerated PMMA depolymerization [37]. By-product acetone formed above 250 °C and maintained a concentration change pattern similar to MMA. At 350 °C from t=30 min, the quantity of methanol surpassed that of MAA. Extra methanol may be result of the direct hydrolysis of PMMA to Poly(MMA-co-MAA) copolymer chains, which subsequently forms acid anhydride groups on the chain via dehydration (Fig. 5.7).

On-line MS monitored the evolution of CO and CO_2 during reaction (Fig. 5.6b). A weak signal of m/z=44 suggested that PMMA hydrolysis yielded a minor production of CO_2. The signal of CO increased starting from 250 °C and peaked around 350 °C. Acetone and CO

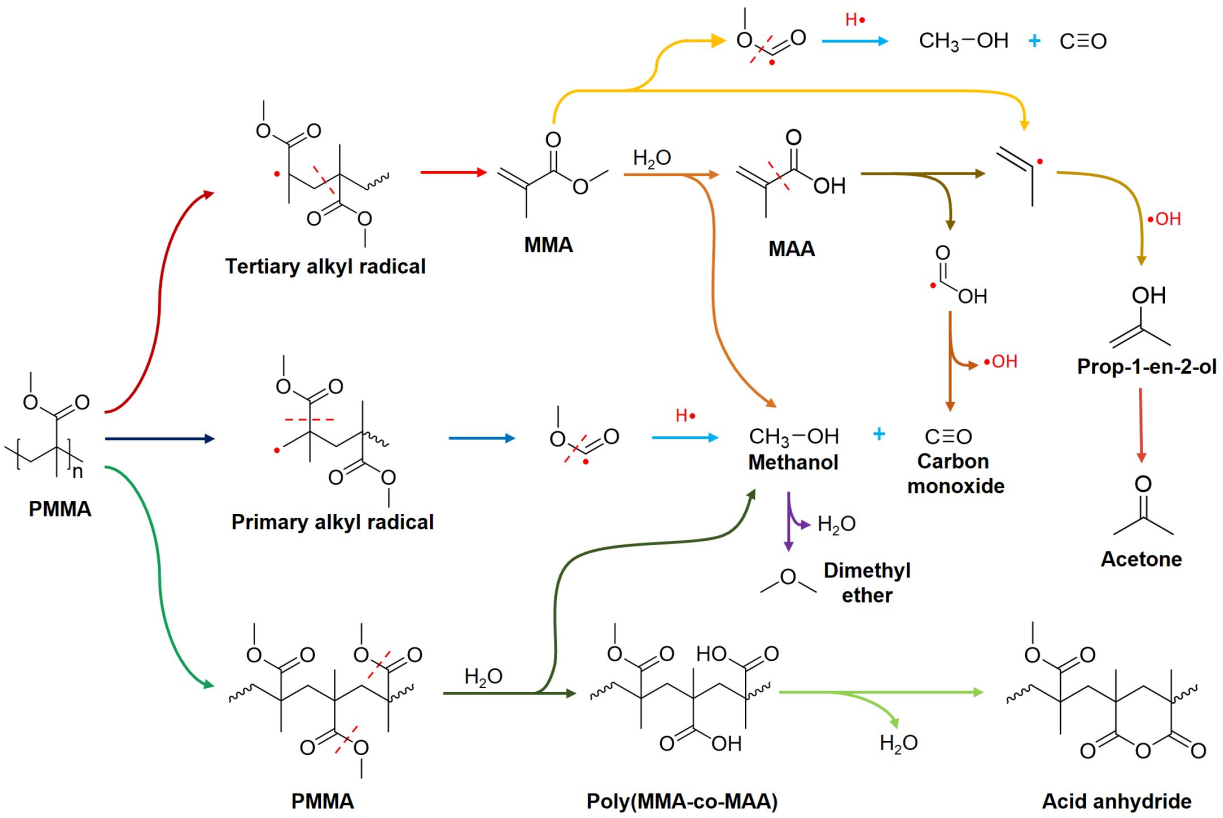

Figure (5.7) PMMA hydrolysis mechanism over zeolite Y. Coloured arrows represent different reactions. FTIR spectra of PMMA residues in C-HY(80) reacted at 350 °C validated the formation of Poly(MMA-co-MAA) acid anhydride. Primary by-products, acetone and CO, derived from MAA cracking over acid sites on zeolite Y.

both appeared at the same temperature.

To further elucidate the relationship between CO and acetone, we performed blank tests by feeding only MMA or MAA into the reactor (Supplementary Fig. 5.11). Non-catalytic hydrolysis of MMA at 350 °C did not produce any liquid product. However, catalytic hydrolysis of MMA over HY(80) at 350 °C produced a small amount of MAA, methanol and a trace of acetone(Supplementary Fig. 5.11a). While non-catalytic hydrolysis of MAA also did not generate any decomposition products at 350 °C, catalytic hydrolysis of MAA over HY(80) at 350 °C yielded a considerable amount of acetone (Supplementary Fig. 5.11b). Catalytic hydrolysis of MAA produced CO at the same conditions (Supplementary Fig. 5.11d).

Higher bond orders indicate stronger molecular stability. Even though C−C bond (bond order=1.224) between carboxyl group and C=C double bond in MAA has higher bond order than C−C bond (bond order=1.201) between ester group and C=C double bond in MMA (Fig. 5.5a & c), the dominant formation route of acetone and CO is the scission of C−C bond between carboxyl group and C=C double bond in MAA since MAA predominated over HY(80) during reaction.

Here, we proposed a PMMA hydrolysis mechanism over HY(80) at 350 °C based on experimental data and literature (Fig. 5.7). Random chain scission of PMMA at 350 °C generated tertiary alkyl radicals, followed by unzipping to produce MMA monomer. Subsequently, HY(80) hydrolyzed MMA to MAA and methanol on acid sites. MAA further cracked into formic acid radicals and 2-propenyl radicals at 350 °C. Dehydroxylation of formic acid radicals resulted in CO, while 2-propenyl radical combined one hydroxyl group to form prop-1-en-2-ol that was further isomerized to acetone. Cracking of MMA may produce 2-propenyl radical and $CH_3O(CO)\cdot$ free radical directly. Random chain scission of PMMA generated a small amount of primary alkyl radicals which readily resulted in $CH_3O(CO)\cdot$ free radical fragment. Protonation of $CH_3O(CO)\cdot$ fragment produce methanol and CO. Further dehydration of methanol yielded a trace of dimethyl ether (DME). A small amount of PMMA was partially hydrolyzed to Poly(MMA-co-MAA) copolymer, followed by dehydration to form six-member glutaric anhydride (Fig. 5.7).

Conclusions

Upcycling PMMA to MAA instead of MMA is a viable alternative to recycle both post-processed industrial scraps and cuttings and end-of-life PMMA, offering prominent technical, economic, and market benefits. In this study, we introduced a heterogeneous catalytic hydrolysis method to directly convert PMMA to MAA over zeolite -fresh, activated, regenerated and desilicated zeolites. H-type zeolite Y with SiO_2/Al_2O_3 ratio of 80 exhibited the highest MAA yield and selectivity. PMMA thermolysis to MMA followed by MMA catalytic hydrolysis over zeolite Y to MAA produced a high concentration of MAA monomer. Coke primarily formed on the surface of medium strong acid sites and so temporarily deactivated Brønsted acid sites. Kinetic diameter estimation of MMA and MAA suggested that coke predominantly formed in the channels of zeolites with large pores. Small-pore ZSM-5 have stronger cracking capacity, while large-pore zeolite Y demonstrated superior hydrolysis performance. Acetone appeared with CO at higher hydrolysis temperature (>250 °C). Acetone produced during PMMA hydrolysis primarily by decarboxylation of MAA monomer. The existence of acid anhydride group in the reacted residues proved partial hydrolysis of PMMA chains to Poly(MMA-co-MAA) copolymer, and subsequent dehydration to six-member glutaric anhydride. For subsequent research, we suggest to extend the feed from virgin PMMA to post-processed industrial scraps and cuttings and end-of-life PMMA plastic, and design specific pilot and industrial scale reactors for direct conversion of PMMA to MAA, along with a techno-economic assessment.

Acknowledgements

The authors thank Dr. Jean-Luc Dubois at Trinseo France SAS for discussion and revising; Prof. Liang Wu at Shanghai Jiao Tong Univeristy for Gaussian 16 license; Tian Lu at Beijing Kein Research Centre for Natural Sciences for Multiwfn program; Jean-Philippe Masse at Polytechnique Montreal for TEM-EDS and XRD analysis. This work was supported by the Natural Sciences and Engineering Research Council of Canada (ALLRP-573784-22 CRSNG) and Arkema & Lavergne (CDT 051087).

5.5 Supplementary information for article 2

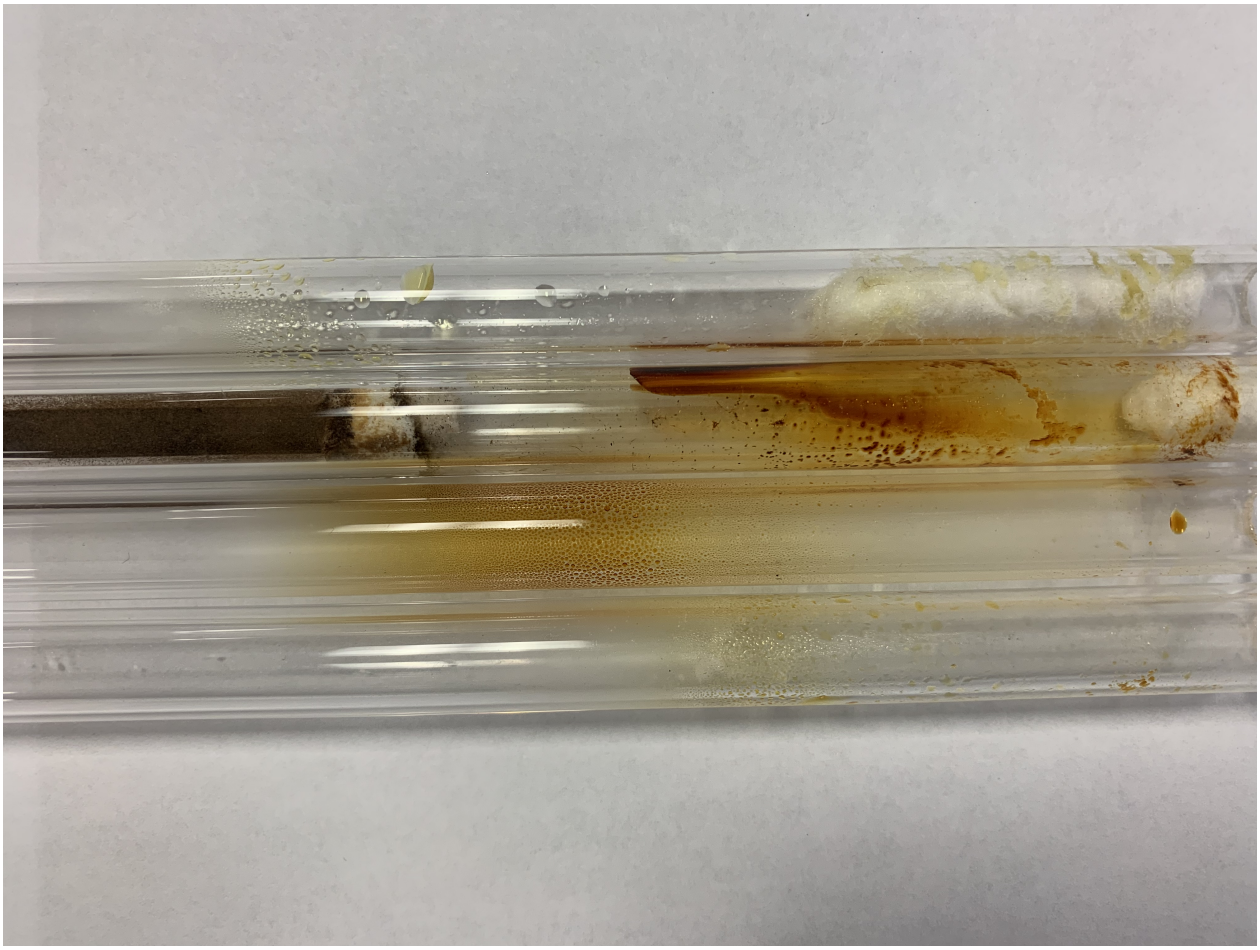

Figure (5.8) MMA repolymerization byproducts in PMMA-to-MMA recycling routes. The yellow repolyermzaition residues that formed in reactors and condensers during PMMA catalytic/non-catalytic pyrolysis reduced MMA yield and resulted in higher MMA purification cost.

Table (5.1) Carbon balance of PMMA hydrolysis over different zeolites

Samples	T °C	X_{PMMA}[a] %	Y_{MAA} %	Y_{MeOH} %	Y_{MMA} %	$Y_{Acetone}$ %	S_{MAA} %	S_{MeOH} %	S_{MMA} %	$S_{Acetone}$ %	C in residues[b] mol %	CO mol %	CO_2 mol %	CH_4 mol %	Recovered C mol %
HY(80)	350	97	54	15	2	3	56	15	3	3	10	3.4	0.8	0.0	88
HY(80)-rep	350	97	56	16	3	2	58	16	3	2	10	3.4	0.9	0.0	91
HY(80)	330	74	43	12	1	3	58	16	1	5	32	3.3	0.8	0.0	95
HY(80)	370	99	55	14	4	2	56	14	4	2	6	3.5	0.9	0.1	86
HY(60)	350	96	49	14	2	5	51	15	2	5	15	3.9	0.8	0.0	89
HY(30)	350	96	41	13	2	5	42	14	2	5	20	4.2	0.9	0.0	86
Hβ(360)	350	92	51	14	2	6	55	16	2	6	15	3.6	0.7	0.0	92
HZSM-5(200)	350	96	45	13	3	11	47	14	3	12	6	4.5	1.0	0.0	84
HZSM-5(80)	350	98	24	7	1	13	25	7	1	13	6	7.5	0.9	0.0	60
HMOR(20)	350	98	40	2	3	3	41	2	3	3	13	4.5	0.9	0.1	67
R-HY(80)	350	95	51	15	2	2	53	15	3	2	12	3.4	0.8	0.0	86
M0.5	350	98	21	7	19	0	21	8	19	0	7	3.4	0.9	0.0	59
M1	350	99	18	5	25	0	18	5	25	0	5	3.3	0.8	0.0	57
M2	350	98	19	7	17	0	20	8	18	0	7	3.4	1.3	0.0	56
HY(80) on PMMA[c]	350	97	47	6	0	0	48	6	0	0	6	5.8	1.5	0.0	66
PMMA (blank)	350	95	0	0	56	0	0	0	59	0	5	0.0	0.7	0.0	61

Note: T-temperature, rep.-repetition, a-determined by TGA, b-measured by LECO, c-HY(80) layer covered on the surface of PMMA powder.

Liquid products detected by GCMS contains MAA, methanol, MMA and acetone. GC-TCD quantified CO, CO_2 and CH_4 in the gas phase. LECO measured total carbon residues for carbon balance and TGA determined the amount of unreacted PMMA and coke for conversion calculation.

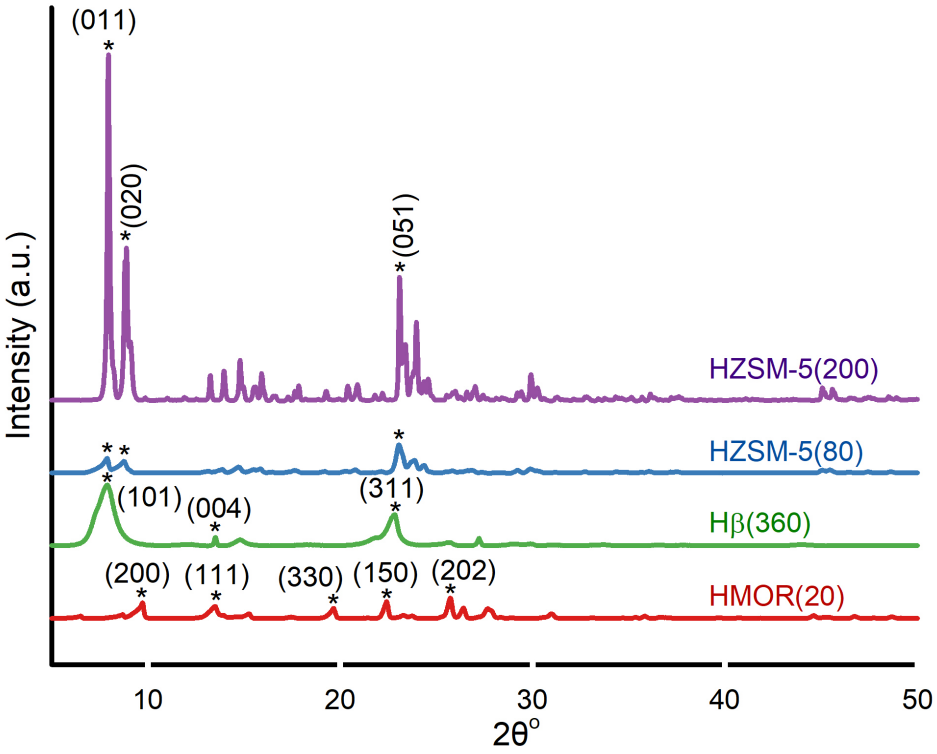

Figure (5.9) X-ray powder diffraction over HZSM-5(200), HZSM-5(80), Hβ(360) and HMOR(20)

Table (5.2) Physico-chemical properties of fresh zeolites, regenerated HY(80), desilicated HY(80) and coked HY(80) zeolites

Sample	Si/Al[a]	S_{BET}	V_{tot}	Average D_v	V_{micro}	S_{micro}	S_{meso}	d_p[b]			
								Medium size	Mean size	D[10]	D[90]
		$m^2\,g^{-1}$	$cm^3\,g^{-1}$	Å	$cm^3\,g^{-1}$	$m^2\,g^{-1}$	$m^2\,g^{-1}$	µm	µm	µm	µm
Commercial zeolites											
HY(80)	102	741	0.59	15	0.26	498	242	2.87	3.00	2.03	4.18
HY(60)	-	767	0.58	15	0.26	504	263	4.08	4.82	2.33	8.39
HY(30)	-	731	0.58	19	0.27	523	208	3.25	4.54	1.89	9.10
Hβ(360)	150	550	0.39	17	0.21	413	137	1.04	1.10	0.84	1.38
Activated zeolites											
HZSM-5(200)	104	381	0.24	15	0.06	110	270	2.18	2.23	1.76	2.78
HZSM-5(80)	-	403	0.29	17	0.12	242	161	1.68	1.71	1.22	2.21
HMOR(20)	11	440	0.36	17	0.19	384	56	2.67	4.12	1.54	9.11
Regenerated HY zeolite											
R-HY(80)	107	786	0.60	15	0.27	534	252	-	-	-	-
Desilicated HY zeolites											
M0.5	58	128	0.43	39	0.004	10	118	2.49	3.38	1.51	6.73
M1	46	43	0.29	86	0.003	6	37	2.17	2.42	1.37	3.77
M2	27	82	0.45	87	0.004	10	72	2.34	2.49	1.70	3.45
M3	6	95	0.21	17	0.003	8	87	2.60	2.66	2.05	3.36
Coked HY zeolite											
C-HY(80)	58	-	-	-	-	-	-	-	-	-	-

Note:d_p-particle size; a-calculated by XPS; b-measured by PSD

Table (5.3) Acidic properties of fresh, regenerated, coked, and desilicated Zeolite Y (µmol g^{-1}).

Sample	Weak[a]	Medium strong[a]	Brønsted[b]	Lewis[b]	B/L ratio	Brønsted[b]	Lewis[b]	B/L ratio
			150 °C			350 °C		
HY(80)	95	52	15	170	0.09	6.4	49	0.13
HY(60)	240	340	-	-	-	-	-	-
HY(30)	850	910	-	-	-	-	-	-
R-HY(80)	150	210	8.8	250	0.04	3.2	62	0.05
M0.5	300	0	20	53	0.37	8.3	18	0.46
C-HY(80)	230	0	3.4	83	0.04	2.7	12	0.21

Note: a-measured by NH_3-TPD; b-measured by Py-IR

Table (5.4) Pore dimension of different zeolites

Zeolite	Framework Type	Channel diameter, Å
Zeolite Y	FAU	12-ring [111] channels: 7.4 × 7.4
Zeolite β	BEA	12-ring [100] channels: 6.6 × 6.7
Zeolite β	BEA	12-ring [001] channels: 5.6 × 5.6
Mordenite	MOR	12-ring [001] channels: 6.5 × 7.0
Mordenite	MOR	8-ring [001] channels between 12-ring channels: 2.6 × 5.7
ZSM-5	MFI	10-ring [010] channels: 5.3 × 5.6
ZSM-5	MFI	10-ring [100] channels: 5.1 × 5.5

Data source: Database of Zeolite Structures (http://www.iza-structure.org/databases/)

Table (5.5) Molecular weight of PMMA in reacted HY(60) sample

PMMA residues in	M_n	M_w	Dispersity
HY(60)	18000	39000	2.15

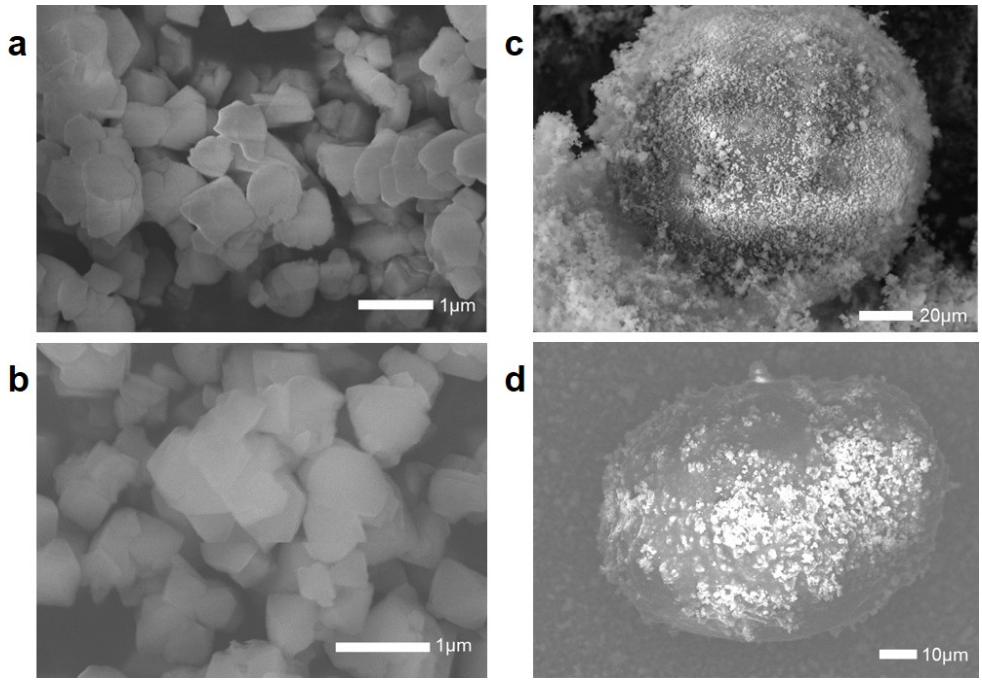

Figure (5.10) SEM images of fresh HY(80) (**a**), R-HY(80) (**b**), unreacted PMMA sphere covered by HY(80) particles (**c**), and PMMA sphere covered by HY(80) particles preheated at 350 °C for 2 min under steam atmosphere (**d**).

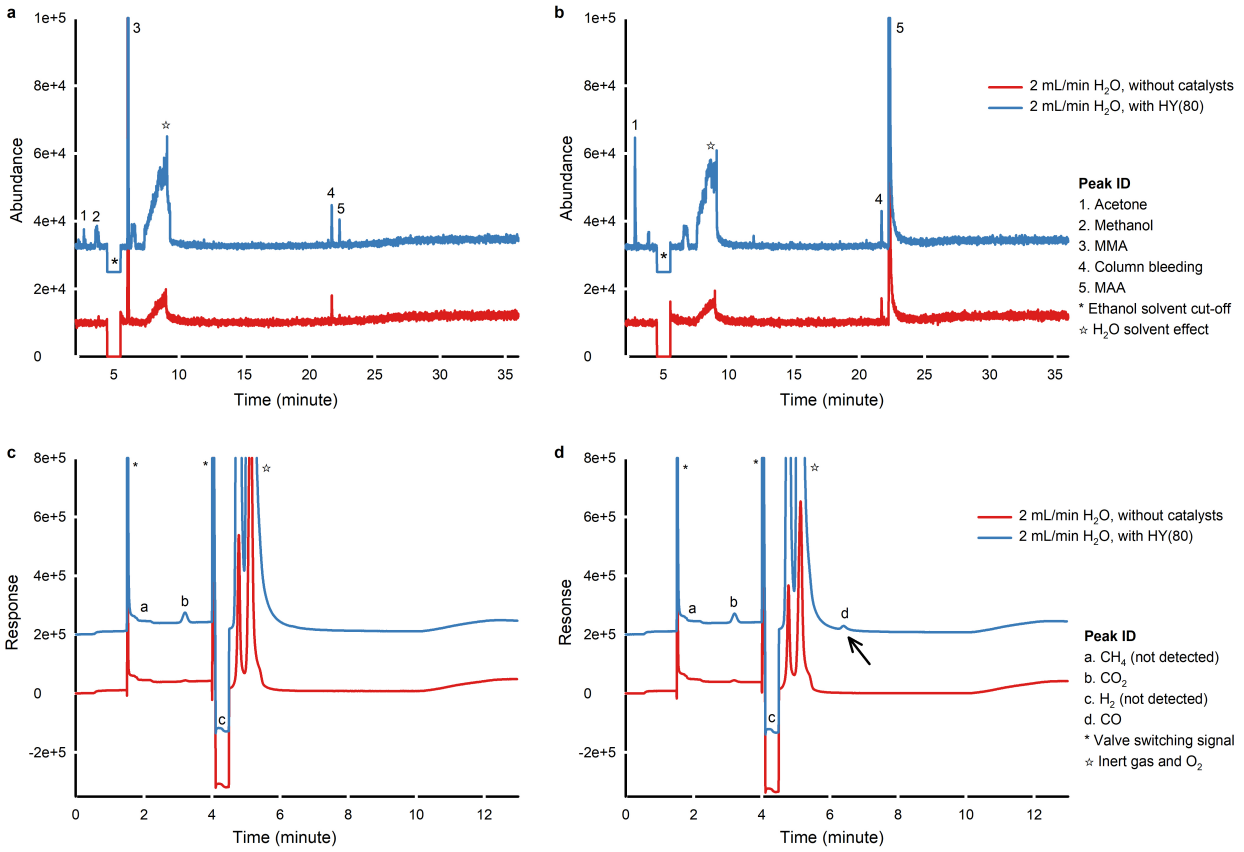

Figure (5.11) Catalytic and non-catalytic hydrolysis of MMA and MAA. **a**, GCMS results of MMA hydrolysis with and without HY(80) at 350 °C with 2 mL min^{-1} of water injection. **b**, GCMS results of MAA hydrolysis with and without HY(80) at 350 °C with 2 mL min^{-1} of water injection. **c**, GC-TCD gas detection results of MMA hydrolysis with and without HY(80) at 350 °C with 2 mL min^{-1} of water injection. Catalytic hydrolysis of MMA over HY(80) produced a small amount of CO_2. **d**, GC-TCD gas detection results of MAA hydrolysis with and without HY(80) at 350 °C with 2 mL min^{-1} of water injection. Catalytic hydrolysis of MAA over HY(80) produced a small amount of CO and CO_2.

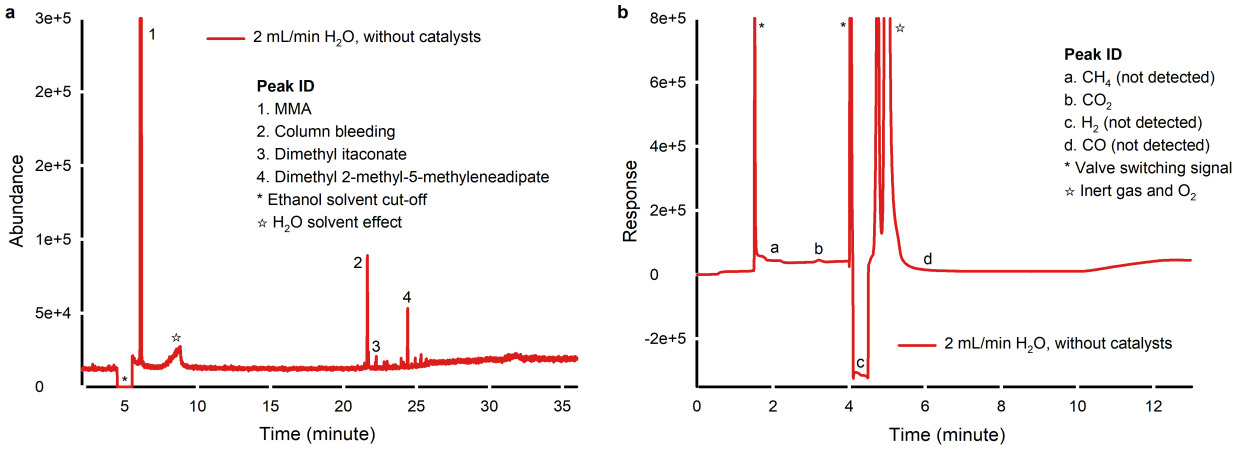

Figure (5.12) PMMA blank hydrolysis without catalysts at 350 °C under steam conditions (2 mL min^{-1} of water injection). **a**, GCMS results of PMMA non-catalytic degradation. **b**, GC-TCD gas detection results of PMMA non-catalytic degradation.

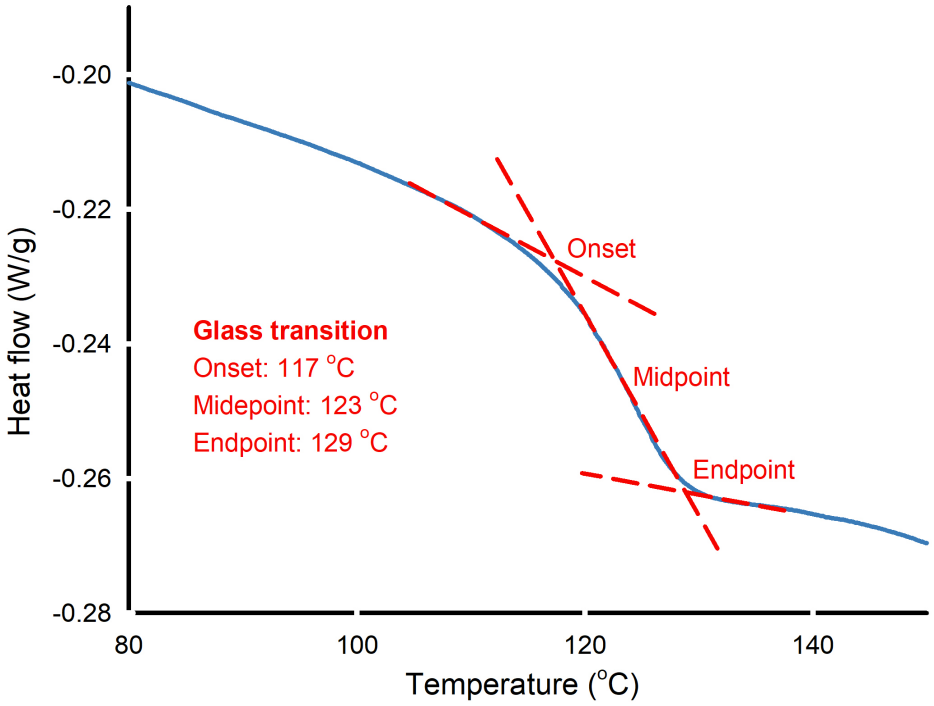

Figure (5.13) DSC results of PMMA powder showed onset T_g=117 °C, midpoint T_g=123 °C and endpoint T_g=129 °C.

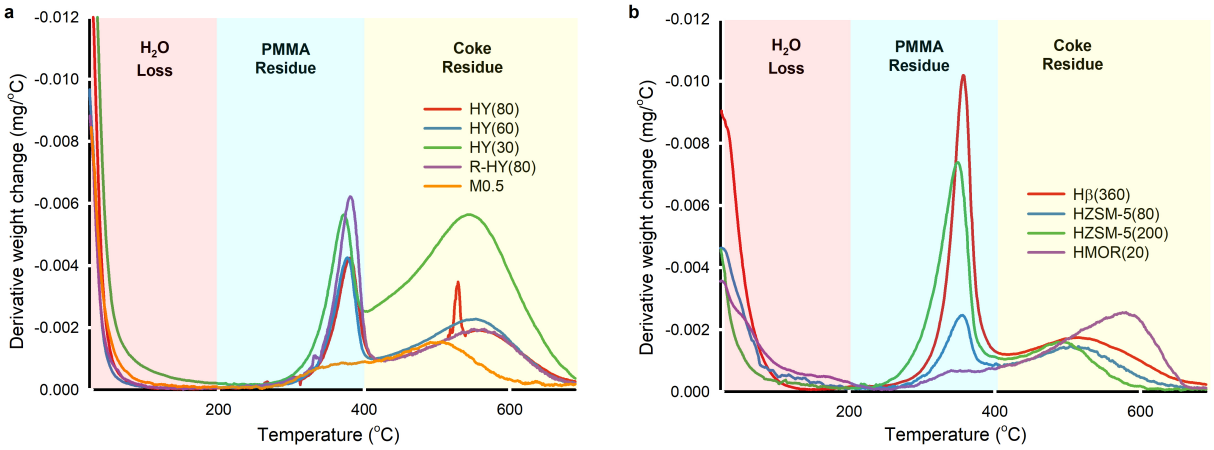

Figure (5.14) The first derivative of the TGA curves of solid residues for fresh, regenerated and desilicated zeolite Y reacted at 350 °C (**a**), and activated HZSM-5(200), HZSM-5(80), HMOR(20) and fresh Hβ(360) reacted at 350 °C (**b**) under air atmosphere (60 mL min^{-1}) with a heating ramp of 5 °C min^{-1}. Weight loss under 200 °C was attributed to H_2O loss, while weight loss between 200 °C and 400 °C was attributed to PMMA residues. Coke residues corresponded to temperature higher than 400 °C.

Table (5.6) XPS elemental identification and quantification in HY(80)

Name	Structure	Peak BE eV	FWHM eV	Area (P), CPS eV	Atomic %
Al2p	Al in zeolite	74.7	2.46	542	0.3
Si2p3	Si in zeolite	103.3	1.71	50300	30.7
C1s A	C−C and/or C=C	284.1	1.65	7740	2.9
C1s B	C−O	285.4	1.65	2980	1.1
C1s C	C=O and/or O−C−O	287.5	1.65	796	0.3
O1s A	O in zeolite	533.0	2.01	440000	61.6
O1s B	Adsorbed H_2O	535.4	2.01	21600	3.0

Abbreviations: BE, binding energy; FWHM, full-width-at-half-maximum; CPS, counts per second

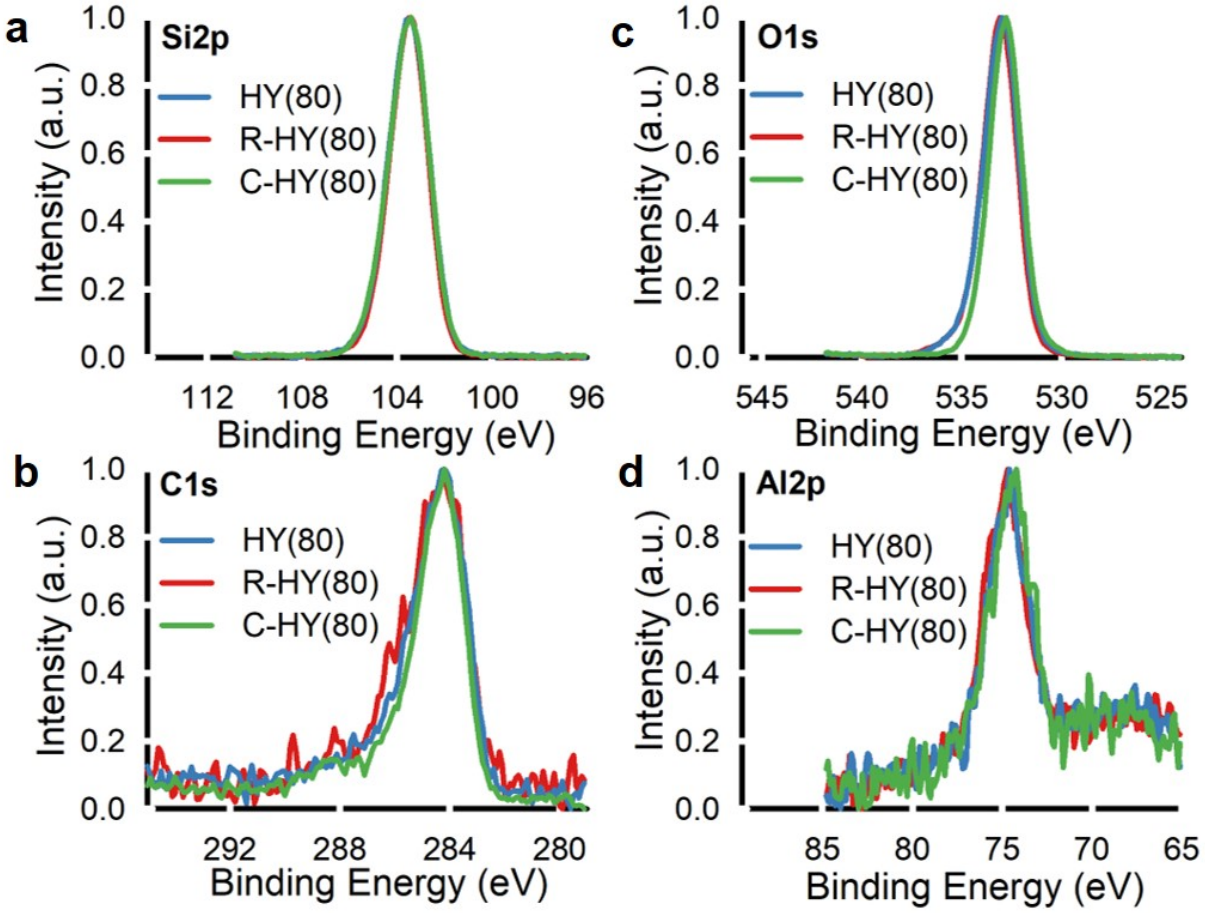

Figure (5.15) XPS spectra comparison for Si2p (**a**), C1s (**b**), O1s (**c**) and Al2p (**d**) over HY(80), R-HY(80), and C-HY(80).

Table (5.7) XPS elemental identification and quantification in R-HY(80)

Name	Structure	Peak BE eV	FWHM eV	Area (P), CPS eV	Atomic %
Al2p A	Al in zeolite	74.9	2.60	540	0.3
Si2p3	Si in zeolite	103.3	1.60	5660	32.0
C1s A	C-C and C=C	284.2	1.89	3570	1.2
C1s B	C-O	286.0	1.89	1320	0.5
C1s C	O-C=O	288.5	1.89	490	0.2
O1s A	O in zeolite	533.1	1.94	484000	62.8
O1s B	Adsorbed H_2O	535.6	1.94	23500	3.0

Abbreviations: BE, binding energy; FWHM, full-width-at-half-maximum; CPS, counts per second

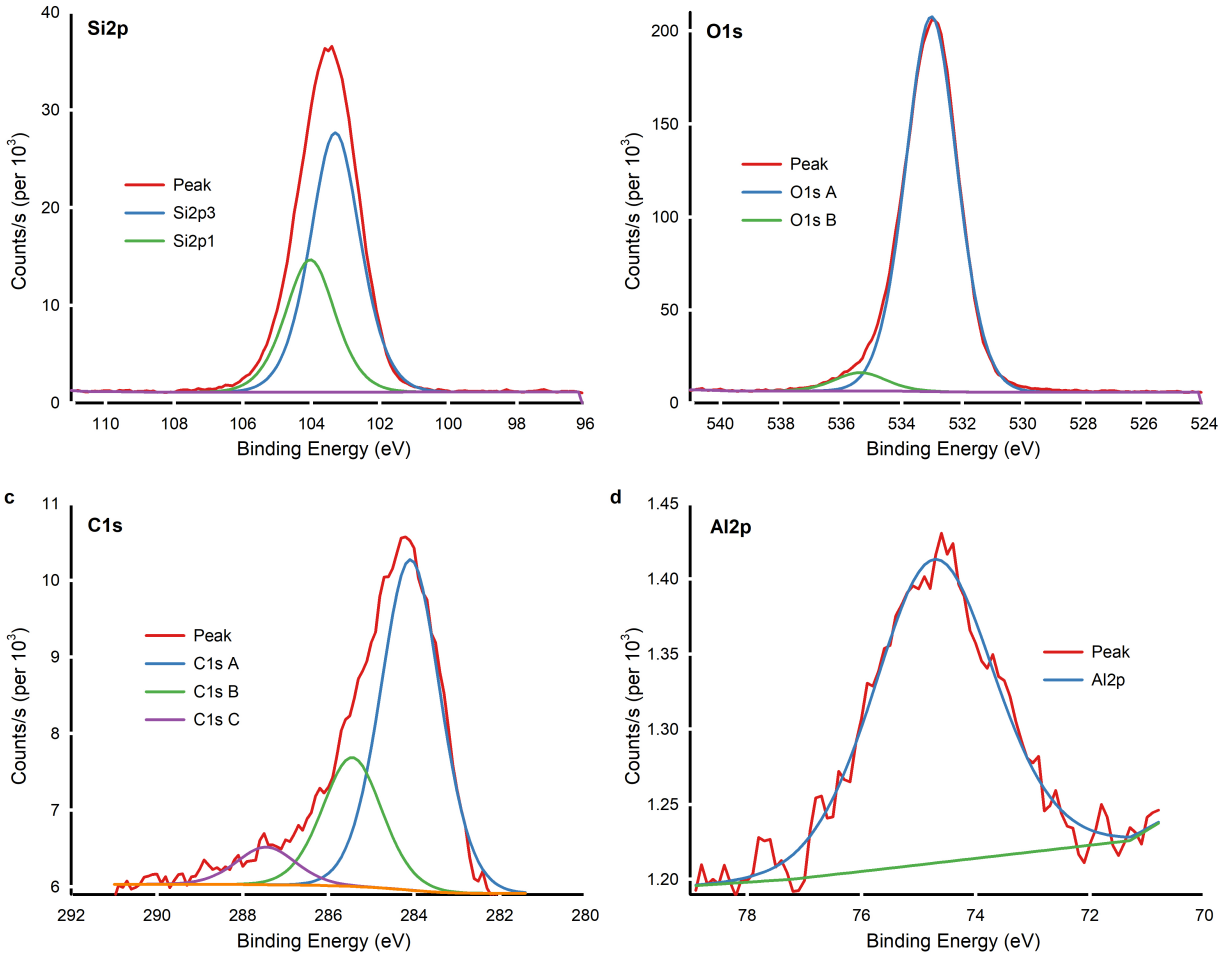

Figure (5.16) XPS of HY(80)

Table (5.8) XPS elemental identification and quantification in C-HY(80)

Name	Structure	Peak BE eV	FWHM eV	Area (P), CPS eV	Atomic %
Al2p A	Al in zeolite	74.4	2.43	570	0.4
Si2p3	Si in zeolite	103.3	1.73	50000	29.2
C1s A	C-C and C=C	284.2	1.68	17000	6.0
C1s B	C-O	285.9	1.68	3240	1.2
C1s C	O-C=O	288.3	1.68	1670	0.6
O1s A	O in zeolite	532.8	1.82	470000	62.7

Abbreviations: BE, binding energy; FWHM, full-width-at-half-maximum; CPS, counts per second

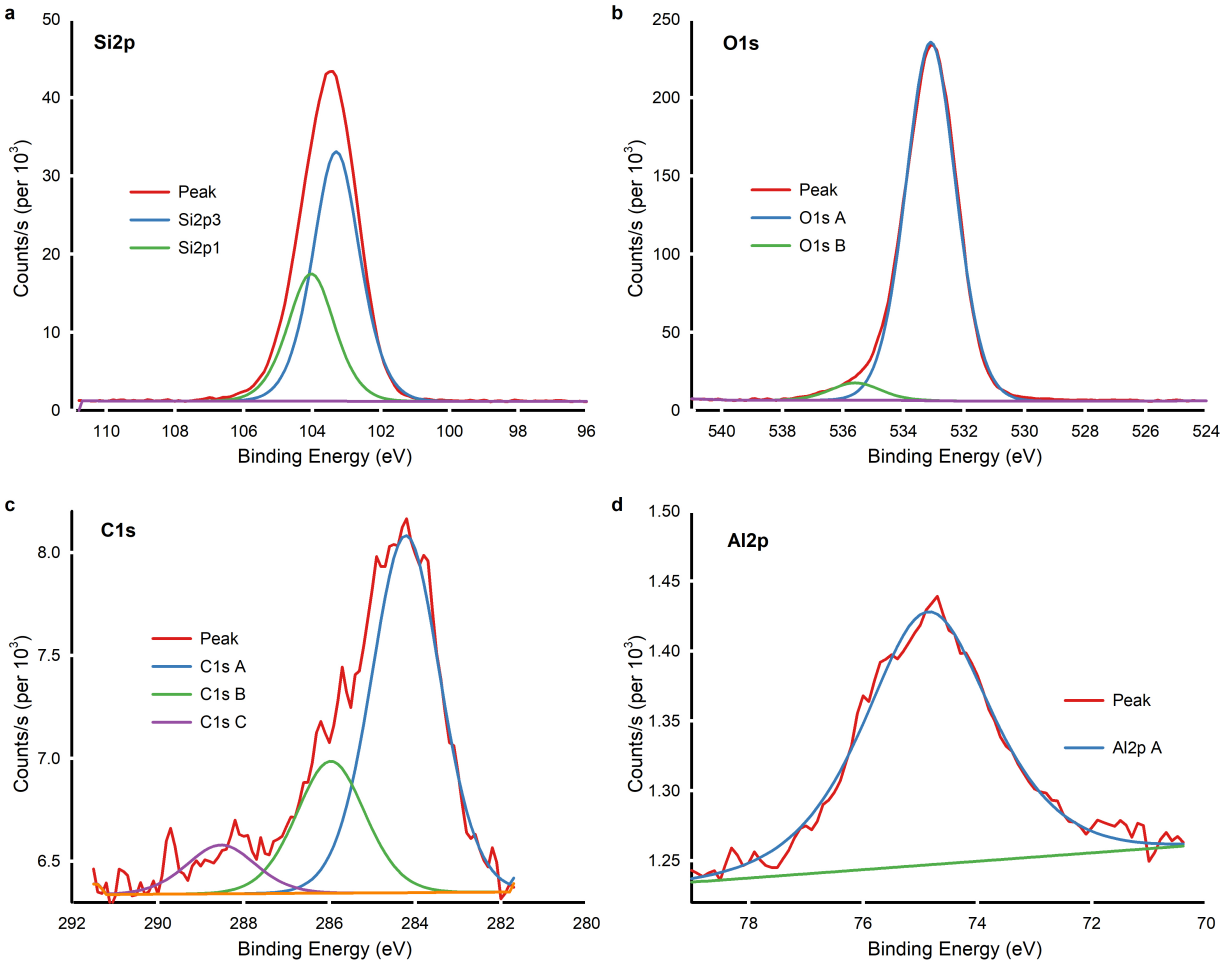

Figure (5.17) XPS of R-HY(80)

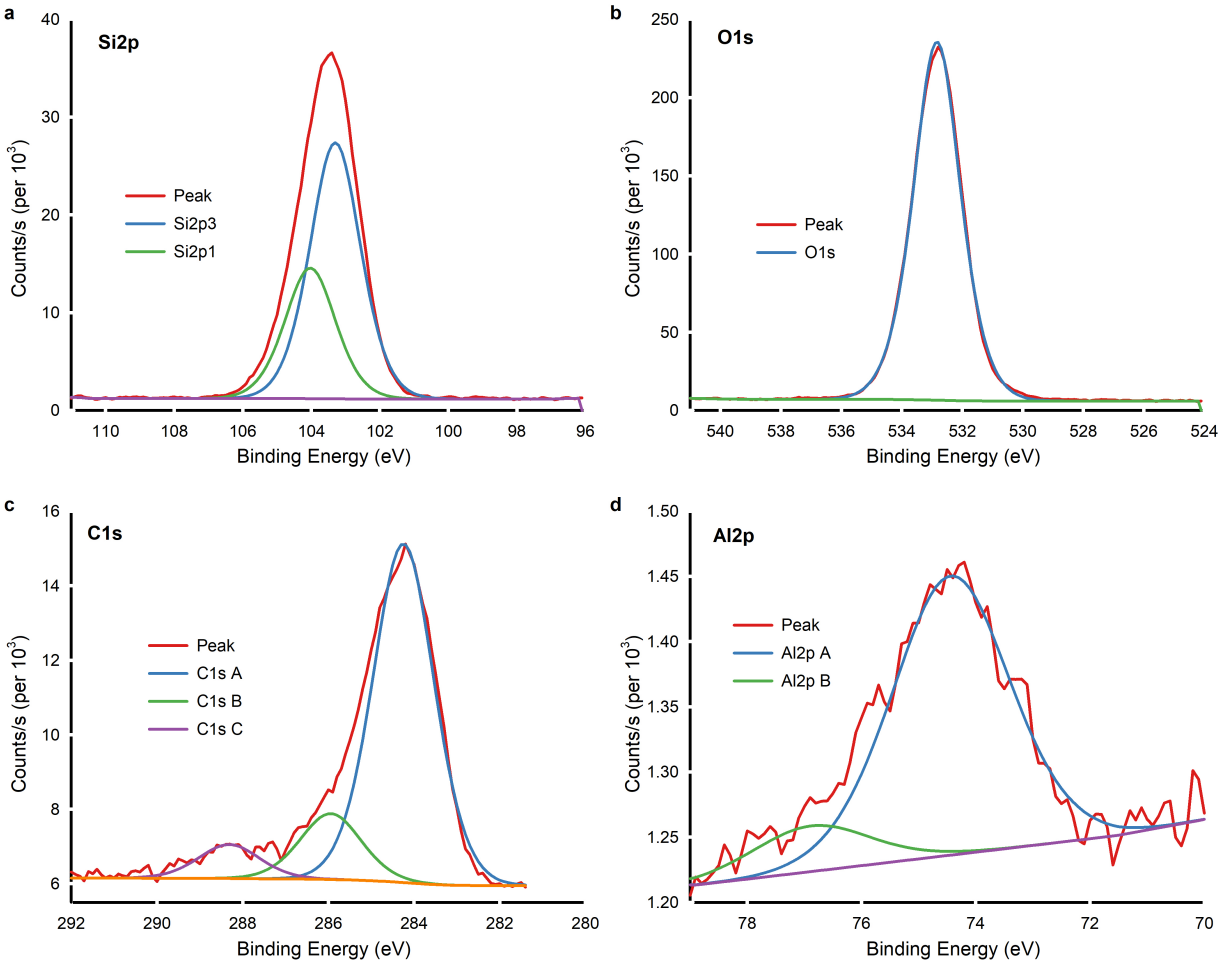

Figure (5.18) XPS of C-HY(80)

Table (5.9) XPS elemental identification and quantification in M0.5

Name	Structure	Peak BE eV	FWHM eV	Area (P), CPS eV	Atomic %
Al2p A	Al in zeolite	75.4	2.91	1500	0.5
Si2p3 A	Si in zeolite	103.3	1.83	78000	25.1
Si2p3 B	Si in other forms	104.8	1.83	13500	4.4
C1s A	C-C	284.5	1.99	24000	4.9
C1s B	C-O	286.2	1.99	7700	1.6
C1s C	O-C=O	288.3	1.99	3600	0.7
O1s A	O in zeolite	532.9	2.18	800000	62.4
Na1s	Na from NaOH	1072.2	3.15	4400	0.1
N1s	N from NH_3NO_3	399.7	2.79	1300	0.2

Abbreviations: BE, binding energy; FWHM, full-width-at-half-maximum; CPS, counts per second

Table (5.10) XPS elemental identification and quantification in M1

Name	Structure	Peak BE eV	FWHM eV	Area (P), CPS eV	Atomic %
Al2p	Al in zeolite	75.0	2.49	1900	0.7
Si2p3	Si in zeolite	103.3	1.82	92000	30.2
C1s A	C-C	284.9	1.99	11000	2.3
C1s B	C-O	286.6	1.99	4100	0.8
C1s C	O-C=O	288.8	1.99	1800	0.4
O1s A	O in zeolite	532.9	2.06	820000	65.0
Na1s	Na from NaOH	1072.8	2.46	5300	0.2
N1s	N from NH_3NO_3	402.5	2.65	600	0.1

Abbreviations: BE, binding energy; FWHM, full-width-at-half-maximum; CPS, counts per second

Table (5.11) XPS elemental identification and quantification in M2

Name	Structure	Peak BE eV	FWHM eV	Area (P), CPS eV	Atomic %
Al2p	Al in zeolite	74.9	2.43	3200	1.1
Si2p3	Si in zeolite	103.1	1.97	92000	29.5
C1s A	C-C	284.5	1.74	10000	2.1
C1s B	C-O	285.9	1.74	5900	1.2
C1s C	C=O	287.7	1.74	2000	0.4
C1s D	O-C=O	289.3	1.74	1200	0.2
O1s A	O in zeolite	532.6	2.05	840000	64.8
Na1s	Na from NaOH	1072.5	2.61	13000	0.4
N1s	N from NH_3NO_3	401.5	3.35	1500	0.2

Abbreviations: BE, binding energy; FWHM, full-width-at-half-maximum; CPS, counts per second

CHAPTER 6 ARTICLE 3 – REACTIVE EXTRUSION UPCYCLING OF POLYMETHYL METHACRYLATE TO METHYL METHACRYLATE AND METHACRYLIC ACID

Yanfa Zhuang, Tien-Dat Nguyen, Mahdi Sharifian, J ean-Luc D ubois, A bdellah A jji, and Gregory S. Patience

Submitted in Chemical Engineering Journal on December 23, 2024

6.1 Abstract

The global production of polymethyl methacrylate (PMMA) reached 4 million tonnes annually, yet only 10 % of PMMA, primarily post-industrial scraps, is recycled. Recycling end-of-life PMMA, which often contains additives or composite components, poses challenges in achieving crude methyl methacrylate (MMA) monomer with comparable purity to post-industrial scraps. Hydrolyzing end-of-life PMMA presents a viable alternative to produce methacrylic acid (MAA) and simplifies t he p urification pr ocess of cr ude MM A. However, current PMMA hydrolysis is limited to lab-scale and batch operations in fluidized/fixed beds and stirred tank reactors. In this study, we demonstrate a lab-scale, two-stage reactive hydrolysis extrusion system for the continuous conversion of injection- and extrusion-grade PMMA scraps into MMA and/or MAA at 330 °C to 370 °C. Residence time distribution (RTD) tests characterized the hydrodynamics of the screw configuration for PMMA extrusion, revealing that lower screw speed and feeding rate increase reaction time. A Plackett-Burman design identified temperature and catalyst type as significant factors for MM A hy dr olysis. Under optimized conditions, hydrolysis extrusion without any catalysts achieved the highest MMA yield of 89 % and 96 % PMMA conversion. Hydrolysis extrusion with 10 % H-type zeolite Y with an SiO_2/Al_2O_3 ratio of 80 at 370 °C resulted in a 5.3 % MAA yield, a 67 % MMA yield, and near-complete PMMA conversion. Liquid acid catalysts directly hydrolyzed PMMA to poly(MMA-co-MAA) copolymer and/or PMAA, followed by dehydration of two adjacent acid groups to form six-member glutaric anhydride. KOH solution hydrolyzed PMMA to poly(MMA-co-MAA) and/or PMAA potassium salt.

6.2 Introduction

Industry produces 400 million tonnes of plastic waste annually [219], with only 9 % being recycled [220]. Over 80 % of plastic waste is either trashed in landfills, incinerated, or discarded into the environment [65], creating a critical environmental crisis. Commercially used plastics contain various additives, such as colorants, flame retardants, plasticizers, and antioxidants [221]. These additives increase risks to environmental organisms and complicate the recycling process.

Polymethyl methacrylate (PMMA), also known as acrylic glass, Plexiglas, Perspex, and Altuglas, is an optically transparent, lightweight thermoplastic with good impact strength, excellent weather resistance, and scratch resistance [1, 2]. Annually, the industry produces around 4 million tonnes of PMMA for optical, electronic, and construction applications, but only 10 % of PMMA is collected to be recycled in the EU. Most waste PMMA is incinerated or landfilled [66]. Recycled PMMA predominantly comes from post-industrial cast sheets, extrusion sheets, or injection molded parts, which can be mechanically recycled into new PMMA products or thermolyzed into high-purity regenerated MMA (r-MMA) [2]. End- of-life PMMA containing additives or composite components requires chemical recycling, but producing r-MMA of similar purity as post-industrial PMMA scraps is more challenging.

Thermolyzing PMMA above 350 °C in an inert atmosphere yields 70 % to 90 % monomer at over 90 % r-MMA purity [4]. PMMA depolymerization follows a radical reaction mechanism [3, 67]. Commercial reactors, include molten metal baths, fluidized beds, reactive twin-screw extruders, augers, rotating drums, dry distillation stills, rotating paddles, and stirred tank reactors [3, 67, 68]. Fillers or additives such as metals, glass fibers, granite, and colorants in end-of-life PMMA lower monomer yield and introduce impurities, increasing purification costs in downstream processing [5, 222]. Crude r-MMA may contain oligomers and impurities like methyl acrylate, ethyl acrylate, methyl pyruvate, methyl or ethyl propionate, methyl isobutyrate, methyl 2-methylbutyrate, and pentanedioic acid, 2,4-dimethyl-, monomethyl ester [6–8]. Some impurities have close boiling points (BP) or molecular structures to MMA, complicating the separation and purification of crude r-MMA. For instance, ethyl acrylate has a boiling point almost identical to MMA (100 °C vs. 101 °C) and an odor threshold over 20 times lower than MMA [9, 10]. Crude r-MMA recycled from low- quality scraps with more impurities requires higher purification costs, and some impurities remain difficult to eliminate completely. This limits the application of r-MMA in strictly regulated markets for producing high-quality PMMA products.

To reduce the downstream purification costs of crude r-MMA generated from low-quality end-of-life PMMA, Chub et al. [5, 16] proposed a new route to convert PMMA into methacrylic acid (MAA) instead of MMA. MAA has a boiling point of 162 °C and many other different physico-chemical properties [223], which makes it easier to separate from the liquid products. The purified MAA can then be converted into MMA as a monomer or sold as a specialty chemical.

MAA, a colorless carboxylic acid with a pungent odor, is mainly used as co-monomer in paints, adhesives, leather treatment, fiber processing, and as a rubber modifier [11]. It is also used as a precursor to synthesize its esters (MMA), copolymers with other monomers, and MAA salts [14]. The market size for MAA, other than as an intermediate, is approximately 10 % of the MMA market. New MMA plants using ethylene as a feedstock are expected to come online in the coming years. These plants do not co-produce MAA, which will further increase the market demand for MAA.

Industrial MAA production primarily relies on the acetone-cyanohydrin (ACN) process and the oxidation of isobutylene or ethylene-based methacrolein [14, 15]. HCN and cyanide intermediates are the major feedstocks for the ACN process, while alternative oxidation routes consume substantial amounts of fossil-fuel-derived feedstocks. The industrial viability of greener production methods, such as converting biomass-derived citric acid or citramalic acid to MAA via decarboxylation and dehydration at 250 °C [224], are hindered by low yields and poor atom economy [14, 225]. The economic benefits of producing MAA from PMMA scraps are substantial. This process not only facilitates the management of larger volumes of PMMA waste but also aligns the market demand for MAA with the available supply of PMMA waste. Additionally, the BP and melting points (MP) of the involved compounds facilitate purification compared to PMMA thermolysis to MMA. For instance, methyl isobutyrate (BP 90 °C) hydrolyzes to isobutyric acid (BP 155 °C, MP −47 °C), and ethyl acrylate (BP 100 °C) hydrolyzes to acrylic acid (BP 141 °C), both of which can be easily separated from MAA (BP 162 °C, MP 15 °C) [13].

Current recycling of PMMA to MAA is constrained to lab-scale fluidized/ fixed bed reactors [5, 16, 69] and stirred tank reactors [2, 17]. The primary reaction mechanism involves a series of steps where PMMA is thermally depolymerized into MMA, which is subsequently hydrolyzed into MAA. However, the acidic solid catalysts used in this process deactivate

after each batch reaction. To date, continuous recycling of PMMA into MAA has not been reported.

In fixed-bed [69] and fluidized-bed [5,16] reactors, previous studies have tested only gram-scale quantities of virgin PMMA powder, achieving an MAA yield of over 50 % without accounting for energy consumption or unit recycling costs. In stirred-tank reactors [2, 17], researchers primarily used waste artificial marble containing 40 % PMMA and 60 % aluminum hydroxide ($Al(OH)_3$) to recover MMA and MAA, with MMA as the dominant product. However, stirred-tank processes operate in batch mode, necessitating downstream reactor cleaning, which could lead to high operational costs in industrial applications.

Reactive extrusion, which combines conventional physical melt extrusion with chemical reactions in a single screw or twin-screw extruder, is a promising method to produce continuously crude r-MMA from scraps [67, 226]. The European project MMAtwo demonstrated a continuous reactive extrusion thermolysis process, converting extrusion, injection, and cast grade scraps into MMA monomer with yields between 80 % and 90 % at the pilot scale [56].

In this study, we developed a lab-scale two-stage reactive extrusion hydrolysis system (Fig. 6.1) to convert injection- and extrusion-grade scraps into MMA and/or MAA at temperatures ranging from 330 °C to 370 °C. The first-stage single screw extruder served as a feeder, injecting melt into the second-stage twin-screw extruder where it degraded further. The designed intermeshing co-rotating twin-screw extruder provides self-cleaning capabilities, enabling the efficient extrusion of unreacted residues and solid catalysts [226]. We injected a fluorescent tracer to study the residence time distribution (RTD) of PMMA melt along the twin-screw extruder. Additionally, we applied a Plackett-Burman design to identify the optimal conditions for degradative extrusion before further optimizing operational parameters [227]. Both multiphase extrusion using solid powder catalysts (H-type zeolite Y-80 and gamma Al_2O_3) and homogeneous extrusion with liquid catalysts (KOH, H_2SO_4, and phosphotungstic acid hydrate (PTA) solutions) were investigated. We compared two degassing methods: vacuum and atmospheric degassing. MMA was the predominant condensed product, regardless of the presence of steam and/or catalyst. Notably, multiphase extrusion of PMMA with zeolite Y-80 at 370 °C converted almost all the PMMA but the yield was only 5.3 % when a single catalyst was used to recycle injection-grade scraps.

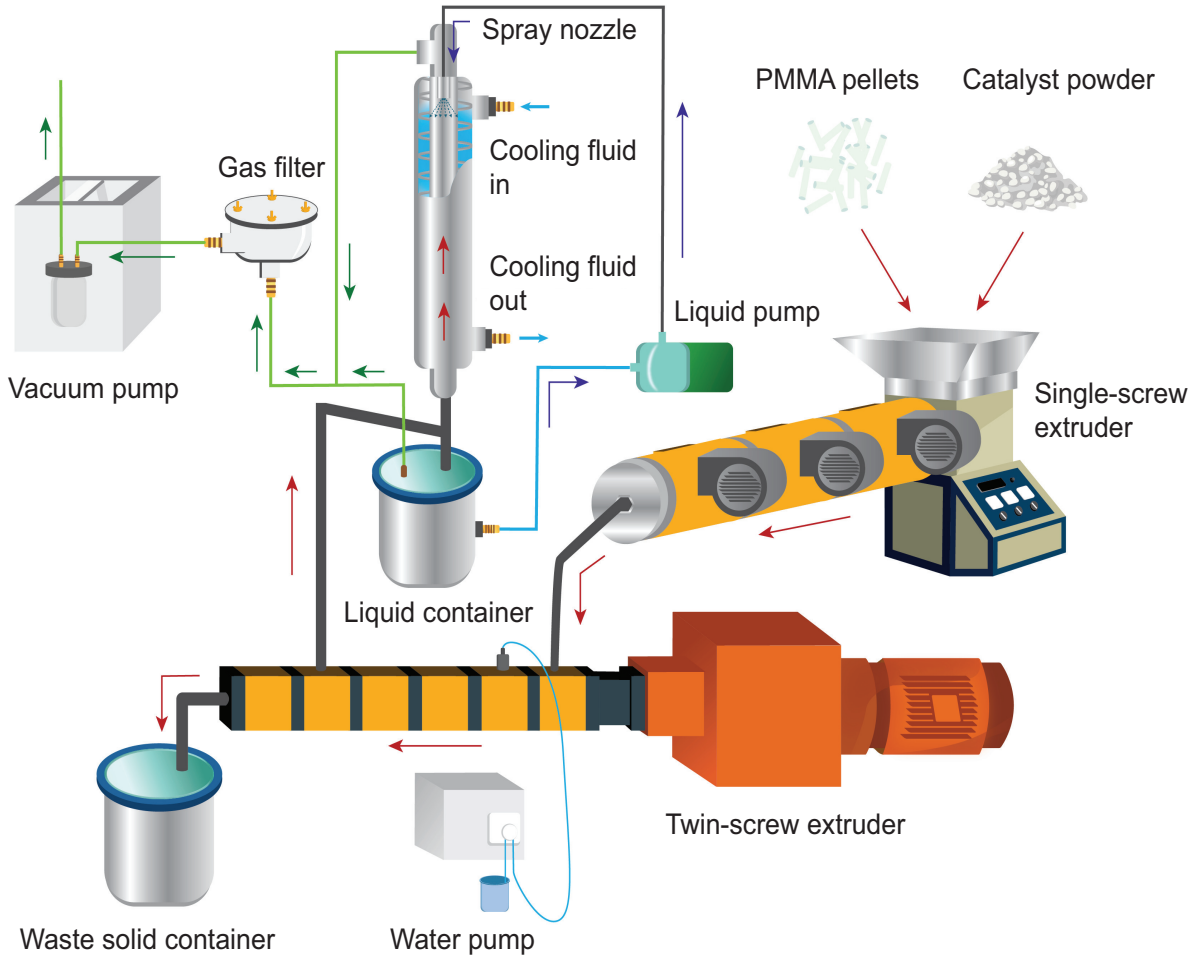

Figure (6.1) **Setup of the two-stage reactive extrusion hydrolysis system.** The single screw extruder was connected to the twin-screw extruder, functioning as a feeder. A vacuum degassing and circulation condensation system was employed to collect the liquid products.

6.3 Experimental

6.3.1 Materials

Injection-grade PMMA scraps and extrusion-grade PMMA scraps were provided by Montreal Polymers. Virgin PMMA granules (M_w=100 000 g mol^{-1}) were supplied by Altuglas. We purchased gamma Al_2O_3 (PURALOX SCCa-5/200) from Sasol and H-type zeolite Y (CBV780, SiO_2/Al_2O_3 mole ratio=80, 780 m g^{-2}) powder from Zeolyst. Phosphotungstic acid hydrate (PTA) was obtained from Thermo Scientific Chemicals. Isopropyl alcohol (≥99.8 %, GC grade) and GC-MS calibration standard MAA (99 % with 250 ppm MEHQ as inhibitor), methanol (≥99.9 %, HPLC grade), and acetone (≥99.9 %, HPLC grade) were

sourced from Sigma-Aldrich. MMA (≥99.6 % with 6-tert-Butyl-2,4-xylenol) was purchased from TCI America. Anhydrous ethanol (HPLC grade) was provided by Commercial Alcohols. Potassium hydroxide (reagent grade, 90 %) and the fluorescent tracer anthracene were also purchased from Sigma-Aldrich. Sulfuric acid (70 % w/w) was obtained from Anachemia, and solvent acetone (≥99.6 %, ACS reagent) was sourced from Thermo Scientific Chemicals.

6.3.2 Characterization

N_2 adsorption

A Quantachrome Autosorb-1 analyzer characterized the surface area and porosity of the gamma Al_2O_3 catalyst. The Al_2O_3 powder was vacuum degassed at 350 °C for 12h. The specific surface area of Al_2O_3 was determined using the multi-point Brunauer-Emmett-Teller (BET) method in the P/P_0 range of 0.05 to 0.30 [228]. The adsorbed N_2 volume at $P/P_0 = 0.99$ was used to estimate the total pore volume. The t-plot method in the t range of 3.5 Å to 5.0 Å was used to determine the volume of micropores and the specific surface area of mesopores. The average pore size and pore size distribution were estimated using the Barrett-Joyner-Halenda (BJH) model [228].

Particle size distribution (PSD)

A Horiba LA950 laser diffractometer measured the particle size distribution (PSD) of the powder.

Scanning electron microscopy with energy dispersive X-ray spectroscopy (SEM/EDS)

A small piece of the extrudate was cut using pliers. The cut section, created by the pliers, was oriented upward for SEM analysis. Prior to scanning, a thin layer of gold (Au) was sputter-coated onto the sample surface to enhance conductivity. The morphology and elemental mapping of the extrudes were analyzed using a JEOL JSM-7600F Scanning Electron Microscope (SEM) equipped with a Schottky field emission gun and an Oxford Instruments X-MaxN Energy Dispersive Spectroscopy (EDS) detector. The accelerating voltage was set to 5.0 kV for imaging.

Fourier-transform infrared spectroscopy (FTIR)

A PerkinElmer Spectrum 65 FTIR spectrometer detected the functional groups of PMMA extrudates and scraps. The solid extrudates and scraps were dissolved in acetone and kept at room temperature for 12 h. The supernatant was separated and dropped onto the surface of the spectrometer's sample chamber. After the acetone evaporated, a thin film formed on the chamber surface. The spectrometer then scanned the film from 4000 to 600 cm^{-1}.

Gel permeation chromatography (GPC)

The molecular weight (Mw) of PMMA scraps was measured with a Thermo Scientific UltiMate 3000 HPLC system equipped with two tandem Shodex GPC columns, KF-803L and KF-804L. The system was calibrated with the Shodex PMMA calibration kit, STANDARD M-75. The GPC system utilized a Refractive Index (RI) detector and tetrahydrofuran (THF) as the eluent. The temperature of the RI detector and the columns was maintained at 35 °C, and the eluent flow rate was kept at 1 mL min^{-1}. All PMMA scraps were dissolved in THF prior to injection.

Thermogravimetric analysis (TGA)

Thermogravimetric degradation curves of PMMA scraps and extrudates were determined using a TA Instruments Q500 or Q550 Thermogravimetric Analyzer. All samples were heated from room temperature to 700 °C at a rate of 5 °C min^{-1} under a nitrogen atmosphere with a flow rate of 60 mL min^{-1}.

Differential scanning calorimetry (DSC)

The glass transition temperature (T_g) of PMMA scraps was measured using a TA Instruments DSC Q-2000 differential scanning calorimeter. The samples, encapsulated in aluminum pans, were kept at 135 °C for 10 min to eliminate thermomechanical history, followed by cooling to 40 °C. Each sample was heated to 180 °C at a rate of 10 °C min^{-1} and then cooled to 40 °C under a nitrogen atmosphere with a flow rate of 50 mL min^{-1}. This heating and cooling cycle was repeated three times, with the second heating cycle used to plot the DSC curve.

6.3.3 Liquid products analysis

The liquid products were quantitatively and qualitatively analyzed using an Agilent 7890A/5975C Gas Chromatography-Mass Spectrometry (GC-MS) system equipped with an Agilent 7693 Autosampler. A 30-meter Agilent J&W DB-Wax UI column (polyethylene glycol stationary phase) with an inner diameter of 0.25 mm and a film thickness of 0.25 µm was used to separate the components. For qualitative analysis, the MSD scanned the m/z ratio in the range of 29 to 500 in full scan mode. For quantitative analysis, selected ion monitoring (SIM) mode was employed to scan acetone (m/z=43 and 58), methanol (m/z=31), MMA (m/z=41, 69, and 100), and MAA (m/z=41 and 86). The concentration of the four components was quantified using an external calibration method. Anhydrous ethanol was used as the solvent for all calibration standards and samples.

The PMMA conversion (X_{PMMA}), product selectivity (S_i), and yield (Y_i) were calculated using the following formulas:

$$X_{\mathrm{PMMA}} = (1 - \frac{\text{mass of extrudates - catalyst fed}}{\text{mass of PMMA fed}}) \times 100\% \tag{6.1}$$

$$S_i = \frac{\text{moles of product i} \times \text{carbon number in product i}}{\text{MMA moles in degraded PMMA} \times 5} \times 100\% \tag{6.2}$$

$$Y_i = \frac{\text{moles of product i} \times \text{carbon number in product i}}{\text{MMA moles in PMMA fed} \times 5} \times 100\% \tag{6.3}$$

where i means different liquid products (i.e. MMA, MAA, MeOH and acetone).

To simplify the calculation of PMMA conversion, we assume that the extrudates consist solely of unreacted PMMA and catalysts. This assumption holds despite the presence of additional components such as carbon deposits and partially hydrolyzed PMMA in the extrudates. However, PMMA remains the predominant polymer residue in the extrudates.

6.3.4 Experimental set-up

PMMA scraps or PMMA scrap-solid catalyst blends were fed into a two-stage extruder system (Fig. 6.1). The first-stage extruder was an SJ30 single screw extruder (diameter D=30 mm, length to diameter ratioL/D=25:1) with three heating zones, manufactured by Zhangji-

agang MC Machinery Co., Ltd. The second-stage extruder was a T20 co-rotating twin-screw extruder (D=22.4 mm, L/D=46:1) manufactured by Nanjing Huaju Machinery Co., Ltd. The temperature profile along the twin-screw extruder is presented in Fig. 6.4.

The screw configuration of the twin-screw extruder consists of a feeding zone, liquid injection zone, reaction zone, degassing zone, and compression zone (Supplementary Fig. 6.1). Two reverse conveying screw elements were configured separately before the liquid injection zone and the degassing zone to build melt pressure. An AZURA P 4.1S pump injected liquid from the third barrel of the second-stage extruder. A 304 stainless steel AB double-wall fin heat exchanger (L=0.975 m, D=0.05 m) condensed the condensable gaseous products from the degassing port. A 304 stainless steel vacuum container connected to the bottom of the heat exchanger collected condensed products, while another vacuum container collected residues from the die of the second-stage extruder. To aid in the condensation of products, a magnetic drive water circulating pump transported liquid from the liquid container to a spray nozzle placed at the top of the heat exchanger.

During the vacuum degassing process, a vacuum pump was applied to the condenser and the liquid container. The vacuum pump was removed for the atmospheric degassing process.

PMMA exhibits low viscosity above 300 °C. In the designed screw and barrel configuration (Supplementary Fig. 6.1), the second barrel (feeder barrel) is set at 220 °C, ensuring that PMMA behaves as a viscous polymer. To prevent backflow of gas and melt, we incorporated reverse screw elements before the liquid injection zone, creating a choked zone.

The third to fifth barrels constitute the reaction zone, where PMMA melt transitions to a low-viscosity, water-like state. In these zones, shear forces primarily serve to renew material surfaces and enhance mixing. However, the depolymerization and hydrolysis reactions in this system are primarily driven by heat rather than shear forces.

From the degassing zone to the final compression zone (sixth and seventh barrels), the temperature is maintained at or below 250 °C, where shear forces facilitate the extrusion of unreacted materials. The reaction barrels operating above 330 °C involve a degradative reactive extrusion process, significantly reducing polymer viscosity.

Although PMMA exhibits low viscosity and a water-like flow behaviour above 330 °C, we still consider it to be in a melt state. The generated monomers, MMA and MAA, transitions to the gas phase at temperatures above 300 °C. The designed reaction system constitutes a complex heterogeneous system involving melt-solid-gas interactions.

6.3.5 Experimental procedure

The PMMA feeding rate corresponded to the screw rotation speed of the single screw extruder. Blends of PMMA scraps and powder catalysts, or PMMA scraps alone, were fed from the hopper into the first-stage extruder. The melt was then transferred into the second barrel of the second-stage extruder. To avoid severe PMMA melt degradation before the liquid injection zone, the three heating zones on the first-stage extruder were maintained at 200 °C, and the connector between the two stages of the extruder, and the second barrel of the twin-screw extruder were kept at 220 °C.

A liquid pump injected liquid from the third barrel of the twin-screw extruder during the melt extrusion process. PMMA depolymerization/hydrolysis commenced from the third to the sixth barrels. The last barrel (i.e., the seventh barrel) of the twin-screw extruder was kept at 220 °C to terminate the PMMA depolymerization and extrude the residues. The operating temperature (250 °C or 300 °C) of the degassing barrel was lower than the reaction temperature (330 °C, 350 °C or 370 °C) in the third to fifth barrels. The third to fifth barrels constitute the reaction zone, where PMMA melt transitions to a low-viscosity, water-like state.

The rotation speed of the twin-screw extruder was maintained at 240 rpm, 300 rpm, or 360 rpm. A chiller set at 3.5 °C cooled the condenser. The collection of hydrolyzed or thermolyzed products began once the reaction temperature was reached. Each trial was conducted for 1 h. The feeding rate for each trial was either $0.5\,\mathrm{kg\,h^{-1}}$ or $0.75\,\mathrm{kg\,h^{-1}}$.

For the DOE tests, 1.5 L of a 20:80 (L:L) ethanol-water solution was added to the liquid container to generate a spray prior to reaction. For reactions under optimized operating conditions, 1 L of pure ethanol was used in the liquid container to form a spray and absorb condensable gaseous components. Residues from the die of the twin-screw extruder were weighed to calculate PMMA conversion. Liquid in the container was collected and analyzed by GC-MS.

6.3.6 Residence time distribution (RTD) measurement

During the extrusion of virgin PMMA, 0.1 g of the fluorescent tracer anthracene was injected at the position of the liquid injector (Supplementary Fig. 6.1a). Extrudates were collected every minute and subsequently dissolved in a mixture of isopropyl alcohol and acetone in a 3:2 ratio (L:L). The fluorescence of the PMMA solutions, placed in a 384-well plate, was quantitatively measured using a TECAN Spark multimode microplate reader. The monochromator was set to an excitation wavelength of 397 nm and an emission wavelength of 352 nm.

We characterized the hydrodynamics with an axial dispersion model to fit [229, 230]:

$$\frac{\partial C}{\partial \theta} + \frac{\partial C}{\partial \xi} = \frac{1}{N_{\mathrm{Pe}}} \frac{\partial^2 C}{\partial^2 \xi} \tag{6.4}$$

where C is the normalized relative fluorescence intensity (RFI), $\theta{=}tu/Z$ is the non-dimensional time, $u{=}Q/A$ is the melt velocity, Q is the melt volume feeding rate, and A is the internal cross-sectional area of the die, Z is the extrusion length (0.773 m), $\xi{=}z/Z$ is the non-dimensional length, Pe is the dimensionless Peclet number defined as $N_{\mathrm{Pe}}{=}uZ/D$, and D is the axial dispersion coefficient.

The injection of the fluorescence tracer is considered to be in the form of a bolus pulse. The exact analytic solution for the bolus pulse function is [229]:

$$G'(\theta) = G(\theta) - H(\theta - \tau)G(\theta - \tau) \tag{6.5}$$

$$H(\theta - \tau) = \begin{cases} 0, \theta \leq \tau \\ 1, \theta > \tau \end{cases} \tag{6.6}$$

$$G(\theta) = 0.5 \left[\mathrm{erfc} \sqrt{\frac{N_{\mathrm{Pe}}}{4\theta}} (1 - \theta) + e^{N_{\mathrm{Pe}}} \mathrm{erfc} \sqrt{\frac{N_{\mathrm{Pe}}}{4\theta}} (1 + \theta) \right] \tag{6.7}$$

where, $\tau{=}t_d u/Z$ is the non-dimensional time length of the pulse injection, and t_d is the delay time from tracer injection to the first extrusion. Tracer was injected from the liquid injector position (Supplementary Fig. 6.1a).

For the pulse injection, the mean residence time ($\bar{t}$) can be expressed in both continuous and

discrete forms as follows [231]:

$$\bar{t} = \frac{\int_0^\infty tC(t)dt}{\int_0^\infty C(t)dt} = \frac{\sum t_i C_i \Delta t_i}{\sum C_i \Delta t_i} \tag{6.8}$$

where, Δt_i is 1 min, as samples were collected at 1-minute intervals.

We normalized the relative fluorescence intensity (RFI) data and the model to ensure that the area under the curves equals one:

$$Y_i = \frac{C_i}{\sum C_i \Delta t} \tag{6.9}$$

$$\sum Y_i = 1 \tag{6.10}$$

The Peclet number characterizes the extrusion hydrodynamics by determining the number of continuous stirred tank reactors (CSTRs) in series [229]:

$$N_{\mathrm{CSTR}} = \frac{N_{\mathrm{Pe}}}{2} + 1 \tag{6.11}$$

6.3.7 Design of experiments (DOE)

To determine the optimal reaction operating conditions, we employed a Plackett-Burman design with five factors, each evaluated at two levels (Table 6.1).

Table (6.1) Factors and levels selection for design of experiments (DOE)

No.	Factor	Level 1	Level 2
Factor 1	T (°C)	330	350
Factor 2	N_{TSE} (rpm)	240	360
Factor 3	Q_{PMMA} ($\mathrm{g\,h^{-1}}$)	500	750
Factor 4	Scrap	Injection	Extrusion
Factor 5	Catalyst	HY(80)	Al_2O_3

Note: T-temperature, N_{TSE}-screw rotation speed of twin-screw extruder, Q_{PMMA}-PMMA scrap feeding rate.

The Plackett-Burman design (Table 6.2) consists of 12 unique runs without any repetitions. The experimental results were analyzed using Minitab Statistical Software 22 (trial version). To analyze the factorial design, the categorical factors scrap type (factor 4) and catalyst type

(factor 5) were assigned low values of -1 (injection, Al_2O_3) and high values of 1 (extrusion, HY(80)).

Table (6.2) Plackett–Burman design including five factors at two levels

Run	Block	T °C	N_{TSE} rpm	Q_{PMMA} g h^{-1}	Scrap	Catalyst
1	1	350	240	0.75	Injection	Al_2O_3
2	1	330	240	0.5	Injection	Al_2O_3
3	1	350	360	0.5	Extrusion	Al_2O_3
4	1	350	360	0.5	Extrusion	HY(80)
5	1	330	240	0.75	Extrusion	HY(80)
6	1	350	360	0.75	Injection	HY(80)
7	1	330	360	0.5	Injection	Al_2O_3
8	1	330	240	0.5	Extrusion	HY(80)
9	1	330	360	0.75	Injection	HY(80)
10	1	350	240	0.75	Extrusion	Al_2O_3
11	1	330	360	0.75	Extrusion	Al_2O_3
12	1	350	240	0.5	Injection	HY(80)

Note: The catalyst constitutes 1.8 % by weight of the PMMA scraps. The rate of H_2O injection is set to 1.2 times the theoretical amount required for the reaction converting MMA to MAA and methanol.

Vacuum degassing improves efficiency and is widely used in devolatilization during polymer extrusion. However, MMA water vapor mist that forms in the condensation and collection steps reduces yield. Therefore, we excluded degassing type as a factor in the DOE.

6.4 Results and discussion

6.4.1 Residence time distribution (RTD) test and modelling

Screw speed, feeding rate, temperature, and screw profile affect the mixing pattern and residence time distribution (RTD) within a twin-screw extruder. Increasing screw speed or decreasing feeding rate reduces the fill fraction of materials in the extruder [232]. A lower degree of fill enhances axial mixing within the extruder, as evidenced by the decreased Peclet (N_{Pe}) number. The N_{Pe} number, the reciprocal of the dispersion number, quantifies the extent of axial mixing or backmixing [231, 233]. A lower N_{Pe} number indicates enhanced axial mixing, which improves the contact between catalysts and the PMMA melt or MMA. Conversely, a higher N_{Pe} number suggests more pronounced plug flow behavior and reduced

interactions between degradation products and PMMA. This condition helps minimize selectivity towards certain impurities, such as isobutyrate. Controlling N_{Pe} in the extruder is crucial for optimizing the balance between mixing to achieve uniformity and minimizing backmixing to maintain product quality.

A fluorescence tracer was introduced at the liquid injector port (Supplementary Fig. 6.1a). Increasing the screw speed from 240 rpm to 300 rpm at a feeding rate of $0.5\,\mathrm{kg\,h^{-1}}$ and a temperature of 220 °C shifted the RTD curves to shorter times, indicating a decreased mean residence time $\bar{t}$ (Fig. 6.2a). Additionally, this increase in screw speed reduced the N_{Pe} value from 17.6 to 16.6, demonstrating that higher screw speeds enhance axial mixing.

At a screw speed of 240 rpm and a temperature of 220 °C, increasing the feeding rate from $0.5\,\mathrm{kg\,h^{-1}}$ to $0.75\,\mathrm{kg\,h^{-1}}$ shifted the RTD curves to the left and reduced the $\bar{t}$ to 9.4 min, but increased the N_{Pe} (Fig. 6.2b). The higher feeding rate resulted in a greater degree of fill, which weakens axial mixing [232, 234].

Reducing the extrusion temperature from 220 °C to 200 °C at a screw speed of 240 rpm and a feeding rate of $0.5\,\mathrm{kg\,h^{-1}}$ decreased the N_{Pe} from 17.6 to 12, while slightly increasing the mean residence time, $\bar{t}$, from 11.7 min to 12.8 min (Fig. 6.2c). At higher processing temperatures, the viscosity and density of the melt decrease, enhancing the melt velocity (u). However, elevated temperatures also accelerate the thermal motion of molecules, leading to an increase in the axial dispersion coefficient (D). To prevent thermal degradation of PMMA during the RTD tests, we avoided higher extrusion temperatures. Within the temperature range of 200 °C to 220 °C, the increase in the axial dispersion coefficient (D) had a more pronounced effect on N_{Pe} than the corresponding increase in melt velocity (u).

Reactive extrusion hydrolysis involves a melt-solid-gas heterogeneous state, where effective mixing of catalysts with the melt and steam is crucial. While reduced axial mixing (higher N_{Pe}) decreases the formation of impurities, plug flow-like extrusion also reduces the axial mixing of catalysts within the PMMA melt. This degrades contact between catalysts and MMA, reducing MAA yield. Conversely, longer residence times enhance PMMA depolymerization by increasing PMMA conversion. However, extending the residence time decreases the overall productivity of the reactive extrusion hydrolysis process. Therefore, optimizing the axial mixing extent (N_{Pe} number) and residence time is essential to achieve high PMMA conversion and yield of MMA and/or MAA while minimizing impurity levels.

6.4.2 Design of experiments (DOE)

To identify the key factors affecting reactive extrusion degradation, we employed a Plackett-Burman design of experiments. PMMA conversion (X_{PMMA}), yield (Y_i), selectivity (S_i), and recovered carbon (carbon balance) responded to five selected factors (Table 6.3). The Pareto charts revealed that no factors significantly affected X_{PMMA}, Y_{MMA}, Y_{MAA}, S_{MMA}, S_{MeOH}, or recovered carbon (Supplementary Fig. 6.3a-c, e, g-h). However, temperature and catalyst type significantly affected Y_{MeOH} and S_{MAA} (Supplementary Fig. 6.3d & f), which correspond to the MMA hydrolysis reaction. Vacuum degassing resulted in an irreversible loss of volatile vapors.

The X_{PMMA} of both extrusion- and injection-grade scraps increased as the temperature rose from 330 °C to 350 °C. A lower PMMA feeding rate, resulting in longer residence times, leads to increased PMMA conversion. Increasing the feeding rate shortens the residence time of the PMMA melt within the extruder and reduces axial mixing [235]. Although screw speed (N_{TSE}) did not significantly affect X_{PMMA} and MMA hydrolysis, increasing N_{TSE} decreased the residence time of the melt but enhanced axial mixing [236].

PMMA hydrolysis is a tandem reaction process. First, PMMA thermally depolymerizes to MMA, followed by the catalytic hydrolysis of MMA to MAA [5, 16]. At higher reaction temperatures, the kinetics of PMMA depolymerization are faster than those of MMA hydrolysis, resulting in a much higher yield of MMA compared to MAA. The generation rate of MMA is primarily determined by barrel temperature and the mean residence time in the reaction zones of the twin-screw extruder, although mechanical shear also slightly contributes to PMMA degradation [237].

Selectivity to MAA was higher over HY(80) compared to Al_2O_3. The weight ratio of catalysts in the PMMA feed is set at 1.8 %. This low catalyst/PMMA ratio may not achieve a high MAA yield due to insufficient contact between PMMA or MMA and the catalysts.

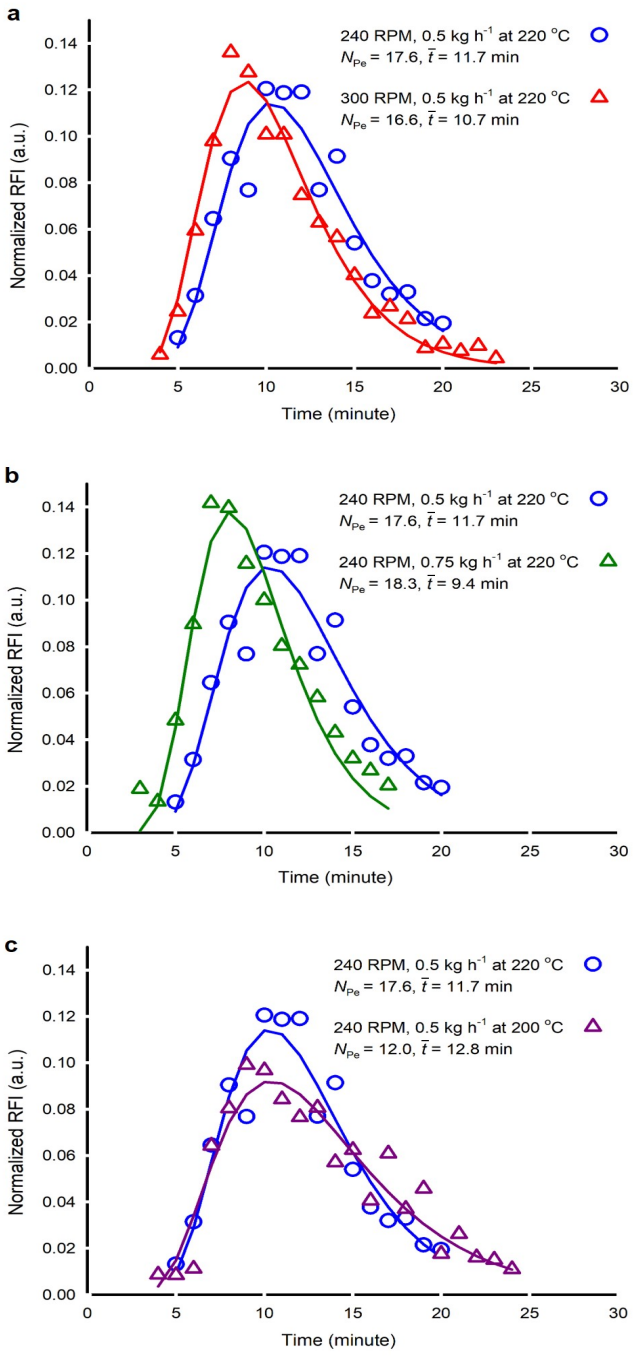

Figure (6.2) **Residence time distribution (RTD) of reaction zones in a twin-screw extruder.** The hollow symbols represent normalized relative fluorescence intensity (RFI) curves, while the solid lines are the simulated RTD curves using the axial dispersion model. N_{Pe} denotes the Peclet number, and $\bar{t}$ represents the mean residence time. **a**, Normalized RTD at different screw speeds for a feeding rate of $0.5\,\mathrm{kg\,h^{-1}}$ at $220\,^{\circ}\mathrm{C}$. **b**, Normalized RTD at different feeding rates at 240 rpm and $220\,^{\circ}\mathrm{C}$. **c**, Normalized RTD at different extrusion temperatures for a feeding rate of $0.5\,\mathrm{kg\,h^{-1}}$ at 240 rpm.

Table (6.3) Design of experiments (DOE) and results of DOE

Run	Scrap	Cat.	$Q_{cat.}$ $g\,h^{-1}$	Q_{H_2O} $mL\,min^{-1}$	Degassing	T °C	Q_{PMMA}[a] $g\,h^{-1}$	N_{TSE} rpm	X_{PMMA} %	Y_{MMA} %	Y_{MAA} %	Y_{MeOH} %	S_{MMA} %	S_{MAA} %	S_{MeOH} %	Recovered C[b] mol %
1	Injection	Al_2O_3	13.6	2.7	Vacuum	350	740	240	33	6.3	0.7	0.2	19.1	2.2	0.5	74.3
2	Injection	Al_2O_3	8.9	1.8	Vacuum	330	488	240	24	3.1	0.2	0.1	13.1	0.9	0.4	79.7
3	Extrusion	Al_2O_3	9.0	1.8	Vacuum	350	491	360	43	5.0	1.0	0.2	11.4	2.3	0.5	62.9
4	Extrusion	HY(80)	9.0	1.8	Vacuum	350	493	360	19	6.8	1.1	0.5	35.9	5.6	2.4	89.5
5	Extrusion	HY(80)	14.2	2.7	Vacuum	330	775	240	4	0.9	0.5	0.2	23.3	11.9	5.9	97.8
6	Injection	HY(80)	13.6	2.7	Vacuum	350	740	360	31	13.8	0.9	0.3	44.3	2.8	1.1	83.9
7	Injection	Al_2O_3	8.9	1.8	Vacuum	330	488	360	24	3.5	0.2	0.1	14.4	0.9	0.4	79.6
8	Extrusion	HY(80)	9.0	1.8	Vacuum	330	493	240	3	1.6	0.4	0.3	55.8	15.0	9.2	99.4
9	Injection	HY(80)	13.6	2.7	Vacuum	330	740	360	4	2.6	0.6	0.2	59.6	14.0	5.3	99.1
10	Extrusion	Al_2O_3	13.4	2.7	Vacuum	350	733	240	25	4.3	0.7	0.2	16.9	2.8	0.7	79.9
11	Extrusion	Al_2O_3	13.4	2.7	Vacuum	330	733	360	10	1.0	0.1	0.1	9.7	0.7	0.5	90.7
12	Injection	HY(80)	9.0	1.8	Vacuum	350	491	240	51	20.4	1.2	0.5	40.3	2.4	0.9	71.5

Note: T-temperature, cat.-catalyst, $Q_{cat.}$-feeding rate of catalyst, Q_{H_2O}-liquid H_2O injection rate, Q_{PMMA}-PMMA scrap feeding rate, N_{TSE}-screw rotation speed of twin-screw extruder. a-PMMA feeding by a single screw extruder, b-considering carbon in residues and quantitatively analyzed liquid components MMA, MAA, methanol and a trace of acetone. Yield and selectivity to acetone were excluded in this table due to low concentration.

6.4.3 Properties of PMMA scraps

Injection-grade scraps contain only one type of PMMA, while extrusion- grade scraps include both white and red components (Fig. 6.3a & b). FTIR analysis exhibited a prominent peak at 1728 cm^{-1}, corresponding to the C=O stretch vibration. Additionally, two adjacent peaks were observed at 2952 cm^{-1} and 3000 cm^{-1}, attributed to the C-H stretching vibrations of $-CH_2$ and $-CH_3$, respectively [238–240] (Fig. 6.3c). These characteristic peaks confirm that all scraps are composed of only PMMA.

The midpoint glass transition temperature (T_g) of injection-grade scraps (T_g=109 °C) is higher than that of the white (T_g=90 °C) and red (T_g=101 °C) components in extrusion-grade scraps (Fig. 6.3d). The T_g of all scraps ranges from 55 °C to 130 °C, indicating an atactic tacticity [215]. Higher T_g values are closer to syndiotactic tacticity, while lower T_g values are closer to isotactic tacticity [241]. The lack of a melting point in the DSC curves indicates that the used PMMA is amorphous and further confirms that it is atactic [242].

Thermogravimetric analysis revealed that injection-grade scraps began to degrade at a lower temperature of 250 °C compared to the white and red components in extrusion-grade scraps in N_2 (Fig. 6.3e). The white and red components in extrusion-grade scraps exhibited similar thermal degradation behavior, starting to lose weight at 280 °C. Injection-grade scraps and white extrusion-grade scraps left residues of approximately 1 % to 2 %, while red extrusion-grade scraps had 6 % non-thermally degradable residues. These residues are due to fillers or additives in the scraps.

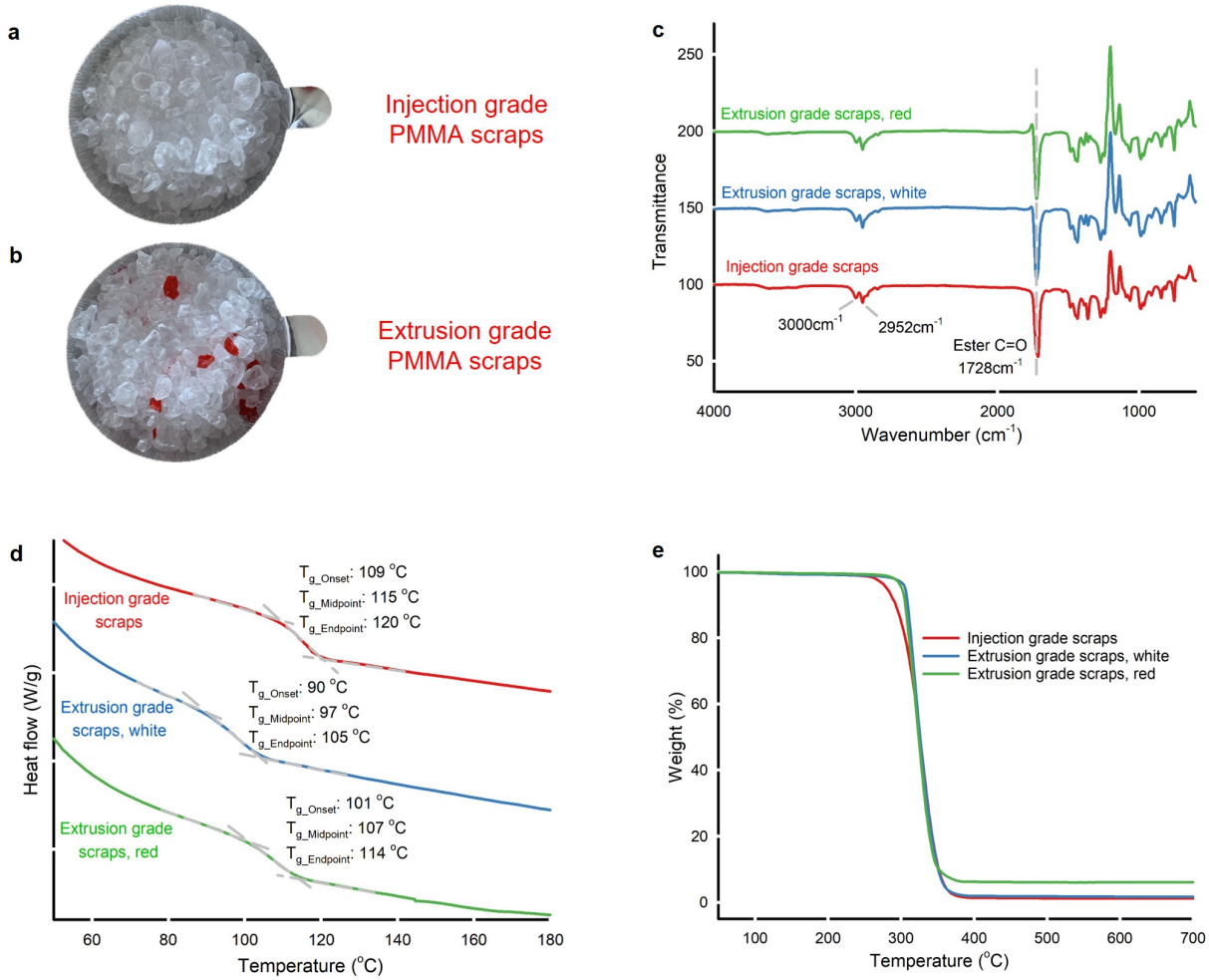

Figure (6.3) **Properties of injection-grade and extrusion-grade PMMA scraps.** Injection-grade scraps consist of only one type of PMMA, while extrusion-grade scraps predominantly contain white PMMA with a small amount of red PMMA. **a**, Physical image of injection-grade PMMA scraps. **b**, Physical image of extrusion-grade PMMA scraps. **c**, FTIR spectra of injection-grade and extrusion-grade scraps from 4000 to 600 cm^{-1}. **d**, DSC curves of injection-grade and extrusion-grade scraps were recorded from 40 °C to 180 °C at a heating rate of 10 °C min^{-1} under a nitrogen atmosphere with a flow rate of 50 mL min^{-1}. **e**, Thermogravimetric curves of injection-grade and extrusion-grade scraps under N_2 atmosphere (60 mL min^{-1}) with a heating ramp of 5 °C min^{-1}.

6.4.4 Optimization of extrusion reaction conditions

To increase the reaction time of PMMA depolymerization and MMA hydrolysis within the twin-screw extruder, we found that a lower screw speed and feeding rate are preferred. Following DOE experiments, we tested higher reaction temperatures and higher weight ratios of HY(80) to PMMA feed. Under optimized conditions, we fed 0.5 kg h^{-1} of PMMA scraps or

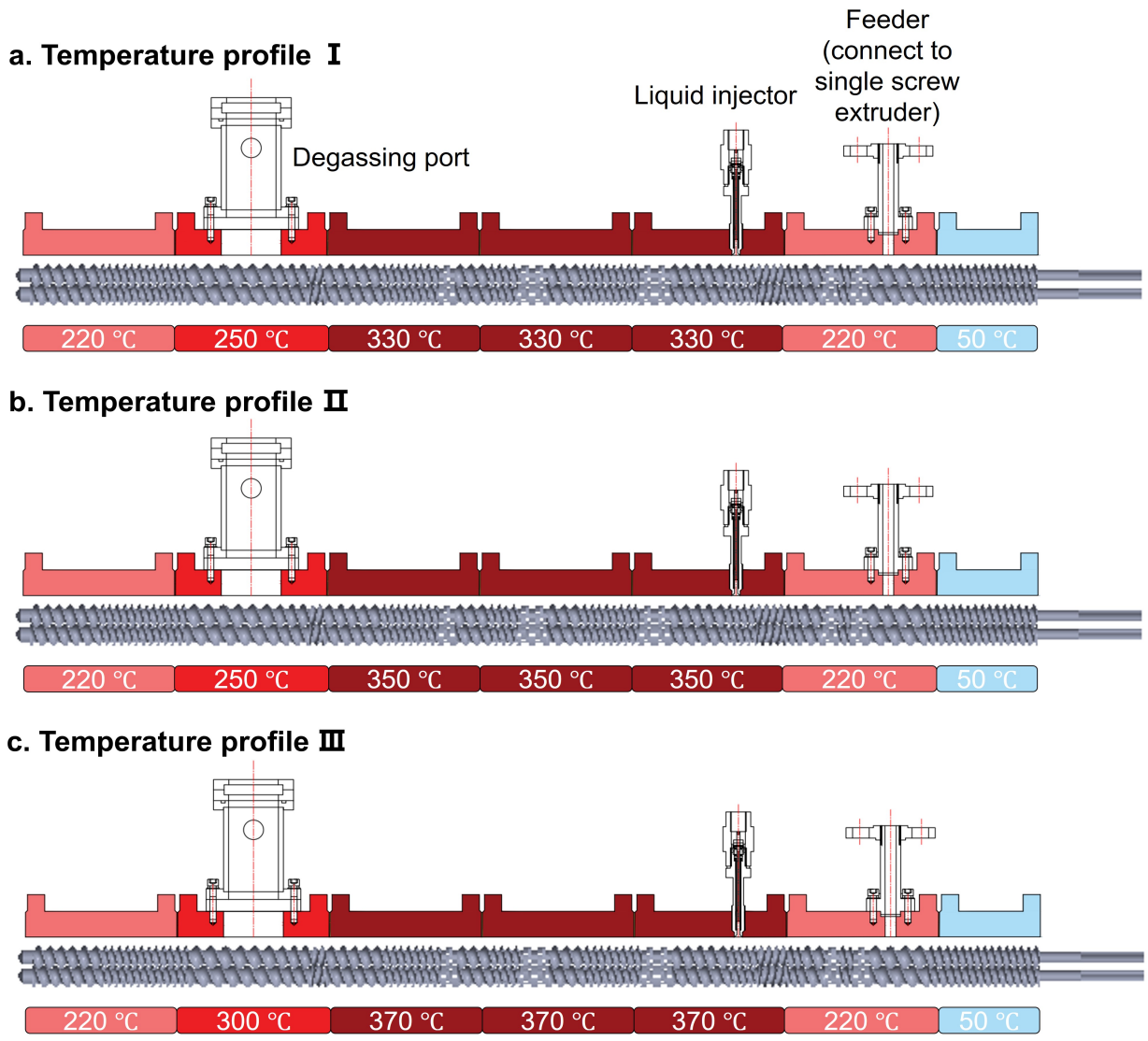

Figure (6.4) **Temperature profiles of PMMA reactive extrusion hydrolysis along the twin-screw extruder.** The first barrel is set at 50 °C to protect the gearbox from overheating during direct melt injection. The second barrel is set at 220 °C to ensure successful melt injection while minimizing melt degradation. The final barrel is also set at 220 °C to cool the melt and terminate the degradation reaction. **a**, Temperature profile I features a maximum degradative extrusion temperature of 330 °C and a degassing temperature of 250 °C. **b**, Temperature profile II features a maximum degradative extrusion temperature of 350 °C and a degassing temperature of 250 °C. **c**, Temperature profile III features a maximum degradative extrusion temperature of 370 °C and a degassing temperature of 300 °C.

mixtures of PMMA scraps and solid catalysts at a screw speed of 240 rpm. Injection-grade scraps depolymerize at lower temperatures compared to extrusion-grade scraps. Based on the DOE tests, we focused on recycling injection-grade scraps. To achieve higher PMMA conversion (X_{PMMA}), we increased the temperature of the reaction zones from 330 °C/350 °C to 370 °C and the degassing temperature from 250 °C to 300 °C (Fig. 6.4).

To compare the hydrolysis effects of solid and liquid catalysts, we used solid HY(80) catalyst and liquid catalysts including PTA, KOH, and H_2SO_4. To increase the contact between solid HY(80) and the PMMA melt, we increased the weight ratio of HY(80) to PMMA feed from 1.8 % (as used in DOE) to 10 %. Within the reaction zones, the components in the extruder exist in a melt-solid-gas heterogeneous state. Increasing the steam fraction in this heterogeneous system may contribute to higher PMMA depolymerization and MMA hydrolysis rates. In this work, at a feeding rate of 0.5 kg h^{-1}, we increased the water injection rate from 1.8 mL min^{-1} to 3.6 mL min^{-1}.

Impact of catalysts on hydrolysis and extrusion processes

Compared to hydrolysis extrusion with HY(80), PTA, KOH, and H_2SO_4, non-catalytic hydrolysis extrusion (N10) without catalysts at 370 °C and with 3.6 mL min^{-1} water injection exhibited the highest yield of MMA (Y_{MMA}=89 %) (Fig. 6.5a & Table 6.4). At 370 °C, pyrolysis extrusion (N11) without steam and catalysts achieved the second highest MMA yield (Y_{MMA}=75 %), though the PMMA conversion was lower at 82 % compared to the PMMA conversion (X_{PMMA}=96 %) in non-catalytic hydrolysis extrusion. This confirms that steam accelerates PMMA thermal depolymerization.

Hydrolysis extrusion with 10 % HY(80) at 370 °C (N4) resulted in a near-complete PMMA conversion (X_{PMMA}=100 %). Under the combined presence of 10 % HY(80) and PTA solution (N6), hydrolysis extrusion at 370 °C showed a PMMA conversion of 98 % but a lower MMA yield (Y_{MMA}=57 %) compared to hydrolysis extrusion with 10 % HY(80) (N4) alone (Y_{MMA}=67 %). The co-injection of PTA solution and solid HY(80) (N6) slightly increased the MAA yield from 5.3 % to 5.5 % compared to hydrolysis extrusion with 10 % HY(80).

Between co-injection of PTA and HY(80) (N6) and single injection of HY(80) (N4), the yields of MAA and methanol were similar, but the presence of PTA reduced the MMA yield by 15 %, indicating that PTA catalyzed the conversion of PMMA or MMA to other by-products.

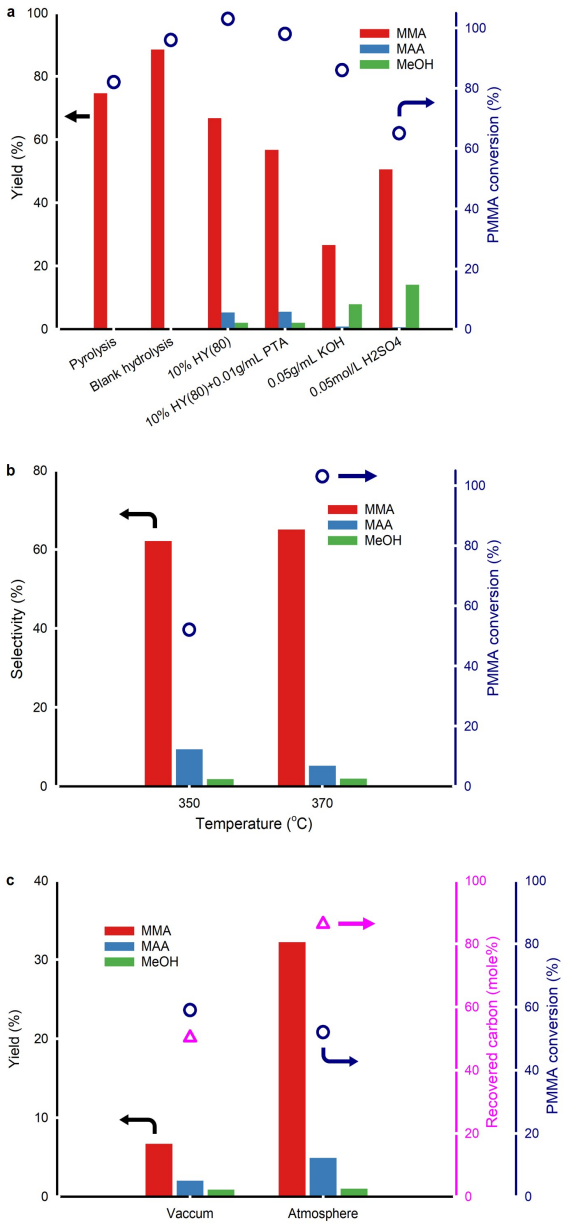

Figure (6.5) **PMMA reactive extrusion hydrolysis with and without catalysts.** The optimized twin-screw rotation speed is 240 rpm, with a scrap feeding rate of 0.5 kg h^{-1}. **a**, Yields of MMA, MAA, and MeOH (left axis, bar), and PMMA conversion (right axis, hollow circle) with and without catalysts at 370 °C for a one-hour reaction, with a liquid injection rate of 3.6 mL min^{-1} and under atmospheric degassing, excluding pyrolysis. **b**, The effect of hydrolysis temperature on the selectivity to MMA, MAA, and MeOH (left axis, bar), and PMMA conversion (right axis, hollow circle) for a one-hour reaction with 10 % HY(80) feeding and a liquid injection rate of 3.6 mL min^{-1} under atmospheric degassing. **c**, The effect of degassing methods on the yields of MMA, MAA, and MeOH (left axis, bar), and the recovered carbon (right axis, pink hollow triangle), as well as PMMA conversion (right axis, dark blue hollow circle) for a one-hour reaction at 350 °C with 10 % HY(80) feeding and a liquid injection rate of 3.6 mL min^{-1}.

Table (6.4) Reactive extrusion hydrolysis of PMMA to MMA and MAA

Run	Scrap	Cat.	Q_{Liquid}[a] mL min^{-1}	Degassing	T °C	Q_{PMMA} g h^{-1}	N_{TSE} rpm	X_{PMMA} %	Y_{MMA} %	Y_{MAA} %	Y_{MeOH} %	S_{MMA} %	S_{MAA} %	S_{MeOH} %	Recovered C[b] mol %
N1	Injection	0.01 g mL^{-1} PTA	3.6	Vacuum	350	500	240	62	22	1.2	1.1	36	2.0	1.8	62
N2	Injection	0.01 g mL^{-1} PTA	3.6	Vacuum	330	500	240	12	2	0.3	0.4	13	2.4	3.0	90
N3	Injection	10 % HY(80)	3.6	Vacuum	350	450	240	59	7	2.0	0.9	11	3.4	1.5	50
N4	Injection	10 % HY(80)	3.6	Atmosphere	370	444	240	100	67	5.3	2.0	65	5.2	1.9	71
N5	Injection	10 % HY(80)	3.6	Atmosphere	350	444	240	52	32	4.9	1.0	62	9.4	1.8	86
N6	Injection	10 % HY(80)+0.01 g mL^{-1} PTA	3.6	Atmosphere	370	444	240	98	57	5.5	2.0	58	5.7	2.0	66
N7	Injection	0.05 g mL^{-1} KOH	3.6	Atmosphere	370	500	240	86	27	0.8	7.9	31	0.9	9.2	49
N8	Injection	0.05 mol L^{-1} H_2SO_4	3.6	Atmosphere	370	458	240	65	51	0.6	14.0	77	0.9	21.4	100
N9	Injection	None (H_2O only)	3.6	Vacuum	350	500	240	31	8	1.0	0.2	25	3.2	0.6	78
N10	Injection	None (H_2O only)	3.6	Atmosphere	370	500	240	96	89	0.0	0.1	92	0.0	0.1	92
N11	Injection	None	0.0	Atmosphere	370	500	240	82	75	0.0	0.0	91	0.0	0.0	93

Note: a-Q_{Liquid}-H_2O or solutions injection rate, b-considering carbon in extrudates and quantitatively analyzed liquid components MMA, MAA, methanol and a trace of acetone.

At a hydrolysis extrusion temperature of 370 °C, the injection of KOH (N7) and H_2SO_4 (N8) exhibited PMMA conversions of 86 % and 65 %, respectively. Hydrolysis extrusion with KOH (N7) resulted in the lowest MMA yield (Y_{MMA}=27 %) and a methanol yield of 7.9 %. Hydrolysis extrusion with H_2SO_4 (N8) produced a MAA yield of 0.6 % and the highest methanol yield (Y_{MeOH}=14 %) among all tests.

Both strong acids and strong alkalis are common ester hydrolysis catalysts. H_2SO_4 directly converts PMMA into PMAA or poly(MMA-co-MAA) copolymer and methanol by hydrolyzing ester groups on the PMMA chain [217, 243]. In contrast, KOH solution reacts with ester groups on PMMA to form PMAA potassium salt or poly(MMA-co-MAA) potassium salt and methanol [243, 244]. Hydrolysis extrusion with H_2SO_4 (N8) or KOH (N7) solution produced a significantly higher yield of methanol compared to MAA (Table 6.4), confirming that direct hydrolysis of PMMA generates additional methanol.

Impact of temperature on hydrolysis and extrusion processes

At a screw speed of 240 rpm and under atmospheric degassing, increasing the reaction temperature from 350 °C (N5) to 370 °C (N4) increased PMMA conversion from 52 % to 100 % (Fig. 6.5b & Table 6.4). At 370 °C (N4), injection-grade scraps were almost completely degraded. The selectivity to MMA increased from 62 % at 350 °C to 65 % at 370 °C, indicating that the temperature rise had a minimal effect on S_{MMA}. The selectivity to methanol remained nearly unchanged, while the selectivity to MAA was almost halved, dropping from 9.4 % at 350 °C to 5.2 % at 370 °C. This suggests that a lower reaction temperature (i.e., 350 °C) favors MMA hydrolysis, despite higher temperatures (i.e., 370 °C) accelerating PMMA depolymerization. At higher temperatures, the rate of PMMA depolymerization exceeds that of MMA hydrolysis, indicating that the depolymerization reaction has a higher activation energy than MMA hydrolysis [193]. We attribute the observed difference in S_{MAA} to the over-cracking of MAA at 370 °C.

Impact of degassing method on hydrolysis and extrusion processes

Degassing method determines the carbon balance of hydrolysis extrusion. At a screw speed of 240 rpm and a reaction temperature of 350 °C, hydrolysis extrusion with 10 % HY(80) under vacuum degassing (N3) yielded only 6.7 % MMA (Fig. 6.5c & Table 6.4). The PMMA conversion was 59 %, but the recovered carbon percentage was merely 50 %, indicating signif-

icant weight loss due to vacuum degassing. In contrast, atmospheric degassing (N5) resulted in a PMMA conversion of 52 % and a substantially higher recovered carbon percentage of 86 %.

Vacuum degassing enhanced the devolatilization of gaseous components from the extruder. However, it also created mists, complicating the condenser's ability to condense these gaseous components [245]. Consequently, product losses during vacuum degassing were attributed to the vacuum pump discharge. Atmospheric degassing, on the other hand, proved more effective for product collection. Steam acted as a stripping agent, facilitating devolatilization, thereby allowing atmospheric conditions to effectively cool the condensable gaseous components [58].

6.4.5 Solid residues analysis

Hydrolysis extrusion at 330 °C and 350 °C resulted in a high amount of residues containing unreacted PMMA, catalysts and by-products (≥38 %) (Table 6.4). FTIR confirmed that non-catalytic hydrolysis at 350 °C without catalysts (N9) and hydrolysis extrusion with 10 % HY(80) (N3) produced only PMMA residues with catalysts, indicating PMMA depolymerization followed by MMA hydrolysis (Fig. 6.6a & Fig. 6.7). Hydrolysis extrusion with PTA solution at 330 °C (N2) also left PMMA residues. However, residues obtained after hydrolysis extrusion with PTA solution at 350 °C exhibited two twin peaks at 1762 cm^{-1} and 1806 cm^{-1}, attributed to the acid anhydride group [246]. Specifically, the double peaks at 1762 cm^{-1} and 1806 cm^{-1} correspond to the structure of intramolecular six-member glutaric anhydride formed between two adjacent carboxyl groups [216, 217]. During hydrolysis extrusion, in addition to MMA hydrolysis, PTA also hydrolyzed partial esters groups on PMMA directly to form acid groups. Subsequently, two adjacent carboxyl groups dehydrated to form six-member glutaric anhydride on the PMMA chain (Fig. 6.7). PMMA hydrolysis to PMAA can also be catalyzed by strong acids, such as sulfuric acid [217].

Thermogravimetric analysis (TGA) revealed two major mass loss stages between 230 °C and 380 °C, and between 380 °C and 500 °C in the residues obtained from PMMA hydrolysis extrusion with PTA at 350 °C (N1). In contrast, residues from PMMA extrusion with PTA at 330 °C (N2) exhibited a single mass loss stage between 250 °C and 400 °C (Fig. 6.6b).

The single mass loss stage in N2 residues (250 °C to 400 °C) and the first-stage mass loss in N1

residues (230 °C to 380 °C) were attributed to PMMA thermal depolymerization. However, the second-stage mass loss (380 °C to 500 °C) in N1 residues was attributed to the thermal degradation of acid anhydride. During thermal degradation of PMAA, PMAA dehydrates at around 220 °C to form acid anhydride, which exhibits a maximum degradation rate at approximately 410 °C [216]. This result further confirmed the formation of poly(MMA-co-MAA) copolymer during hydrolysis extrusion with PTA solutions and the presence of acid anhydride groups on the extrudates.

The residues obtained from hydrolysis extrusion with 10 % HY(80) at 350 °C (N3) displayed a shifted weight loss curve, starting from 250 °C and ending at 400 °C, indicating that HY(80) increases the PMMA degradation temperature (Fig. 6.6b). A slight weight loss after 396 °C was attributed to the continuous reversible dehydration of the HY(80) framework [247] and the dehydration of coke formed in HY(80) during hydrolysis extrusion.

Morphological analysis revealed a dense surface on residues obtained from PMMA hydrolysis extrusion with PTA at 350 °C (N1) (Fig. 6.6c) and a porous surface on residues obtained from PMMA hydrolysis extrusion with 10 % HY(80) (N3) (Fig. 6.6d). Both N1 and N3 residues were extruded under vacuum degassing conditions. The liquid PTA solutions did not induce significant pores or cracks. However, the solid HY(80) powder adhered to the PMMA surface, resulting in an uneven texture. The large pores and cracks were attributed to bubble collapse during the process. The hydrolysis extrusion functioned similarly to a forming process.

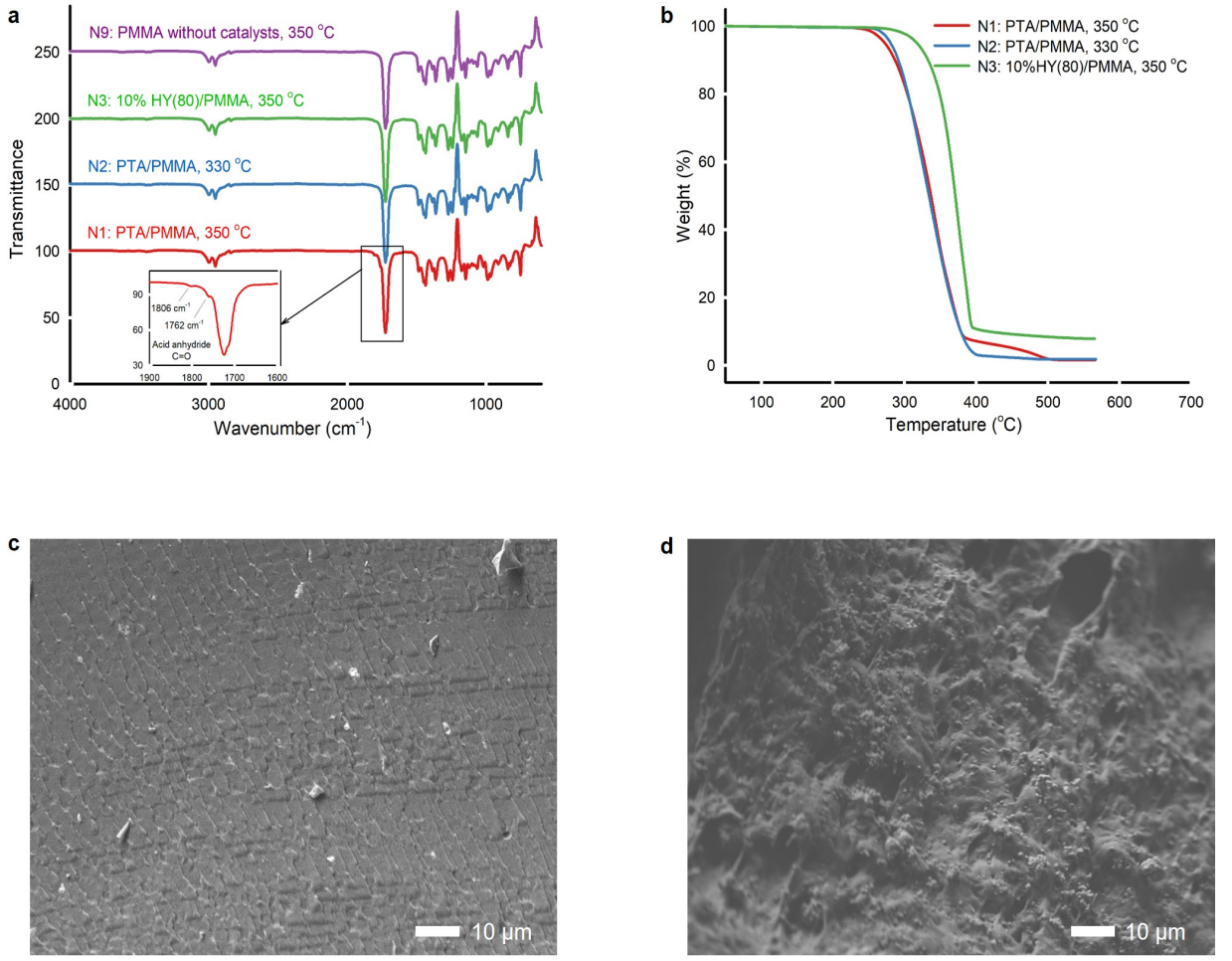

Figure (6.6) **Analysis of solid residue after PMMA reactive extrusion hydrolysis.** All reactions were conducted for one hour with a twin-screw rotation speed of 240 rpm and a liquid injection rate of 3.6 mL min^{-1}. **a**, FTIR spectra of the extrudates from 4000 to 600 cm^{-1}. **b**, Thermogravimetric curves of the extrudates under N_2 atmosphere (60 mL min^{-1}) with a heating ramp of 5 °C min^{-1}. **c**, SEM images of PTA/PMMA (N1) extrudates. **d**, SEM images of 10 % HY(80)/PMMA (N3) extrudates.

6.4.6 Mechanism of hydrolysis extrusion

Without steam, PMMA thermally depolymerizes into MMA monomer via a free radical mechanism [3, 67]. We propose a PMMA hydrolysis extrusion mechanism over solid HY(80) and liquid PTA and sulfuric acid solutions based on experimental data (Fig. 6.7). PMMA thermal depolymerization without catalysts dominated during the hydrolysis extrusion. Random chain scission above 330 °C produced tertiary alkyl radicals, which subsequently underwent unzipping to generate MMA monomer [7]. Some MMA monomers were hydrolyzed into MAA

and methanol over HY(80) or acid catalysts in the reaction zones (≥330 °C). Most MMA did not contact the catalyst during extrusion, resulting in high MMA yield and low MAA yield. A small amount of primary alkyl radicals was generated during random chain scission, followed by the formation of $CH_3O(CO)\cdot$ free radical fragments [67]. $CH_3O(CO)\cdot$ free radical fragments combined with a proton to generate methanol and CO [69]. This mechanism generates additional methanol beyond what is produced by the hydrolysis of PMMA and MMA.

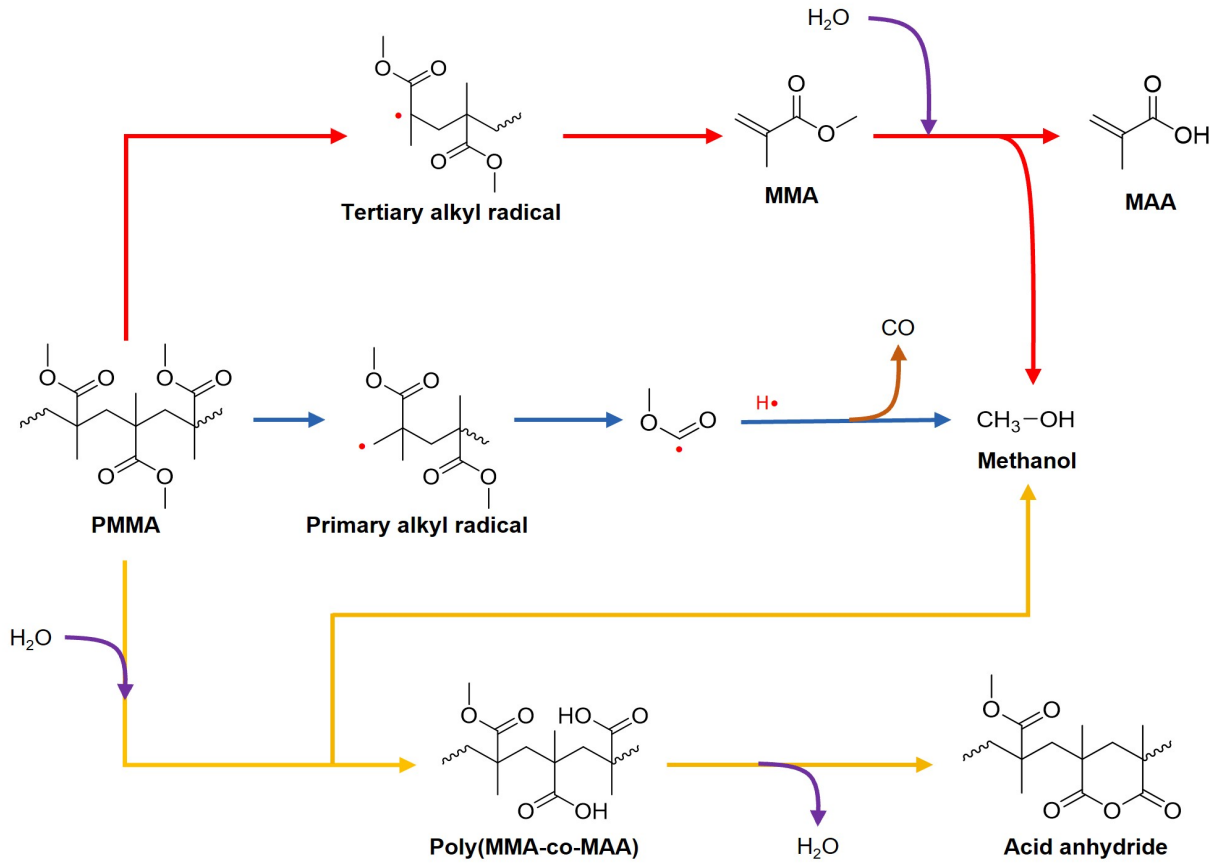

Figure (6.7) **Mechanism of PMMA hydrolysis extrusion with solid HY(80) and liquid acid solutions**

With HY(80) and liquid acid solutions, some PMMA chains were hydrolyzed to poly(MMA-co-MAA) copolymer and methanol, followed by the dehydration of two adjacent acid groups to form six-member glutaric anhydride. Glutaric anhydride may undergo further decomposition, resulting in the formation of a hydrocarbon backbone and gaseous byproducts. Diluted sulfuric acid (0.05 mol L^{-1}) hydrolyzed PMMA into poly(MMA-co-MAA) copolymer and/or PMAA more effectively than PTA solutions (0.01 g mL^{-1}) and HY(80) at 370 °C. Acetone, which results from the over-cracking of MMA and MAA during PMMA pyrolysis or hydrol-

ysis [5], was insignificant in the hydrolysis extrusion due to low concentration. We did not investigate gaseous products as our focus was primarily on the non-gaseous components.

Hydrolysis extrusion with a strong alkaline (KOH) solution produced methanol by directly hydrolyzing PMMA to poly(MMA-co-MAA) and/or PMAA potassium salt, along with partial MMA hydrolysis to MAA. Concurrently, PMMA depolymerization and direct hydrolysis to poly(MMA-co-MAA) and/or PMAA potassium salt occurred.

6.5 Conclusion

Reactive extrusion offers a continuous method for recycling PMMA scraps, producing MMA and/or MAA. In this process, gaseous products are collected from the degassing barrel via vacuum or atmospheric devolatilization, while solid residues are extruded from the die. The continuous operation feature of reactive extrusion makes it an ideal alternative to traditional PMMA recycling reactors, such as stirred tanks, molten metal reactors, and fluidized beds. In this study, we developed a lab-scale two-stage reactive extrusion system to recycle injection- and extrusion-grade PMMA scraps at 330 °C to 370 °C. A first-stage single screw extruder, acting as a melt feeder, injected PMMA melt with/without solid catalysts into a second-stage twin-screw reactive extruder. The direct feeding of melt into the twin-screw extruder, combined with the designed screw configuration, created a dynamic sealing zone prior to the liquid injection and reaction zones.

RTD tests conducted prior to all REX tests showed that lower screw speed and feeding rate increased melt mean residence time, ensuring sufficient reaction time within the extruder. However, extended residence times would lead to reduced productivity and negatively impact the economics of reactive extrusion recycling of PMMA. A Plackett-Burman design identified catalyst type and temperature as significant factors for MMA hydrolysis within the reactive extruder. Based on DOE results, we optimized the reaction temperature profile along the second-stage twin-screw extruder, achieving the highest reaction temperature of 370 °C and the highest degassing temperature of 300 °C. Along with the optimized reaction temperature profile, increasing the water injection rate to 3.6 mL min^{-1} and switching from vacuum to atmospheric degassing yielded the highest MMA yield (Y_{MMA}=89 %) and 96 % PMMA conversion without any catalysts. Under optimized conditions, increasing the weight ratio of HY(80) to PMMA to 10 % resulted in a 5.3 % yield to MAA and a 67 % yield to MMA, as well as near-complete PMMA conversion. The synergies of solid HY(80) and PTA solutions

achieved the highest yield to MAA (Y_{MAA}=5.5 %) and 98 % PMMA conversion. The low yield to MAA was attributed to a much faster PMMA depolymerization rate compared to MMA hydrolysis and an insufficient amount of hydrolysis catalysts. Solid residue analysis revealed that direct hydrolysis of PMMA to poly(MMA-co-MAA) occurred with PTA catalysts. Extrusion hydrolysis with diluted H_2SO_4 solution (0.05 mol L^{-1}) achieved the highest yield to methanol (Y_{MeOH}=14 %), indicating that the diluted strong acid solution directly hydrolyzed PMMA to PMAA or poly(MMA-co-MAA) copolymer, with PMMA depolymerization (Y_{MMA}=51 %). The obtained PMAA or poly(MMA-co-MAA) copolymer tends to form six-member glutaric anhydride via further dehydration. A strong alkaline (KOH) solution directly hydrolyzed PMMA to produce poly(MMA-co-MAA) and/or PMAA potassium salt and methanol.

6.6 Acknowledgements

The authors thank Polymer Montreal for providing extrusion- and injection-grade PMMA scraps; and Prof. Davide Brambilla and Shihao Pei at Université de Montréal for fluorescence testing. This work was supported by the Natural Sciences and Engineering Research Council of Canada (ALLRP-573784-22 CRSNG) and Arkema & Lavergne (CDT 051087).

6.7 Supplementary information for article 3

Supplementary Table (6.5) Molecular weight of virgin PMMA and scraps

PMMA type	M_n $g\,mol^{-1}$	M_w $g\,mol^{-1}$	Dispersity
Virgin PMMA (Altuglas)	99499	116216	1.2
Injection grade scraps	53626	103360	1.93
Extrusion grade scraps, white	46341	101434	2.2
Extrusion grade scraps, red	119423	177626	1.5

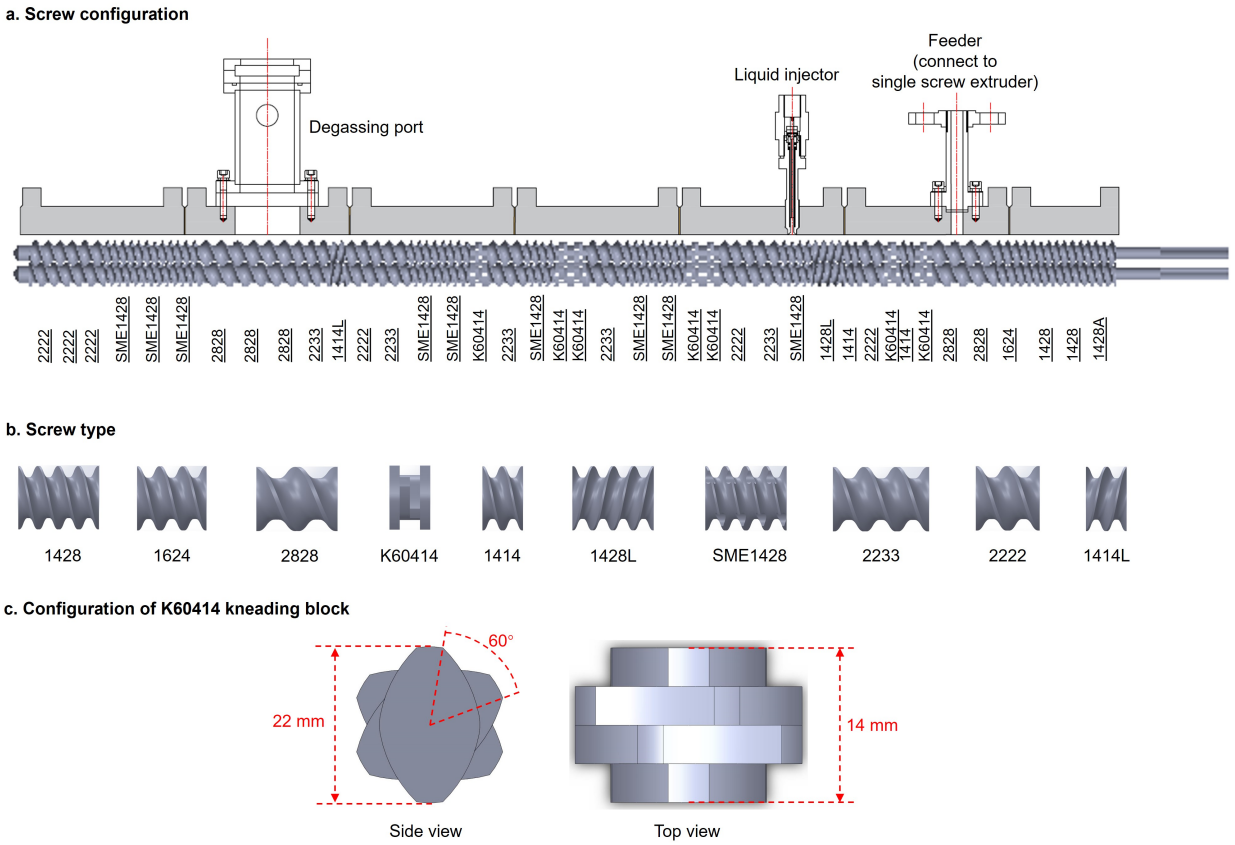

Supplementary Fig. (6.1) Screw configuration (**a**), screw type (**b**), and K60414 kneading block configuration (**c**) of the T20 twin-screw reactive extruder. K60414 kneading block has a 60° disc angle, a length of 14 mm, and consists of four discs.

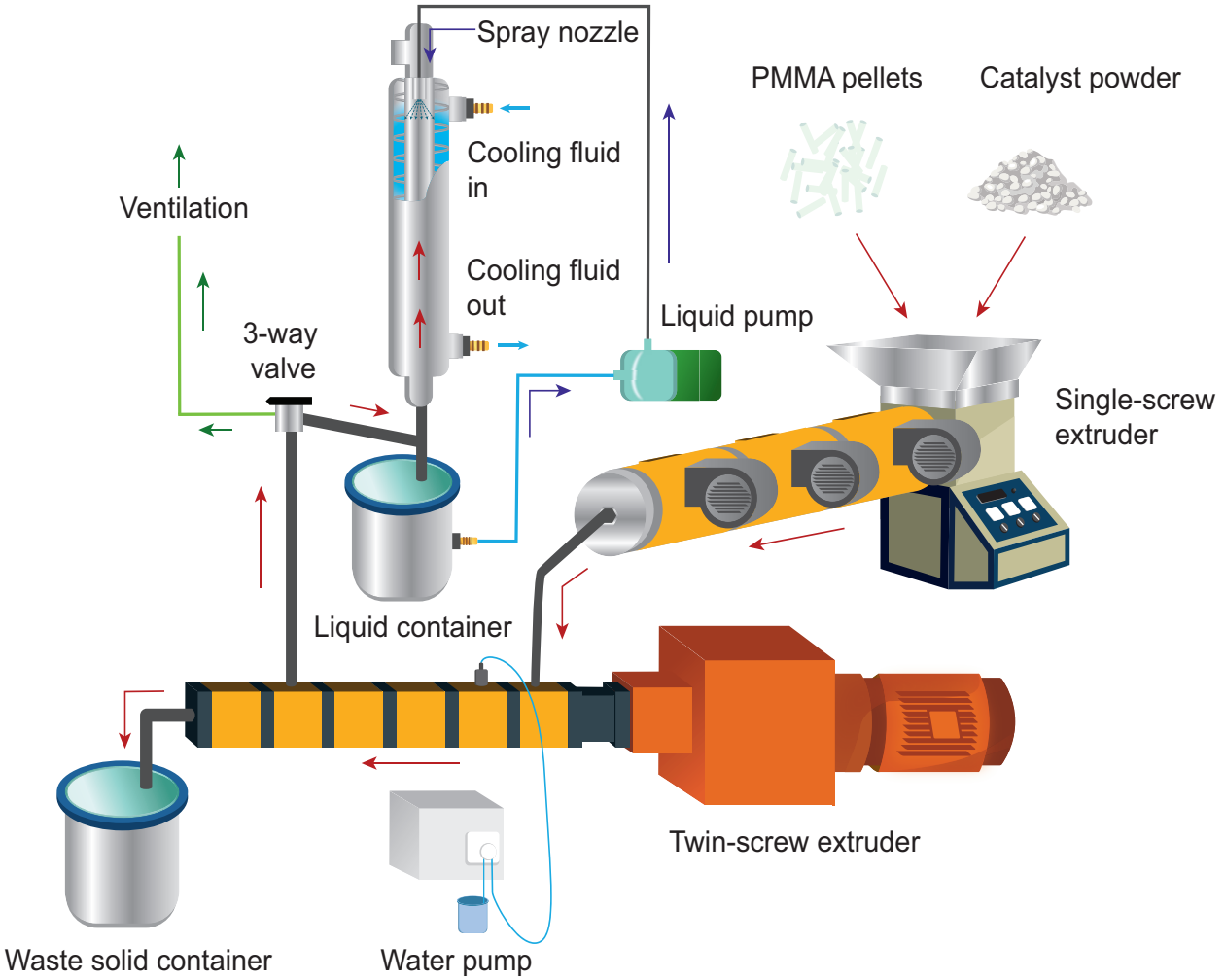

Supplementary Fig. (6.2) Scheme for a two-stage reactive extrusion hydrolysis system with atmospheric degassing design

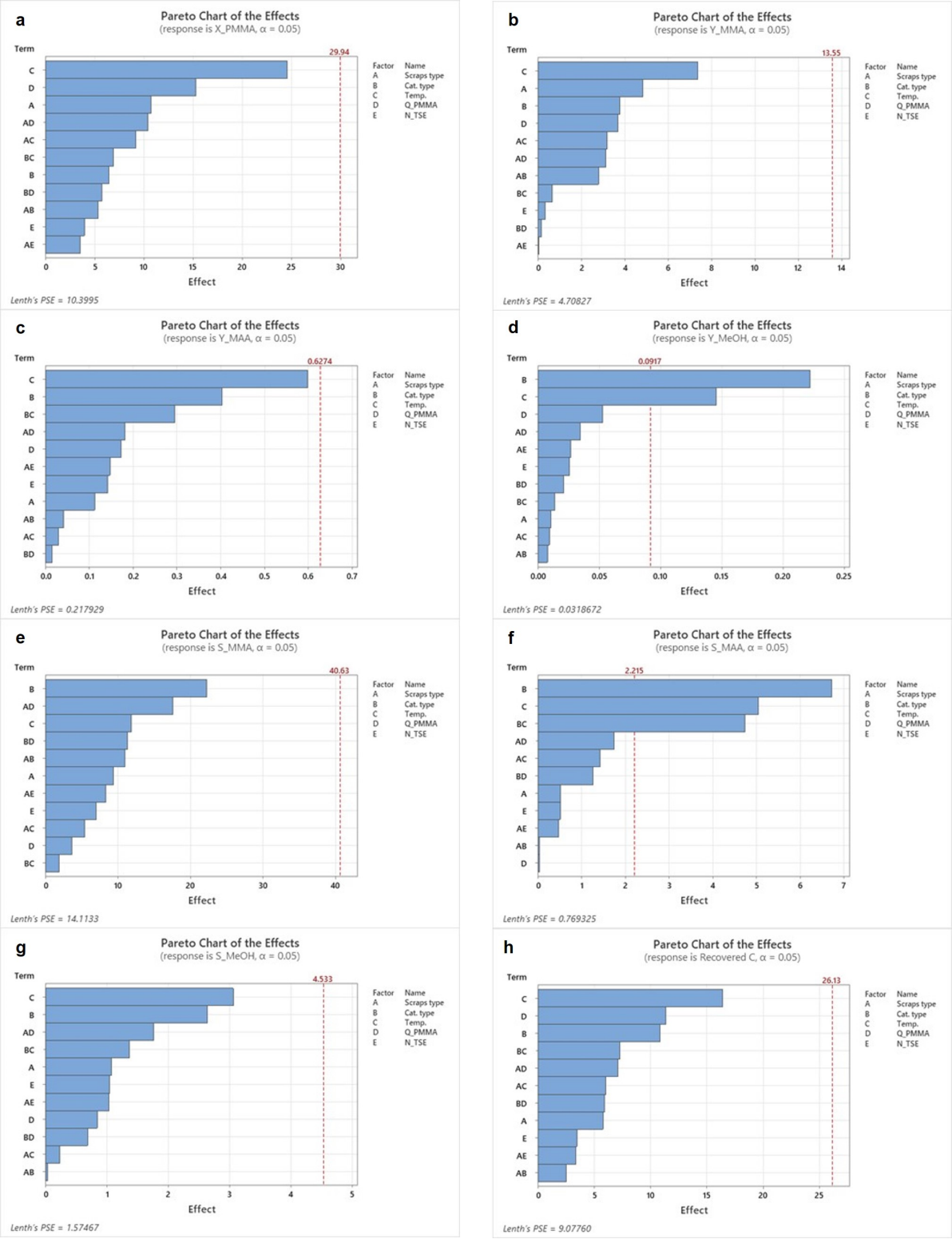

Supplementary Fig. (6.3) Pareto charts of the effects. Each factorial regression model includes terms up to the second order. Factor A-Scraps type; B-Catalyst type; C-Temperature; D-Q_{PMMA}; E-N_{TSE}

Supplementary Table (6.6) Physico-chemical properties and particle size of commercial Al_2O_3

Sample	S_{BET}	V_{tot}	Average D_v	V_{micro}	S_{micro}	S_{meso}	$d_p{}^a$			
							Medium size	Mean size	$D[10]$	$D[90]$
	$m^2\,g^{-1}$	$cm^3\,g^{-1}$	Å	$cm^3\,g^{-1}$	$m^2\,g^{-1}$	$m^2\,g^{-1}$	µm	µm	µm	µm
Al_2O_3	197	0.53	48	0.001	4	192	72.66	74.65	56.78	93.17

Note:d_p-particle size; a-measured by PSD

CHAPTER 7 GENERAL DISCUSSION

Over 80 % of waste plastic ends up in landfills, incinerators, or as litter in the environment. Incineration for heat recovery is a relatively simple and direct method to extract value from plastic; however, it poses significant risks of air pollution and greenhouse gas emissions. Compared to common plastics such as polyethylene (PE) and polypropylene (PP), PMMA waste is more valuable. Pyrolysis of PMMA yields over 90 % MMA monomer at 400 °C. While mechanical recycling of PMMA into new products or composites has lower operating and capital expenses, its application is limited to relatively clean, post-industrial scraps. However, end-of-life PMMA typically contains fillers and additives, making mechanical recycling impractical. Chemical recycling offers a more versatile solution, capable of processing all types of PMMA waste. Recovering MMA monomer from clean, post-industrial PMMA waste is often economically viable, incentivizing industry collection and recycling efforts. However, when PMMA waste is mixed with high levels of fillers, additives, or combined with other plastics, the purification costs for crude r-MMA increase significantly, making the recycling process challenging to sustain profitability.

This PhD project focused on recycling PMMA into MAA, rather than MMA, through a continuous catalytic reactive extrusion process. MAA offers an advantage over MMA due to its simpler purification process, effectively addressing impurities that are challenging to remove in crude r-MMA. The study validated the technical feasibility of continuous reactive hydrolysis extrusion for converting PMMA into MAA and/or MMA. Both MAA and MMA represent valuable products derived from the chemical recycling of PMMA. The co-generation of MMA and MAA is difficult to avoid due to the faster kinetics of PMMA depolymerization compared to the hydrolysis of MMA to MAA.

The first part of this project reviewed the use of REX in polymer functionalization, polymerization, and depolymerization. Applications of REX in plastic depolymerization (chemical recycling) have been reported. Degradative extrusion has been employed to reduce molecular weight (partial depolymerization) or to recover monomers/chemicals (complete thermal degradation). The depolymerization of PMMA via REX to produce crude r-MMA has been developed and applied. However, several alternatives to PMMA depolymerization exist, including stirred tanks, molten metal baths, dry distillation, rotating drums, and fluidized beds. REX may not always be the optimal route for producing MMA from end-of-life PMMA,

which constitutes the majority of PMMA waste. In this review, we identified key parameters and examined the characteristics of various screws, barrels, and extruders, providing a theoretical foundation for designing a reactive hydrolysis extrusion system. Extruders are the most commonly used polymer processing equipment, and retrofitting existing or older extruders for plastic degradative recycling can help reduce the capital expenditure (CAPEX) of recycling systems, as degradative recycling typically does not require new or high-precision extruders. Twin-screw extruders are particularly suitable reactors for degradative extrusion recycling. However, scaling up REX systems for high-throughput production of monomers or chemicals from waste plastics remains a significant challenge.

In the second part of this project, we developed a fixed-bed reactor to screen suitable catalysts for the direct hydrolysis of PMMA and to elucidate a comprehensive reaction mechanism. Reactive hydrolysis extrusion requires substantial amounts of samples, so we used a lab-scale fixed-bed reactor for more efficient catalyst screening and reaction mechanism studies. In our initial screening tests, we employed a Brabender batch mixer and observed that zeolites were more effective hydrolysis catalysts for MAA production compared to metal oxides, such as Al_2O_3. By directly mixing PMMA with zeolites and introducing heat and steam, we achieved an MAA yield of 56 % (close to the theoretical maximum yield of 68.8 %) using H-type zeolite Y with an SiO_2/Al_2O_3 molar ratio of 80. We compared various commercial zeolites (zeolite Y, zeolite β, ZSM-5, and Mordenite) as well as regenerated and desilicated zeolite Y. The shape selectivity of the microporous networks was found to influence zeolite deactivation due to coke formation, while the acidity of the zeolitic framework significantly affected MAA yield and product distribution. High steam injection rates ($2\,mL\,min^{-1}$ of liquid water) and high zeolite loading ratio (50 %) were applied in the screening tests. However, such conditions are impractical for reactive hydrolysis extrusion at scale. We identified several side reactions that impacted MAA yield. For example, over-cracking of MMA and MAA produced by-products such as CO and acetone. Additionally, direct hydrolysis of the PMMA chain generated Poly(MMA-co-MAA) copolymer, while radical cracking of the PMMA chain formed $CH_3O(CO)\cdot$, leading to the production of extra methanol. This study confirmed that the direct hydrolysis of PMMA to MAA is a tandem reaction. PMMA first undergoes thermal depolymerization to form MMA, which is subsequently converted to MAA in situ over zeolite catalysts.

In the final part of this project, we designed and tested a lab-scale two-stage reactive hydrolysis extrusion system for the continuous conversion of injection-grade and extrusion-grade PMMA scraps. Injection-grade PMMA, closely resembling post-industrial scrap, has fewer

additives, whereas extrusion-grade PMMA, representative of end-of-life scrap, contains a mixture of PMMA scraps and higher additive content. The primary goal was to produce a high yield of MAA. However, due to the faster kinetics of PMMA depolymerization compared to MMA hydrolysis, the process resulted in the co-generation of MMA and MAA. With low zeolite loading (10 %) and low water injection rate ($3.6\,\mathrm{mL\,min^{-1}}$), the maximum MAA yield achieved was 5.3 %, while the system primarily produced MMA. We utilized a single-screw extruder to inject a mixture of molten PMMA and solid catalysts into a twin-screw extruder. This approach optimizes the reaction zones within the twin-screw extruder, allocating them primarily for hydrolysis reactions, and reduces the need for additional costly feeders. However, the single screw extruder imposes limitations on the ability to feed high ratios of solid catalysts, which may impact the overall efficiency of the process. In the absence of catalysts, steam-assisted thermolysis of injection-grade PMMA achieved nearly complete conversion at 370 °C, outperforming PMMA pyrolysis at the same temperature. We tested both solid catalysts (zeolite Y and Al_2O_3) and liquid catalysts (H_2SO_4, KOH, and PTA). Strong acid or base liquid catalysts tended to directly hydrolyze the PMMA chain rather than converting MMA to MAA. Consistent with earlier findings, acetone was identified as a by-product of over-cracking MMA and MAA. However, only trace amounts of acetone were detected in the extrusion tests, suggesting its formation requires high zeolite catalyst loading and a high stream of MAA. Degassing methods were found to be critical for collecting and condensing liquid products. Vacuum degassing led to the formation of MMA mist, which was difficult to condense, whereas atmospheric degassing minimized mist formation. Steam serves as an effective stripping agent, significantly enhancing devolatilization. Ethanol was employed to condense and absorb the degassing products, achieving a high recovery rate for MMA and MAA (>90 %). By recirculating the ethanol-condensed product mixture to absorb and condense new outputs, we developed a key step to enhance monomer recovery rates.

Both residence time distribution (RTD) and strain distribution function (SDF) are important for understanding reactive extrusion processes. However, this project specifically aims to validate the potential of the extruder as a chemical reactor for PMMA recycling. While the extruder's mixing capabilities have been widely studied in the context of polymer processing, our focus is on its function as a reactor. Measuring the SDF is particularly challenging due to the complexity of the screw design and configuration. Although we attempted to simulate both SDF and RTD, the intricate screw geometry posed significant difficulties in obtaining reliable results. In contrast, the RTD analysis provides meaningful insights into the extrusion hydrodynamics. Specifically, the Peclet number derived from RTD enables characterization of flow behavior and estimation of the number of CSTRs in series—metrics that are highly

relevant to reactor modeling in chemical reaction engineering.

Before the start of this project, there had been no reported attempts in either industry or academia to convert waste PMMA into MAA. Chemical recycling of PMMA had primarily focused on MMA production. Since this project began, three parallel studies—conducted within our research group—have explored the conversion of PMMA to MAA using different reactor systems: fluidized/fixed bed reactors [5, 16], stirred tank reactors [17], and reactive extruder [248].

This project specifically focuses on developing a reactive extrusion process for recycling PMMA into MAA. All three reactor systems demonstrated co-generation of MMA and MAA during PMMA hydrolysis. While the fluidized/fixed bed and stirred tank reactors operated in batch mode, the reactive extrusion system developed in this work represents the first reported continuous process for PMMA-to-MAA conversion.

To the best of our knowledge, no similar studies outside our research group were reported in the literature during the course of this project. The results of this work are consistent with the findings from the other two parallel projects. Notably, Olga et al. [5] proposed a simplified PMMA hydrolysis mechanism without investigating zeolite catalyst deactivation in detail. In contrast, this project presents a more comprehensive reaction mechanism that includes the primary MAA formation pathway and relevant side reactions, along with an in-depth analysis of zeolite catalyst deactivation [69, 248].

CHAPTER 8 CONCLUSION

8.1 Summary of Works

Waste PMMA is a valuable form of solid plastic waste. Pyrolyzing PMMA results in a high MMA monomer yield of 70 % to 90 %. However, the recycling of PMMA primarily focuses on post-processed industrial scraps and cuttings, while end-of-life PMMA, which dominate the waste PMMA stream, are less commonly targeted. Fillers and additives in end-of-life PMMA reduce the purity of crude r-MMA, which increases purification costs. Some impurities in crude r-MMA exhibit properties similar to MMA, making them difficult to eliminate completely. This challenge limits the use of r-MMA in strictly regulated markets that require high-quality PMMA products.

Upcycling PMMA to MAA, instead of MMA, presents an alternative approach. This method not only produces the specialty chemical MAA but also avoids the high costs associated with purifying crude r-MMA. In this project, we developed a continuous reactive hydrolysis extrusion process to recycle both post-industrial and end-of-life PMMA for the production of MAA and/or MMA. This marks the first experimental validation of REX in the hydrolysis upcycling of PMMA for MAA production.

We began by reviewing the principles, design considerations, and applications of REX to establish a theoretical foundation for designing a degradative REX system. A twin-screw extruder equipped with feeding, reaction, and degassing zones was identified as an ideal reactor for plastic degradative extrusion.

To identify a suitable zeolite hydrolysis catalyst and elucidate the reaction mechanism for PMMA hydrolysis recycling to MAA, we developed a fixed-bed reactor. Among the zeolites tested—zeolite Y, zeolite β, ZSM-5, and Mordenite—H-type zeolite Y (SiO_2/Al_2O_3 ratio = 80) achieved the highest MAA yield of 56 % (with a theoretical maximum yield of 68.8 %) and MAA selectivity of 58 % at 350°C. Coke formation within the framework of large-pore zeolites caused reversible deactivation of medium-strong acid and Brønsted acid sites. Direct hydrolysis of the PMMA chain led to the formation of a Poly(MMA-co-MAA) copolymer, while cracking of the PMMA groups generated $CH_3O(CO)\cdot$ radicals, resulting in the production of additional methanol. Over-cracking of MAA and MMA resulted in impurities such as ace-

tone and CO. Our screening tests identified zeolite Y as the most effective hydrolysis catalyst.

In the final step, we developed a lab-scale, two-stage reactive hydrolysis extrusion system for the continuous conversion of post-industrial and end-of-life PMMA into MMA and/or MAA. The co-generation of MMA and MAA proved difficult to avoid due to the faster kinetics of PMMA depolymerization to MMA compared to MMA hydrolysis to MAA, leading to MMA predominating in the product stream rather than MAA. We validated the performance of zeolite Y in the developed reactive hydrolysis extrusion system and also tested other solid catalyst (Al_2O_3) and liquid catalysts (H_2SO_4, KOH, and phosphotungstic acid). The reactive hydrolysis extrusion achieved an MAA yield of 5.3 % and MMA yield of 67 % over zeolite Y at 370°C. The conversion of PMMA to MAA followed a tandem reaction route, where PMMA was first depolymerized into MMA, followed by MMA catalytic hydrolysis to MAA over zeolite Y. In contrast, liquid acid and base catalysts tended to directly hydrolyze the PMMA chain. We also confirmed that atmospheric degassing was more effective than vacuum degassing in the collection and condensation of liquid products. Finally, PMMA hydrolysis without catalysts achieved near-complete conversion and the highest MMA yield of 89 % at 370°C. Steam significantly enhances the depolymerization of PMMA.

8.2 Limitations

Reactive hydrolysis extrusion over solid zeolite catalysts involves a complex solid-melt-gas heterogeneous system, with few reference cases available to guide the design of such systems.

Feeding a high ratio of powder with PMMA in a single-screw extruder is challenging, making it difficult to achieve high zeolite loadings. Additionally, using large amounts of solid zeolite is costly, necessitating consideration of catalyst recycling. To avoid local rapid cooling in the liquid injection barrel (the first reaction barrel), we are limited in the water injection rate, which cannot be increased significantly. With zeolite loading limited to 10 % and the water injection rate restricted to $3.6\,\mathrm{mL\,min^{-1}}$, the contact between MMA, zeolite, and steam is not enough. The faster kinetics of PMMA depolymerization compared to MMA hydrolysis further reduces MAA yield. Hydrolysis requires the involvement of the catalyst, steam, and MMA.

The reactive twin-screw extruder is equipped with only four reaction barrels, including a de-

gassing barrel, which limits the extent of the hydrolysis reaction. PMMA depolymerization typically occurs at higher temperatures than MMA hydrolysis, and elevated temperatures accelerate the over-cracking of MAA and MMA. This necessitates balancing recycling productivity with product yield.

Injecting liquid catalysts creates a liquid-melt-gas heterogeneous system. The use of strong acids and bases will predominantly hydrolyze the PMMA chain, producing methanol and Poly(MMA-co-MAA) copolymers/salts rather than hydrolyzing MMA to MAA.

The co-generation of MMA and MAA is difficult to avoid when both reactions occur in the same zones within the extruder. The reactive extrusion of PMMA with zeolite Y led to its rapid deactivation, primarily caused by pore blockage.

We analyzed the gaseous products generated during PMMA hydrolysis upcycling in the fixed-bed reactor. However, since the focus was on the more valuable liquid products and the collection of non-condensable gaseous products poses challenges, their study was not pursued in the reactive hydrolysis extrusion system.

8.3 Recommendations for future research

A comprehensive understanding of solid-melt-gas or liquid-melt-gas heterogeneous systems would significantly enhance the design and modelling of reactors.

We developed the configuration of screws and barrels and designed the connection between the single screw extruder and the twin-screw extruder. Future research would explore the impact of various screw and barrel configurations and evaluate the direct feeding of a solid mixture of PMMA and catalyst powder, eliminating the need for a single screw extruder as a feeder.

To increase MAA yield, we recommend separating the injection points for steam and catalysts and dividing the reaction zones into two distinct sections: a PMMA depolymerization zone in the presence of steam and an MMA hydrolysis zone. This separation would allow each reaction to occur under its optimal temperature conditions. The use of a side feeder or injector for introducing liquid or solid catalysts after the PMMA depolymerization zone could

also provide better control over the MMA/MAA ratio. Specifically, the first reaction zone can be operated at temperatures above 350 °C to 370 °C to induce the thermal depolymerization of PMMA into MMA. The resulting MMA, along with unreacted PMMA, then flows into a second reaction zone, where hydrolysis is carried out at temperatures below 250 °C. In this zone, thermal depolymerization of PMMA ceases, and hydrolysis becomes the dominant reaction. A dynamic sealing zone between the two regions is necessary to prevent backflow of gaseous products. A portion of the molten PMMA is conveyed from the first to the second zone to serve as a lubricant for the screws. Integrating multiple reaction zones in this manner requires a longer extruder, which increases the mean residence time of the PMMA melt. However, this configuration allows better control over the residence time distributions of MMA and MAA. In particular, the residence time of MAA may be shortened, minimizing the risk of over-cracking, while the MMA residence time may increase due to its passage through both reaction zones.

Identifying an optimal catalyst is crucial. While reusing liquid catalysts is more challenging than reusing solid catalysts, a techno-economic analysis comparing their use would precede process commercialization.

The gaseous products from the degassing barrel include steam, MMA, MAA, methanol, and CO. To further hydrolyze MMA into MAA, a tandem reactor could be installed at the degassing port outlet. We attempted to use a fixed-bed reactor loaded with powdered zeolite Y at this location, but unstable flow pressures rendered the test unsuccessful. A fixed-bed reactor with structured zeolite catalysts or a fluidized bed reactor may provide a more effective solution for secondary MMA hydrolysis.

Future research would also address the purification of MAA and MMA from the extrusion products, which contain significant amounts of water and solvents (e.g., ethanol). Liquid-phase hydrolysis of condensed liquid products using common hydrolysis catalysts could facilitate the conversion of residual MMA to MAA, supporting subsequent product purification.

Beyond technical optimization, future work should also include a comprehensive LCA study. This analysis would be valuable for assessing the economic feasibility of the PMMA-to-MAA pathway and for comparing the carbon footprint of MAA production from waste PMMA with that from conventional feedstocks.

REFERENCES

[1] U. Ali, K. J. B. A. Karim, and N. A. Buang, "A review of the properties and applications of poly (methyl methacrylate)(PMMA)," *Polymer Reviews*, vol. 55, no. 4, pp. 678–705, 2015.

[2] J. De Tommaso and J.-L. Dubois, "Risk analysis on PMMA recycling economics," *Polymers*, vol. 13, no. 16, p. 2724, 2021.

[3] E. Esmizadeh, S. Khalili, A. Vahidifar, G. Naderi, and C. Dubois, "Waste polymethyl methacrylate (PMMA): Recycling and high-yield monomer recovery," in *Handbook of Ecomaterials*, L. Martínez, O. Kharissova, and B. Kharisov, Eds. Cham: Springer International Publishing, 2018, pp. 1–33.

[4] M. Newborough, D. Highgate, and J. Matcham, "Thermal depolymerisation of polymethyl-methacrylate using mechanically fluidised beds," *Applied Thermal Engineering*, vol. 23, no. 6, pp. 721–731, 2003.

[5] O. V. Chub, N. Saadatkhah, J.-L. Dubois, and G. S. Patience, "Fluidized bed poly (methyl methacrylate) thermolysis to methyl methacrylate followed by catalytic hydrolysis to methacrylic acid," *Applied Catalysis A: General*, vol. 638, p. 118637, 2022.

[6] K. Gkaliou, L. Benedini, Z. Sárossy, C. D. Jensen, U. B. Henriksen, and A. E. Daugaard, "Recycled PMMA prepared directly from crude MMA obtained from thermal depolymerization of mixed PMMA waste," *Waste Management*, vol. 164, pp. 191–199, 2023.

[7] C. B. Godiya, S. Gabrielli, S. Materazzi, M. S. Pianesi, N. Stefanini, and E. Marcantoni, "Depolymerization of waste poly (methyl methacrylate) scraps and purification of depolymerized products," *Journal of Environmental Management*, vol. 231, pp. 1012–1020, 2019.

[8] W. Kaminsky and J. Franck, "Monomer recovery by pyrolysis of poly (methyl methacrylate)(PMMA)," *Journal of Analytical and Applied Pyrolysis*, vol. 19, pp. 311–318, 1991.

[9] B. Meek, J. W. Bridges, A. Fasey, and U. G. Sauer, "Evidential requirements for the regulatory hazard and risk assessment of respiratory sensitisers: methyl methacrylate as an example," *Archives of Toxicology*, vol. 97, no. 4, pp. 931–946, 2023.

[10] S. Kleinbeck, M. Schäper, M. Pacharra, M. L. Lehmann, K. Golka, M. Blaszkewicz, T. Brüning, and C. van Thriel, "A short-term inhalation study to assess the reversibility of sensory irritation in human volunteers," *Archives of Toxicology*, vol. 94, pp. 1687–1701, 2020.

[11] G. Swift, "Acrylic (and methacrylic) acid polymers," *Encyclopedia of Polymer Science and Technology*, vol. 1, 2002.

[12] K. Sunitha, R. Sadhana, D. Mathew, and R. N. C.P., "Novel superabsorbent copolymers of partially neutralized methacrylic acid and acrylonitrile: Synthesis, characterization and swelling characteristics," *Designed Monomers and Polymers*, vol. 18, no. 6, pp. 512–523, 2015.

[13] J. Dubois, "Recovery of (meth) acrylic resin by depolymerization and hydrolysis," Aug. 29 2023, US Patent 11,739,192.

[14] M. J. D. Mahboub, J.-L. Dubois, F. Cavani, M. Rostamizadeh, and G. S. Patience, "Catalysis for the synthesis of methacrylic acid and methyl methacrylate," *Chemical Society Reviews*, vol. 47, no. 20, pp. 7703–7738, 2018.

[15] K. Nagai and T. Ui, "Trends and future of monomer-MMA technologies," *Sumitomo Chem*, vol. 2, pp. 4–13, 2004.

[16] O. V. Chub, J.-L. Dubois, and G. S. Patience, "Tandem fluidized bed/milli-second fixed bed reactor produces methacrylic acid from poly (methyl methacrylate)," *Applied Catalysis A: General*, vol. 647, p. 118887, 2022.

[17] J. De Tommaso, F. Galli, T. D. Nguyen, Y. Zhuang, J.-L. Dubois, and G. S. Patience, "Waste artificial marble pyrolysis and hydrolysis," *Waste Management*, vol. 195, pp. 129–144, 2025.

[18] J. Maris, S. Bourdon, J.-M. Brossard, L. Cauret, L. Fontaine, and V. Montembault, "Mechanical recycling: Compatibilization of mixed thermoplastic wastes," *Polymer Degradation and Stability*, vol. 147, pp. 245–266, 2018.

[19] J. Datta and P. Kopczyńska, "From polymer waste to potential main industrial products: Actual state of recycling and recovering," *Critical Reviews in Environmental Science and Technology*, vol. 46, no. 10, pp. 905–946, 2016.

[20] R. Clift, "Overview clean technology—the idea and the practice," *Journal of Chemical Technology & Biotechnology*, vol. 68, no. 4, pp. 347–350, 1997.

[21] B. Gautam, T.-H. Tsai, and J.-T. Chen, "Towards sustainable solutions: A review of polystyrene upcycling and degradation techniques," *Polymer Degradation and Stability*, p. 110779, 2024.

[22] M. Marczewski, E. Kamińska, H. Marczewska, M. Godek, G. Rokicki, and J. Sokołowski, "Catalytic decomposition of polystyrene. the role of acid and basic active centers," *Applied Catalysis B: Environmental*, vol. 129, pp. 236–246, 2013.

[23] European Parliament and Council, "Directive 2008/98/EC of the European Parliament and of the Council of 19 November 2008 on waste and repealing certain Directives," https://eur-lex.europa.eu/legal-content/EN/TXT/?uri=CELEX:32008L0098, 2008, Official Journal of the European Union, L 312, 22.11.2008, pp. 3–30.

[24] A. R. Prado, A. G. Leal-Junior, C. Marques, S. Leite, G. L. De Sena, L. C. Machado, A. Frizera, M. R. Ribeiro, and M. J. Pontes, "Polymethyl methacrylate (PMMA) recycling for the production of optical fiber sensor systems," *Optics Express*, vol. 25, no. 24, pp. 30 051–30 060, 2017.

[25] G. Kočevar and A. Kržan, "Recycling of an acrylate–glass fiber reinforced polyester composite," *Journal of Material Cycles and Waste Management*, vol. 20, no. 2, pp. 1106–1114, 2018.

[26] Y.-B. Zhao, X.-D. Lv, and H.-G. Ni, "Solvent-based separation and recycling of waste plastics: A review," *Chemosphere*, vol. 209, pp. 707–720, 2018.

[27] S. Gouli, J. Poulakis, and C. Papaspyrides, "Solvent recycling of poly (methyl methacrylate) decorative sheets," *Advances in Polymer Technology: Journal of the Polymer Processing Institute*, vol. 13, no. 3, pp. 207–211, 1994.

[28] H. W. Moeller, *Progress in polymer degradation and stability research*. Nova Publishers, 2007.

[29] D. S. Achilias, "Chemical recycling of polymers. the case of poly (methyl methacrylate)," in *Proceedings of the International Conference on Energy & Environmental Systems, Chalkida, Greece*, 2006, pp. 8–10.

[30] A. Rahimi and J. M. García, "Chemical recycling of waste plastics for new materials production," *Nature Reviews Chemistry*, vol. 1, no. 6, p. 0046, 2017.

[31] K. Smolders and J. Baeyens, "Thermal degradation of PMMA in fluidised beds," *Waste Management*, vol. 24, no. 8, pp. 849–857, 2004.

[32] N. Grassie and H. Melville, "Thermal degradation of polymethylmethacrylate," *Bulletin des Sociétés Chimiques Belges*, vol. 57, no. 4-6, pp. 142–153, 1948.

[33] S. L. Madorsky, "Rates of thermal degradation of polystyrene and polyethylene in a vacuum," *Journal of Polymer Science*, vol. 9, no. 2, pp. 133–156, 1952.

[34] W. Kaminsky and C. Eger, "Pyrolysis of filled PMMA for monomer recovery," *Journal of Analytical and Applied Pyrolysis*, vol. 58, pp. 781–787, 2001.

[35] G. Lopez, M. Artetxe, M. Amutio, G. Elordi, R. Aguado, M. Olazar, and J. Bilbao, "Recycling poly-(methyl methacrylate) by pyrolysis in a conical spouted bed reactor," *Chemical Engineering and Processing: Process Intensification*, vol. 49, no. 10, pp. 1089–1094, 2010.

[36] B.-S. Kang, S. G. Kim, and J.-S. Kim, "Thermal degradation of poly (methyl methacrylate) polymers: Kinetics and recovery of monomers using a fluidized bed reactor," *Journal of Analytical and Applied Pyrolysis*, vol. 81, no. 1, pp. 7–13, 2008.

[37] Y.-H. Hu and C.-Y. Chen, "The effect of end groups on the thermal degradation of poly (methyl methacrylate)," *Polymer Degradation and Stability*, vol. 82, no. 1, pp. 81–88, 2003.

[38] G. Madras, J. Smith, and B. J. McCoy, "Degradation of poly (methyl methacrylate) in solution," *Industrial & Engineering Chemistry Research*, vol. 35, no. 6, pp. 1795–1800, 1996.

[39] Z. Ahmad, N. Al-Awadi, and F. Al-Sagheer, "Thermal degradation studies in poly (vinyl chloride)/poly (methyl methacrylate) blends," *Polymer Degradation and Stability*, vol. 93, no. 2, pp. 456–465, 2008.

[40] K. Pielichowski and J. Njuguna, *Thermal degradation of polymeric materials*. iSmithers Rapra Publishing, 2005.

[41] T. Kashiwagi, A. Inaba, J. E. Brown, K. Hatada, T. Kitayama, and E. Masuda, "Effects of weak linkages on the thermal and oxidative degradation of poly (methyl methacrylates)," *Macromolecules*, vol. 19, no. 8, pp. 2160–2168, 1986.

[42] F. Sasse and G. Emig, "Chemical recycling of polymer materials," *Chemical Engineering & Technology*, vol. 21, no. 10, pp. 777–789, 1998.

[43] S. R. Valandro, P. C. Lombardo, A. L. Poli, M. A. Horn Jr, M. G. Neumann, and C. C. S. Cavalheiro, "Thermal properties of poly (methyl methacrylate)/organomodified montmorillonite nanocomposites obtained by in situ photopolymerization," *Materials Research*, vol. 17, no. 1, pp. 265–270, 2014.

[44] A. Barlow, R. Lehrle, J. Robb, and D. Sunderland, "Polymethylmethacrylate degradation—kinetics and mechanisms in the temperature range 340 to 460 c," *Polymer*, vol. 8, pp. 537–545, 1967.

[45] D. M. King, J. A. Spencer II, X. Liang, L. F. Hakim, and A. W. Weimer, "Atomic layer deposition on particles using a fluidized bed reactor with in situ mass spectrometry," *Surface and Coatings Technology*, vol. 201, no. 22-23, pp. 9163–9171, 2007.

[46] W. Kaminsky, M. Predel, and A. Sadiki, "Feedstock recycling of polymers by pyrolysis in a fluidised bed," *Polymer Degradation and Stability*, vol. 85, no. 3, pp. 1045–1050, 2004.

[47] D. G. Lovering, *Molten salt technology*. Springer, 2014.

[48] J. Domingo and D. Cabanero, "Process and device for regeneration of monomer from polymethyl methacrylate," *Spanish Patent*, vol. 192909, 1949.

[49] W. Kaminsky, J. Menzel, and H. Sinn, "Recycling of plastics," *Conservation & Recycling*, vol. 1, no. 1, pp. 91–110, 1976.

[50] M. Newborough, D. Highgate, and P. Vaughan, "Thermal depolymerisation of scrap polymers," *Applied Thermal Engineering*, vol. 22, no. 17, pp. 1875–1883, 2002.

[51] S. Khangkham, "Catalytic degradation of poly (methyl methacrylate) by zeolites and regeneration of used zeolites via ozonation," Ph.D. dissertation, INPT, 2012.

[52] J. Roegiers, J. Pieters, and F. Ronsse, "Heat and mass transfer modelling of auger reactors," *Ghent University, Ghent*, 2016.

[53] G. Allan, T. E. Loop, and J. D. Flynn, "Biomass and waste plastics to neodiesel and valuable chemicals via supercritical water," Nov. 15 2011, US Patent 8,057,666.

[54] H. Tokushige, A. Kosaki, and T. Sakai, "Method for continuously thermally decomposing synthetic macro-molecule materials," May 25 1976, US Patent 3,959,357.

[55] W. Michaeli and K. Breyer, "Polymer recycling—status and perspectives," in *Macromolecular Symposia*, vol. 135, no. 1. Wiley Online Library, 1998, pp. 83–96.

[56] MMAtwo, "MMAtwo in position to benchmark its results with state of the art virgin and regenerated MMA," 2022, https://www.mmatwo.eu (accessed: March 2023).

[57] Z. Tadmor and C. G. Gogos, *Principles of Polymer Processing*. John Wiley & Sons, 2013.

[58] C. Martin and B. Haight, "Devolatilization via twin-screw extrusiontheory, tips, and test results," in *Pharmaceutical Extrusion Technology*, I. Ghebre-Sellassie, C. E. Martin, F. Zhang, and J. DiNunzio, Eds. Boca Raton: CRC Press, 2018, pp. 325–335.

[59] H. F. Giles Jr, E. M. Mount III, and J. R. Wagner Jr, *Extrusion: The Definitive Processing Guide and Handbook*. Norwich, NY: William Andrew, 2004.

[60] R. Wilczynski and J. Jerrick Juliette, "Methacrylic acid and derivatives," *Kirk-Othmer Encyclopedia of Chemical Technology*, 2000.

[61] D. Broell, H. Siegert, H. Hiltner, and T. Krauss, "Process for preparing methacrylic acid," Jul. 29 2014, US Patent 8,791,296.

[62] J.-L. Dubois, "Recovery of (meth)acrylic resin by depolymerization and hydrolysis," Oct. 31 2019, WO2019207264.

[63] D. Packet, "A method for the direct hydrolysis of fatty acid esters to the corresponding fatty acids," Oct. 15 2003, European Patent 1,352,891.

[64] O. V. Chub, J. Dubois, and G. S. Patience, "Tandem fluidized bed/milli-second fixed bed reactor produces methacrylic acid from poly(methyl methacrylate)," *Applied Catalysis A: General*, vol. 647, p. 118887, 2022.

[65] R. S. Lampitt, S. Fletcher, M. Cole, A. Kloker, S. Krause, F. O'Hara, P. Ryde, M. Saha, A. Voronkova, and A. Whyle, "Stakeholder alliances are essential to reduce the scourge of plastic pollution," *Nature Communications*, vol. 14, no. 1, p. 2849, 2023.

[66] M. Sponchioni and S. Altinok, "Poly (methyl methacrylate): Market trends and recycling," in *Advances in Chemical Engineering*, D. Moscatelli and M. Pelucchi, Eds. Cambridge: Elsevier, 2022, vol. 60, pp. 269–287.

[67] E. K. Moens, K. De Smit, Y. W. Marien, A. D. Trigilio, P. H. Van Steenberge, K. M. Van Geem, J.-L. Dubois, and D. R. D'hooge, "Progress in reaction mechanisms and reactor technologies for thermochemical recycling of poly (methyl methacrylate)," *Polymers*, vol. 12, no. 8, p. 1667, 2020.

[68] J. Dubois, "Guidelines for PMMA depolymerization at pilot and industrial scale," 2022, https://www.researchgate.net/ (accessed: April 2022).

[69] Y. Zhuang, N. Saadatkhah, T.-D. Nguyen, J. De Tommaso, C. Y. J. Ng, C. Wang, A. Ajji, and G. S. Patience, "Upcycling polymethyl methacrylate to methacrylic acid," *Reaction Chemistry & Engineering*, vol. 10, no. 1, pp. 237–250, 2025.

[70] P. N. Bhandari, *Chemical modification of polysaccharides using reactive extrusion.* Lincoln: The University of Nebraska-Lincoln, 2012.

[71] D. Misiura and T. M. Majka, "An overview on obtaining foamed pet by reactive extrusion," *Technical Transactions*, vol. 115, no. 4, pp. 97–102, 2018.

[72] A. Gallos, G. Paës, F. Allais, and J. Beaugrand, "Lignocellulosic fibers: a critical review of the extrusion process for enhancement of the properties of natural fiber composites," *RSC Advances*, vol. 7, no. 55, pp. 34 638–34 654, 2017.

[73] D. E. Crawford, "Extrusion–back to the future: Using an established technique to reform automated chemical synthesis," *Beilstein Journal of Organic Chemistry*, vol. 13, no. 1, pp. 65–75, 2017.

[74] M. A. Mohsin, T. Abdulrehman, and Y. Haik, "Reactive extrusion of polyethylene terephthalate waste and investigation of its thermal and mechanical properties after treatment," *International Journal of Chemical Engineering*, vol. 2017, pp. 1–10, 2017.

[75] L. Janssen, *Reactive Extrusion Systems.* Boca Raton, FL: CRC Press, 2004.

[76] K. Stober and J. Amos, "Method of polymerizing styrene," 1950, US Patent 2,530,409.

[77] G. Meyuhas, A. Moses, Y. Reibenbach, and Z. Tadmor, "Continuous polymerization in extruder reactor," *Journal of Polymer Science: Polymer Letters Edition*, vol. 11, no. 2, pp. 103–111, 1973.

[78] G. Beyer and C. Hopmann, *Reactive Extrusion: Principles and Applications.* Hoboken: John Wiley & Sons, 2018.

[79] C. Tzoganakis, "Reactive extrusion of polymers: a review," *Advances in Polymer Technology*, vol. 9, no. 4, pp. 321–330, 1989.

[80] E. Gatt, L. Rigal, and V. Vandenbossche, "Biomass pretreatment with reactive extrusion using enzymes: A review," *Industrial Crops and Products*, vol. 122, pp. 329–339, 2018.

[81] L. Asaro, M. Gratton, S. Seghar, and N. A. Hocine, "Recycling of rubber wastes by devulcanization," *Resources, Conservation and Recycling*, vol. 133, pp. 250–262, 2018.

[82] T. Goto, S. Ashihara, T. Yamazaki, I. Okajima, T. Sako, Y. Iwamoto, M. Ishibashi, and T. Sugeta, "Continuous process for recycling silane cross-linked polyethylene using supercritical alcohol and extruders," *Industrial & Engineering Chemistry Research*, vol. 50, no. 9, pp. 5661–5666, 2011.

[83] B. Xue, H. He, Z. Zhu, J. Li, Z. Huang, G. Wang, M. Chen, and Z. Zhan, "A facile fabrication of high toughness poly (lactic acid) via reactive extrusion with poly (butylene succinate) and ethylene-methyl acrylate-glycidyl methacrylate," *Polymers*, vol. 10, no. 12, p. 1401, 2018.

[84] F. Magliozzi, G. Chollet, E. Grau, and H. Cramail, "Benefit of the reactive extrusion in the course of polyhydroxyurethanes synthesis by aminolysis of cyclic carbonates," *ACS Sustainable Chemistry & Engineering*, vol. 7, no. 20, pp. 17 282–17 292, 2019.

[85] P. Simonetti, R. Nazir, A. Gooneie, S. Lehner, M. Jovic, K. A. Salmeia, R. Hufenus, A. Rippl, J.-P. Kaiser, C. Hirsch, B. Rubi, and S. Gaan, "Michael addition in reactive extrusion: A facile sustainable route to developing phosphorus based flame retardant materials," *Composites Part B: Engineering*, vol. 178, p. 107470, 2019.

[86] G. S. Patience, "Experimental methods in chemical engineering: Preface," *Canadian Journal of Chemical Engineering*, vol. 96, pp. 2312—2316, 2018.

[87] J. K. Fink, *Reactive Polymers: Fundamentals and Applications: A Concise Guide to Industrial Polymers*. Leoben, Austria: William Andrew, 2017.

[88] S. Al-Malaika, *Reactive Modifiers for Polymers*. Birmingham, UK: Springer Science & Business Media, 2012.

[89] J. D. Patterson, *Continuous Depolymerization of Poly (ethylene terephthalate) via Reactive Extrusion*. Raleigh, North Carolina: North Carolina State University, 2007.

[90] M. Xanthos, *Reactive Extrusion: Principles and Practice*. Weinheim, Germany: Hanser Publishers, 1992.

[91] A. E. Hamielec and H. Tobita, *Polymerization Process, Industrial Polymers Handbook*. Weinheim: Wiley-VHC, 2001.

[92] N. Saadatkhah, A. Carillo Garcia, S. Ackermann, P. Leclerc, M. Latifi, S. Samih, G. S. Patience, and J. Chaouki, "Experimental methods in chemical engineering: Thermogravimetric analysis—tga," *Canadian Journal of Chemical Engineering*, vol. 98, no. 1, pp. 34–43, 2020.

[93] C. Martin, "Processing thermoplastic urethanes via twin screw extrusion," in *Szycher's Handbook of Polyurethanes*, 2nd ed., M. Szycher, Ed. Boca Raton: CRC Press, 2012, ch. 29, pp. 873–896.

[94] J.-P. Harvey, N. Saadatkhah, G. Dumont-Vandewinkel, S. L. Ackermann, and G. S. Patience, "Experimental methods in chemical engineering: Differential scanning calorimetry—dsc," *Canadian Journal of Chemical Engineering*, vol. 96, no. 12, pp. 2518–2525, 2018.

[95] CPM Extrusion Group, "Components-our range of products and services," 2021, https://www.centuryextrusion.com (accessed: June 2021).

[96] Extricom GmbH, "Components for twin screw extruders, conveying and kneading elements," 2021, http://jmlordinternational.com (accessed: June 2021).

[97] Clarivate Analytics, "Web of Science™ Core Collection," 2021, http://apps.webofknowledge.com (accessed: June 2021).

[98] N. J. van Eck and L. Waltman, "Software survey: Vosviewer, a computer program for bibliometric mapping," *Scientometrics*, vol. 84, pp. 523–538, 2010.

[99] F. Jbilou, P. Dole, P. Degraeve, C. Ladaviere, and C. Joly, "A green method for polybutylene succinate recycling: Depolymerization catalyzed by lipase b from candida antarctica during reactive extrusion," *European Polymer Journal*, vol. 68, pp. 207–215, 2015.

[100] P. Kiliaris, C. Papaspyrides, and R. Pfaendner, "Reactive-extrusion route for the closed-loop recycling of poly (ethylene terephthalate)," *Journal of Applied Polymer Science*, vol. 104, no. 3, pp. 1671–1678, 2007.

[101] J. Yang, X. Kong, D. Xu, W. Xie, and X. Wang, "Evolution of the polydispersity of ammonium polyphosphate in a reactive extrusion process: Polycondensation mechanism and kinetics," *Chemical Engineering Journal*, vol. 359, pp. 1453–1462, 2019.

[102] B. Turlier, J. Gimenez, L. Goujard, A. Rousseau, N. Ylla, V. Bounor-Legaré, and F. Fenouillot, "Synthesis of potentially biobased poly (hexamethylene sebacate) via reactive extrusion," *Polymer*, vol. 226, p. 123644, 2021.

[103] B. Kim and K. Kim, "Cross-linking of polypropylene by peroxide and multifunctional monomer during reactive extrusion," *Advances in Polymer Technology*, vol. 12, no. 3, pp. 263–269, 1993.

[104] A. Demongeot, R. Groote, H. Goossens, T. Hoeks, F. Tournilhac, and L. Leibler, "Cross-linking of poly (butylene terephthalate) by reactive extrusion using zn (ii) epoxy-vitrimer chemistry," *Macromolecules*, vol. 50, no. 16, pp. 6117–6127, 2017.

[105] M. Takamura, T. Nakamura, T. Takahashi, and K. Koyama, "Effect of type of peroxide on cross-linking of poly (l-lactide)," *Polymer Degradation and Stability*, vol. 93, no. 10, pp. 1909–1916, 2008.

[106] D. Shi, J. Yang, Z. Yao, Y. Wang, H. Huang, W. Jing, J. Yin, and G. Costa, "Functionalization of isotactic polypropylene with maleic anhydride by reactive extrusion: mechanism of melt grafting," *Polymer*, vol. 42, no. 13, pp. 5549–5557, 2001.

[107] G.-H. Hu, J.-J. Flat, and M. Lambla, "Exchange and free radical grafting reactions in reactive extrusion," in *Makromolekulare Chemie. Macromolecular Symposia*, vol. 75. Hoboken: Wiley, 1993, pp. 137–157.

[108] W. Stevels, A. Bernard, P. V. D. Witte, P. Dijkstra, and J. Feijen, "Block copolymers of poly (l-lactide) and poly (ε-caprolactone) or poly (ethylene glycol) prepared by reactive extrusion," *Journal of Applied Polymer Science*, vol. 62, no. 8, pp. 1295–1301, 1996.

[109] J. Bonilla-Cruz, M. Dehonor, E. Saldívar-Guerra, and A. González-Montiel, "Polymer modification: Functionalization and grafting," in *Handbook of Polymer Synthesis, Characterization, and Processing*, E. Saldívar-Guerra and E. Vivaldo-Lima, Eds. New Jersey: Wiley Online Library, 2013, ch. 10, pp. 205–223.

[110] D. Carlson, L. Nie, R. Narayan, and P. Dubois, "Maleation of polylactide (pla) by reactive extrusion," *Journal of Applied Polymer Science*, vol. 72, no. 4, pp. 477–485, 1999.

[111] Y.-M. Corre, J. Duchet, J. Reignier, and A. Maazouz, "Melt strengthening of poly (lactic acid) through reactive extrusion with epoxy-functionalized chains," *Rheologica Acta*, vol. 50, no. 7, pp. 613–629, 2011.

[112] M. R. Thompson, C. Tzoganakis, and G. L. Rempel, "Alder ene functionalization of polypropylene through reactive extrusion," *Journal of Applied Polymer Science*, vol. 71, no. 3, pp. 503–516, 1999.

[113] G. Montaudo, M. S. Montaudo, E. Scamporrino, and D. Vitalini, "Mechanism of exchange in polyesters: composition and microstructure of copolymers formed in the melt mixing process of poly (ethylene terephthalate) and poly (ethylene adipate)," *Macromolecules*, vol. 25, no. 19, pp. 5099–5107, 1992.

[114] P. Zhan, J. Chen, A. Zheng, H. Shi, F. Chen, D. Wei, X. Xu, and Y. Guan, "The trommsdorff effect under shear and bulk polymerization of methyl methacrylate via reactive extrusion," *European Polymer Journal*, vol. 122, p. 109272, 2020.

[115] J.-P. Puaux, P. Cassagnau, G. Bozga, and I. Nagy, "Modeling of polyurethane synthesis by reactive extrusion," *Chemical Engineering and Processing: Process Intensification*, vol. 45, no. 6, pp. 481–487, 2006.

[116] G. Shishuang, Z. Ying, Z. Anna, and H. Xiao, "Polystyrene prepared by reactive extrusion: kinetics and effect of processing parameters," *Polymers for Advanced Technologies*, vol. 15, no. 4, pp. 185–191, 2004.

[117] Y.-J. Sun, G.-H. Hu, M. Lambla, and H. K. Kotlar, "In situ compatibilization of polypropylene and poly (butylene terephthalate) polymer blends by one-step reactive extrusion," *Polymer*, vol. 37, no. 18, pp. 4119–4127, 1996.

[118] Y.-J. Sun, R. J. Willemse, T. Liu, and W. E. Baker, "In situ compatibilization of polyolefin and polystyrene using friedel—crafts alkylation through reactive extrusion," *Polymer*, vol. 39, no. 11, pp. 2201–2208, 1998.

[119] A. Ghanbari, Z. Mousavi, M.-C. Heuzey, G. S. Patience, and P. J. Carreau, "Experimental methods in chemical engineering: Rheometry," *Canadian Journal of Chemical Engineering*, vol. 98, no. 7, pp. 1456–1470, 2020.

[120] A. Bérard, B. Blais, and G. S. Patience, "Experimental methods in chemical engineering: Residence time distribution—rtd," *Canadian Journal of Chemical Engineering*, vol. 98, no. 4, pp. 848–867, 2020.

[121] P. Cassagnau, V. Bounor-Legaré, and F. Fenouillot, "Reactive processing of thermoplastic polymers: a review of the fundamental aspects," *International Polymer Processing*, vol. 22, no. 3, pp. 218–258, 2007.

[122] C. Rauwendaal, *Understanding Extrusion*. Munich: Carl Hanser Verlag GmbH Co KG, 2018.

[123] G. S. Patience, *Experimental Methods and Instrumentation for Chemical Engineers*, 2nd ed. Amsterdam: Elsevier B.V., 2017.

[124] D. A. Sievers, E. M. Kuhn, J. J. Stickel, M. P. Tucker, and E. J. Wolfrum, "Online residence time distribution measurement of thermochemical biomass pretreatment reactors," *Chemical Engineering Science*, vol. 140, pp. 330–336, 2016.

[125] A. L. Gregor, Gerstorfer, and J. Miethlinger, "Determining the residence time distribution of various screw elements in a co-rotating twin-screw extruder by means of fluorescence spectroscopy," in *AIP Conference Proceedings*. Linz, Autria: AIP Publishing LLC, 2015, vol. 1664, no. 1, p. 020005.

[126] A. Poulesquen, B. Vergnes, P. Cassagnau, A. Michel, S. Carneiro, and J. A. Covas, "A study of residence time distribution in co-rotating twin-screw extruders. part ii: Experimental validation," *Polymer Engineering & Science*, vol. 43, no. 12, pp. 1849–1862, 2003.

[127] A. J. Gomes, C. N. Lunardi, F. S. Rocha, and G. S. Patience, "Experimental methods in chemical engineering: Fluorescence emission spectroscopy," *Canadian Journal of Chemical Engineering*, vol. 97, no. 8, pp. 2168–2175, 2019.

[128] L. Hilliou and J. A. Covas, "In-process rheological monitoring of extrusion-based polymer processes," *Polymer International*, vol. 70, no. 1, pp. 24–33, 2021.

[129] P. Cassagnau, V. Bounor-Legaré, and B. Vergnes, "Experimental and modelling aspects of the reactive extrusion process," *Mechanics & Industry*, vol. 20, no. 8, p. 803, 2019.

[130] M. O. Guerrero-Pérez and G. S. Patience, "Experimental methods in chemical engineering: Fourier transform infrared spectroscopy—ftir," *Canadian Journal of Chemical Engineering*, vol. 98, no. 1, pp. 25–33, 2020.

[131] M. O. Guerrero-Pérez, G. S. Patience, and M. A. Bañares, "Experimental methods in chemical engineering:raman," *Canadian Journal of Chemical Engineering*, vol. 99, no. 1, pp. 97–107, 2021.

[132] A. Y. Malkin and S. G. Kulichikhin, *Rheokinetics: rheological transformations in synthesis and reactions of oligomers and polymers*. Heidelberg: John Wiley & Sons, 2008.

[133] J. Biesenberger, R. Kumar, R. Garritano, and J. Starita, "Rheokinetics for reactive polymer processing," *Polymer Engineering & Science*, vol. 25, no. 5, pp. 301–304, 1985.

[134] K. Yasuda, "A multi-mode viscosity model and its applicability to non-newtonian fluids," *Journal of Textile Engineering*, vol. 52, no. 4, pp. 171–173, 2006.

[135] C. Carrot, P. Revenu, and J. Guillet, "Rheological behavior of degraded polypropylene melts: from mwd to dynamic moduli," *Journal of Applied Polymer Science*, vol. 61, no. 11, pp. 1887–1897, 1996.

[136] K. Kohlgrüber, *Co-Rotating Twin-Screw Extruder, Co-Rotating Twin-Screw Extruders: Fundamentals, Technology, and Applications*. München: Carl Hanser Verlag GmbH & Co, 2007.

[137] E. O. Rodríguez, "Numerical simulations of reactive extrusion in twin screw extruders," Ph.D. dissertation, University of Waterloo, 2009.

[138] T. Ishikawa, T. Amano, S.-I. Kihara, and K. Funatsu, "Flow patterns and mixing mechanisms in the screw mixing element of a co-rotating twin-screw extruder," *Polymer Engineering & Science*, vol. 42, no. 5, pp. 925–939, 2002.

[139] E. Ortiz-Rodriguez and C. Tzoganakis, "Scaling-up a reactive extrusion operation: A one-dimensional simulation analysis," *International Polymer Processing*, vol. 25, no. 3, pp. 242–250, 2010.

[140] K. Ganzeveld and L. Janssen, "Scale-up of counter-rotating closely intermeshing twin screw extruders without and with reactions," *Polymer Engineering & Science*, vol. 30, no. 23, pp. 1529–1536, 1990.

[141] G.-H. Hu, Y. Khalfalla, and K. Y. Benyounis, *Reactive Polymer Processing: Fundamentals of REX*. Amsterdam: Elsevier, 2016.

[142] C. Jepson, "Future extrusion studies," *Industrial & Engineering Chemistry*, vol. 45, no. 5, pp. 992–993, 1953.

[143] J. Pittman and K. Rashid, "Heat transfer in recirculating extruder channel flow," *Journal of Polymer Engineering*, vol. 5, no. 1, pp. 1–48, 1985.

[144] A. Suresh, S. Chakraborty, K. Kargupta, and S. Ganguly, "Low-dimensional models for describing mixing effects in reactive extrusion of polypropylene," *Chemical Engineering Science*, vol. 63, no. 14, pp. 3788–3801, 2008.

[145] K. De Smit, T. Wieme, Y. W. Marien, P. H. Van Steenberge, D. R. D'hooge, and M. Edeleva, "Multi-scale reactive extrusion modelling approaches to design polymer

synthesis, modification and mechanical recycling," *Reaction Chemistry & Engineering*, vol. 7, no. 2, pp. 245–263, 2022.

[146] L. Zhu, K. A. Narh, and K. S. Hyun, "Investigation of mixing mechanisms and energy balance in reactive extrusion using three-dimensional numerical simulation method," *International Journal of Heat and Mass Transfer*, vol. 48, no. 16, pp. 3411–3422, 2005.

[147] W. Michaeli, A. Greefenstein, and U. Berghaus, "Twin-screw extruders for reactive extrusion," *Polymer Engineering & Science*, vol. 35, no. 19, pp. 1485–1504, 1995.

[148] SC-Consultants, "Simulation for twin screw extruder," 2022, https://www.scconsultants.com (accessed: April 2022).

[149] F. Berzin, B. Vergnes, S. Canevarolo, A. Machado, and J. Covas, "Evolution of the peroxide-induced degradation of polypropylene along a twin-screw extruder: Experimental data and theoretical predictions," *Journal of Applied Polymer Science*, vol. 99, no. 5, pp. 2082–2090, 2006.

[150] S. P. Dubey, H. A. Abhyankar, V. Marchante, J. L. Brighton, K. Blackburn, C. Temple, B. Bergmann, G. Trinh, and C. David, "Modelling and validation of synthesis of poly lactic acid using an alternative energy source through a continuous reactive extrusion process," *Polymers*, vol. 8, no. 4, p. 164, 2016.

[151] L. Zhu, K. A. Narh, and K. S. Hyun, "Evaluation of numerical simulation methods in reactive extrusion," *Advances in Polymer Technology: Journal of the Polymer Processing Institute*, vol. 24, no. 3, pp. 183–193, 2005.

[152] L. Zhu, "3-d numerical simulation of reactive extrusion and its application to polymerization of ε-caprolactone in co-rotating twin-screw extruders," Ph.D. dissertation, New Jersey Institute of Technology, 2004.

[153] Y. Zong, H. Tang, and L. Zhao, "3-d numerical simulations for polycondensation of poly (p-phenylene terephthalamide) in twin screw extruder," *Polymer Engineering & Science*, vol. 57, no. 11, pp. 1252–1261, 2017.

[154] D. Sun, X. Zhu, and M. Gao, "3d numerical simulation of reactive extrusion processes for preparing pp/tio2 nanocomposites in a corotating twin screw extruder," *Materials*, vol. 12, no. 4, p. 671, 2019.

[155] R. Ibañez, F. Casteran, C. Argerich, C. Ghnatios, N. Hascoet, A. Ammar, P. Cassagnau, and F. Chinesta, "On the data-driven modeling of reactive extrusion," *Fluids*, vol. 5, no. 2, p. 94, 2020.

[156] F. Castéran, R. Ibanez, C. Argerich, K. Delage, F. Chinesta, and P. Cassagnau, "Application of machine learning tools for the improvement of reactive extrusion simulation," *Macromolecular Materials and Engineering*, vol. 305, no. 12, p. 2000375, 2020.

[157] N. Saadatkhah, S. Aghamiri, M. R. Talaie, and G. S. Patience, "Flame-assisted spray pyrolysis to size-controlled LiyAlxMn2-xO4: a supervised machine learning approach," *CrystEngComm*, vol. 20, no. 46, pp. 7590–7601, 2018.

[158] J. Panerati, M. A. Schnellmann, C. Patience, G. Beltrame, and G. S. Patience, "Experimental methods in chemical engineering: Artificial neural networks–anns," *The Canadian Journal of Chemical Engineering*, vol. 97, no. 9, pp. 2372–2382, 2019.

[159] J. Golba, B. Thiele, and C. Gogos, "Reactive extrusion: Industry icons impart their insights," 2020, https://www.ptonline.com/blog/post/reactive-extrusion-industry-icons-impart-their-insights (accessed: June 2021).

[160] H. Vahabi, F. Laoutid, K. Formela, M. R. Saeb, and P. Dubois, "Flame-retardant polymer materials developed by reactive extrusion: Present status and future perspectives," *Polymer Reviews*, vol. early access 10.1080/15583724.2022.2052897, pp. 1–31, 2022.

[161] S. Martey, B. Addison, N. Wilson, B. Tan, J. Yu, J. R. Dorgan, and M. J. Sobkowicz, "Hybrid chemomechanical plastics recycling: Solvent-free, high-speed reactive extrusion of low-density polyethylene." *ChemSusChem*, vol. 14, no. 19, pp. 4280–4290, 2021.

[162] L. Verny, N. Ylla, F. D. Cruz-Boisson, É. Espuche, R. Mercier, G. Sudre, and V. Bounor-Legaré, "Solvent-free reactive extrusion as an innovative and efficient process for the synthesis of polyimides," *Industrial & Engineering Chemistry Research*, vol. 59, no. 37, pp. 16 191–16 204, 2020.

[163] T.-T. Li, L.-F. Feng, X.-P. Gu, C.-L. Zhang, P. Wang, and G.-H. Hu, "Intensification of polymerization processes by reactive extrusion," *Industrial & Engineering Chemistry Research*, vol. 60, no. 7, pp. 2791–2806, 2021.

[164] S. Seck, S. Magana, A. Prébé, P. Buvat, J. Bigarré, J. Chauveau, B. Ameduri, J.-F. Gérard, and V. Bounor-Legaré, "New fluorinated polymer-based nanocomposites via combination of sol-gel chemistry and reactive extrusion for polymer electrolyte membranes fuel cells (pemfcs)," *Materials Chemistry and Physics*, vol. 252, p. 123004, 2020.

[165] K. Formela, Ł. Zedler, A. Hejna, and A. Tercjak, "Reactive extrusion of bio-based polymer blends and composites-current trends and future developments." *Express Polymer Letters*, vol. 12, no. 1, 2018.

[166] T. J. Gutiérrez and G. A. Valencia, "Reactive extrusion-processed native and phosphated starch-based food packaging films governed by the hierarchical structure," *International Journal of Biological Macromolecules*, vol. 172, pp. 439–451, 2021.

[167] B. K. Baek, J. W. Shin, J. Y. Jung, S. M. Hong, G. J. Nam, H. Han, and C. M. Koo, "Continuous supercritical decrosslinking extrusion process for recycling of crosslinked polyethylene waste," *Journal of Applied Polymer Science*, vol. 132, no. 6, 2015.

[168] S. Ulitzsch, T. Bäuerle, M. Stefanakis, M. Brecht, T. Chassé, G. Lorenz, and A. Kandelbauer, "Synthesis of an addition-crosslinkable, silicon-modified polyolefin via reactive extrusion monitored by in-line raman spectroscopy," *Polymers*, vol. 13, no. 8, p. 1246, 2021.

[169] L. P. Barros, S. V. Canevarolo, D. Klein, and J. Maia, "On-line atr-mir for real-time quantification of chemistry kinetics along the barrel in extrusion-based processes," *Polymer Testing*, vol. 103, p. 107350, 2021.

[170] T. Rohe, W. Becker, A. Krey, H. Nägele, S. Kölle, and N. Eisenreich, "In-line monitoring of polymer extrusion processes by nir spectroscopy," *Journal of Near Infrared Spectroscopy*, vol. 6, no. 1, pp. 325–332, 1998.

[171] OECD, *Global Plastics Outlook: Economic Drivers, Environmental Impacts and Policy Options*. Paris: OECD Publishing, 2022.

[172] X. Yuan, X. Wang, B. Sarkar, and Y. S. Ok, "The covid-19 pandemic necessitates a shift to a plastic circular economy," *Nature Reviews Earth & Environment*, vol. 2, no. 10, pp. 659–660, 2021.

[173] K. S. Khoo, L. Y. Ho, H. R. Lim, H. Y. Leong, and K. W. Chew, "Plastic waste associated with the covid-19 pandemic: Crisis or opportunity?" *Journal of Hazardous Materials*, vol. 417, p. 126108, 2021.

[174] T. M. Adyel, "Accumulation of plastic waste during covid-19," *Science*, vol. 369, no. 6509, pp. 1314–1315, 2020.

[175] N. Ebner and E. Iacovidou, "The challenges of covid-19 pandemic on improving plastic waste recycling rates," *Sustainable Production and Consumption*, vol. 28, pp. 726–735, 2021.

[176] A. L. P. Silva, J. C. Prata, T. R. Walker, D. Campos, A. C. Duarte, A. M. Soares, D. Barcelò, and T. Rocha-Santos, "Rethinking and optimising plastic waste management under covid-19 pandemic: policy solutions based on redesign and reduction of single-use plastics and personal protective equipment," *Science of the Total Environment*, vol. 742, p. 140565, 2020.

[177] B. Joseph, J. James, N. Kalarikkal, and S. Thomas, "Recycling of medical plastics," *Advanced Industrial and Engineering Polymer Research*, vol. 4, no. 3, pp. 199–208, 2021.

[178] M. Bachmann, C. Zibunas, J. Hartmann, V. Tulus, S. Suh, G. Guillén-Gosálbez, and A. Bardow, "Towards circular plastics within planetary boundaries," *Nature Sustainability*, vol. 6, no. 5, pp. 599–610, 2023.

[179] R. Geyer, R. J. Jenna, and L. L. Kara, "Production, use, and fate of all plastics ever made," *Science Advances*, vol. 3, no. 7, p. e1700782, 2017.

[180] MarketsandMarkets, "Polymethyl methacrylate (PMMA) market," 2022, https://www.marketsandmarkets.com/Market-Reports/polymethyl-methacrylate-pmma-market-715.html (accessed: August 2022).

[181] P. Research, "Polymethyl methacrylate (PMMA) market size, report," 2021, https://www.precedenceresearch.com/polymethyl-methacrylate-market (accessed: April 2023).

[182] D. D'Hooge, Y. W. Marien, and J. L. Dubois, *Polymer Circularity Roadmap: Recycling of Poly(methyl Methacrylate) as a Case Study*. Berlin: Walter de Gruyter, 2022.

[183] T. C. Research and D. I. S. (CORDIS), "Innovative acrylic(PMMA- polymethyl methacrylate) recycling technology complying with regulations," 2022, https://cordis.europa.eu/project/id/856103/reporting (accessed: August 2022).

[184] M. Sponchioni and S. Altinok, "Poly (methyl methacrylate): Market trends and recycling," in *Advances in Chemical Engineering*. New York: Elsevier, 2022, vol. 60, no. 1, pp. 269–287.

[185] T. Kashiwagi, T. Hirata, and J. E. Brown, "Thermal and oxidative degradation of poly (methyl methacrylate) molecular weight," *Macromolecules*, vol. 18, no. 7, pp. 1410–1418, 1985.

[186] USEPA, "Ethyl acrylate," 2016, https://www.epa.gov/sites/default/files/2016-09/documents/ethyl-acrylate.pdf (accessed: March 2023).

[187] E. K. Moens, Y. W. Marien, F. L. Figueira, A. D. Trigilio, K. De Smit, K. M. Van Geem, P. H. Van Steenberge, and D. R. D'hooge, "Coupled matrix-based monte carlo modeling for a mechanistic understanding of poly (methyl methacrylate) thermochemical recycling kinetics," *Chemical Engineering Journal*, vol. 475, p. 146105, 2023.

[188] H. Narita, S. Okamoto, and S. Machida, "The polymerization mechanism of methyl methacrylate initiated with ceric ion," *Die Makromolekulare Chemie: Macromolecular Chemistry and Physics*, vol. 125, pp. 15–23, 1969.

[189] R. Buter, Y. Y. Tan, and G. Challa, "Radical polymerization of methyl methacrylate in the presence of stereoregular poly (methyl methacrylate). iv. influence of solvent type," *Journal of Polymer Science: Polymer Chemistry Edition*, vol. 11, pp. 2975–2989, 1973.

[190] F. Fenouillot, J. Terrisse, and T. Rimlinger, "Polymerization of methyl methacrylate at high temperature with 1-butanethiol as chain transfer agent," *Journal of Applied Polymer Science*, vol. 72, pp. 1589–1599, 1999.

[191] IARC, "Some industrial chemicals." in *IARC Monographs on the Evaluation of the Carcinogenic Risk of Chemicals to Humans*, vol. 60. Geneva: World Health Organization, 1994, pp. 1–560.

[192] BMT, "Methyl methacrylate (MMA)," 2023, https://cargohandbook.com (accessed: March 2023).

[193] O. V. Chub, J. Dubois, and G. S. Patience, "Zeolite Y hydrolyses methyl methacrylate to methacrylic acid in the gas phase," *Chemical Engineering Journal*, vol. 459, p. 141479, 2023.

[194] T. Map, "291614 esters of methacrylic acid," 2023, https://www.trademap.org/ (accessed: March 2023).

[195] N. Mehio, S. Dai, and D. Jiang, "Quantum mechanical basis for kinetic diameters of small gaseous molecules," *The Journal of Physical Chemistry A*, vol. 118, pp. 1150–1154, 2014.

[196] T. Lu and F. Chen, "Multiwfn: A multifunctional wavefunction analyzer," *Journal of Computational Chemistry*, vol. 33, pp. 580–592, 2012.

[197] D. Masih, S. Rohani, J. N. Kondo, and T. Tatsumi, "Low-temperature methanol dehydration to dimethyl ether over various small-pore zeolites," *Applied Catalysis B: Environmental*, vol. 217, pp. 247–255, 2017.

[198] M. M. J. Treacy and J. B. Higgins, *Collection of Simulated XRD Powder Patterns for Zeolites Fifth (5th) Revised Edition*. Amsterdam: Elsevier, 2007.

[199] P. B. Raja, K. R. Munusamy, V. Perumal, and M. N. M. Ibrahim, "Characterization of nanomaterial used in nanobioremediation," in *Nano-Bioremediation: Fundamentals and Applications*, M. I. Hafiz, B. Muhammad, and A. N. Tuan, Eds. Amsterdam: Elsevier, 2022, pp. 57–83.

[200] S. Liu, P. A. Kots, B. C. Vance, A. Danielson, and D. G. Vlachos, "Plastic waste to fuels by hydrocracking at mild conditions," *Science Advances*, vol. 7, p. eabf8283, 2021.

[201] M. Gackowski and J. Datka, "Acid properties of hierarchical zeolites Y," *Molecules*, vol. 25, p. 1044, 2020.

[202] J. Zuo, W. Chen, J. Liu, X. Duan, L. Ye, and Y. Yuan, "Selective methylation of toluene using CO_2 and H_2 to para-xylene," *Science Advances*, vol. 6, p. eaba5433, 2020.

[203] J. Lü, S. Zhou, K. Ma, M. Meng, and Y. Tian, "The effect of P modification on the acidity of HZSM−5 and P−HZSM−5/CuO-ZnO-Al_2O_3 mixed catalysts for hydrogen production by dimethyl ether steam reforming," *Chinese Journal of Catalysis*, vol. 36, pp. 1295–1303, 2015.

[204] M. A. Makarova and J. Dwyer, "FTIR analysis of the hydroxyl region in US−Y zeolites," *The Journal of Physical Chemistry*, vol. 97, pp. 6337–6338, 1993.

[205] M. Xie, Y. Li, U. J. Etim, H. Lou, W. Xing, P. Wu, X. Liu, P. Bai, and Z. Yan, "Enhanced catalytic performance of the FCC catalyst with an alumina matrix modified by the zeolite Y structure-directing agent," *Industrial & Engineering Chemistry Research*, vol. 58, pp. 5455–5463, 2019.

[206] L. Wang, A. Wang, X. Li, F. Zhou, and Y. Hu, "Highly acidic mesoporous aluminosilicates prepared from preformed HY zeolite in Na_2SiO_3 alkaline buffer system," *Journal of Materials Chemistry*, vol. 20, pp. 2232–2239, 2010.

[207] W. Dong, Z. Shen, B. Peng, M. Gu, X. Zhou, B. Xiang, and Y. Zhang, "Selective chemical conversion of sugars in aqueous solutions without alkali to lactic acid over a Zn−Sn−Beta lewis acid-base catalyst," *Scientific Reports*, vol. 6, p. 26713, 2016.

[208] Z. Shen, L. Kong, W. Zhang, M. Gu, M. Xia, X. Zhou, and Y. Zhang, "Surface amino-functionalization of Sn – Beta zeolite catalyst for lactic acid production from glucose," *RSC Advances*, vol. 9, pp. 18 989–18 995, 2019.

[209] N. V. Vlasenko, Y. N. Kochkin, G. M. Telbiz, O. V. Shvets, and P. E. Strizhak, "Insight into the active site nature of zeolite H – BEA for liquid phase etherification of isobutylene with ethanol," *RSC Advances*, vol. 9, pp. 35 957–35 968, 2019.

[210] W. Zhang, P. Wang, C. Yang, and C. Li, "A comparative study of n-butane isomerization over H – Beta and H – ZSM – 5 zeolites at low temperatures: effects of acid properties and pore structures," *Catalysis Letters*, vol. 149, pp. 1017–1025, 2019.

[211] S. Li, A. Zheng, Y. Su, H. Zhang, L. Chen, J. Yang, C. Ye, and F. Deng, "Brønsted/lewis acid synergy in dealuminated HY zeolite: a combined solid-state NMR and theoretical calculation study," *Journal of the American Chemical Society*, vol. 129, pp. 11 161–11 171, 2007.

[212] D. S. Zasukhin, I. A. Kasyanov, Y. G. Kolyagin, A. I. Bulygina, K. C. Kharas, and I. I. Ivanova, "Evaluation of zeolite acidity by ^{31}P MAS NMR spectroscopy of adsorbed phosphine oxides: Quantitative or not?" *ACS Omega*, vol. 7, pp. 12 318–12 328, 2022.

[213] J. N. Kondo, R. Nishitani, E. Yoda, T. Yokoi, T. Tatsumi, and K. Domen, "A comparative IR characterization of acidic sites on HY zeolite by pyridine and CO probes with silica–alumina and γ-alumina references," *Physical Chemistry Chemical Physics*, vol. 12, pp. 11 576–11 586, 2010.

[214] C. Baerlocher and L. McCusker, "Database of zeolite structures," 2023, http://www.iza-structure.org/databases/ (accessed: January 2023).

[215] L. Chang and E. Woo, "Tacticity effects on glass transition and phase behavior in binary blends of poly (methyl methacrylate) s of three different configurations," *Polymer Chemistry*, vol. 1, pp. 198–202, 2010.

[216] B. Ho, Y. Lee, and W. Chin, "Thermal degradation of polymethacrylic acid," *Journal of Polymer Science Part A: Polymer Chemistry*, vol. 30, pp. 2389–2397, 1992.

[217] J. Semen and J. Lando, "The acid hydrolysis of isotactic and syndiotactic poly (methyl methacrylate)," *Macromolecules*, vol. 2, pp. 570–575, 1969.

[218] D. Breck, *Zeolite Molecular Sieves: Structure, Chemistry, and Use.* Hoboken: Wiley, 1973.

[219] E. Erickson, "Shaping a federal strategy for chemical recycling: Moving toward sensible applications of emerging technologies in us plastic waste management," *Environmental Progress & Sustainable Energy*, p. e14333, 2024.

[220] B. T. Nicholls and B. P. Fors, "Closing the loop on thermoset plastic recycling," *Science*, vol. 384, no. 6692, pp. 156–157, 2024.

[221] B. Hu, S. Wang, J. Yan, H. Zhang, L. Qiu, W. Liu, Y. Guo, J. Shen, B. Chen, C. Shi, and X. Ge, "Review of waste plastics treatment and utilization: Efficient conversion and high value utilization," *Process Safety and Environmental Protection*, 2024.

[222] S. El-Bashir, N. Althumairi, and N. Alzayed, "Durability and mechanical performance of PMMA/stone sludge nanocomposites for acrylic solid surface applications," *Polymers*, vol. 9, no. 11, p. 604, 2017.

[223] M. Pirmoradi and J. R. Kastner, "Synthesis of methacrylic acid by catalytic decarboxylation and dehydration of carboxylic acids using a solid base and subcritical water," *ACS Sustainable Chemistry & Engineering*, vol. 5, no. 2, pp. 1517–1527, 2017.

[224] Y. Wu, M. Shetty, K. Zhang, and P. J. Dauenhauer, "Sustainable hybrid route to renewable methacrylic acid via biomass-derived citramalate," *ACS Engineering Au*, vol. 2, no. 2, pp. 92–102, 2021.

[225] J. Lebeau, J. P. Efromson, and M. D. Lynch, "A review of the biotechnological production of methacrylic acid," *Frontiers in Bioengineering and Biotechnology*, vol. 8, p. 207, 2020.

[226] Y. Zhuang, N. Saadatkhah, M. S. Morgani, T. Xu, C. Martin, G. S. Patience, and A. Ajji, "Experimental methods in chemical engineering: Reactive extrusion," *The Canadian Journal of Chemical Engineering*, vol. 101, no. 1, pp. 59–77, 2023.

[227] R. L. Plackett and J. P. Burman, "The design of optimum multifactorial experiments," *Biometrika*, vol. 33, no. 4, pp. 305–325, 1946.

[228] R. Bardestani, G. S. Patience, and S. Kaliaguine, "Experimental methods in chemical engineering: specific surface area and pore size distribution measurements—BET, BJH, and DFT," *The Canadian Journal of Chemical Engineering*, vol. 97, no. 11, pp. 2781–2791, 2019.

[229] M. Sharifian, N. Hudon, E. Pahija, and G. S. Patience, "Feedback control strategy of Fischer–Tropsch process in a micro-gtl plant," *Chemical Engineering Research and Design*, 2024.

[230] A. Bérard, B. Blais, and G. S. Patience, "Residence time distribution in fluidized beds: diffusion, dispersion, and adsorption," *Advanced Powder Technology*, vol. 32, no. 5, pp. 1677–1687, 2021.

[231] O. Levenspiel, *Chemical Reaction Engineering*. New York: John Wiley & Sons, 1998.

[232] N. Frame, "Operational characteristics of the co-rotating twin-screw extruder," *The Technology of Extrusion Cooking*, pp. 1–51, 1994.

[233] E. N. Kimuli, I. I. Onyemelukwe, B. Benyahia, and C. D. Rielly, "Characterisation of axial dispersion in a meso-scale oscillatory baffled crystalliser using a numerical approach," in *Computer Aided Chemical Engineering*, A. Espuña, M. Graells, and L. Puigjaner, Eds. Barcelona: Elsevier, 2017, vol. 40, pp. 223–228.

[234] P. Ainsworth, S. Ibanoglu, and G. D. Hayes, "Influence of process variables on residence time distribution and flow patterns of tarhana in a twin-screw extruder," *Journal of Food Engineering*, vol. 32, no. 1, pp. 101–108, 1997.

[235] H. Fang, F. Mighri, A. Ajji, P. Cassagnau, and S. Elkoun, "Flow behavior in a corotating twin-screw extruder of pure polymers and blends: Characterization by fluorescence monitoring technique," *Journal of Applied Polymer Science*, vol. 120, no. 4, pp. 2304–2312, 2011.

[236] L. Kotamarthy, S. Karkala, A. Dan, A. D. Román-Ospino, and R. Ramachandran, "Investigating the effects of mixing dynamics on twin-screw granule quality attributes via the development of a physics-based process map," *Pharmaceutics*, vol. 16, no. 4, p. 456, 2024.

[237] C. Capone, L. Di Landro, F. Inzoli, M. Penco, and L. Sartore, "Thermal and mechanical degradation during polymer extrusion processing," *Polymer Engineering & Science*, vol. 47, no. 11, pp. 1813–1819, 2007.

[238] B.-S. Lee, Y.-J. Chen, T.-C. Wei, T.-L. Ma, and C.-C. Chang, "Comparison of antibacterial adhesion when salivary pellicle is coated on both poly (2-hydroxyethyl-methacrylate)-and polyethylene-glycol-methacrylate-grafted poly (methyl methacrylate)," *International Journal of Molecular Sciences*, vol. 19, no. 9, p. 2764, 2018.

[239] A. M. Bakr, A. Darwish, A. Azab, M. E. El Awady, A. A. Hamed, and A. Elzwawy, "Structural, dielectric, and antimicrobial evaluation of PMMA/CeO_2 for optoelectronic devices," *Scientific Reports*, vol. 14, no. 1, p. 2548, 2024.

[240] M. Khalifa, A. M. El Sayed, S. M. Kassem, and E. Tarek, "Synthesis, structural, optical, and thermal properties of $LaFeO_3$/poly (methyl methacrylate)/poly (vinyl acetate) nanocomposites for radiation shielding," *Scientific Reports*, vol. 14, no. 1, p. 3672, 2024.

[241] M. A. Forte, R. M. Silva, C. J. Tavares, and R. F. e. Silva, "Is poly (methyl methacrylate)(PMMA) a suitable substrate for ALD?: A review," *Polymers*, vol. 13, no. 8, p. 1346, 2021.

[242] J. D. Menczel, L. Judovits, R. B. Prime, H. E. Bair, M. Reading, and S. Swier, "Differential scanning calorimetry (DSC)," *Thermal analysis of polymers: Fundamentals and applications*, pp. 7–239, 2009.

[243] N. A. Platé, A. D. Litmanovich, and Y. V. Kudryavtsev, "Theoretical considerations on the reactions in polymer blends," in *Modification and Blending of Synthetic and Natural Macromolecules*, F. Ciardelli and S. Penczek, Eds. Dordrecht: Springer, 2004, pp. 241–281.

[244] J. Kang, X. Li, Y. Zhou, and L. Zhang, "Supramolecular interaction enabled preparation of high-strength water-based adhesives from polymethylmethacrylate wastes," *Iscience*, vol. 26, no. 2, 2023.

[245] Y. Kikuchi, M. Hirao, H. Sugiyama, S. Papadokonstantakis, K. Hungerbühler, T. Ookubo, and A. Sasaki, "Design of recycling system for poly (methyl methacrylate)(PMMA). part 2: process hazards and material flow analysis," *The International Journal of Life Cycle Assessment*, vol. 19, pp. 307–319, 2014.

[246] J. Cervantes-Uc, J. Cauich-Rodríguez, H. Vázquez-Torres, and A. Licea-Claveríe, "TGA/FTIR study on thermal degradation of polymethacrylates containing carboxylic groups," *Polymer Degradation and Stability*, vol. 91, no. 12, pp. 3312–3321, 2006.

[247] G. Cruciani, "Zeolites upon heating: Factors governing their thermal stability and structural changes," *Journal of Physics and Chemistry of Solids*, vol. 67, no. 9-10, pp. 1973–1994, 2006.

[248] Y. Zhuang, T. D. Nguyen, M. Sharifian, J.-L. Dubois, A. Ajji, and G. Patience, "Reactive extrusion recycling of polymethyl methacrylate to methyl methacrylate and methacrylic acid," *Chemical Engineering Journal*, vol. 515, p. 162709, 2025.